Charting New Territory in Bis(imino)pyridine Coordination Chemistry

Titel Jurca

Thesis submitted to the
Faculty of Graduate and Postdoctoral Studies
In partial fulfillment of the requirements for the degree of

Doctorate in Philosophy
In
Chemistry

Ottawa-Carleton Chemistry Institute
University of Ottawa

Supervisor: *Professor Darrin Richeson*

I would like to dedicate this thesis to my parents. Without their love and support, none of this would have been possible.

Acknowledgements

First and foremost, I would like to thank my supervisor, Dr. Darrin Richeson, without whose support, none of this work would have been possible. Our many discussions over the years not only shaped the course of this thesis, but also the approach I take as a scientist. I would also like to thank my committee members, Dr. David Bryce, Dr. Muralee Murugesu, and Dr. Sean Barry who have provided me valuable insights and direction, and restrained my desire to coordinate ligands to just about every element on the periodic table!

I would also like to acknowledge Dr. Serge Gorelsky, whose computational work is featured throughout this thesis. Without his expertise and insight, many of these projects would not have been realised. Similarly, I would like to thank crystallographers Tara Kell, Glen Yap and Ilia Korobkov. Without their work, and particularly Dr. Korobkov's, this thesis could not have been realised. The work of Glenn Facey and his staff past and present has also helped me a great deal, especially in the last few weeks of the writing process.

I would like to thank members of the Richeson group past and present who have made my time in the lab an enjoyable experience. I would also like to thank all my friends in the department, some of whom I have had the pleasure of collaborating with, and have shared many great experiences over the years.

Last but not least, I would like to thank my family. The support and encouragement I have received from my parents helped me get through the difficult times. I would also like to thank my girlfriend Sophie. Her presence in my life and encouragement has been very important to me. Without my loved ones, this task would have been far more difficult to complete.

Publications

The following publications were both directly related to, or derived from work reported in this thesis.

- "Capturing In^+ Monomers in a Neutral Weakly Coordinating Environment" **T. Jurca**, J. Lummiss, T. J. Burchell, S. I. Gorelsky, D. S. Richeson, *J. Am. Chem. Soc.,* **2009**, 131, 4608-4609.
- "Disproportionation and radical formation in the coordination of "GaI" with bis(imino)pyridines" **T. Jurca**, K. Dawson, I. Mallov, T. Burchell, G. P. A. Yap, D. S. Richeson, *Dalton Trans.,* **2010***,* 39, 1266-1272.
- "Multinuclear Solid-State Magnetic Resonance Study of In^+ and Ag^+ in Neutral Weakly Coordinating Environments" A. Y. H. Lo, **T. Jurca**, D. S. Richeson, D. L. Bryce, *J. Phys. Chem. Let. ,***2010***,* 1, 3078-3084.
- "Harnessing Low-Valent Metal Centers through Non-Bonding Orbital Interactions" **T. Jurca**, I. Korobkov, G. P. A. Yap, S. I. Gorelsky, D. S. Richeson. *Inorg. Chem.,* **2010**, 49 (22), 10635–10641.
- "Novel pincer complexes of Ag(I), coordination of toluene and their comparison with indium analogues" **T. Jurca**, S. I. Gorelsky, I. Korobkov, D. S. Richeson. *Dalton Trans.,* **2011**, 40, 4394-4396.
- "Single-Molecule Magnet Behavior with a Single Metal Center Enhanced Through Peripheral Ligand Modifications" **T. Jurca**, A. Farghal, P. H. Lin, I. Korobkov, M. Murugesu, D. S. Richeson, *J. Am. Chem. Soc.*, **2011**, 133, 15814–15817.
- "Using $^{69/71}$Ga Solid-State NMR and ^{127}I NQR as Probes to Elucidate the Composition of "GaI"" C. M. Widdifield, **T. Jurca**, D. S. Richeson, D. L. Bryce, *Polyhedron*, **2012**, 35, 1, 96-100.
- "The Interplay of Metal and Supporting Ligand in Labile Coordination to Pincer Complexes of Ag(I)" **T. Jurca**, S. Ouanounou, I. Korobkov, S. I. Gorelsky, D. S. Richeson, *Dalton Trans.,* **2012**, 41, 4765-4771.
- "The 2,2'-Diindolylmethane Dianion Supporting Scaffold for Group 15 Compounds" I. Mallov, H. Spinney, **T. Jurca**, S. I. Gorelsky, T. J. Burchell, D. S. Richeson, *Inorganica Chimica Acta,* **2012**, *accepted* ICA15023.
- "Non-Covalent Interactions of Metal Cations and Arenes Probed with Thallium(I) Complexes, How Low Can You Go?" **T. Jurca**, I. Korobkov, S. I. Gorelsky, D. S. Richeson, *Submitted.*
- "Changing the *fac* of Rhenium(I) Carbonyl Chemistry; Synthesis and Characterization of Neutral Low Valent Bis(imino)pyridine Pincer Complexes" **T. Jurca**, W.C. Chen, S. Michel, I. Korobkov, T.G. Ong, D.S. Richeson, *Submitted.*

More to come...

Abstract

This work was initially launched to study the synthesis of low-valent group 13 compounds bearing the bis(imino)pyridine ligand framework. Since its inception, this project has grown beyond the boundaries of group 13 to include low valent tin, silver, and rhenium. Alongside the reports of novel coordination compounds, we utilized computational chemistry to uncover unprecedented interactions which challenge conventional concepts of bonding. Synthesis, characterization, and complimentary computational studies are presented herein.

Chapter 1 presents a historical overview of the bis(imino)pyridine ligand as well as our synthetic methodology and characterization of new ligand variants we have contributed to the literature.

Chapter 2 presents the synthesis of a series of In(I) and In(III) bis(imino)pyridine complexes with varied sterics. Ligand-metal interaction and effect of ligand steric bulk on complex stability, as well as computational studies highlighting weak covalent interactions will be discussed.

Chapter 3 presents the synthesis of Ga(III) bis(imino)pyridine complexes. Reactivity with "GaI" synthon as well as varied-stoichiometry one-pot synthesis attempts to generate low valent Ga-bis(imino)pyridine complexes will be discussed.

Chapter 4 presents the synthesis of a series of Tl(I) bis(imino)pyridine complexes with varied sterics analogous to the approach taken with indium(I). Unprecedented weak ligand-metal as well as Tl-arene interactions will be discussed.

Chapter 5 presents the synthesis of a series of Sn(II) bis(imino)pyridine complexes with varied sterics and halide substituents. Preferential cation-anion pair formation and attempted reactivity will be discussed.

Chapter 6 presents the synthesis of a series of Ag(I) bis(imino)pyridine complexes with varied sterics. Resulting ligand-metal interactions as well as reactivity towards Lewis basic donor ligands will be discussed.

Chapter 7 presents the synthesis of first crystallographically authenticated examples of rhenium(I) pincer complexes utilizing the bis(imino)pyridine ligand.

Chapter 8 presents a general conclusion to the work.

Table of Contents

Summary of Figures

Summary of Tables

Chapter 1: *Ligand Design and Synthesis*

[1.1] Introduction

Put in its simplest terms, a ligand is defined as the atoms or groups joined to the central atom in an inorganic coordination entity.[1] Complexes wherein the central metal atom binds to inorganic (non-carbon) ligands have long been known, and often referred to as classical or Werner complexes. As inorganic chemists, our fundamental understanding and preliminary intuitions regarding metal-ligand (M-L) interaction are derived from these classical bonding concepts; the metal centre is a polyvalent Lewis acid (electron pair acceptor) and the ligand, via lone pairs is a Lewis base (electron pair donor). This interaction results in the formation of a Lewis adduct, whereby two electrons are donated to the metal centre per each ligand coordination site; an example being $L_nB + {:}NH_3 \rightarrow L_nB\text{-}NH_3$.[2,3]

The advancement of inorganic and organometallic chemistry has been intimately linked with that of ligand design. The judicious choice of ligand, and fine tuning thereof, has profound influence on complex stability and reactivity. Tantamount to the advances in organometallic and inorganic chemistry is our increasing understanding of molecular orbitals. Employing modern computational techniques, our understanding of M-L interactions has grown beyond that of our predecessors. While classical bonding models are pivotal for shaping our fundamental understanding of M-L bonding, an advanced understanding of M-L interactions aided by computational efforts is paramount to developing new compounds and uncovering hitherto unexplored reactivity.

---

[1] Red Book: IUPAC Nomenclature of Inorganic Chemistry. Third Edition, Blackwell Scientific Publications, Oxford, **1990**, 146.
[2] R.H. Crabtree, The Organometallic Chemistry of the Transition Metals, Fourth Edition, Wiley-Interscience, A John Wiley & Sons Inc. Publication, USA, **2005**, 2.
[3] L_n refers to other ligands present on the metal centre.

[1.2] The Advent of Bis(imino)pyridine Chemistry

With the goal of uncovering unprecedented structure and bonding arrangements and concomitant novel reactivity, we were attracted to the bis(imino)pyridine scaffold and its potential for the isolation of reactive main-group metal centres via kinetic stabilization afforded by implementation of steric bulk. The bis(imino)pyridine ligand class is defined by its binding pocket, consisting of a pyridine backbone, and two imine side-arms. Variability is introduced by altering substituents on the imine group; N-bound side-arms (R') or C-bound groups on the imine backbone (R) traditionally featuring H or CH_3 (Scheme 1.1a). The active binding pocket thereby consists of 3 N-based lone pair donors, and to a first approximation, can be considered a classical, three electron pair Werner complex. The first example of the bis(imino)pyridine class came from a study of pyridine and imine based ligands by Stoufer and Busch in 1956; they reported the bis(hydrazone)pyridine ligand (Scheme 1.1b). The ligands were initially employed in an effort to synthesize and characterize a series of Fe(II), Co(II), and Ni(II)-halide complexes.[4] Interest in the ligand class was rejuvenated when Alyea and Merrell reported the first bis(arylimino)pyridine in 1974 (Scheme 1.1c). It was subsequently used to synthesize a series of Ni(II), Cu(II), Zn(II), and Cd(II)-halide complexes.[5] Although most commonly used modern variants of this ligand class are in fact bis(arylimino)pyridines, the naming convention used is the broad term "bis(imino)pyridine", and will remain the term used for the remainder of this thesis.

[4] R.C. Stoufer, D.H. Busch, *J. Am. Chem. Soc*. **1956**, *78*, 6016.
[5] (a) E.C. Alyea, P.H. Merrell, *Synth. React. Inorg. Met.-Org. Chem.* **1974**, 4. 535. (b) E.C. Alyea, P.H. Merrell, *Inorg. Chim. Acta*, **1978**, 28, 91. (c) E.C. Alyea, L. Ecott, P.H. Merrell, *Inorg. Chim. Acta*, **1982**, 59, 25.

Scheme 1.1

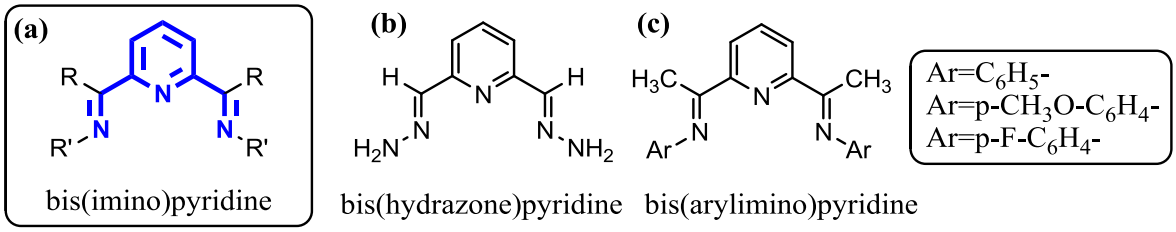

It was however not until the late 1990's that the bis(imino)pyridine ligand garnered widespread and sustained attention. The revitalized interest arose from a discovery by Gibson, Brookhart, and Dupont, that sterically encumbered bis(imino)pyridine complexes of Fe and Co exhibit unprecedentedly high ethylene polymerization activity (Scheme 1.2).[6] The utility of the bis(imino)pyridine supported precatalysts prompted a wide ranging and sustained advancement of the bis(imino)pyridine ligand class. A 2007 review from Gibson *et al.* highlights 49 different symmetric aryl substitution patterns, not taking into account potential substitutional variation on the imine C-backbone (Scheme 1.2 "R"), or asymmetric examples bearing different aryl groups.[7] Today, bis(imino)pyridine chemistry has grown to cover an appreciable portion of the periodic table ranging from Al to Zn, with diverse applications not limited to but including catalysis, optoelectronic devices, and single molecule magnets.[7,8]

Scheme 1.2

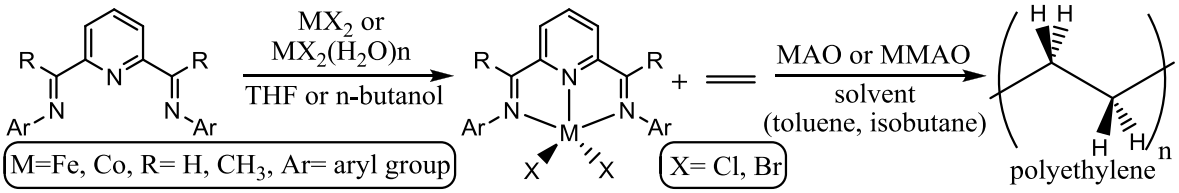

[6] (a) B.L. Small, M. Brookhart, *J. Am. Chem. Soc*., **1998**, 120, 7143. (b) B.L. Small, M. Brookhart, A.M.A. Bennett, *J. Am. Chem. Soc*., **1998**, 120, 4049. (c) G.J.P. Britovsek, V.C. Gibson, B.S. Kimberley, P.J. Maddox, S.J. McTavish, G.A. Solan, A.J.P. White, D.J. Williams, *Chem. Commun*., **1998**, 849.

[7] V.C. Gibson, C. Redshaw, G.A. Solan, *Chem. Rev*., **2007**, 107, 1745.

[8] (a) R. Fan, Y.Yang, Y. Yin, W. Hasi, Y. Mu, *Inorg. Chem*., **2009**, 48, 6034. (b) T. Jurca, A. Farghal, P.H. Lin, I. Korobkov, M. Murugesu, D. S. Richeson, *J. Am. Chem. Soc.*, **2011**, *133*, 40, 15814.

[1.3] Aspects of Ligand Non-Innocence

Although the 3 N-lone pair donors in the binding pocket suggest classical M-L bonding behaviour for bis(imino)pyridines, the reality is much more complex. Bis(imino)pyridine ligands can act as both classical σ-donors as well as π-acceptors, akin to CO. However unlike CO where metal centred electron pairs are delocalized to the ligand; bis(imino)pyridines exhibit single electron transfer from M-L. The electron accepting capacity of this ligand class is credited for its remarkable ability to stabilize metals in a wide variety of oxidation states.[9] Another important facet of bis(imino)pyridine ligand non-innocence is complex decomposition via deprotonation of imine bound CH_3, accompanied by subsequent loss of imine functionality. Several examples have been reported by both the Gambarotta and Gibson groups utilizing Li, Mg, and Zn; reports indicate a mixture of products, including a methylated pyridine-N, and deprotonation of imine bound CH_3 to generate C=C on the ligand backbone (Scheme 1.3 highlights the result of MeLi ligation and subsequent decomposition).[10]

Scheme 1.3

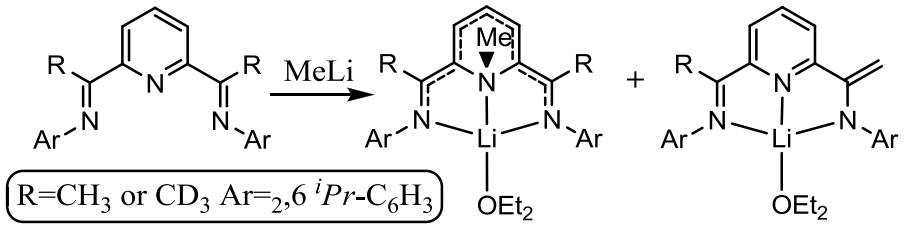

The bis(imino)pyridine chemistry of a significant range of transition metals is well documented, however that of the main group elements, and specifically group 13 remain largely

[9] D. Zhu, P.H.M. Budzelaar, *Organometallics,* **2008,** *27,* 2699.
[10] (a) I. Korobkov, S. Gambarotta, G.P.A. Yap, P.H.M. Budzelaar, *Organometallics* **2002**, *21*, 3088. (b) I.J. Blackmore, V.C. Gibson, P.B. Hitchcock, C.W. Rees, D.J. Williams, A.J. P. White, *J. Am. Chem. Soc*., **2005**, 127, 6012.

unexplored.[11,12] The scope of this thesis is to expand the utility of the bis(imino)pyridine ligand for use with group 13 metals, with the target of stabilizing their less stable, and consequently more exotic low-valent states. While ligand non-innocence has been exploited and well studied for catalysis by various groups, ligand centred decomposition pathways could prove detrimental when attempting to stabilize reactive low valent states of main group metals {Al(I), Ga(I), Ga(II), and In(I)}.[13]

[1.4] Synthetic Methodology for Bis(imino)pyridine Ligands

To circumvent ligand based decomposition via imine-C bound groups (CH_3 or H), we chose to employ a less common variant of the bis(imino)pyridine ligand class; by functionalizing the imine backbone with phenyl groups we can hinder facile H abstraction. Following the procedure reported by Estruelas *et al.*; Friedel-Crafts acylation of 2,6-dicarbonylpyridinedichloride is used to generate 2,6-dibenzoylpyridine (**i**) which serves as the starting point for bis(imino)pyridine synthesis (Scheme 1.4).[14] From (**i**), with the desired aniline (Ar-NH_2), there are two common pathways to generate bis(imino)pyridine ligands with phenyl backbones (**iii**), (Scheme 1.4 **a** and **b**). Approach (**a**) proceeds via a 5 coordinate L-$NiCl_2$ (**ii**) intermediate and subsequent removal of $NiCl_2$ by passage through aminopropylsilicagel to generate (**iii**) (reported by Estruelas *et al*.[14]). Although (**a**) is uncomplicated, we chose to negate it in order to avoid potential trace $NiCl_2$ contamination and reactivity/competition with our target

[11] T. Jurca, J. Lummiss, T.J. Burchell, S.I. Gorelsky, D.S. Richeson, *J. Am. Chem. Soc.*, **2009**, *131* (13), pp 4608–4609.

[12] Prior to our first publication on bis(imino)pyridine complexes of In(I) (ref 11), there were no systematically targeted main group bis(imino)pyridine complexes; (a) R.J. Baker, C. Jones, C.M. Kloth, D.P. Mills *New J. Chem*. **2004**, *28*, 20l7; Isolated a Ga(III) species while screening a broad ligand scope with "GaI" synthon. (b) J. Scott, S. Gambarotta,I. Korobkov, Q. Knijnenburg, B. de Bruin, P.H.M. Budzelaar, *J. Am. Chem. Soc*., **2005**, 127, 17204; isolated Al(III) radical species serendipitously while working on Fe precatalysts. (c) G. Reeske, A.H. Cowley *Chem. Commun.* **2006**, 4856; isolated As species among broader range ligand scope to isolate cyclic arsenic cations.

[13] A.M. Archer, M.W. Bouwkamp, M.P. Cortez, E. Lobkovsky, P.J. Chirik, *Organometallics,* **2006,** 25, 4269.

[14] M.A. Esteruelas, A.M. Lopez, L. Mendez, M. Olivan, E. Onate, *Organometallics,* **2003**, 22*,* 395.

low valent main group reagents. Instead we followed approach (**b**), a slightly modified version from that reported by Kleigrewe *et al*.[15] A mixture of (**i**), aniline, and catalytic *p*-toluenesulfonic acid is refluxed in toluene at 160°C for 48 hours, employing a Dean-Stark apparatus to remove H_2O and drive the reaction forward. A light downward flow of N_2 from atop the reflux condenser is maintained to prevent solvent evaporation in light of the elevated temperature used. Subsequent isolation and purification is detailed in sections [1.4] and [1.5]. Although (**b**) represents a lengthy multi-day process, (**iii**) is generally obtained in good yield with high purity.

Scheme 1.4

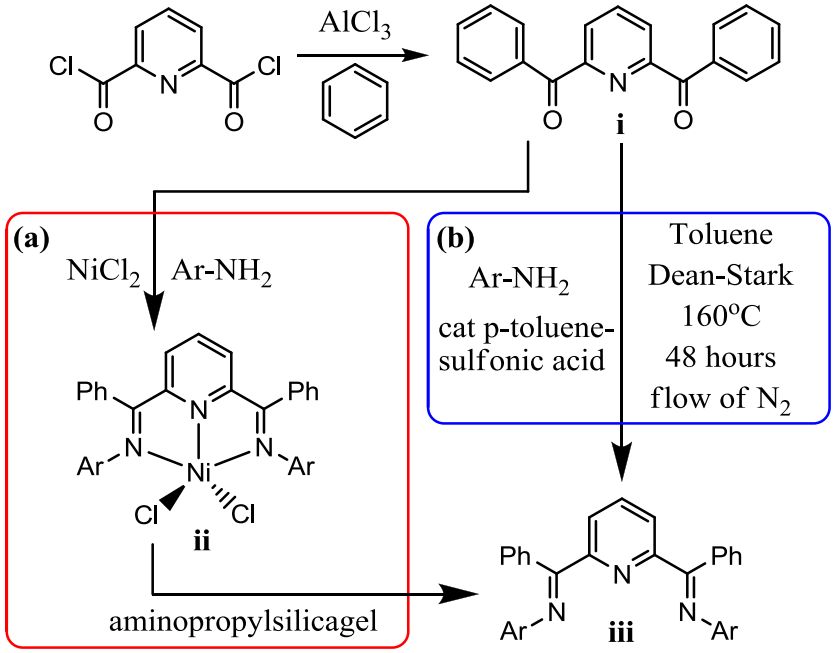

[1.5] Ligand Synthesis and Characterization

Utilizing methodology (**b**) as outlined in Scheme 1.4, we targeted the synthesis of four bis(imino)pyridine ligands bearing phenyl substituents on the imine backbone (Scheme 1.5).

[15] N. Kleigrewe, W. Steffen, T. Blömker, G.Kehr, R. Fröhlich, B. Wibbeling, G. Erker, J.C. Wasilke, G. Wu, G.C. Bazan, *J. Am. Chem. Soc.*, **2005**, 127, 40, 13955.

Following identical reaction procedure as outlined prior, a mixture of (**i**), a minimum of 2.1 equivalents aniline, and catalytic *p*-toluenesulfonic acid was refluxed in toluene at 160°C for 48 hours, employing a Dean-Stark apparatus, under a light flow of N_2. The solution was concentrated *in vacuo* to yield a thick brown paste, then re-dissolved in a minimal amount of cold methanol and held at -20°C overnight to form bright yellow precipitate. The precipitate was washed with either a cold methanol or 9:1 hexanes/ether solution to remove excess aniline, and dried to yield analytically pure ligand (**1A-D**).[16] Deviations from the general synthesis and workup procedure are detailed in section [1.5].

Scheme 1.5

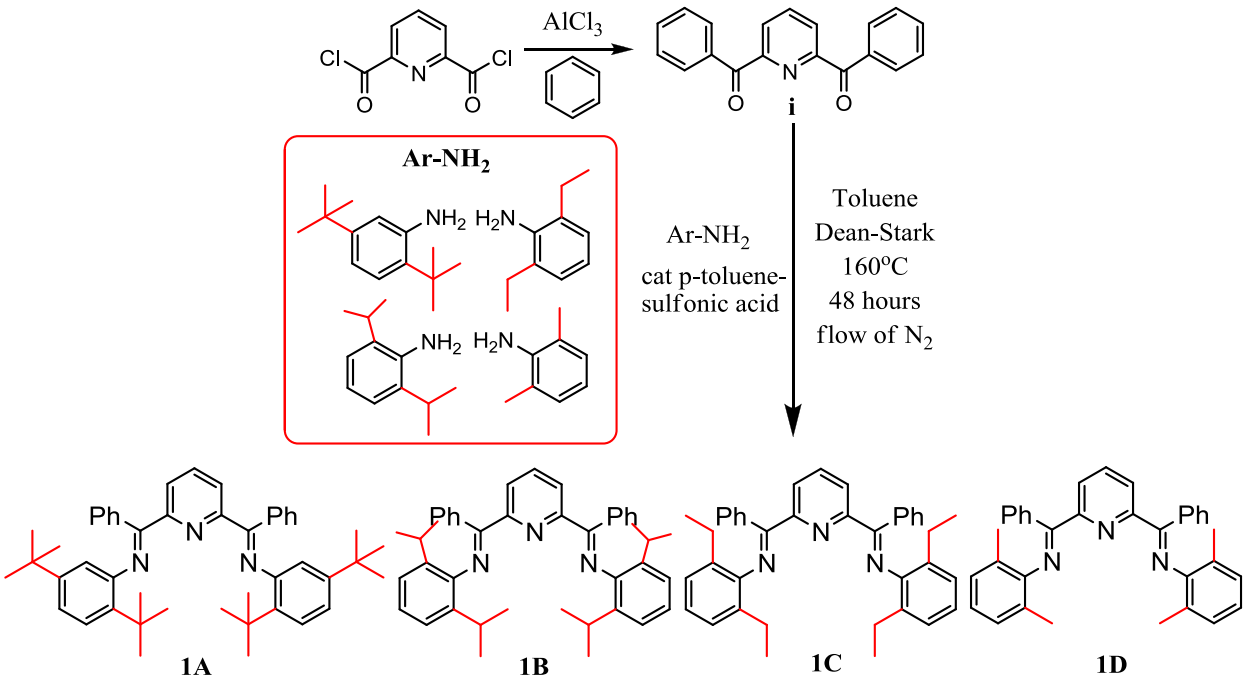

The anilines ($Ar\text{-}NH_2$) selected for our target ligand range are 2,5-ditertbutylaniline, 2,6-diisopropylaniline, 2,6-diethylaniline, and 2,6-dimethylaniline (Scheme 1.5). All four attempts successfully afforded their corresponding bis(imino)pyridine ligands (**1A-D**) in moderate to high

[16] Elemental analysis of **1A-D** returns C, H, N values within the accepted 0.4% range.

yields (39-96%). As can be seen in Scheme 1.5, the judicious choice of aniline reagents yielded a ligand range with systematically decreasing steric bulk surrounding the N,N,N' binding pocket (left to right); 2,5-ditertbutylaniline substituted **1A** representing the highest degree of steric bulk, and 2,6-dimethylaniline substituted **1D** representing the lowest. This array of sterically varied ligands affords us the opportunity to refine the synthesis, and study the stability and reactivity of our target low-valent complexes and their analogues. These results will be discussed throughout the following chapters.

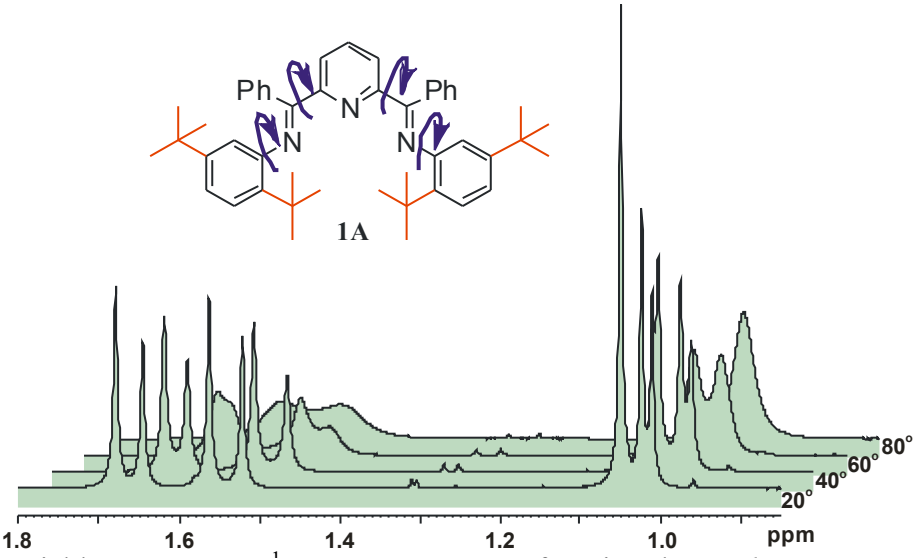

Figure 1.1: Variable temperature ^{1}H NMR spectrum of **1A** in toluene-*d*8 at 20, 40, 60 and 80 ^{o}C. These spectra show the averaged rotation about C-C and C-N bonds resulting in several conformers observed in room temperature solution. Similar behaviour was observed in the ^{13}C NMR.

Principal characterization of **1A-D** was performed with ^{1}H and ^{13}C NMR, and confirmed by elemental analysis. However, NMR characterization proved to be unexpectedly demanding. As can be seen in Figure 1.1, at room temperature several rotational isomers, arising from the pyridine-2,6-carbon to imine-carbon bond, as well as the imine-nitrogen to 2-aryl-carbon bond, are observed. Taking into account potential for asymmetric structures, one could envision a multitude of potential conformers. Ultimately this results in room temperature NMR spectra that

are difficult to analyze. Figure 1.1 highlights the ^{1}H alkyl region of **1A** (δ0.9-1.8ppm) in toluene-*d8*; at 20^{o}C, there are seven visible peaks attributed to the tertbutyl (^{t}Bu) proton signals. As temperature is increased in 20^{o} increments, rotation around the single bonds increases and peaks begin to coalesce at around 80^{o}C. However, this is not sufficient to achieve complete coalescence, and higher temperatures go beyond the safe user range for toluene-*d8*. As such, ^{1}H and ^{13}C spectra were obtained in dimethylsulfoxide-*d6* (DMSO-*d6*) at 115^{o}C. A figure showing coalescence in DMSO-*d6* could not be achieved, as **1A-D** do not become soluble until higher temperatures are reached. While the presence of multiple conformers makes NMR characterization of free ligand difficult, it becomes a valuable probe for reactivity with metals. Once ligated to a metal centre, the ligand adopts a near-planar conformation (N,N,N' plane), resulting in a simplified NMR spectrum, thus affording a quick probe to verify complex formation.[17]

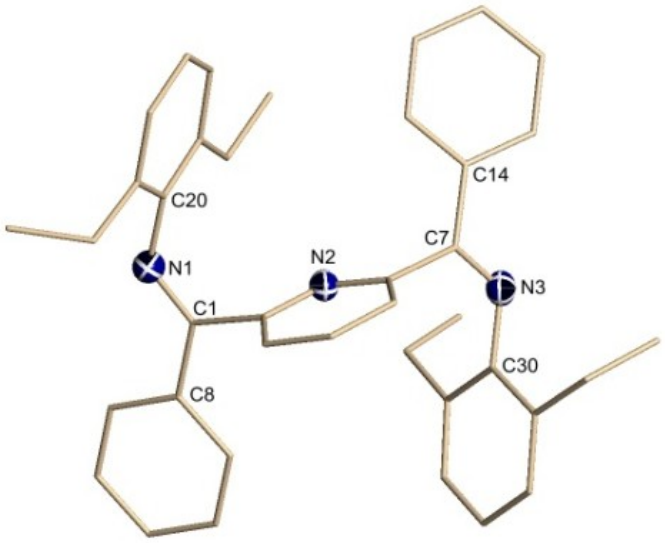

Figure 1.2: Structure of **1C** from single crystal X-ray data, see Table 1.2 for a list of select bonds and angles.

[17] Although infrequent, bis(imino)pyridines can ligate some metal centres to generate multiple conformers at room temperature. See Chapter 3 for examples of Ga(III) bis(imino)pyridines.

There was no concerted effort made to obtain crystallographic data for **1A-D**, nonetheless crystals suitable for X-ray crystallography were obtained for **1C** from a saturated solution of ether with hexanes as counter-solvent.[18] A list of relevant bond lengths and angles is provided in Table 1.2. As can be seen in Figure 1.2, **1C** adopts an asymmetric structure, with the diethyl-substituted aryl groups pointing away from each other to minimize repulsion. Figure 1.2 highlights just one of the many conformers **1A-D** can adopt in the solution state. Further crystallographic details are provided in section 1.6, Table 1.1.

[1.6] Experimental Details for Synthesis and Characterization of Ligands

General Methods. Reactions were performed using standard Schlenk technique under a flow of N_2, subsequent work-up was performed under lab atmosphere. All solvents were purchased from Fisher Scientific and used as received. Compound (**i**) was synthesized according to published procedure, all other chemicals were purchased from Aldrich and used without further purification. NMR spectra were run on a Bruker Avance 300 MHz spectrometer with deuterated dimethylsulfoxide as a solvent and internal standard. Elemental analyses for **1A, 1B, 1C** and **1D** were performed by Midwest Microlab LLC.

(1A) ***2,6-Bis{1-[(2,5-ditertbutylphenyl)imino]-benzyl}pyridine***: A 250mL round bottom flask was charged with 2,6-dibenzoylpyridine (1.0g 3.48mmol), 2,5-di-tert-butylaniline (1.5g, 7.31mmol), *p*-toluenesulfonic acid (0.1g) in toluene (150mL). A Dean Stark trap was attached to the flask and the reaction mixture was placed under nitrogen atmosphere and heated to reflux (160°C) for 48 h. The solution turned brown and a brown precipitate formed. The mixture was concentrated *in-vacuo*, resulting in a thick brown paste, which was subsequently dissolved in cold methanol with ice cubes, resulting in a yellow precipitate. The yellow product was collected

[18] Crystals are colourless needles, collected alongside targeteted Tl(I) bis(imino)pyridines. See Chapter 4.

by filtration and washed with a minimal amount of cold 9:1 hexanes:ether solution to remove aniline impurities. The filtrate was reduced again to a thick paste and the procedure was repeated several times. A bright yellow powder was isolated in 89% yield (2.055g). Elemental analysis calculated (%) for $C_{47}H_{55}N_3$: C, 85.28; H, 8.37; N, 6.35, found C, 84.68; H, 8.73; N, 6.12. E/I mass spectrometry shows M+ peak at 661 m/z. Room temperature ^{1}H NMR ($CDCl_3$, 300 MHz) and ^{13}C NMR ($CDCl_3$, 75 MHz) showed a multitude of peaks which could not be properly assigned due to constant rotation of bonds in the molecule. ^{1}H NMR at 115 ^{o}C (*d*-methyl sulfoxide, 300 MHz) collapses to 2 *tert*-butyl signals, the aromatic region is however very broad and cannot be accurately assigned: δ 8.20-6.90 (br m, 17 H, Ar-H), 6.21 (br s, 2H, Ar-H), 1.39(br s, 18H, ^tBu), 0.99(br s, 18H, ^tBu). ^{13}C NMR at 115 ^{o}C (*d*-methyl sulfoxide, 75 MHz) collapses to 4 peaks for *tert*-butyl signals, and 10 aromatic signals, with several others which could not be properly assigned due to broadening: δ 148.5 (Ar-CH), 147.9(Ar-CH), 138.7(Ar-CH), 129.1(Ar-CH), 128.4(Ar-CH), 128.3(Ar-CH), 126.1(Ar-CH), 120.8(Ar-CH), 118.8(Ar-CH), 131.6(Ar-CH), 99.9(Ar-CH), 35.0(Ar-^tBu, C-$(CH_3)_3$), 33.8 (Ar-^tBu, C-$(CH_3)_3$), 31.1(Ar-^tBu, CH_3), 30.5(Ar-^tBu, CH_3).

(1B) ***2,6-Bis{1-[(2,6-diisopropylphenyl)imino]-benzyl}pyridine:*** A 250mL round bottom flask was charged with 2,6-dibenzoylpyridine (1.0g 3.48mmol), 2,6-diisopropylaniline (1.4g, 11.94mmol), *p*-toluenesulfonic acid (0.1g) in toluene (150mL). A Dean Stark trap was attached to the flask and the reaction mixture was placed under nitrogen atmosphere and heated to reflux (160°C) for 48 h. The reaction mixture was cooled down and concentrated *in vacuo* to give a dark yellow oil. Cold methanol was added and mixed for several minutes, causing the product to precipitate as a yellow solid which was filtered off and rinsed with cold methanol. The filtrate was reduced to about half the initial volume under vacuum, and then placed in the fridge, causing

additional product to precipitate, which was filtered off and again rinsed with cold methanol. The product was obtained as a yellow powder with a yield of 49% (1.04g). MS (EI) *m/z* 605 (M^+). Room temperature ^{1}H NMR ($CDCl_3$, 300 MHz) and ^{13}C NMR ($CDCl_3$, 75 MHz) showed a multitude of peaks which could not be properly assigned due to constant rotation of bonds in the molecule. ^{1}H NMR at 115 ^{o}C (*d*-methyl sulfoxide, 300 MHz) collapses to 1 *iPr* signal, the aromatic region remains very broad and cannot be accurately assigned: δ 7.82(br t, 1 H, py, *p*-CH), 7.55-7.20 (br m, 12 H, Ar-H), 6.94 (br s, 6H, Ar-H), 2.90(m, 4H, ^{i}*Pr*), 1.00(d, 24H, ^{t}*Bu*). ^{13}C NMR at 115 ^{o}C (*d*-methyl sulfoxide, 75 MHz) collapses to 3 peaks for *iPr* signals, and 11 aromatic signals, with several others which could not be properly assigned due to broadening: δ 164.6 (C=N imine), 155.2(py, *o*-C=N), 146.2(Ar-CH), 136.8(Ar-*i*-C), 135.5(Ar-CH), 130.1(Ar-CH), 128.9(Ar-CH), 128.1(Ar-CH), 123.7(Ar-CH), 123.2(Ar-CH), 122.7(Ar-CH), 28.2(Ar-^{i}*Pr*, CH-(CH_3)$_2$), 22.9(Ar-^{i}*Pr*, CH_3), 22.3(Ar-^{i}*Pr*, CH_3).

(1C) ***2,6-Bis{1-[(2,6-diethylphenyl)imino]-benzyl}pyridine:*** A mixture of 2,6-dibenzoylpyridine (1.0 g, 3.48 mmol), a slight excess of 2,6-diethylaniline (1.143 g, 7.66 mmol), p-toluenesulfonic acid (0.1 g) in toluene (150 mL) was refluxed, using a Dean Stark Trap in a sand bath at 160°C for 48 hours. The work-up was performed under lab atmosphere conditions. The reaction mixture was cooled down and the solvent was removed under vacuum to give a dark yellow oil. Cold methanol was added, and the solution was held at -20^{o}C for 48 hours, over which point a multitude of large yellow rectangular crystals formed. The solvent was removed by filtration and the crystals washed with cold methanol and hexanes. The crystals were then crushed to a fine pale yellow powder, and held under vacuum for 72 hours to remove remaining methanol. A very fine pale yellow powder was collected in moderate 39% yield (750 mg), but in high purity: elemental analysis for $C_{39}H_{39}N_3$ Calculated: C, 85.21; H, 7.15; N, 7.64 Found: C,

85.13; H, 7.17; N, 7.63. Crystals suitable for X-ray crystallography were grown via saturated solution of ether with hexanes as counter-solvent and being held at -20^{o}C for several days. Room temperature ^{1}H NMR ($CDCl_3$, 300 MHz) and ^{13}C NMR ($CDCl_3$, 75 MHz) showed a multitude of peaks which could not be properly assigned due to constant rotation of bonds in the molecule. ^{1}H NMR (T = 115 ^{o}C, d_6-dimethyl sulfoxide, 300 MHz) δ 7.77(br t, 1 H, py, *p*-CH), 7.52-7.27 (br m, 12 H, Ar-H), 6.93 (br m, 6H, Ar-H), 2.37(br s, 8H, CH_2), 1.07(t, 12H, CH_3). ^{13}C NMR (T = 115 ^{o}C, d_6-dimethyl sulfoxide, 75 MHz) δ 164.9 (C=N imine), 155.0(py, *o*-C=N), 147.5(Ar-CH), 137.4(Ar-*i*-C), 136.8(Ar-CH), 131.0(Ar-CH), 130.3(Ar-*i*-C), 128.7(Ar-CH), 128.2(Ar-CH), 125.5(Ar-CH), 123.3(Ar-CH), 122.8(Ar-*i*-C), 24.4(-CH_2), 13.3(-CH_3).

(1D) ***2,6-Bis{1-[(2,6-dimethylphenyl)imino]-benzyl}pyridine:*** A mixture of 2,6-dibenzoylpyridine (2.0 g, 6.96 mmol), an excess of 2,6-dimethylaniline (3.0 g, 24.7 mmol), p-toluenesulfonic acid (0.1 g) in toluene (150 mL) was refluxed, using a Dean Stark Trap in a sand bath at 160°C for 48 hours. The work-up was performed under lab atmosphere conditions. The reaction mixture was cooled down and the solvent was removed under vacuum to give a dark yellow oil. Cold methanol was added, and the solution was held at -20^{o}C for 48 hours, over which point a bright yellow precipitate formed. The precipitate was filtered off, and washed with cold methanol and hexanes to afford a fine yellow powder. Solvent was removed under vacuum to afford a very fine yellow powder in 96% yield (3.34 g), but in high purity: elemental analysis for $C_{35}H_{31}N_3$ Calculated: C, 85.16; H, 6.33; N, 8.51 Found: C, 85.30; H, 6.47; N, 8.41. Room temperature ^{1}H NMR ($CDCl_3$, 300 MHz) and ^{13}C NMR ($CDCl_3$, 75 MHz) showed a multitude of peaks which could not be properly assigned due to constant rotation of bonds in the molecule. ^{1}H NMR (T = 115 ^{o}C, d_6-dimethyl sulfoxide, 300 MHz) δ 8.20-7.65(br m, 3 H, py, CH), 7.39 (v br s, 10 H, Ar-H), 6.89 (br m, 6H, Ar-H), 1.99(m, 12H, CH_3).^{13}C NMR (T = 115 ^{o}C, d_6-dimethyl

sulfoxide, 75 MHz) δ 165.7 (C=N imine), 155.2(py, *o*-C=N), 148.6(Ar-CH), 137.5(Ar-*i*-C), 136.9(Ar-CH), 130.3(Ar-*i*-C), 128.5(Ar-CH), 128.2(Ar-CH), 127.6(Ar-CH), 125.3(Ar-CH), 122.9(Ar-CH), 122.7(Ar-*i*-C), 18.1(-CH_3).

[1.7] X-ray Crystallographic Information: Ligand

Table 1.1: Summary of Data Collection and Crystallographic Parameters for **1C.***

Empirical formula	$[C_{39}H_{39}N_3]$
Formula weight	549.73
Temperature (K)	200(2)
λ (Å)	0.71073
Crystal system	Orthorhombic
Space group	Pbca
a (Å)	13.3319(6)
b (Å)	19.5052(10)
c (Å)	23.9734(12)
α (deg)	90.00
β (deg)	90.00
γ (deg)	90.00
V (Å ^{3})	6234.1(5)
Z	8
ρ (calc) (Mg/m^3)	1.171
μ (mm^{-1})	0.068
Absorption correction	Semi-empirical from equivalents
Final R indices [I>2σ(I)]	
R1[a]	0.0497
*w*R2[b]	0.1023

[a] $R1 = \Sigma \left| |F_o| - |F_c| \right| / \Sigma |F_o|$. [b] $wR2 = \left(\Sigma w \left(|F_o| - |F_c| \right)^2 / \Sigma w |F_o|^2 \right)^{1/2}$

*structure files available from CCDC

Table 1.2: Select bond lengths and angles for **1C**.

Select bond lengths (Å)		**Select bond angles (°)**	
N1-C1	1.277(2)	N1-C1-C2	122.85(18)
N1-C20	1.425(3)	N1-C1-C8	120.12(19)
N3-C7	1.279(2)	N3-C7-C6	122.31(18)
N3-C30	1.420(3)	N3-C7-C14	119.46(19)
N2-C2	1.341(2)	C1-C2-N2	114.78(17)
N2-C6	1.345(2)	C2-N2-C6	117.15(17)
C1-C8	1.482(3)	C7-C6-N2	114.55(18)
C7-C14	1.478(3)	C20-N1-C1	119.84(18)
		C30-N3-C7	121.75(18)

[1.8] Prelude to the Remainder of the Thesis

The remainder of the thesis can be broken down into two parts: First, our attempts at synthesizing and subsequently characterizing novel group 13 and 14 (In^{I}, Ga^{III}, Tl^{I}, and Sn^{II}) complexes bearing the bis(imino)pyridine ligand framework. Second, an extension of our work to transition metal analogues of the group 13 metals: Ag^{I} because of its similar size/charge characteristics to In^{I}, and Tl^{I}, and Re^{I} as it fits the theme of low valent oxidation states. The general breakdown is presented below.

Chapter 2: Synthesis of a series of In^{I} bis(imino)pyridine complexes with varied sterics. Ligand-metal interaction and effect of ligand steric bulk on complex stability will be discussed.

Chapter 3: Synthesis of Ga^{III} bis(imino)pyridine complexes and ligand radical species. Reactivity with "GaI" synthon as well as varied-stoichiometry one-pot synthesis attempts to generate low valent Ga-bis(imino)pyridine complexes will be discussed.

Chapter 4: Synthesis of a series of Tl^{I} bis(imino)pyridine complexes with varied sterics. Ligand-Metal interactions, as well as Tl-arene interactions will be discussed.

Chapter 5: Synthesis of a series of Sn^{II} bis(imino)pyridine complexes with varied sterics and halide substituents. Preferential cation-anion pair formation and reactivity will be discussed.

Chapter 6: Synthesis of a series of Ag^{I} bis(imino)pyridine complexes with varied sterics. Ligand-metal interactions will be discussed and analogy to main group congeners, as well as reactivity towards Lewis basic donor ligands (unsaturated C-C and C-N bonds as well as pyridine N-lone pair donors) will be discussed.

Chapter 7: Synthesis of Re^{I} bis(imino)pyridine complexes utilizing both solution and solid-state techniques. Refining reaction conditions towards formation of previously difficult to access Re^{I} pincer type complex and attempted reactivity will be discussed.

Chapter 8: A general conclusion of our findings will be provided.

Chapter 2: *Indium(I) and Indium(III), Weak Covalent Interactions*

[2.1] In(I) Coordination Compounds

Barring thallium(I), indium(I) has the next most stable low valent oxidation state of the group 13 elements, which all prefer the M(III) state. As such, it is no surprise that the chemistry of In(I) is thus comparatively rich. The stability/reactivity characteristics of In(I) are intrinsically related to its valence electron distribution; high energy $5s^2$ electrons which remain primarily localized on the indium centre. Owing to the localized $5s^2$ electron pair, In(I) can be regarded as a Lewis base, unlike the smaller M(III) group 13 elements (B(III), Al(III), Ga(III) and In(III)), which are classically known as strongly Lewis acidic. However, the high energy $5s^2$ electron pair also makes the indium centre prone to oxidation, or in the absence of oxidizing agents, disproportionation to indium metal and In(III) or In-In bonded In(II) species.[19]

The nature of In(I) presents inherent difficulties in synthesizing discrete In(I) monomeric molecular compounds. The requirements for which are a non-oxidizing substituent (X) on the In(I)-X starting material, and the use of sterically encumbered ligands (L). In the absence of sufficient steric bulk, L-In-X aggregates to form dimeric, trimeric, or larger multi-centre cluster like complexes.[20] Although there is a wealth of complexes in which indium is retained in the +1 valence state, the body of monomeric molecular In(I) compounds is quite small. In an extensive 2007 review by Pardoe *et al*, there are only 14 such examples reported.[19] Their common structural feature is the use of sterically demanding support ligands of the *o*-terphenyl, *β*-

[19] J.A.J. Pardoe, A.J. Downs, *Chem. Rev.* **2007**, 107, 2.
[20] (a) M.S. Hill, P.B. Hitchcock, R. Pongtavornpinyo, R. *Angew. Chem., Int. Ed.* **2005**, 44, 4231. (b) Organoindium Compounds 1; *Gmelin Handbook of Inorganic and Organometallic Chemistry,* 8th ed.; Springer-Verlag: Berlin and Heidelberg, Germany, 1991, pp 372-385. (c) W. Uhl, R. Graupner, M. Layh, U. Schultz, *J. Organomet. Chem.* **1995**, 493, C1.

diketiminato, tris(pyrazolyl)borate, and phosphacyclopentadienyl class.[21] The common synthetic route to these monomeric molecular indium(I) compounds, as well as their related oligomeric derivatives, is via metathesis of an indium(I) halide starting material with an alkali-metal derivative of the target ligand (typically a Li-Ligand complex).[19, 22]

The most notable early work in monomeric molecular indium(I) compounds is that from the Powers group. Utilizing the sterically demanding *o*-terphenyl ligand system, well separated In(I) monomers bearing a unique mono-coordinate L-M interaction were achieved (Scheme 2.1 i).[21a] As a testament to the importance of ligand steric bulk, one need only look at later work from the Power group; a near identical *o*-terphenyl ligand system with aryl *p*-substituted isopropyl groups removed is no longer able to stabilize the In(I) monomeric compound, leading to the formation of an In-In dimer (Scheme 2.1 ii). The resulting In-In bond is quite weak, and in the presence of bulky Lewis acid $B(C_6F_5)_3$, is broken to yield the LIn- $B(C_6F_5)_3$ adduct pair, further evidencing the Lewis basic nature of In(I) (Scheme 2.1 iii). [21b]

Scheme 2.1

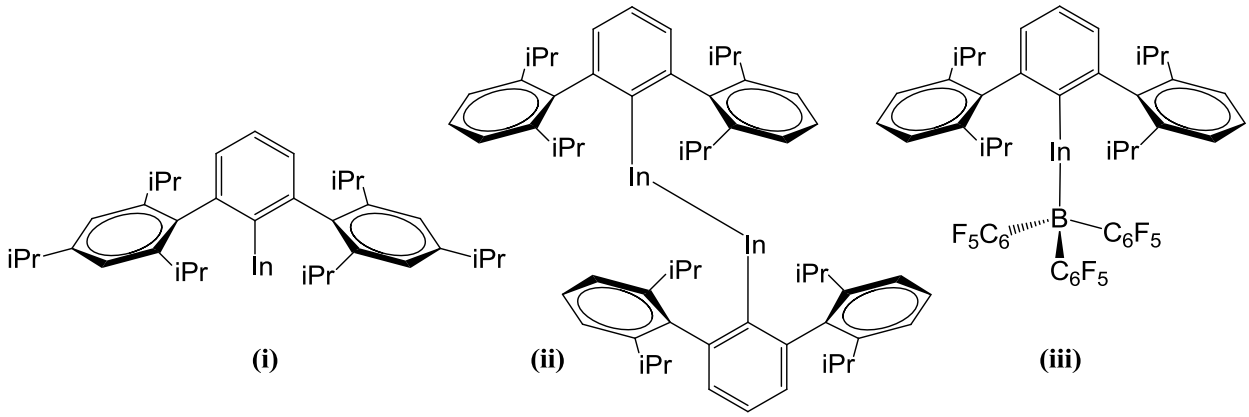

(i) **(ii)** **(iii)**

[21] (a)S.T. Haubrich, P.P. Power, *J. Am. Chem. Soc.* **1998**, 120, 2202, (b) R.J. Wright, A.D. Phillips, N.J. Hardman, P.P. Power, *J. Am. Chem. Soc.* **2002**, 124, 8538 (c) G.K.B. Clentsmith, F.G.N. Cloke, M.D. Francis, J.C. Green, P.B. Hitchcock, J.F. Nixon, J.L. Suter, D.M. Vickers, *Dalton Trans*. **2000**, 1715. (d) A. Frazer, B. Piggott, M.B. Hursthouse, M. Mazid, *J. Am. Chem. Soc.* **1994**, *116*, 4127.

[22] An exception being the phosphoacylcyclopentadienyl compounds which were accessed via co-condensation of In metal vapour with *t*BuC=P at 77K, see ref. 21c.

[2.2] In(I)Triflate Synthon

The common synthetic access point to low valent indium chemistry has traditionally been indium(I) halides or InCp* (Cp*=C_5Me_5). These synthons, however, have inherent drawbacks for use in solution state inorganic synthesis, with the biggest hindrance being very high insolubility, making reactions where there isn't a strong driving force, such as metathesis, more difficult. Paired with their tendency towards oxidation or disproportionation once in the solution state, and instability with increasing temperatures, most traditional In(I) synthons are difficult to work with. In that regard, a breakthrough discovery in In(I) synthons was reported by Macdonald *et al.* in 2004: the development of indium(I)-triflate (InOTf, OTf = CF_3SO_3) as an inert atmosphere and room temperature stable In(I) access point that is highly soluble in a range of organic solvents.[23]

Scheme 2.2

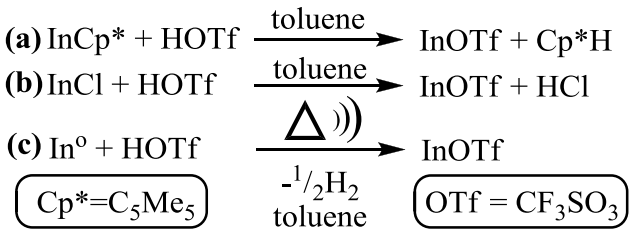

Synthesis of InOTf is achieved through several facile routes (Scheme 2.2). Protonolysis of InCp* via HOTf in a solution of toluene yields InOTf and Cp*H (Scheme 2.2 a). Alternatively, addition of HOTf to a toluene suspension of InCl, a relatively inexpensive commercially available compound, followed by removal of volatiles and pentane wash yields InOTf and HCl by-product (Scheme 2.2 b). Both methods afford high yields (> 80%), which are reportedly only diminished by mechanical loss.[23] Although the use of InCl is convenient, it was found by both the Macdonald group and by experimental observation in our own group that

[23] C.L.B. Macdonald, A.M. Corrente, C.G. Andrews, A. Taylor, B.D. Ellis, *Chem. Commun.* **2004**, 250.

InOTf prepared in this manner contains chloride ion contaminants. In the right chemical environment, the presence of these chloride ions can initiate a reaction process leading to the formation of undesired In(III) complexes (*vide infra*). An alternative synthetic approach to InOTf was reported by the Macdonald group which circumvents the use of InCl, thereby eliminating unwanted chloride based side reactions. Sonication of indium metal in the presence of triflic acid in a solution of toluene at 40°C affords InOTf in 92% yield with only H_2 as by-product (Scheme 2.2 c).[24]

InOTf was successfully used by the Macdonald group to synthesize an In(I)-[18]crown-6 complex (Scheme 2.3). At that time, this was the only intact monomeric In(I) complex behaving as a Lewis acid (receives electron donation from crown ether O-atoms), whereas all previous attempts to ligate bases to In(I) salts resulted in disproportionation.[25] The reported ligation of a neutral Lewis basic ligand to an In(I) metal centre has direct implications to the potential ligation of bis(imino)pyridines to form indium(I)bis(imino)pyridine compounds. As such, our efforts were focused on the InOTf synthon; we utilized the InCl precursor method (Scheme 2.2 b), as at the time, the preferable chloride free sonication method (Scheme 2.2 c) was not yet reported.

Scheme 2.3

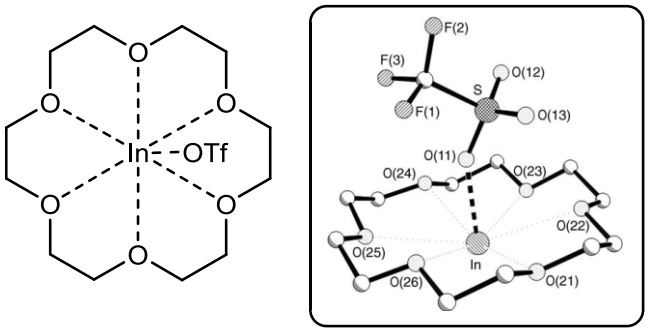

[24] B.F.T. Cooper, C.L.B. Macdonald, *New J. Chem*., **2010**, 34, 1551.
[25] C.G. Andrews, C.L.B. Macdonald, *Angew. Chem., Int. Ed.* **2005**, 44, 7453.

[2.3] Results and Discussion: Ligation of Bis(imino)pyridines to InOTf and $InCl_3$

The first low-valent, main group metal complex of the bis(imino)pyridine ligand class was prepared when the soluble and readily accessible In(I) synthon, $In(O_3SCF_3)$, was allowed to react with ligand **1A** (Scheme 2.4) to provide an excellent isolated yield (76%) of the bright orange compound **2.1**. The bulky steric environment provided by the 2,5-$^{t}Bu_2C_6H_3$ substituents of the imine function in **1A** were a key feature of the observed species. The identity of this species as the bis(imino)pyridine complex $[\{2,5\text{-}^{t}Bu_2C_6H_3N{=}CPh\}_2(NC_5H_3)]In^{+}(OTf)^{-}$ **2.1** was established by single crystal X-ray analysis and the results for the cationic component summarized in Figure 2.1 and Tables 2.2, 2.3 and 2.4.[11]

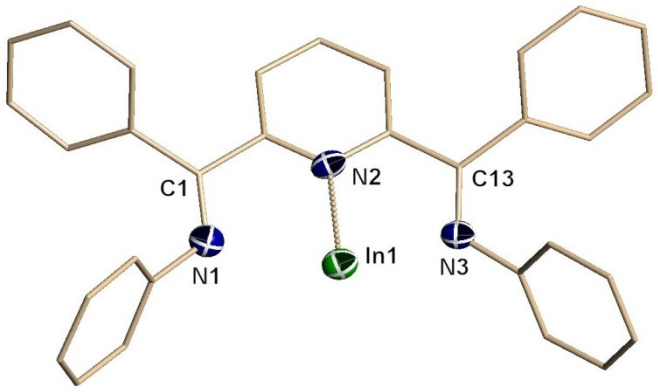

Figure 2.1. X-ray structure of the $[\{2,5\text{-}^{t}Bu_2C_6H_3N{=}C(Me)\}_2(NC_5H_3)]In^{+}$ cation of compound **2.1.** Hydrogen atoms, ^{t}Bu groups and triflate counter-ion have been omitted for clarity. Selected bond lengths and angles are given in Tables 2.3 and 2.4.

Compound **2.1** is monomeric with a long In-N2 bond distance of 2.495(5)Å.[26] The most direct comparisons to **2.1** can be made with In(I) complexes of anionic ligands. For example, the In-N bond distance in the two coordinate β-diketiminate complex $[In\{(NDippCMe)_2CH\}]$ is

[26] This distance is similar to that in the metastable complex InBr·TMEDA. S.P., Green, C. Jones, A. Stasch, *Chem. Commun.* **2008**, 6285.

2.27Å.[27] Furthermore, for the three coordinate tris(3,5-di-*tert*-butylpyrazolyl)hydroborato In(I) these distances averaged *ca.* 2.47Å[28] and for the four coordinate amidinato species [DippNC(tBu)NDipp]In(I) an In–N distance of 2.329(5)Å was observed.[29] The In centre in **2.1** lies slightly out of the pyridine plane (11.5°). The In-N_{imine} distances, In-N1 2.748(6)Å and In-N3 2.689(6)Å, are well beyond the sum of van der Waals radii for In and N. Furthermore, the long In-O(triflate) distance (In-O2 7.975Å) was consistent with no or very little coordination of the anion.[23,25] The shortest In/triflate contact observed for **2.1** is to an F atom of the CF_3 group at a distance of 6.485Å. Within **2.1**, the imine C=N distances (N1-C1 1.281(9)Å, N3-C13 1.283(9)Å) are comparable to those for the free ligand and the carbon centers of the imine moieties are planar. The SO bonds within the triflate anion are essentially equivalent and range from 1.406(7)Å to 1.425(6)Å with an average value of 1.417Å, a value which is consistent with a non-coordinated anion. All of these structural features point to the fact that **2.1** displayed a very weakly coordinated In centre in spite of the presence of additional sites for coordination. Interestingly, the structural features for the singly coordinated cation **2.1** are reminiscent of the In(*o*-terphenyl) monomer 2,6-$(Tripp)_2C_6H_3In$ (Scheme 2.1, i).[21a]

Scheme 2.4

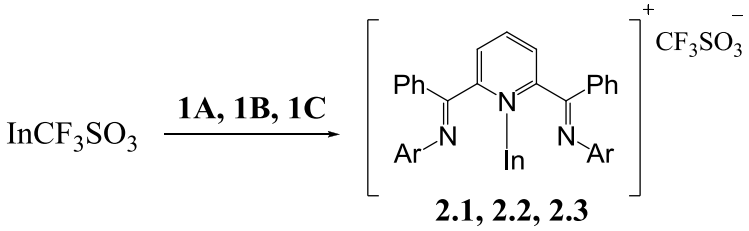

2.1, 2.2, 2.3

2.1: Ar = 2,5^t*Bu*(C_6H_3) **2.2**: Ar = 2,6^i*Pr*(C_6H_3) **2.3**: Ar = 2,6CH_2CH_3(C_6H_3)

[27] M.S. Hill, P.B. Hitchcock, *Chem Commun*. **2004**, 1818.
[28] M.C. Kuchta, H.V.R. Dias, S.G. Bott, G. Parkin, *Inorg. Chem.* **1996**, 35, 943.
[29] C. Jones, P.C. Junk, J.A. Platts, D.Rathmann, A. Stasch, *Dalton Trans*. **2005**, 2497.

To ascertain the effects of ligand steric bulk (around the In(I) bonding pocket) on L-In(I) interaction and potentially isolate further examples of weakly bound In(I) complexes, we turned to ligands **1B** and **1C**. While ligand **1A** bears 2,5-^{t}Bu(C_6H_3) groups on the imine nitrogens, **1B** and **1C** represent a systematic reduction of steric load via subsequent exclusion of CH_3 groups (2,6-^{i}Pr(C_6H_3) and 2,6-Et(C_6H_3) respectively). Like **1A**, ligands **1B** and **1C** also react smoothly with In(OSO_2CF_3), to provide orange compounds **2.2** and **2.3** in isolated yields of 63% and 39%, respectively (Scheme 2.4). A clear indication of the steric demands of these two ligand systems was reflected in the NMR spectra of **2** and **3**. Specifically, the appearance of diastereotopic Me groups for **2.2** and diastereotopic CH_2 groups for **2.3** was consistent with hindered rotation of the N_{imine}-Ar′ bonds in these compounds. Complex **2.2** displayed two broad, equal intensity doublets for the ^{i}Pr methyl groups and the uniqueness of these groups was confirmed by the appearance of two singlets for these methyl groups in the ^{13}C NMR spectrum of **2.2**. Attempts to carry out NMR measurements for the ethyl compound **2.3** in $CDCl_3$ resulted in decomposition and subsequent acquisition of complicated multi-component spectra. These observations have been attributed to traces of HCl in the $CDCl_3$, which resulted in conversion of **2.3** to an In^{3+} species.[30]

The detailed structural features of **2.2** and **2.3** were established by single crystal X-ray analysis studies, which confirmed these species as the bis(imino)pyridine complexes [{2,6-$R_2C_6H_3N$=CPh}$_2$(NC_5H_3)]$In^{+}(OTf)^{-}$ (R = iPr, **2.2**; Et, **2.3**). Pictorial representations for the structures of **2.2** and **2.3** are presented in Figures 2.2 and 2.3 with a summary of bonding parameters presented in Tables 2.2, 2.3 and 2.4. The general structural features for the cations in compounds **2.2** and **2.3** are evocative of those observed for **2.1**. In particular the In-N_{py} distances (**2.2** In1-N2 2.502(5)Å, **2.3** In1-N2 2.501(8)Å) are the same as was observed in **2.1**.

[30] T. Jurca, I. Korobkov, G.P.A. Yap, S.I. Gorelsky, D. S. Richeson, *Inorg. Chem.* **2010**, 49, 22, 10635.

Furthermore, the In-N_{imine} distances for **2.2** (In1-N1 2.664Å, In1-N3 2.679Å) and **2.3** (In1-N1 2.731Å, In1-N3 2.636Å) are greater than the sum of the van der Waals radii for these two elements. Again, like compound **2.1**, the imine C=N distances within **2.2** and **2.3** are comparable to those for the free ligand.

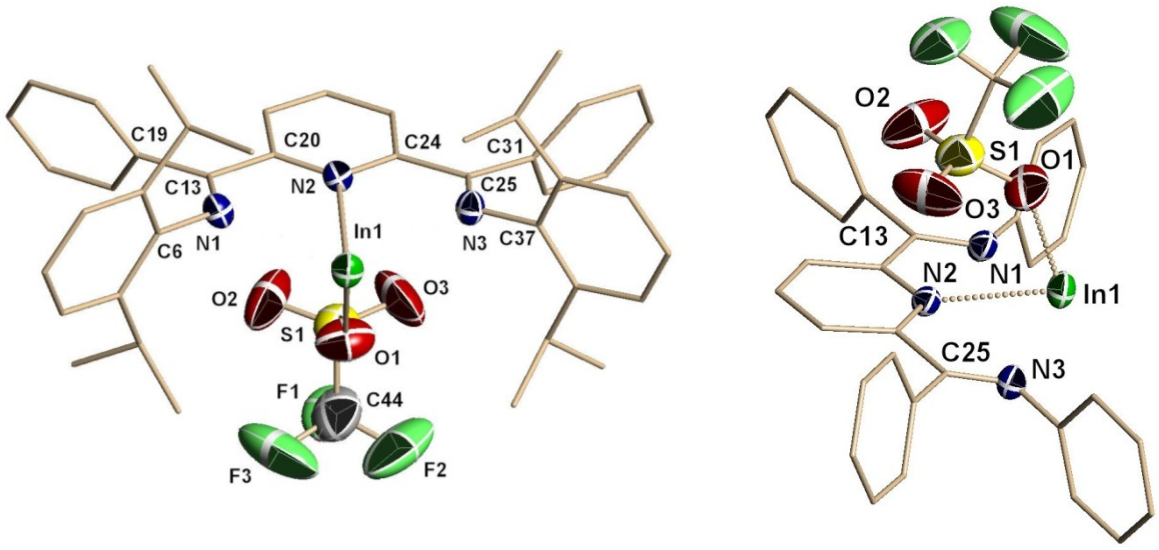

A **B**

Figure 2.2. X-ray structure (A: top view, B: side view) of compound **2.2**, with hydrogen atoms (A and B) and ^{i}Pr groups (B) omitted for clarity. Selected bond lengths and angles are given in Tables 2.3 and 2.4.

The reduction of the size of the aryl substituents in **2.2** and **2.3**, compared to **2.1**, allowed for a closer approach of the OTf⁻ anions to the In centres. For compound **2.2** the shortest In-O (In1-O1) distance was 2.462(6)Å while for compound **2.3** a slightly longer distance for In1-O1 of 2.532(7) Å was obtained. For comparison, these distances are shorter than those reported for In(OTf) (In–O 2.579(6)Å and 2.589(6)Å)[23] but considerably longer than in InOTF[18]crown-6 where the In-O distance was 2.370(2)Å.[25] The orientation of the triflate anions in compounds **2.2** and **2.3** suggests an alignment of the negative charge density of the triflate O and F centres with δ+ charges on the imino-carbon ligand sites (i.e. **2.2** C13, C25; **2.3** C7, C13). The specific

differences in triflate anion orientation for **2.2** and **2.3**, as shown in Figures 2.2 and 2.3, is likely an indication for a low energy barrier to reorganization of the anion.

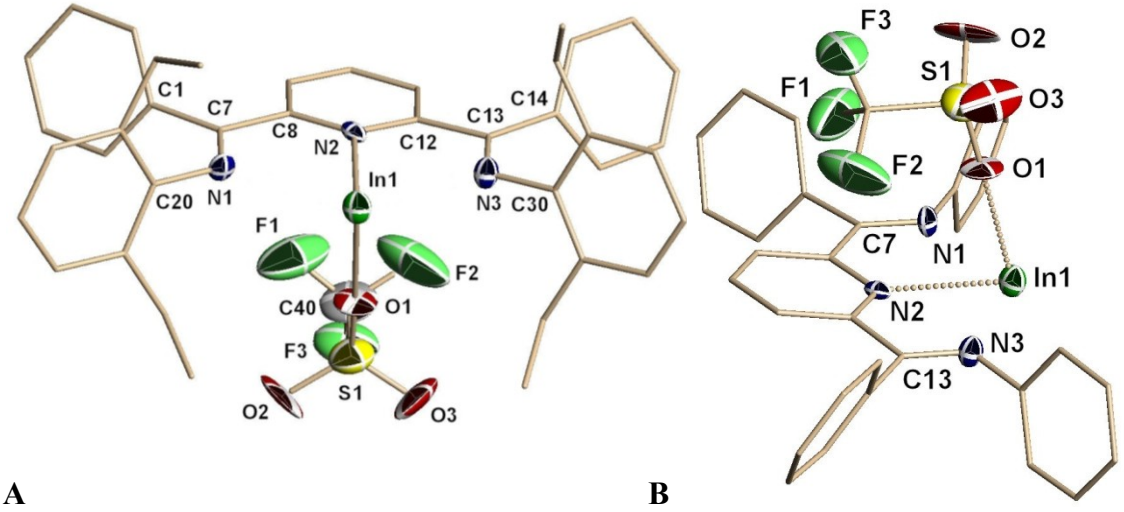

Figure 2.3. X-ray structure (A: top view, B: side view) of compound **2.3**, with hydrogen atoms (A and B) and ethyl groups (B) omitted for clarity. Selected bond lengths and angles are given in Tables 2.3 and 2.4.

In striking contrast to the syntheses of the In (I) compounds **2.1-2.3**, ligand **1D** reacted with $In(O_3SCF_3)$, to generate a red reaction mixture (Scheme 2.5). From this mixture was isolated an In(III) bis(imino)pyridine complex, $[\{2,6\text{-}Me_2C_6H_3N{=}CPh\}_2(NC_5H_3)]In(OTf)_2Cl$ **2.4**, possessing two OTf^- ($^-O_3SCF_3$) anions and one chloride ion (Figure 2.4). Large yellow block-like crystals were isolated and subjected to elemental analysis confirming homogeneity of the crystallized product. When these reactions were repeated using different precursor batches they consistently yielded product **2.4**. We attribute the appearance of the chloride ligand in compound **2.4** to a slight impurity arising from the synthesis of InOTf. Compound **2.4** displayed distorted octahedral coordination geometry for In (III) with the coordination sphere consisting of a planar, tridentate bis(imino)pyridine ligand $\{2,6\text{-}Me_2C_6H_3N{=}CPh\}_2(NC_5H_3)$ with the remaining three

coordination sites occupied by two, *trans*-oriented triflate anions and a chloride anion.. The In1-O1 distance of 2.269(3)Å and the observed S-O bond distances of the triflate anion (S1-O1 1.476Å, S1-O2 1.424Å, S1-O3 1.431Å) are consistent with coordination of O1.[23,31]

Scheme 2.5

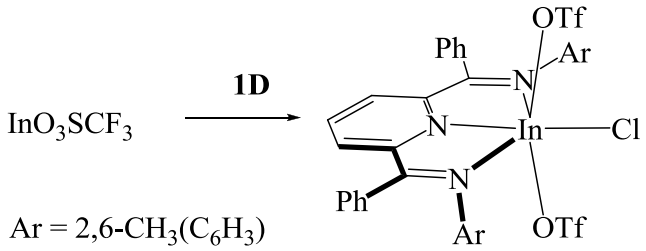

2.4

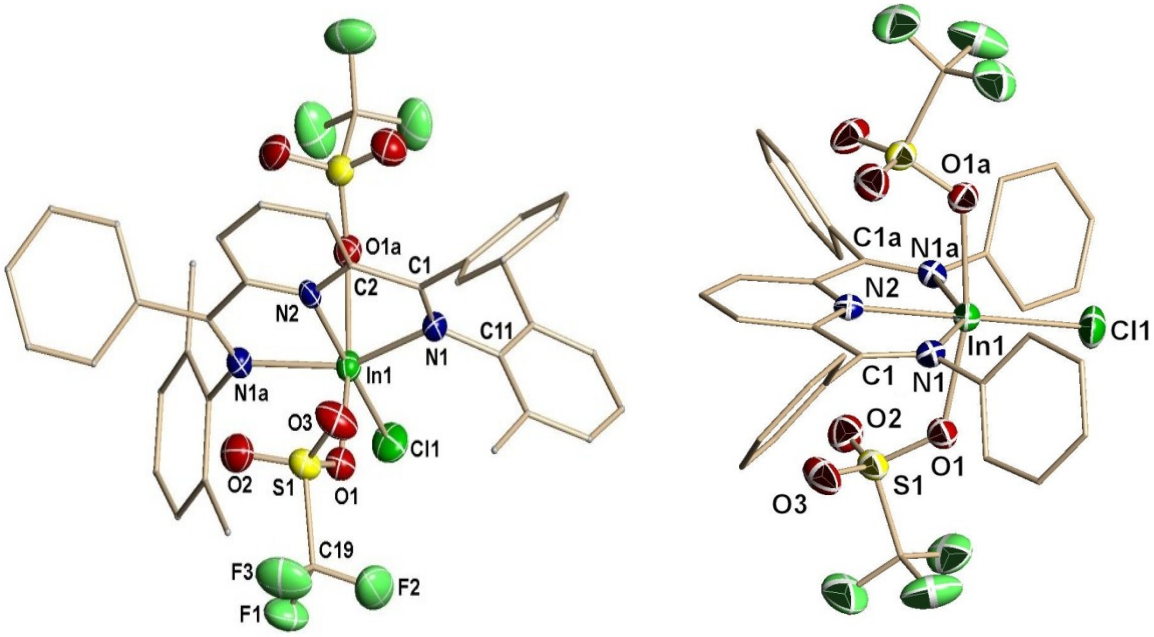

A **B**

Figure 2.4. X-ray structure of compound **2.4**, with hydrogen atoms (A and B) and methyl groups (B) omitted for clarity. Selected bond lengths and angles are given in Table 2.5.

[31]C.G. Andrews, C.L.B. Macdonald, *J. Organomet. Chem*. **2005**, *690*, 5090.

To establish a comparison to a specifically targeted In(III) complex, we sought to react ligand **1A** with commercially available $InCl_3$, The combination of **1A** with $InCl_3$ in a 1:2 stoichiometric ratio resulted in red-orange solution and yielded the bright yellow powder **2.5** in 73% yield (Scheme 2.6). Coordination of the ligand in a symmetrical fashion was clearly indicated by the appearance of a simplified ^{1}H NMR spectrum of the ^{t}Bu substituents that now appeared as two singlets of appropriate integration. Single crystal X-ray analysis for this unique In complex revealed a well-separated cation/anion pair with the cationic portion of compound **2.5**, [{2,4-^{t}BuC$_6$H$_3$N=C(Me)}$_2$(NC$_5$H$_3$)]InCl$_2^+$, shown in Figure 2.5. The geometry of the indium centre within this constituent is distorted trigonal bipyramidal with the three-fold plane (Σ angles = 359.9°) defined by the N2 with Cl1 and Cl2 centres. The limitations of ligand geometry led to a pseudoaxial N1-In-N3 angle of only 142.6(6)°. The two five-membered rings resulting from the coordination of the pyridyl and imine moieties display a sum of internal angles of 539 and 539.5, values that are ideal for planar rings. Overall, structural features of **2.5** are comparable with the metrical parameters of compound **2.4**. Average In-N distances of 2.27 Å and In-Cl distances of 2.33 Å are observed for **2.5**, compared with 2.21 Å and 2.31 Å respectively for **2.4**.

Scheme 2.6

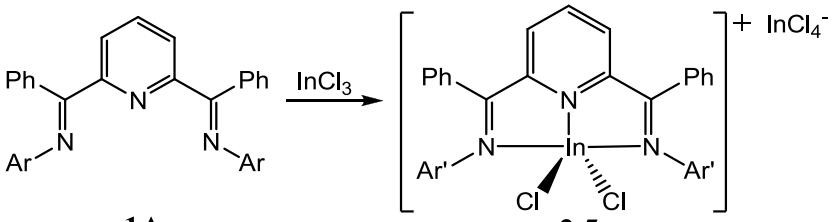

1A **2.5**

Ar=2,5-^{t}BuC$_6$H$_3$

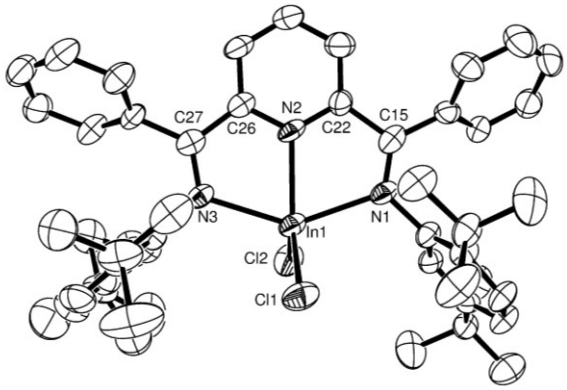

Figure 2.5. X-ray structure of the $[\{2,5\text{-}^{t}BuC_6H_3N{=}C(Me)\}_2(NC_5H_3)]InCl_2^+$, cation of compound **2.5** with hydrogen atoms and the $InCl_4^-$ counter-ion omitted for clarity. Selected bond lengths and angles are given in Table 2.5.

[2.4] Indium Complexes: Computational Evaluation

With the collaborative efforts of Dr. Serge I. Gorelsky, a DFT computational study with the B3LYP functional and the mixed DZVP/TZVP basis set was undertaken to obtain a thorough understanding of the electronic nature of the indium[bis(imino)pyridine]$^+$ cations and the interactions of the cation with the OTf$^-$ anion in compounds **2.1-2.3**. Optimizations for compounds **2.1-2.3** gave structures that were in agreement with the experimental structures. In the case of compound **2.1**, the natural population analysis (NPA) for the valence configuration of the In(I) center was $5s^{1.93}$ $5p^{0.20}$ and the NPA-derived charge of the In atom was +0.86 a.u.. These results indicated that much of the cationic charge remains on the In ion, with only 0.14e are transferred from the ligand to In^+ in the complex. Analysis for the cation component of **2.2**

gave very similar results with a charge on the indium centre of +0.83 a.u., with only 0.17e transferred from the ligand in this case.[32]

These results were convincingly supported by the bond order analysis. In the case of the cation of **2.1**, Mayer bond order values for In-N1/In-N3 and In-N2 interactions are only 0.23 and 0.28, respectively. Similarly, for the cation in **2.2**, the In-N_{imine} (In-N1/In-N3) interactions corresponded to a bond order of 0.19 while an In-N2 bond order of 0.22 was obtained. These values are all substantially lower than the expected indices of 1.00 for single bonds. The Wiberg bond indices calculated in the natural atomic orbital basis are only 0.07-0.10, also consistent with very weak In-ligand interactions. These observations are also in harmony with the extremely long In-N distances in these species. Ultimately, analysis of the electronic structures of the cations point toward only nominal covalent interactions of the In cation with the ligand.

While the triflate anion of **2.1** was well beyond bonding distance, the shortest OTf$^-$ contact in **2.2** was at an In-O distance of 2.462(6)Å. A careful examination of the cation/anion pair alignment observed in both the crystallographic (Fig. 2.2) and computational structures of **2.2** suggests a significant electrostatic component to the interaction energy for the ion pair. Specifically, the negatively charged oxygen atoms of triflate (the average NPA charge of O is -0.94 a.u.) are positioned over the sites of positive charge localization of the cation: In, C_{imine} (C13, C25 = +0.30 a.u.) and C_{py} (C20, C24 = +0.17 a.u.). The results of energy decomposition analysis support that the major component of the interaction energy between the two ions (E_{int}= -82.9 kcal mol^{-1}) is, in fact, electrostatic with only approximately 40% of the cation/anion energy due to orbital interactions (E_{orb}=-32.7 kcal mol^{-1}).

[32] For comparison, the NPA-derived charge of the Ge(II) centre in the complex (Ge·cryptand[2.2.2])$^{2+}$(O_3SCF_3)$^-_2$, which displayed minimal coordination between the cryptand ligand and Ge, was +1.38 a.u. and corresponded to 0.62 electrons being donated to the Ge(II) ion: P.A. Rupar, V.N. Staroverov, K.M. Baines, *Science* **2008** *322* 1360.

The orbital contributions to the interaction energy were explored in more detail by examining the specifics of the electron transfer from the triflate anion to the indium[bis(imino)pyridine]$^+$ cation through a fragment orbital population analysis. Only 0.21 electrons are transferred from the anion to the cation and, of these, only 0.10 electrons are transferred to a cation fragment orbital that has a significantly In-based component. This lowest unoccupied fragment orbital (LUFO+2) is 85% In 5*p* in nature. This analysis provided further validation that the indium centre in the cation receives only minor electron donation from the OTf$^-$ anion with the bulk of electron donation actually going to the ligand component of the In[bis(imino)pyridine]$^+$ cation. The donation from the triflate to indium corresponds to an In-OTf bond order of only 0.17. Furthermore, an optimization for the indium[bis(imino)pyridine]$^+$ cation in **2.2** was also carried out in the absence of the OTf$^-$ anion. The computed structure for this cation yielded In-N distances that are in agreement with the experimental In-N distances in **2.2** (In-N_{py}:2.57Å vs. 2.502(5)Å exp and In-N_{imine}: 2.63Å vs 2.66Å exp). These results also point to electrostatic rather than orbital interaction for the association of the anion with the cation in **2.2**.

In an attempt to evaluate the role of both ligand sterics and of the counterion in our computational analysis of the cation, a DFT optimization of the model cation [{C_6H_5N=CPh}$_2$(NC_5H_3)]In$^+$, with unsubstituted phenyl groups, was performed. Under these model conditions, the computed values for the In-N_{py} (2.52Å) and the In-N_{imine} (2.63Å) distances are essentially identical to the crystallographic values obtained for **2.1-2.3**. Significantly, this model system analysis again displayed only nominal bonding between the bis(imino)pyridine ligand and the In$^+$ centre with bond orders for the In-N_{py} of 0.27 and for In-N_{imine} of 0.24.

For the more simplified model compound {In[bis(imino)pyridine]$^+$ cation} with Ar = H, the bonding between the In$^+$ cation and the ligand was analyzed more intimately using a

molecular orbital interaction diagram (Figure 2.6). Three occupied fragment orbitals (HOFO, HOFO-1 and HOFO-3) of the ligand participate in the charge donation to the two sigma-type 5*p* orbitals (p_x and p_z) of the In^+ cation. The In p_y orbital is non-bonding with the ligand π-framework. There is no back donation from the metal into the extended π-system since In 5*s* → L π*, is symmetry forbidden (zero overlap, see Figure 2.6). Only the ligand HOFO-3 mixes with the occupied In 5*s* orbital. For the In[bis(imino)pyridine]$^+$ cations, the lone pair of electrons on In^+ is localized in the 5*s* orbital and the raising of the energy of these electrons is a dominant feature in a de-stabilizing effect on the metal-ligand bonding (Figure 2.6). For the In[bis(imino)pyridine]$^+$ cation with Ar= H, the HOMO of the cation has 74% contribution from In-localized orbitals (Figure 2.6, Table 2.1). Elaboration of the N_{imine}-Ar groups of the In[bis(imino)pyridine]$^+$ cations (Ar = Ph, 2,6-^{i}Pr$_2$C$_6$H$_3$, 2,5-^{t}Bu$_2$C$_6$H$_3$) significantly reduced the contribution from In-localized orbitals and, most importantly, of the lone electron pair in In 5*s* to the HOMO of the cation as summarized in Table 2.1. The resulting reactivity of the In(I) lone pair of electrons is diminished and it is proposed that this effect plays a critical role in leading to the stable complexes **2.1-2.3.**

The decrease in In 5*s* contribution to the HOMO arises primarily from two effects. The first is due to the fact that changing Ar from H to substituted phenyl groups increases the number of occupied electronic levels of the ligand which can mix with the 5*s* orbital and this distributes the In orbital over a larger number of In[bis(imino)pyridine]$^+$ orbitals. The second contribution arises from the fact that as the ligand changes from Ar= H to ligands **1A-1C**, the energy of the occupied orbital of the bis(imino)pyridine fragment that overlaps with the In 5*s* (i.e. the analogue of the HOFO-3 in Figure 2.6) rises in energy. As a result, the mixing between In 5*s* and this

ligand orbital leads to the HOMO that has a lower In character and higher contribution of ligand occupied orbitals.

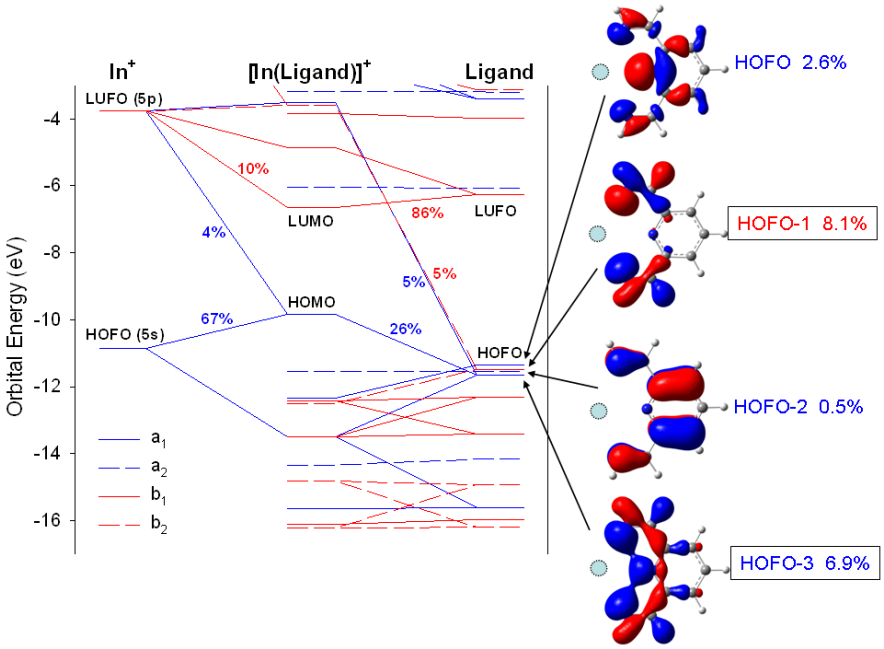

Figure 2.6. Molecular orbital interaction diagram for the di(imino)pyridine ligand (Ar = H) and the In^+ cation. The four highest occupied fragment orbitals (HOFOs) of the ligand and their contribution to the ligand-to-metal charge transfer interactions in the complex (via the % of electron population transferred to the In^+ cation) are shown on the right.

Table 2.1. Energy and % In character in the HOMO of In[bis(imino)pyridine]$^+$ cations.

Ar	**ε_{HOMO} (eV)**	**% In (% In *s*)[a] character in HOMO**
H	-9.84	74% (66%)
Ph	-8.82	57% (47%)
2,6-$^{i}Pr_2C_6H_3$	-8.52	37% (28%)
2,5-$^{t}Bu_2C_6H_3$	-8.56	19% (14%)

[a] Indium *s* orbital contribution (%).

[2.5] Conclusion

The sterically demanding bis(imino)pyridine scaffold readily reacted with the In(I) synthon, $In(O_3SCF_3)$, to allow the preparation, isolation and analysis of a set of unique compounds in which the In^+ cation is involved in only minimal covalent interactions with the ligand and counterion. The In^+ centres in these compounds are electron deficient possessing a 5s lone pair of electrons and three unoccupied p orbitals. Structural features of the compounds point to weak coordination and computational analysis of the two σ-type 5*p* orbitals revealed that they only receive limited electron donation from the ligands. While the reduction in the steric demands of the ligand did allow for closer approach of the triflate counterion to the In centres, the major component of the interaction energy between the two ions was determined to be electrostatic in nature with substantial component of the interaction to be between the ligand and the OTf` anion. The indium centre receives only minor electron donation from the anion.

In line with the observations that ligand sterics play an important role in stabilizing these species, by reducing the ligand steric demands to Ar = 2,6-$Me_2C_6H_3$ the In(III) bis(imino)pyridine complex, [{2,6-$Me_2C_6H_3N$=CPh}$_2$(NC_5H_3)]In$(OTf)_2Cl$ **2.5** was produced. Electronic structure analysis demonstrated that only one ligand donor orbital mixes with the In 5s orbital, and that this four electron interaction decreases as the steric demands of the imino-aryl groups increases leading to the HOMO that is dominated by ligand contributions over the In lone pair. In spite of having three N donor centres, the bis(imino)pyridine ligand, while stabilizing a low valent metal center, provides little charge donation to the metal cation due to the "mismatch" of donor orbital of the ligand and the *sp* metal acceptor orbitals (Figure 2.6).

[2.6] Indium Complex Experimental

General Methods. Reactions were performed in a glovebox with a nitrogen atmosphere, with the exception of ligand synthesis, which was performed using standard Schlenk techniques under a flow of N_2. All solvents were sparged with nitrogen and then dried by passage through a column of activated alumina using an apparatus purchased from Anhydrous Engineering. Deuterated chloroform was dried using activated molecular sieves. Metal halides were purchased from Strem Chemicals and used as received. All other chemicals were purchased from Aldrich and used without further purification. ^{1}H and ^{13}C NMR spectra were run on a Bruker Avance 300 MHz spectrometer with $CDCl_3$, CD_2Cl_2, and DMSO-d_6 as solvents and internal standards. Elemental analyses **2.1**−**2.4**, were performed by Midwest Microlab LLC, Indianapolis, IN, **2.5** was performed by Robertson Microlit Laboratories, Madison, NJ.

(2.1) [In-2,6-Bis{1-[(2,5-ditertbutylphenyl)imino]-benzyl}pyridine][OSO$_2$CF$_3$]: $InOSO_2CF_3$ powder (80 mg, 0.303 mmol) was added to a clear yellow solution of **1A** (200 mg, 0.303 mmol) in 5 mL of toluene. The reaction mixture was sealed and allowed to stir for 6 h. An immediate color change from translucent yellow to translucent red-orange was observed. The solution was then held at -20^{o}C for 24 h, and a small amount of bright orange precipitate formed. This solution was then concentrated in-vacuo to ~1.5 mL and maintained at -20^{o}C for 24 h to produce a bright orange precipitate. The reaction mixture was filtered, washed with 2 x 5 mL hexanes, and dried under vacuum. A bright orange powder of **2.1** was isolated in 76% yield. Crystals suitable for X-ray analysis were grown by layering a saturated solution of diethyl ether with hexanes, and storing at -20^{o}C for several days. ^{1}H NMR ($CDCl_3$, 23^{o}C): δ 7.96-6.63(br m, 19 H, aromatic), 1.43(br s, 18H, ^{t}Bu), 0.88(br s, 18H, ^{t}Bu). ^{13}C NMR ($CDCl_3$). δ 166.5(C=N imine), 156.1(py, *p*-CH), 150.2(py, *m*-CH), 146.1(py, *o*-C=N), 139.7(Ar-^{t}Bu, *i*-C), 139.4(Ph, *o*-CH),

134.4(Ar-^{t}Bu, *o*-CH), 130.0(Ar-^{t}Bu, *p*-CH), 129.4(Ph, *i*-C), 128.6(Ph, *p*-CH), 126.2(Ar-^{t}Bu, *m*-CH), 125.7(Ph, *m*-CH), 122.4(Ar-^{t}Bu, *m*-C), 121.7(Ar-^{t}Bu, *o*-C), 35.5(Ar-^{t}Bu, CH_3), 34.3(Ar-^{t}Bu, CH_3), 31.2(Ar-^{t}Bu, CH_3), 31.0(Ar-^{t}Bu, CH_3). CF_3 carbon broad and unresolved. Sample for elemental analysis was obtained by recrystalizations in THF, resulting in a bis-THF adduct of **2.1** Calculated for $C_{56}H_{71}F_3InN_3O_5S$: C 62.86, H 6.69, N 3.93, Found C 63.25, H 5.87, N 3.98.

(2.2) [In-2,6-Bis{1-[(2,6-diisopropylphenyl)imino]-benzyl}pyridine][OSO$_2$CF$_3$]: $InOSO_2CF_3$ powder (87 mg, 0.331 mmol) was added to a clear yellow solution of **1B** (200 mg, 0.331 mmol) in 5 mL of toluene. The reaction mixture was sealed and allowed to stir for 6 h. An immediate color change from translucent yellow to translucent red-orange was observed, with a gradual change to dark red. The solution was then held at −20 °C for 24 h, and a small amount of orange precipitate formed. This solution was filtered, and the precipitate was washed with 2 × 5 mL of hexanes, and allowed to dry under vacuum. An orange powder of **2** was isolated in 63% yield. Yellow-orange needle like crystals suitable for X-ray analysis were grown by diffusion of hexanes into a saturated tetrahydrofuran (THF) solution of **2.2** and storing at −20 °C for several days. ^{1}H NMR ($CDCl_3$, 23 °C): δ 7.99(t, 1H, py, *p*-CH), 7.68(d, 2H, py, *m*-CH), 7.46−7.28(br m, 10H, Ar−H), 7.16−7.02(br m, 6H, Ar−H) 3.00(br m, 4H, ^{i}Pr-CH), 1.20(br d, 12H, CH_3), 0.91(br d, 12H, CH_3). ^{13}C NMR ($CDCl_3$). δ 167.4(C═N imine), 154.6(py-C), 141.7(py-CH), 140.3(Ar−C), 138.7(py-CH), 133.7(Ar−CH), 130.6(Ar−C), 130.2(Ar−C), 129.6(Ar−CH), 128.7(Ar−CH), 126.3(Ar−CH), 123.8(Ar−CH), 28.6(CH_3), 26.3(*C*HMe_2), 22.7(CH_3). Analysis for $C_{44}H_{47}F_3InN_3O_3S$ Calculated: C, 60.76; H, 5.45; N, 4.83 Found: C, 60.61; H, 5.29; N, 4.82.

(2.3) [In-2,6-Bis{1-[(2,6-diethylphenyl)imino]-benzyl}pyridine][OSO$_2$CF$_3$]: $InOSO_2CF_3$ powder (90 mg, 0.341 mmol) was added to a clear yellow solution of **1C** (194 mg, 0.353 mmol) in 5 mL of hexanes. The reaction mixture was sealed and allowed to stir for 18 h. A gradual

color change from translucent yellow to opaque orange was observed, as the $InOSO_2CF_3$ slowly went into solution. The solution was then held at −20 °C for 24 h, and a pale orange precipitate formed. This solution was filtered, and the precipitate was washed with 5 × 2 mL of hexanes, and allowed to dry under vacuum. The resulting pale orange powder was then dissolved in toluene, and then the solution was passed through a plug of Celite to remove impurities. The solution was then dried under vacuum, resulting in the isolation of a dark orange powder in a modest yield of 39% (108 mg) because of mechanical loss from purification. Dark orange rod-like crystals suitable for X-ray analysis were grown by diffusion of hexanes into a saturated toluene solution of **2.3** and storing at −20 °C for several days. ^{1}H NMR (C_7D_8, 23 °C): δ 7.45(v br s, 4H, Ar−H), 7.26(d, 2H, py, m-CH), 7.09(br s, 2H, Ar−CH), 7.02−6.82(br m, 11H, Ar−H), 2.79(br m, 4H, CH_2), 2.41(br m, 4H, CH_2), 1.20(t, 12H, CH_3). ^{13}C NMR (C_7D_8) δ 168.2 (C═N imine), 155.1(py-CH), 144.1(py-C), 140.5(py-CH), 134.9(Ar−CH), 134.1(Ar−CH), 130.6(Ar−CH), 129.9(Ar−C), 129.7(Ar−CH), 129.6−128.7 (Ar−CH overlapped by C_7D_8 signals), 126.3(Ar−CH), 126.1(Ar−C), 123.9(Ar−C), 25.5(CH_2), 15.4(CH_3). Analysis for $C_{40}H_{39}F_3InN_3O_3S$ Calculated: C, 59.05; H, 4.83; N, 5.16 Found: C, 58.87; H, 4.85; N, 4.98.

(2.4) [In(OSO$_2$CF$_3$)$_2$Cl-2,6-Bis{1-[(2,6-dimethylphenyl)imino]-benzyl}pyridine]: $InOSO_2CF_3$ powder (52.5 mg, 0.199 mmol) was added to a clear yellow solution of **1D** (100 mg, 0.203 mmol) in 5 mL of toluene. The reaction mixture was sealed and allowed to stir for 4 h. An immediate color change from translucent yellow to opaque dark red was observed. The solution was then held at −20 °C for 5 days, and a dark red precipitate formed. This solution was filtered, and the precipitate was washed with 5 × 2 mL hexanes, and allowed to dry under vacuum. A red/bronze powder was isolated in 103 mg. Attempted crystallization in a range of solvents from three separate reactions using different purified precursor batches consistently yielded the same

decomposition product **2.4**. Large block-like crystals could be consistently isolated, and were subjected to elemental analysis, confirming a relative homogeneity of crystallized product. Analysis for $C_{37}H_{31}F_6InClN_3O_6S_2$ Calculated: C 47.17, H 3.32, N 4.46, Found C 46.15, H 3.60, N 4.22.

(2.5) [InCl$_2$-2,6-Bis{1-[(2,5-ditertbutylphenyl)imino]-benzyl}pyridine][InCl$_4$]: $InCl_3$ powder (134 mg, 0.606 mmol) was added to a clear yellow solution of **1A** (200 mg, 0.303 mmol) in 8 mL of toluene. The reaction mixture was sealed and allowed to stir for 6 h. An immediate color change of the solution from translucent yellow to translucent red orange was observed. The solution was then held at -20^{o}C for 72 h, to yield a bright yellow precipitate. This solution was filtered, and the precipitate was washed with 2 x 5 mL hexanes, and allowed to dry under vacuum. A bright yellow powder of 3 was isolated in 73% yield. Crystals suitable for X-ray analysis were grown by layering a saturated solution of toluene with hexanes, and storing at -20^{o}C for several days. ^{1}H NMR ($CDCl_3$, 23^{o}C): δ 8.76(t, 1H, py, *o*-CH), 8.38(d, 2H, py, *m*-CH), 8.29-6.93(br m, 16H, aromatic), 1.37(br s, 18H, ^{t}Bu), 1.10(br s, 18H, ^{t}Bu). ^{13}C NMR ($CDCl_3$). δ 168.7(C=N imine), 167.5(py, *p*-CH), 149.9(py, *m*-CH), 148.4(py, *o*-C=N), 146.6(Ph, *o*-CH), 138.9(Ar-*t*Bu, *o*-CH), 137.7(Ar-^{t}Bu, *p*-CH), 134.4(Ph, *i*-C), 133.3(Ph, *p*-CH), 131.6(Ar-^{t}Bu, *m*-CH), 129.7(Ar-^{t}Bu, *i*-C), 129.1(Ph, *m*-CH), 125.5(Ar-^{t}Bu, *m*-C), 122.4(Ar-^{t}Bu, *o*-C), 36.7(Ar-^{t}Bu, CH_3), 34.9(Ar-^{t}Bu, CH_3), 33.0(Ar-^{t}Bu, CH_3), 31.5(Ar-^{t}Bu, CH_3). Elemental analysis Calculated for $C_{47}H_{55}Cl_6In_2N_3$: C 51.12, H 5.02, N 3.81, Found C 50.81, H 4.95, N 3.74.

[2.7] X-ray Crystallographic Information: Indium Complexes

Table 2.2. Summary of Data Collection and Crystallographic Parameters for **2.1-2.5**. *

Cmpd	**2.1**	**2.2**	**2.3**	**2.4**	**2.5**
Emp. formula	$C_{48}H_{55}F_3InN_3O_3S$	$C_{44}H_{47}F_3InN_3O_3S$	$C_{40}H_{39}F_3InN_3O_3S$	$[C_{37}H_{31}F_6InClN_3O_6S_2]_2[C_7H_8]_4$	$C_{47}H_{55}Cl_6In_2N_3[C_7H_8]_{1.5}$
Formula weight	925.83	869.73	813.62	2252.61	1242.48
T (K)	202(2)	202(2)	200(2)	203(2)	202(2)
λ(Å)	0.71073	0.71073	0.71073	0.71073	0.71073
Crystal system	Triclinic	Monoclinic	Monoclinic	Monoclinic	Monoclinic
Space group	P-1	P2(1)/c	P2(1)/c	C2/c	P2(1)/n
a (Å)	11.344(2)	9.036(3)	8.894(3)	17.539(7)	18.2104(13)
b (Å)	14.775(3)	17.395(5)	15.832(5)	14.032(6)	16.5153(12)
c (Å)	15.361(3)	27.183(8)	26.407(8)	21.970(9)	20.0394(15)
α (deg)	78.425(3)	90.00	90.00	90.00	90.00
β (deg)	69.913(3)	96.858(4)	96.459(6)	108.382(6)	100.6280(10)
γ (deg)	74.980(3)	90.00	90.00	90.00	90.00
V ($Å^3$)	2317.5(8)	4242(2)	3695(2)	5131(4)	5923.5(7)
Z	2	4	4	2	4
ρ(calc) (Mg/m^3)	1.327	1.362	1.463	1.458	1.393
μ (mm^{-1})	0.609	0.661	0.753	0.667	1.087
Abs. corr.	Semi-empirical from equivalents				
Final R indices [I>2σ(I)]					
R1[a]	0.0737	0.0782	0.0706	0.0495	0.0646
*w*R2[b]	0.1856	0.1011	0.1369	0.1275	0.1350

[a] $R1 = \Sigma \left| |F_o| - |F_c| \right| / \Sigma |F_o|$. [b] $wR2 = \left(\Sigma w \left(|F_o| - |F_c| \right)^2 / \Sigma w |F_o|^2 \right)^{1/2}$ *structure files available from CCDC

Table 2.3. Selected Bond Distances for Compounds **2.1-2.3** (Å).

2.1		**2.2**		**2.3**	
C(1)-C(8)	1.500(10)	C(13)-C(20)	1.502(9)	C(7)-C(8)	1.496(12)
C(12)-C(13)	1.488(10)	C(24)-C(25)	1.495(9)	C(12)-C(13)	1.497(12)
In(1)-N(2)	2.495(5)	In(1)-N(2)	2.502(5)	In(1)-N(2)	2.501(8)
In(1)-N(1)	2.747[a]	In(1)-N(1)	2.664[a]	In(1)-N(1)	2.731[a]
In(1)-N(3)	2.689[a]	In(1)-N(3)	2.679[a]	In(1)-N(3)	2.636(7)
In(1)-O(2)	7.975[a]	In(1)-O(1)	2.462(6)	In(1)-O(1)	2.532(7)
N(1)-C(1)	1.281(9)	N(1)-C(13)	1.272(8)	N(1)-C(7)	1.268(11)
N(3)-C(13)	1.283(9)	N(3)-C(25)	1.272(8)	N(3)-C(13)	1.280(12)
N(2)-C(8)	1.329(9)	N(2)-C(20)	1.337(8)	N(2)-C(8)	1.368(11)
N(2)-C(12)	1.340(9)	N(2)-C(24)	1.350(8)	N(2)-C(12)	1.357(10)
N(1)-C(20)	1.426(9)	N(1)-C(6)	1.437(8)	N(1)-C(20)	1.433(11)
N(3)-C(34)	1.432(9)	N(3)-C(37)	1.446(8)	N(3)-C(30)	1.461(12)
O(1)-S(1)	1.425(6)	O(1)-S(1)	1.463	O(1)-S(1)	1.462
O(2)-S(1)	1.408(7)	O(2)-S(1)	1.421	O(2)-S(1)	1.475
O(3)-S(1)	1.419(8)	O(3)-S(1)	1.436	O(3)-S(1)	1.418

[a] distance beyond the recognized bonding parameters in SHELXTL.

Table 2.4. Selected Bond Angles for Compounds **2.1-2.3** (°).

2.1		**2.2**		**2.3**	
O(2)-In(1)-N(2)	--	O(1)-In(1)-N(2)	75.8(2)	O(1)-In(1)-N(2)	76.6(2)
In(1)-O(2)-S(1)	--	In(1)-O(1)-S(1)	138.0(4)	In(1)-O(1)-S(1)	178.3(5)
In(1)-N(2)-C(8)	121.0(4)	In(1)-N(2)-C(20)	120.7(4)	In(1)-N(2)-C(8)	122.0(6)
In(1)-N(2)-C(12)	118.8(4)	In(1)-N(2)-C(24)	120.6(4)	In(1)-N(2)-C(12)	119.3(6)
In(1)-N(1)-C(1)	109.71[b]	In(1)-N(1)-C(13)	116.46[b]	In(1)-N(1)-C(7)	116.65[b]
In(1)-N(3)-C(13)	108.68[b]	In(1)-N(3)-C(25)	115.89[b]	In(1)-N(3)-C(13)	118.4(6)
N(1)-In(1)-N(2)	61.85[b]	N(1)-In(1)-N(2)	63.62[b]	N(1)-In(1)-N(2)	63.56[b]
N(3)-In(1)-N(2)	63.09[b]	N(3)-In(1)-N(2)	63.15[b]	N(3)-In(1)-N(2)	64.7(2)
N(1)-C(1)-C(8)	116.1(6)	N(1)-C(13)-C(20)	118.5(6)	N(1)-C(7)-C(8)	119.6(9)
N(3)-C(13)-C(12)	116.9(6)	N(3)-C(25)-C(24)	118.6(6)	N(3)-C(13)-C(12)	117.6(8)
N(2)-C(8)-C(1)	116.7(6)	N(2)-C(20)-C(13)	117.4(5)	N(2)-C(8)-C(7)	117.6(8)
N(2)-C(12)-C(13)	116.5(6)	N(2)-C(24)-C(25)	116.9(5)	N(2)-C(12)-C(13)	118.7(8)
N(2)-C(8)-C(9)	122.0(6)	N(2)-C(20)-C(21)	122.7(6)	N(2)-C(8)-C(9)	121.5(9)
N(2)-C(12)-C(11)	121.8(7)	N(2)-C(24)-C(23)	122.4(6)	N(2)-C(12)-C(11)	121.8(8)
C(1)-N(1)-C(20)	121.3(6)	C(13)-N(1)-C(6)	120.7(5)	C(7)-N(1)-C(20)	118.7(8)
C(13)-N(3)-C(34)	122.0(6)	C(25)-N(3)-C(37)	120.2(5)	C(13)-N(3)-C(30)	119.0(8)
C(8)-N(2)-C(12)	119.2(6)	C(20)-N(2)-C(24)	117.7(5)	C(8)-N(2)-C(12)	117.7(7)
C(8)-C(9)-C(10)	119.0(7)	C(20)-C(21)-C(22)	118.5(6)	C(8)-C(9)-C(10)	120.3(9)
C(12)-C(11)-C(10)	118.6(7)	C(24)-C(23)-C(22)	119.7(6)	C(12)-C(11)-C(10)	118.0(9)
C(9)-C(10)-C(11)	119.2(6)	C(21)-C(22)-C(23)	118.9(6)	C(9)-C(10)-C(11)	120.6(9)

[b] distance beyond the recognized bonding parameters in SHELXTL.

Table 2.5: Selected Bond Distances, and Bond Angles for Compounds **2.4** and **2.5**(Å).

Selected Bond Lengths (Å)				**Selected Bond Angles (^{o})**			
2.4		**2.5**		**2.4**		**2.5**	
In(1)-N(1)	2.289(3)	In(1)-N(1)	2.295(17)	In(1)-N(2)-C(2)	118.7(2)	In(1)-N(2)-C(22)	118.7(13)
--	--	In(1)-N(3)	2.284(16)	--	--	In(1)-N(2)-C(26)	117.5(14)
In(1)-N(2)	2.171(4)	In(1)-N(2)	2.226(17)	In(1)-N(1)-C(1)	115.2(2)	In(1)-N(1)-C(15)	118.4(14)
In(1)-O(1)	2.269(3)	In(1)-Cl(1)	2.327(6)	--	--	In(1)-N(3)-C(27)	117.3(14)
--	--	In(1)-Cl(2)	2.334(6)	N(1)-C(1)-C(2)	117.4(3)	N(1)-C(15)-C(22)	116(2)
In(1)-Cl(1)	2.3121(16)	In(1)-Cl(3)	4.291[c]	--	--	N(3)-C(27)-C(26)	116.5(19)
N(1)-C(1)	1.285(4)	N(1)-C(15)	1.28(3)	N(2)-C(2)-C(1)	114.8(3)	N(2)-C(22)-C(15)	114.9(19)
--	--	N(3)-C(27)	1.29(2)	--	--	N(2)-C(26)-C(27)	116.2(19)
N(2)-C(2)	1.340(4)	N(2)-C(22)	1.35(3)	N(2)-In(1)-N(1)	73.53(7)	N(2)-In(1)-N(1)	71.0(6)
--	--	N(2)-C(26)	1.33(2)	--	--	N(2)-In(1)-N(3)	72.0(6)
N(1)-C(11)	1.463(4)	N(1)-C(9)	1.44(3)	N(2)-In(1)-Cl(1)	180.000(1)	N(2)-In(1)-Cl(1)	129.1(5)
--	--	N(3)-C(34)	1.47(3)	N(2)-In(1)-O(1)	83.46(6)	N(2)-In(1)-Cl(2)	116.7(5)
S(1)-O(1)	1.476						
S(1)-O(2)	1.424						
S(1)-O(3)	1.431						

[c] represents the bond distance to the nearest Cl of the counterion.

Chapter 3: *Gallium(III) and Ligand Radical Species*

[3.1] Gallium(I) Coordination Compounds

Motivated by our success with In(I), we sought to expand our bis(imino)pyridine chemistry towards the synthesis of monomeric molecular Ga(I) compounds. Although In, and Tl (to be discussed in Chapter 4) are distinguished from their lighter group 13 congeners by increased separation of s and p orbitals resulting in inert-pair effect phenomena which stabilizes the +1 state, the comparative expediency in the development of their application could be attributed to the availability of stable M(I) synthons.[33] However, the availability of a stable, soluble Ga(I) synthon has been comparatively lacking, and it could be argued that is one of the principal reasons for the poorer catalogue of Ga(I) coordination chemistry. To date, the only crystallographically authenticated solid gallium(I)-halides have been reported by the group of Schnöckel, the synthesis of which requires a complex high temperature reactor that is not available to the average research group.[34] Alternatively, "GaI", as reported by Green in 1990, has become the standard low-valent gallium precursor due to its ease of synthesis and broad applicability for organic synthesis, coordination chemistry, and cluster fabrication.[35]

Attempted synthesis of monomeric Ga(I) complexes with "GaI" starting material and donor ligands (phosphines, amines, imines) have thus far been fruitless. "GaI" has a strong tendency to disproportionate, giving a range of Ga(II) and Ga(III) coordination complexes, some exhibiting Ga-Ga bonds.[12a,36] While Ga(I)'s bias towards disproportionation has prevented the synthesis of monomeric Ga(I) complexes via the "GaI" synthon route, "GaI" has afforded a

[33] Commercially available InCl, easily accessible InOTf, and commercially available TlOTf as common synthetic access points to low valent In and Tl chemistry.
[34] H. Schnockel, *Dalton Trans*. **2008**, 4344
[35] M.L.H. Green, P. Mountford, G. J. Smout, S.R. Speel, *Polyhedron*, **1990**, 9, 2763.
[36] Some examples of coordination chemistry: (a) A. Schnepf, C. Doriat, E. Mollhausen H. Schnockel, *Chem. Commun.*, **1997**, 2111. (b) R.J. Baker, C. Jones, *Dalton Trans*., **2005**, 1341.

successful pathway towards Ga clusters, the breadth of which is quite vast, and a more thorough overview is provided by Jones.[12a,36b] Recently, Slattery and Krossing have reported a simple synthetic pathway to Ga(I) salts. Ga metal is oxidized by $Ag[Al\{OC(CF_3)_3\}_4]$ in toluene, or fluorobenzenes using a sonicator as energy source. The resulting complex is a bis-arene Ga(I) cation stabilized by a weakly coordinating $[Al\{OC(CF_3)_3\}_4]^-$ anion (Scheme 3.1). Unlike "GaI" complexes, the stabilized Ga-(H-arene) cation-anion pairs are stable towards disproportionation at room temperature, likely due to the lack of halides which are known to promote it.[37]

Scheme 3.1

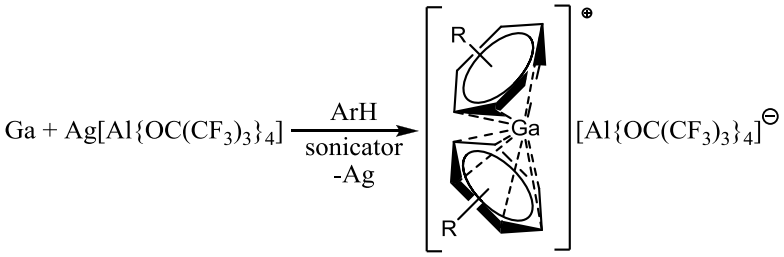

Similar reaction in a mixture of *o*-$C_6H_4F_2$ and toluene led to the partial decomposition of the anion, and the formation of the very stable cation-anion pair (**i**) (Scheme 3.2). The Ga-F contacts of 3.26 Å are shorter than the sum of the Van Der Waals radii (3.34 Å). Unlike the reaction of "GaI" with phosphines, (**i**) reacts with three equivalents of PPh_3 in *o*-$C_6H_4F_2$ to afford (**ii**), without any evidence of disproportionation (Scheme 3.2). The resulting complex is the first structurally characterized homoleptic gallium phosphine complex, of any oxidation state. ^{31}P NMR points to unusually broadened lines, as expected for weak Ga-P interactions. This is supported by MP2/TZVPP calculations on the $[GaPPh_3]^+$ cation which point to a low barrier to phosphine ligand exchange (22 $kJmol^{-1}$). The HOMO is also a Ga-based lone pair comprised of

[37] Wehmschulte, R.J., *Angew. Chem., Int. Ed*., **2010**, 49, 2

mostly s character (93%).[38] The weak E-donor interaction, and predominantly s-character lone pair HOMO is not unlike our work with In(I)-bis(imino)pyridines (Chapter 2).

Scheme 3.2

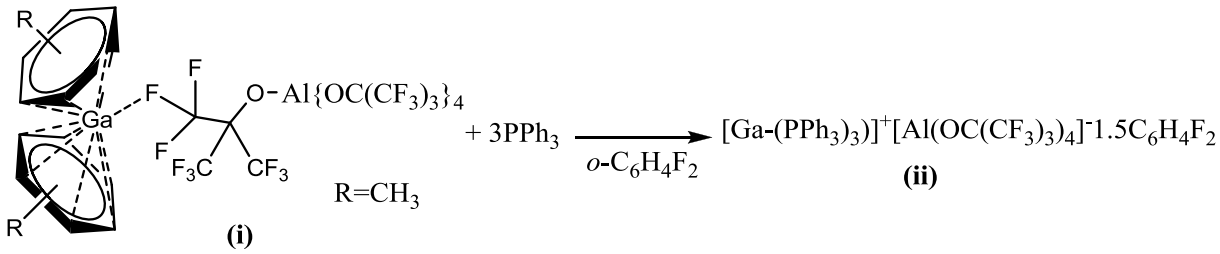

Although these recent developments in the field of Ga(I) chemistry are promising, our work had already been complete and reported prior to their publication. As such our efforts centred on developing the chemistry of the "GaI" synthon (the nature of which is discussed in section 3.2). This was further motivated by the work of Jones. While cataloguing the reactivity of "GaI" with a variety of donor ligands (amines, phosphines etc..), Jones reported a bis(imino)pyridine Ga(III) complex resulting from the disproportionation reaction of "GaI" in the presence of bis(imino)pyridine. The reported yield was only 10% and the complex was not investigated further. The low yield and general ambiguity piqued our interest as to the remainder of the product distribution and the potential for isolation of a low-valent gallium complex using our modified bulky bis(imino)pyridine ligand framework.[12a,36b]

[38] Slattery, J.M., Higelin, A., Bayer, T., Krossing, I., *Angew. Chem. Int. Ed*. **2010**, 49, 3228

[3.2] "GaI"

As may be evident thus far, "GaI" is always represented in quotation marks, owing to the fact that the composition of this material is not entirely known. Based on raman spectroscopy, the conventional interpretation points to a predominant component of $[Ga]_2[Ga_2I_6]$ as well as several subvalent gallium iodides yet to be clearly determined.[12a,36b] However, recent collaborative work with the Bryce group using $^{69/71}$Ga solid-state NMR and ^{127}I nuclear quadrupole resonance (NQR) experiments revealed that ''GaI'' is predominantly two equivalents of Ga(0) metal with two equivalents of GaI_2, where the latter is composed of Ga^+ and GaI_4^- ions. This composition may be represented as $[Ga(0)]_2[Ga]^+[GaI_4]^-$.[39]

Scheme 3.3

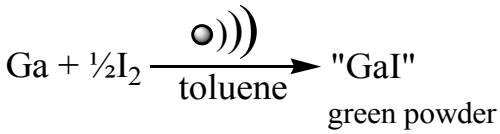

"GaI" was synthesized according to the synthetic procedure reported by Green et al.[35] On a three gram scale, under an atmosphere of N_2, gallium metal was mixed with a half of an equivalent of I_2 in dry toluene. The mixture was placed in an ultrasonic bath, where it was allowed to react for several hours (Scheme 3.3). The resulting fine green powder was filtered, washed with hexanes, dried, and stored under an atmosphere of N_2, under which it remains stable for nearly a year. The synthetic procedure was repeated several times, and reproducibility was confirmed via powder XRD (Figure 3.1).

[39] C.M. Widdifield, T. Jurca, D.S. Richeson, D.L. Bryce, *Polyhedron*, **2012**, 35, 1, 96.

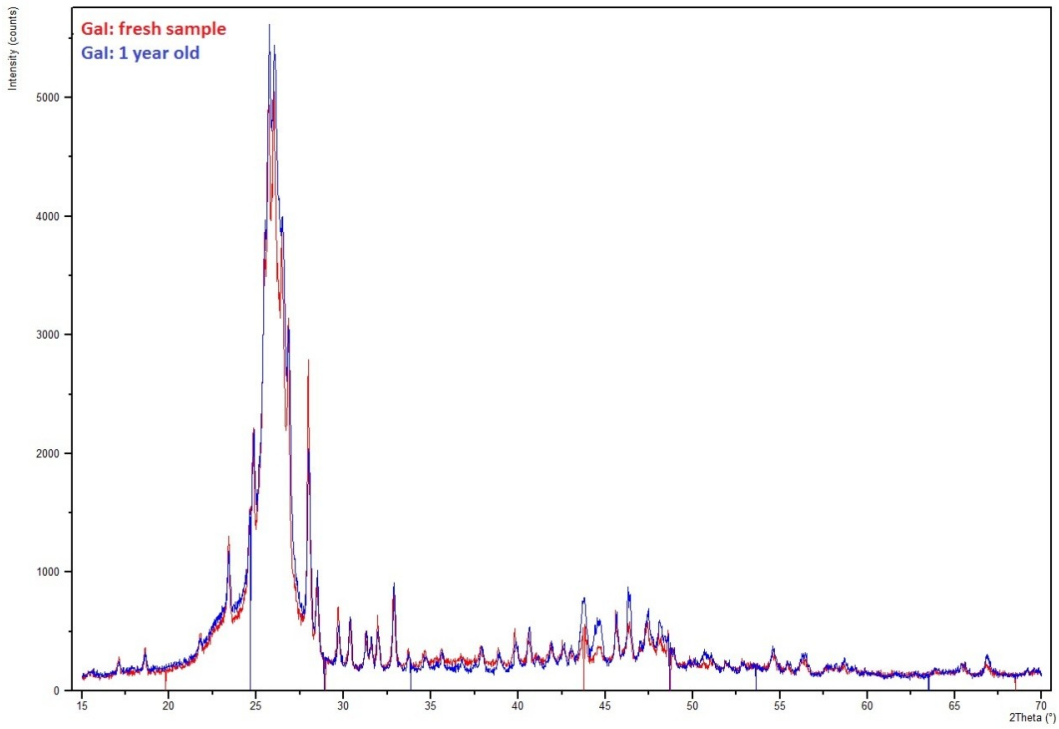

Figure 3.1. Powder XRD pattern of a freshly synthesized sample of "GaI" (red), and a "GaI" sample that has been stored under inert atmosphere at -30^{o}C for one year (blue). The similarity of patterns, as well as the as the consistency in sample colour (i.e., pale green) is indicative of the stability of "GaI" for prolonged periods of time, if stored under a nitrogen atmosphere.

[3.3] Results and Discussion: Ligation of Bis(imino)pyridines to "GaI" and GaI_3

Although the reaction of 2,6-{2,5-$^{t}Bu_2C_6H_3N$=CPh}$_2$(NC_5H_3) (**1A**) with "GaI" proceeded smoothly, this reaction consistently yielded a mixture of products, consisting of a predominantly red solid, a more crystalline orange material, and some insoluble gray powder that appeared to be Ga metal. Attempts to cleanly separate the two soluble solids have, so far, been unsuccessful and the NMR analysis of this mixture is complicated by broadness of the observed resonances. Fortunately, we were able to isolate a small amount of orange single crystals **3.1** (Scheme 3.4). The molecular structure of this Ga(III) species was confirmed

through single crystal X-ray analysis as summarized in Tables 3.1, 3.2 and 3.3 and Figure 3.3. This Ga(III) complex consisted of $[2,6\text{-}\{2,5\text{-}^{t}Bu_2C_6H_3N{=}CPh\}_2(NC_5H_3)]GaI_2^{+}GaI_4^{-}$ as a well-separated cation/anion pair with the cationic portion of compound **3.1**, shown in Figure 3.2. Selected bond distances and angles for this species are presented in Tables 3.2 and 3.3 respectively. The geometry of the gallium centre within this cation is a distorted square pyramid with the four-fold plane defined by the pyridine centre, N2, the two imine nitrogens, N1, N3, and iodine centre I2, with iodine centre I1 as the apex. The limitations of ligand geometry led to the basal imine centres oriented with an N1-Ga-N3 angle of 148.8(2)°. The two five-membered rings resulting from the coordination of the pyridyl and imine moieties are planar. As anticipated the equatorial Ga-N2 distance of 2.017(5)Å is shorter than the axial Ga-Nimine distances of 2.151(5)Å and 2.181(5)Å.

Scheme 3.4

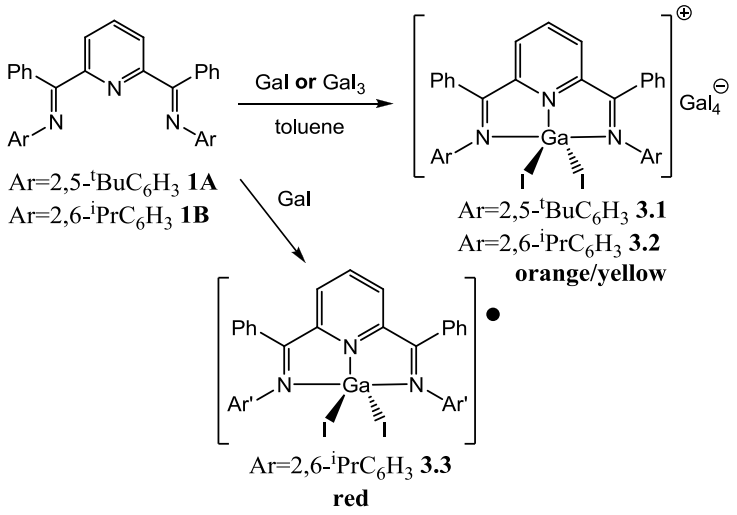

A more direct synthesis of **3.1** was provided by reaction of **1A** with GaI_3 in a stoichiometric ratio of 1:2. The resulting red-orange solution yielded bright orange **3.1** in 93% yield. The room temperature NMR spectra of **3.1** are simplfied relative to that of the free ligand and indicate two conformers for **3.1**. The ratio between these species was

dependent on temperature and solvent. These observations were attributed to atropisomerism arising from restricted rotation of the N-aryl groups in the coordinated 2,6-bis (imino)pyridine ligands of 3.1.[40]

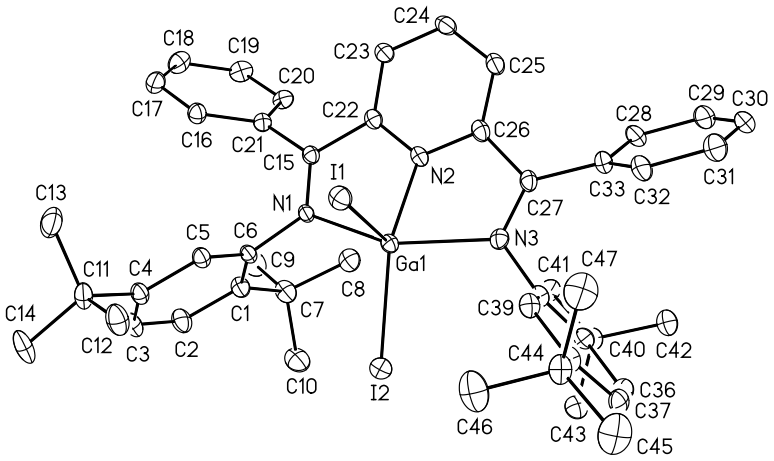

Figure 3.2. X-ray structure of the $[2,6\text{-}\{2,5\text{-}^{t}BuC_6H_3N{=}CPh\}_2(NC_5H_3)]GaI_2^+$ cation of compound **3.1** with hydrogen atoms, the GaI_4^- counter-ion and co-crystallized $CHCl_3$ omitted for clarity.

Clearly, the reaction between "GaI" and **1A** involves more than simple ligand coordination. In an effort to unravel the details of this reaction, obtain simpler spectroscopic data and perhaps determine the identity of the major red product, we replaced the N(2,5-$^{t}Bu_2C_6H_3$) groups of **1A** with the more symmetrical Dipp substituent in ligand **1B**. Similar to the reaction with **1A**, the 1:1 reaction between "GaI" and **1B** produced a rapid color change from the yellow color of the initial solution to red. Along with some gray powder of elemental Ga, two soluble species, one red and the other yellow-orange, were obtained. As we observed from the reaction of ligand **1A**, the major product appears to be the red material.

[40] J. Cámpora, M. Á. Cartes, A. Rodríguez-Delgado, A. M. Naz, P. Palma, C. M. Pérez, D. del Rio, *Inorg. Chem.* **2009**, 48, 3679.

From the reaction, a mixture of crystals for a yellow-orange compound **3.2** and a red compound **3.3** could be isolated and it was fortunate that both of these were suitable for single crystal analysis.

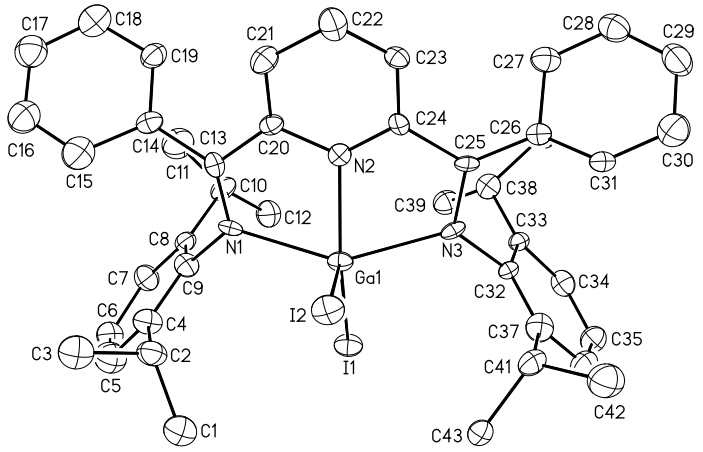

Figure 3.3. X-ray structure of the [2,6-{DippN=CPh}$_2$(NC_5H_3)]GaI_2^+, cation of compound **3.2** with hydrogen atoms, the GaI_4^- counter-ion and co-crystallized THF omitted for clarity.

The structure obtained for the yellow-orange species, **3.2**, is a Ga(III) complex analogous to that of **3.1** and is depicted in Figure 3.3 with selected bond distances and angles presented in Tables 3.2 and 3.3. The cationic component of **3.2** presents the Ga centre in a distorted square pyramid with the four-fold plane defined by the pyridine centre, N2, the two imine nitrogens, N1, N3, and iodine centre I1, with iodine centre I2 as the apex. The basal imine centres (N1-Ga-N3 = 146.0(6)°) exhibit slightly longer bond distances (2.189(17)Å and 2.214(17)Å) than the Ga-N_{py} distance of 2.022(16)Å.

The energetic features for the disproportionation reaction of DippN=C(Me)}$_2$(NC_5H_3) and "GaI" to compound **3.2** and Ga(0) were examined computationally. These DFT computations using the B3LYP functional and DGDZVP basis set supported the

thermodynamic favourability of the disproportionation process with an enthalpy for this reaction of -28.50 kJ/mol (see section 3.7).[41] Consideration of the route to obtain **3.2** lead to an investigation of an *in situ* method to access **3.2** from the elements that is provided by direct sonication of Ga and I_2 with addition of ligand **1B**. The yield of this reaction was directly linked to the stoichiometry of the ratio Ga:I_2 used in the sonication step. A lower yield along with the red product was provided by a 1:1 ratio of "GaI" while the 2:3 ratio, corresponding to GaI_3, provided a 98% yield of **3.2**. These observations are consistent with the observed disproportionation from the "GaI" reagent. Excellent yields (>90%) of **3.2** were also obtained from reaction of **1B** with GaI_3.

Red crystals of **3.3**, the second and a major product from the reaction of "GaI" and **1B**, were also analyzed by single crystal X-ray analysis and the results as well as a direct comparison with the structure of **3.2** are presented in Figure 3.4. Selected bond distances and angles for this compound are presented in Tables 3.2 and 3.3. The first notable feature of these results is the observation that **3.3** is the neutral analogue of the cation of compound **3.2**. Secondly, the similarity of the coordination of ligand **1B** to the GaI_2 unit in these two species and the apparent undistorted nature of the ligand is significant and accentuated by the overlay of the structures of **3.2** and **3.3** shown in Figure 3.5. These features indicate that **3.3** is a radical species.

[41] T. Jurca, K. Dawson, I. Mallov, T. Burchell, G.P.A. Yap, D.S. Richeson, *Dalton Trans*. **2010**, 39, 1266.

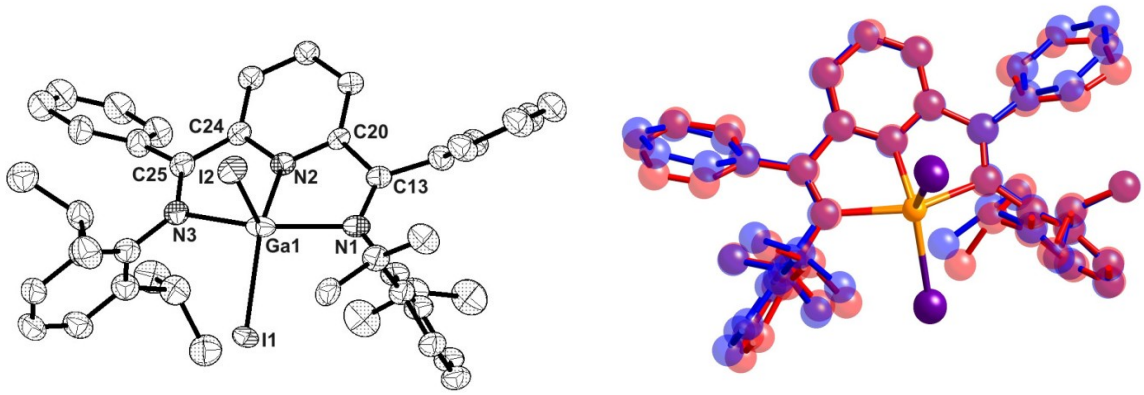

(a) **(b)**

Figure 3.4. (**a**) X-ray structure of compound **3.3** with hydrogen atoms omitted for clarity. (**b**) An overlay of the structures of the cation of compound **3.2**, $[2,6\text{-}\{DippN{=}CPh\}_2(NC_5H_3)]GaI_2^+$ (red), and the radical **3.3**, $[2,6\text{-}\{DippN{=}CPh\}_2(NC_5H_3)]GaI_2$ (blue). Hydrogen atoms have been omitted for clarity.

Although it may be initially tempting to interpret these data as compound **3.3** consisting of a $Ga^{II}I_2$ radical species coordinated by a neutral ligand **1B**, the alternative view that **3.3** is composed of a GaI_2^+ cation coordinated to an anion radical of the ligand is certainly precedented for the non-innocent di(imino)pyridine ligand system.[12b,42] We examined **3.3** by EPR spectroscopy and DFT computations in an effort to more decisively assign the unpaired electron density. The observation of an EPR signal with a g value of 2.0029 confirms the fact that **3.3** possesses radical character and indicates that the free electron is ligand localized. A slightly asymmetric triplet pattern further suggests that the electron predominantly samples one N centre in the ligand (Figure 3.5). A DFT computational study was undertaken to obtain a more thorough understanding of the electronic nature of radical **3.3**. Calculations were carried out with the B3LYP functional and the DGDZVP basis set. The results of these computations place the unpaired electron on the

[42] Q. Knijnenburg, S. Gambarotta, P. H. M. Budzelaar, *Dalton Trans.* **2006**, 5442.

ligand. The SOMO is depicted in Figure 3.6 and consists mainly of a delocalized di(imino)pyridine π* orbital of an anionic ligand with nearly zero contribution from the Ga or I centres. Although the EPR spectrum is consistent with the computational findings, the asymmetry of both the EPR spectrum and the orbitals of the computed SOMO suggest a potentially more complex interaction than has been described. Such a description is currently beyond the scope of this thesis.

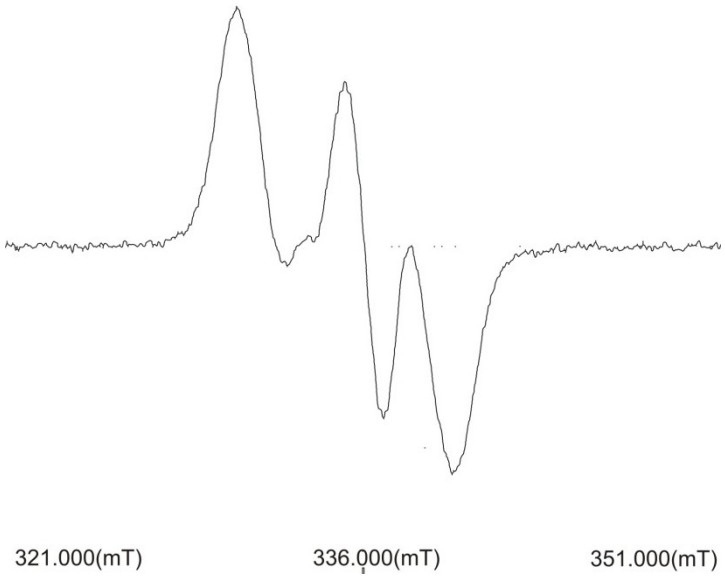

Figure 3.5. Solution EPR spectrum of **3.3** (g = 2.0029).

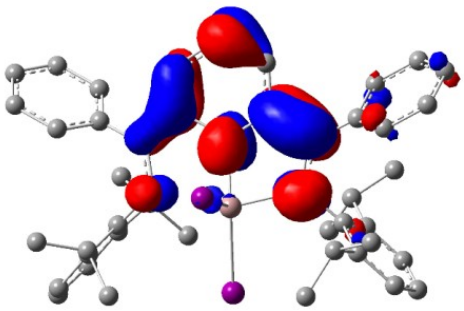

Figure 3.6. The SOMO for the radical [2,6-{DippN=CPh}$_2$(NC_5H_3)]GaI_2 **3.3**. Hydrogen atoms are omitted for clarity. Isovalue = 0.0300.

[3.4] Conclusion

While in some cases "GaI" may provide synthetic access to Ga^{I} species, the coordination of this species with aryl substituted bis(imino)pyridine ligands (**1A** and **1B**) lead to a thermodynamically favourable disproportionation reaction with ultimate isolation of the Ga^{III} species $[2,6\text{-}\{Ar'N{=}CPh\}_2(NC_5H_3)]GaI_2^{+}GaI_4^{-}$ (Ar' = 2,5-$^{t}Bu_2C_6H_3$ **3.1**, 2,6-$^{i}Pr_2C_6H_3$ **3.2**). These observations allowed for the development of a direct, "one-pot" synthesis from elemental Ga and I_2. Apparent intermediates of this reaction were isolated and characterized as neutral radical species **3.3**.

[3.5] Gallium Complex Experimental

General Methods. Unless otherwise stated, reactions were performed in a glovebox with a nitrogen atmosphere. All solvents were sparged with nitrogen and then dried by passage through a column of activated alumina using an apparatus purchased from Anhydrous Engineering. Deuterated chloroform was dried using activated molecular sieves. Metals and metal halides were purchased from Strem Chemicals and used as received. All other reagents were purchased from Aldrich and used without further purification. NMR spectra were run on a Bruker Avance 300 MHz spectrometer with deuterated chloroform as a solvent and internal standard. Elemental analyses were performed by Midwest Microlab LLC, Indianapolis IN. EPR measurements were performed using a JEOL FA-100 X-Band EPR spectrometer equipped with a JEOL ES-UCX2 cylindrical cavity. Samples were held in clear-fused silica tubes (5 mm diameter) purchased from Wilmad. All spectra were recorded over 2 min at 5 mW power, modulation width of 0.025 mT, time constant of 0.03 s, and a sweep width of 30 mT.

***Preparation of "GaI"*:** Based on literature procedure, on a three gram scale, under an atmosphere of N_2, gallium metal was mixed with a half of an equivalent of I_2 in dry toluene, and

placed in a Bransonic ultrasonic cleaning apparatus, where it was allowed to react for several hours (Scheme 3.3). The resulting fine green powder was filtered, washed with hexanes, dried, and stored under an atmosphere of N_2. Due to the high air sensitivity of "GaI", the samples used for powder X-ray diffraction (XRD) experiments were prepared in the glovebox, utilizing a side-loading hermetic sample holder to accommodate air sensitive samples, which was covered with a thin Mylar film adhered to the underside of the holder with nitrocellulose in ethyl acetate (i.e., nail polish).[43] Powder XRD experiments were performed using a Philips X'PERT system with Cu radiation (Cu-Kα, 1.5405980Å), with a 2θ range between 15 and 70°. The diffraction peaks corresponding to the Mylar film are observed between 2θ = 24 – 27°.

***Reaction of [2,6-bis{2,5-^{t}Bu$_2$C$_6$H$_3$N=CPh}$_2$(NC$_5$H$_3$)] (1A) with "GaI"*:** "GaI" powder (59 mg, 0.300 mmol) was added to a clear yellow solution of **1A** (200 mg, 0.300 mmol) in 8 mL of toluene. The reaction mixture changed color immediately from translucent yellow to a dark opaque red/purple. The reaction was sealed and allowed to stir for 4.5 hours and then cooled to -20°C overnight, over which time a dark red precipitate formed. The solution was filtered and a red solid was washed with 10 x 2 mL hexanes, and allowed to dry under vacuum. Dark red powder (0.80 g) was isolated, dissolved in toluene and cooled to -20°C to give a mixture of dark red powder and a small amount of orange powder. Despite multiple attempts, these two compounds could not be completely isolated from each other. The red powder is poorly soluble and shows only very broad ^{1}H signals by NMR. Small dark red crystals that were not suitable for X-ray crystallography could be grown.

(3.1) [2,6-bis{2,5-^{t}Bu$_2$C$_6$H$_3$N=CPh}$_2$(NC$_5$H$_3$)]GaI$_2$(GaI$_4$): GaI$_3$ powder (135 mg, 0.300 mmol) was added to a clear yellow solution of **1A** (100 mg, 0.151 mmol) in 8 mL of toluene.

[43] J. H. Reibenspies, N. Bhuvanesh, *Powder Diffraction*, **2009**, 24 56.

Colour change was immediate as the solution went from translucent yellow to a bright translucent red, gradually becoming opaque. The reaction mixture was sealed and allowed to stir for 6 hours and then cooled to -20°C overnight, over which time a bright orange precipitate formed. The solution was filtered, washed with 10 x 2 mL hexanes, and the solid was allowed to dry under vacuum. A bright orange powder of **3.1** was isolated in 93% yield. Yellow-orange needle like crystals suitable for X-ray analysis were grown by diffusion of hexanes into a saturated $CDCl_3$ solution held at -20°C for several days. ^1H and ^{13}C NMR point to the existence of two conformers in solution. *Conformer A*: ^1H NMR ($CDCl_3$, 300 MHz): δ 9.02(br t, 1 H, py, *p*-CH), 8.53(br d , 2 H, py, *m*-CH), δ 8.13(br m, 2 H, aromatic), 7.80-7.05(br m, 13H, aromatic), δ 6.48(br s, 1 H, aromatic), 1.39(br s, 18H, ^tBu), 0.95(br s, 18H, ^tBu). ^{13}C NMR ($CDCl_3$, 75 MHz). δ 164.8 (C=N imine), 150.1(py, *o*-C=N), 149.8(Ar-CH), 145.2 (Ar-CH), 140.8(Ar, *i*-C), 138.4(Ar-CH), 134.6(Ar-CH), 132.2(Ar, *i*-C), 131.4(Ar-CH), 130.1(Ar-CH), 129.4(Ar-CH), 128.6(Ar-CH), 125.6(Ar-^tBu, C-^tBu), 124.1(Ar-^tBu, C-^tBu), 36.7(Ar-^tBu, C-$(CH_3)_3$), 34.9(Ar-^tBu, C-$(CH_3)_3$), 31.6(Ar-^tBu, CH_3), 31.2(Ar-^tBu, CH_3). *Conformer B*: ^1H NMR ($CDCl_3$, 300 MHz): δ 8.63(br t, 1 H, py, *p*-CH), 8.46(br d , 2 H, py, *m*-CH), 7.80-7.05(br m, 16H, aromatic), 1.36(br s, 18H, ^tBu), 1.01(br s, 18H, ^tBu).^{13}C NMR ($CDCl_3$, 75 MHz). δ 162.1(C=N imine), 149.6(Ar-CH), 145.3(py, *o*-C=N), 142.7(Ar, *i*-C), 138.3(Ar-CH), 133.6(Ar-CH), 131.7 (Ar -CH), 130.6(Ar, *i*-C), 129.9(Ar-CH), 129.2(Ar-^tBu, C-^tBu),128.9(Ar-^tBu, C-^tBu), 126.9(Ar-CH), 124.8(Ar-CH), 121.1 (Ar-CH), 35.3(Ar-^tBu, C-$(CH_3)_3$), 34.5(Ar-^tBu, C-$(CH_3)_3$), 35.3(Ar-^tBu, CH_3), 30.9(Ar-^tBu, CH_3).A sample for elemental analysis was obtained by recrystallization in toluene, resulting in a 4:3 toluene adduct of **3.1**. Calculated for $[C_{47}H_{55}I_6Ga_2N_3]_3[C_7H_8]_4$: C 40.14, H 3.93, N 2.49, Found C 40.03, H 4.14, N 2.80.

Reaction of [2,6-bis{2,6-^{i}Pr$_2$C$_6$H$_3$N=CPh}$_2$(NC$_5$H$_3$)] (1B) and "GaI": "GaI" powder (65 mg, 0.331 mmol) was added to a clear yellow solution of **1B** (200 mg, 0.331 mmol) in 8 mL of toluene. The reaction mixture changed colour immediately from translucent yellow to a dark opaque red and was allowed to stir for 6 hours at room temperature. The reaction mixture was cooled to -20^{o}C and stored overnight. During this period a combination of bright yellow and red precipitate formed. The reaction mixture was filtered and the solid was washed with 10 x 2 mL hexanes then dried under vacuum to yield 160 mg of bright red powder mixed with yellow powder. Despite multiple attempts, these two compounds could not be completely isolated from each other. The red powder is poorly soluble and showed only very broad ^{1}H NMR signals. A combination of orange needle like crystals, and small red rectangular plate-like crystals suitable for X-ray diffraction were grown by diffusion of saturated solution of toluene in hexanes. The orange needle like crystals were identified as compound **3.2**, [2,6-{DippN=CPh}$_2$(NC$_5$H$_3$)]GaI$_2^+$GaI$_4^-$, and the red platelets as complex **3.3**, [2,6-{DippN=CPh}$_2$(NC$_5$H$_3$)]GaI$_2$. Solution state EPR of compound **3.3** provided an asymmetric triplet centered at 336.000 mT. The spectrum is shown in Figure 3.6.

(3.2) [2,6-bis{2,6-^{i}Pr$_2$C$_6$H$_3$N=CPh}$_2$(NC$_5$H$_3$)]GaI$_2$GaI$_4$: *Method 1:* Ga metal (80 mg, 1.15 mmol) and I$_2$ (437mg, 1.72 mmol) were added to a clear yellow solution of **1B** (347 mg, 0.659 mmol) in 15 mL of toluene. The reaction mixture immediately changed color resulting in a deep red solution. The reaction mixture was sealed and sonicated for 3 hours. During this period the solution became an intense opaque yellow/orange colored mixture. The solution was allowed to stir overnight, then filtered, washed with 5 x 2 mL hexanes, and allowed to dry under vacuum. A deep yellow-orange powder of **3.2** was isolated in 98% yield.

Method 2: GaI$_3$ powder (149 mg, 0.331 mmol) was added to a clear yellow solution of **1B**

(100 mg, 0.166 mmol) in 8 mL of toluene. The reaction mixture immediately changed color from translucent yellow to bright translucent red, which gradually become opaque and was sealed and allowed to stir for 6 hours. The reaction mixture was then cooled to -20^{o}C overnight, over which time an yellow-orange precipitate formed. The reaction mixture was filtered and the solid washed with 10 x 2 mL hexanes, and allowed to dry under vacuum. A pale yellow-orange powder of **3.2** was isolated in 92% yield. Yellow-orange needle like crystals of **3.2**, suitable for X-ray analysis, were grown by diffusion of saturated THF solution in hexanes.

^{1}H NMR ($CDCl_3$, 23^{o}C): δ 8.99(t, 1H, py, *p*-CH), 8.49(d, 2H, py, *m*-CH), 7.90-7.05(br m, 16H, aromatic), 3.00(v br s, 4H, *^{i}Pr-CH*), 1.24(br d, 12H, CH_3), 0.89(v br d, 12H, CH_3).^{13}C NMR ($CDCl_3$). δ 167.7(C=N imine), 148.9(py, *o*-C=N), 146.3(py, *m*-CH), 139.5(py, *p*-CH), 134.9(Ph, *o*-CH), 134.1(Ph, *m*-CH), 129.4(Ar-*^{i}Pr*, C-*^{i}Pr*), 129.2(Ar-*^{i}Pr*, CH), 128.9(Ph, *i*-C),128.6(Ph, *p*-CH), 125.7(Ar-*^{i}Pr*, C- *^{i}Pr*), 125.2(Ar-*^{i}Pr*, CH), 29.7(Ar-*^{i}Pr*,CH_3), 26.7(Ar-*^{i}Pr*, CH-$(CH_3)_2$), 24.3(Ar-*^{i}Pr*,CH_3). The sample for elemental analysis was obtained from recrystallization in toluene. Elemental analysis calculated for $[C_{43}H_{47}I_6Ga_2N_3]_3[C_7H_8]$ C 35.42, H 3.26, N 2.73, Found C 35.00, H 3.22, N 2.65.

[3.6] X-ray Crystallographic Information: Gallium Complexes

Table 3.1. Summary of Data Collection and Crystallographic Parameters for **3.1-3.3**.*

Compound	**3.1**	**3.2**	**3.3**
Empirical formula	$C_{47}H_{55}I_6Ga_2N_3$•$(CH_2Cl_2)_3$	$C_{43}H_{47}I_6Ga_2N_3$•(OC_4H_8)	$C_{43}H_{47}GaI_2N_3$
Formula weight	1562.83	1506.73	929.36
Temperature (K)	120(2)	209	202(2)
λ (Å)	0.71073	0.71073	0.71073
Crystal system	Monoclinic	Orthorhombic	Triclinic
Space group	P2(1)/n	P2(1)2(1)2(1)	P1
a (Å)	20.582(8)	10.647(3)	8.411(2)
b (Å)	16.057(7)	19.533(5)	9.720(2)
c (Å)	22.528(9)	27.369(7)	13.536(3)
α (deg)	90	90	76.463(4)
β (deg)	113.432(6)	90	78.265(4)
γ (deg)	90	90	67.402(4)
V ($Å^3$)	6831(5)	5692(3)	985.3(4)
Z	4	4	1
ρ (calc) (Mg/m^3)	1.868	1.842	1.566
μ (mm^{-1})	3.885	4.234	2.298
Absorption correction	Semi-empirical from equivalents		
Final R indices [I>2σ(I)]			
R1[a]	0.0638	0.0897	0.0738
*w*R2[b]	0.1792	0.2232	0.1589

[a] $R1 = \Sigma \left| |F_o| - |F_c| \right| / \Sigma |F_o|$. [b] $wR2 = \left(\Sigma w \left(|F_o| - |F_c| \right)^2 / \Sigma w |F_o|^2 \right)^{1/2}$

*structure files available from CCDC

Table 3.2: Selected bond lengths (Å) for compounds **3.1**-**3.3**.

3.1		**3.2**		**3.3**	
C(15)-C(22)	1.493(8)	C(13)-C(20)	1.48(3)	C(13)-C(20)	1.462(15)
C(26)-C(27)	1.495(9)	C(24)-C(25)	1.50(3)	C(24)-C(25)	1.473(16)
C(25)-C(26)	1.384(10)	C(23)-C(24)	1.36(3)	C(20)-C(21)	1.3900
C(22)-C(23)	1.396(9)	C(20)-C(21)	1.36(3)	C(23)-C(24)	1.3900
C(24)-C(25)	1.384(10)	C(22)-C(23)	1.28(3)	C(21)-C(22)	1.3900
C(23)-C(24)	1.391(9)	C(21)-C(22)	1.46(3)	C(22)-C(23)	1.3900
Ga(1)-I(1)	2.5478(12)	Ga(1)-I(1)	2.512(3)	Ga-I(1)	2.5230(18)
Ga(1)-I(2)	2.5067(12)	Ga(1)-I(2)	2.538(2)	Ga-I(2)	2.562(2)
Ga(1)-N(1)	2.181(5)	Ga(1)-N(1)	2.214(17)	Ga-N(1)	2.171(13)
Ga(1)-N(2)	2.017(5)	Ga(1)-N(2)	2.022(16)	Ga-N(2)	1.952(6)
Ga(1)-N(3)	2.151(5)	Ga(1)-N(3)	2.189(17)	Ga-N(3)	2.334(13)
N(1)-C(6)	1.448(7)	N(1)-C(9)	1.52(3)	N(1)-C(6)	1.433(14)
N(3)-C(34)	1.449(8)	N(3)-C(32)	1.48(2)	N(3)-C(37)	1.426(14)
N(1)-C(15)	1.278(8)	N(1)-C(13)	1.27(3)	N(1)-C(13)	1.318(17)
N(3)-C(27)	1.296(8)	N(3)-C(25)	1.36(3)	N(3)-C(25)	1.321(18)
N(2)-C(26)	1.344(8)	N(2)-C(24)	1.31(2)	N(2)-C(24)	1.3900
N(2)-C(22)	1.323(8)	N(2)-C(20)	1.38(3)	N(2)-C(20)	1.3900

Table 3.3: Selected bond angles (°) for compounds **3.1**-**3.3**.

3.1		**3.2**		**3.3**	
N(2)-Ga(1)-N(3)	76.2(2)	N(2)-Ga(1)-N(3)	75.2(6)	N(2)-Ga-N(3)	75.9(4)
N(2)-Ga(1)-N(1)	75.3(2)	N(2)-Ga(1)-N(1)	76.0(6)	N(2)-Ga-N(1)	77.6(4)
N(2)-Ga(1)-I(2)	143.80(15)	N(2)-Ga(1)-I(2)	95.9(4)	N(2)-Ga-I(2)	103.2(3)
N(2)-Ga(1)-I(1)	100.25(15)	N(2)-Ga(1)-I(1)	144.7(4)	N(2)-Ga-I(1)	143.8(3)
N(2)-C(22)-C(23)	121.7(6)	N(2)-C(20)-C(21)	118.3(19)	N(2)-C(20)-C(21)	120.0
N(2)-C(26)-C(25)	120.7(6)	N(2)-C(24)-C(23)	121.6(18)	N(2)-C(24)-C(23)	120.0
N(2)-C(22)-C(15)	113.3(5)	N(2)-C(20)-C(13)	114.2(18)	N(2)-C(20)-C(13)	112.4(7)
N(2)-C(26)-C(27)	113.7(6)	N(2)-C(24)-C(25)	112.8(18)	N(2)-C(24)-C(25)	115.1(7)
N(1)-C(15)-C(22)	115.3(5)	N(1)-C(13)-C(20)	115.1(19)	N(1)-C(13)-C(20)	116.7(12)
N(3)-C(27)-C(26)	114.2(5)	N(3)-C(25)-C(24)	113.5(16)	N(3)-C(25)-C(24)	116.1(12)
N(1)-C(15)-C(21)	126.4(6)	N(1)-C(13)-C(14)	128(2)	N(1)-C(13)-C(19)	126.1(12)
N(3)-C(27)-C(33)	126.9(6)	N(3)-C(25)-C(26)	122.5(18)	N(3)-C(25)-C(31)	125.3(13)
C(34)-N(3)-Ga(1)	123.2(4)	C(32)-N(3)-Ga(1)	125.8(12)	C(37)-N(3)-Ga	129.7(9)
C(6)-N(1)-Ga(1)	123.3(4)	C(9)-N(1)-Ga(1)	123.7(13)	C(6)-N(1)-Ga	128.3(8)
C(15)-N(1)-Ga(1)	114.4(4)	C(13)-N(1)-Ga(1)	114.2(14)	C(13)-N(1)-Ga	111.3(9)
C(27)-N(3)-Ga(1)	115.5(4)	C(25)-N(3)-Ga(1)	113.1(12)	C(25)-N(3)-Ga	110.0(10)
C(15)-N(1)-C(6)	122.0(5)	C(13)-N(1)-C(9)	120.3(18)	C(13)-N(1)-C(6)	119.6(12)
C(27)-N(3)-C(34)	121.2(5)	C(25)-N(3)-C(32)	121.0(16)	C(25)-N(3)-C(37)	119.8(12)
C(22)-C(15)-C(21)	118.3(5)	C(20)-C(13)-C(14)	117(2)	C(20)-C(13)-C(19)	117.2(10)
C(33)-C(27)-C(26)	118.9(6)	C(24)-C(25)-C(26)	124.0(17)	C(24)-C(25)-C(31)	118.4(11)
C(22)-N(2)-Ga(1)	118.5(4)	C(20)-N(2)-Ga(1)	115.0(13)	C(20)-N(2)-Ga	117.3(4)
C(26)-N(2)-Ga(1)	117.5(5)	C(24)-N(2)-Ga(1)	118.5(13)	C(24)-N(2)-Ga	119.5(4)
C(22)-N(2)-C(26)	121.0(6)	C(20)-N(2)-C(24)	121.3(17)	C(20)-N(2)-C(24)	120.0

[3.7] Computational Evaluation for Disproportionation Reaction

Both the thermochemical analysis of the disproportionation reaction of 2,6-{DippN=CPh}2(NC_5H_3)]GaI in the presence of GaI and the optimization of compound **3.2** were performed with DFT calculations and the B3LYP functional using the Gaussian 03 (revision D.01) suite of programs.[44] The basis set DGDZVP was employed. The compounds and atom in equation 1 were optimized and the results presented in Table 3.4. The enthalpy of atomization for Ga of 276kJ/mol = 0.10518 au/atom was used to calculate the net reaction enthalpy. This data provides a net reaction enthalpy of -0.108552 au = -4.73259 x 10-22 kJ or -28.5003 kJ/mole.

$$[2,6\text{-}\{DippN{=}CPh\}_2(NC_5H_3)]GaI + 5GaI \rightarrow [2,6\text{-}\{DippN{=}CPh\}_2(NC_5H_3)]GaI_2^+ + GaI_4^- + 4Ga(0)_s \quad (\mathbf{1})$$

Table 3.4: Energies of the species in eq. **1** obtained by computation.

Compound Energy (atomic units)	**Compound Energy (atomic units)**
[2,6-{DippN=CPh}$_2$(NC_5H_3)]GaI	-10675.7050987
GaI	-8844.4058746
[2,6-{DippN=CPh}$_2$(NC_5H_3)]GaI_2^+	-17595.430207
GaI_4^-	-29604.2606012
$4Ga(0)_s$	-1924.4328944 - 0.42060

[44] Gaussian 03, Revision D.01, M. J. Frisch, G. W. Trucks, H. B. Schlegel, G. E. Scuseria, M. A. Robb, J. R. Cheeseman, J. A. Montgomery, Jr., T. Vreven, K. N. Kudin, J. C. Burant, J. M. Millam, S. S. Iyengar, J. Tomasi, V. Barone, B. Mennucci, M. Cossi, G. Scalmani, N. Rega, G. A. Petersson, H. Nakatsuji, M. Hada, M. Ehara, K. Toyota, R. Fukuda, J. Hasegawa, M. Ishida, T. Nakajima, Y. Honda, O. Kitao, H. Nakai, M. Klene, X. Li, J. E. Knox, H. P. Hratchian, J. B. Cross, C. Adamo, J. Jaramillo, R. Gomperts, R. E. Stratmann, O. Yazyev, A. J. Austin, R. Cammi, C. Pomelli, J. W. Ochterski, P. Y. Ayala, K. Morokuma, G. A. Voth, P. Salvador, J. J. Dannenberg, V. G. Zakrzewski, S. Dapprich, A. D. Daniels, M. C. Strain, O. Farkas, D. K. Malick, A. D. Rabuck, K. Raghavachari, J. B. Foresman, J. V. Ortiz, Q. Cui, A. G. Baboul, S. Clifford, J. Cioslowski, B. B. Stefanov, G. Liu, A. Liashenko, P. Piskorz, I. Komaromi, R. L. Martin, D. J. Fox, T. Keith, M. A. Al-Laham, C. Y. Peng, A. Nanayakkara, M. Challacombe, P. M. W. Gill, B. Johnson, W. Chen, M. W. Wong, C. Gonzalez, and J. A. Pople, Gaussian, Inc., Wallingford CT, 2004.

Chapter 4: *Thallium(I) and Arene Interactions*

[4.1] Introduction

With a similar covalent radius to indium (1.42Å for In vs 1.45Å for Tl)[45] and commercial availability of analogous triflate starting material (TlOTf), thallium presented a logical progression in our study of low valent group 13 metal reactivity with the bis(imino)pyridine ligand framework. However, unlike In(I), due to inert pair and relativistic effects, thallium has a preference for the +1 oxidation state over the standard +3 observed for the rest of group 13.[46] This increased stability, coupled with near identical charge and radii makes for a compelling contrast to our previous efforts with In(I). Most importantly, it allows us to assess potential weak covalent bonding interactions in an identical system which does not suffer from the strong tendency towards disproportionation as observed in the In(I) systems. Furthermore, we were pleased to find that there were no known bis(imino)pyridine complexes of thallium(I). In fact, and likely due to its toxicity, the body of literature for coordination chemistry of thallium was on the whole quite bare.

Scheme 4.1

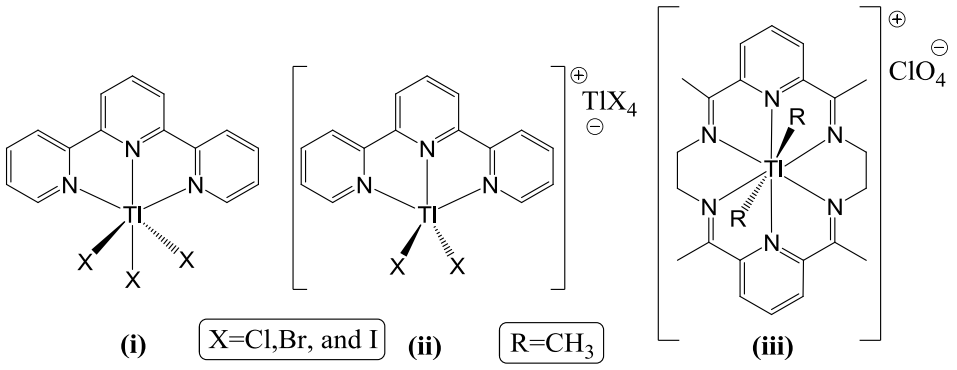

[45] B. Cordero, V.Gómez, A. E. Platero-Prats, M. Revés, J. Echeverría, E. Cremades, F. Barragán and S. Alvarez, *Dalton Trans.*, **2008**, 2832.

[46] G.L. Miessler, D.A. Tarr, Inorganic Chemistry, 3rd ed., Pearson Prentice Hall, **2004**.; Inert pair effect: a metal has an oxidation state that is 2 less than the traditional American group number (group 13 is also refered to as Group IIIA).

The closest compounds we have found to our targeted thallium(I) bis(imino)pyridine complexes are the tripyridine thallium(III) halide derivatives of the form (**i**) and (**ii**) as shown in Scheme 4.1. Ligand geometry is terdentate effectively forming pincer-type complexes. Both monomeric (**i**) and bimetallic cation/anion pairs (**ii**) are observed (as seen with our gallium chemistry). [47] Perhaps the closest to our target bis(imino)pyridine system is the macrocyclic Tl(III) complex (**iii**) reported by Kawasaki *et al*. The complex is essentially two bis(imino)pyridine ligands bound in terdentate fashion, and tethered via the imine functionalities by ethyl groups. The complex is cationic with a perchlorate counterion.[48] These complexes, although similar in their use of N-bound pincer ligands, feature thallium(III) instead of our target thallium(I) species. Furthermore, it has been over 30 years since these complexes have been reported, and no significant strides towards analogous thallium(I) coordination chemistry has been made. Our goal is to synthesize, characterize, and study the bonding features of bis(imino)pyridine complexes of thallium(I).

A growing trend in thallium chemistry over the past twenty years has been the study of thallium arene complexes. Although transition metal arene π-complexes are very common, examples of the main group elements, and particularly of thallium are fairly scarce. Even though these complexes have been known in the literature for over 40 years, it was not until the work of Schmidbaur in 1985 that they were finally crystallographically authenticated.[49] The tetra-gallate cluster (Scheme 4.2 (**i**)) was originally reported in 1968 by Auel *et al*, but structure was never confirmed.[50] The structure features two five coordinate Tl centres interacting with two arene groups, and two seven coordinate Tl centres interacting with single arene groups respectively.

[47] (a) R.A. Walton, *Inorg. Chem*., **1968**, 7, 4, 640., (b) R.A. Walton, *J. Inorg. Nucl. Chem*., **1970**, 32, 2875.
[48] Y. Kawasaki, N. Okuda, *Chem. Lett*., **1982**, 1161.
[49] H. Schmidbaur, W. Bublak, J. Riede, G. Müller *Angew. Chem. Int. Ed. Engl.* **1985**, 24, 414.
[50] Th. Auel, E. L. Amma, *J. Am. Chem. Soc.*, **1968**, *90*, 21, 5941.

The structure is supported by four tetrahedral $GaBr_4$ sites. Since then there have been multiple advances in the development of Tl-arene π-coordination chemistry. The most noteable examples come from the Dias (Scheme 4.2 (**ii**)) and Bochmann groups (scheme 4.2 (**iii**).

Scheme 4.2

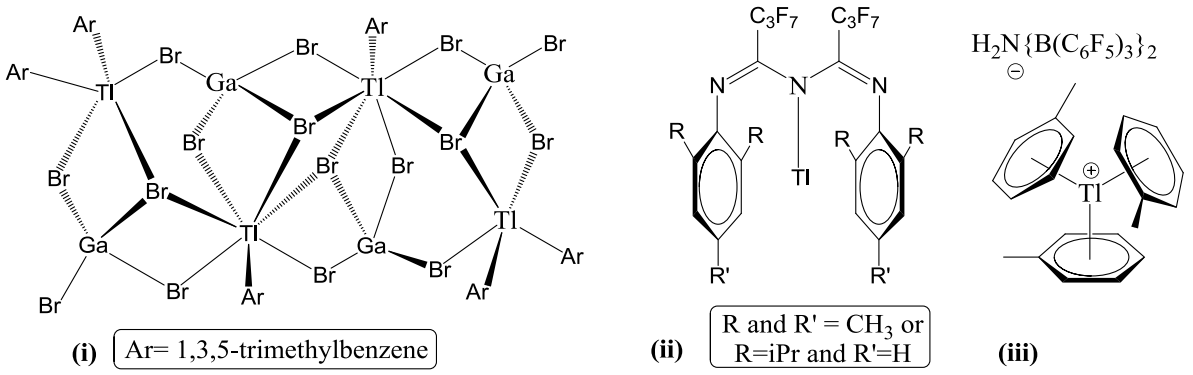

As shown in Scheme 4.2, compound (**ii**) features an anionic triamide ligand N-bound to Tl which undergoes π-interaction with pendant ligand arene groups.[51] The presence of pendant arene arms is not unlike those available on our bis(imino)pyridine ligand (two Ph groups as well as substituted N-aryl groups). The availability of multiple arene sites on our ligand makes it amenable towards either intramolecular or intermolecular interactions with the Tl centre. Recent work from the Bochmann group has shown that the use of bulky, weakly coordinating anions ($H_2N\{B(C_6F_5)_3\}_2^-$) allow for strong Tl-arene π interactions, with no anion contact points. This has lead to the isolation of various sandwhich and tri-arene complexes (Scheme 4.2 (**iii**)).[52] Although the triflate group we intend to use does not bear the same level of steric bulk as the anions used by the Bochmann group, our work with indium shows sufficiently weak binding

[51] H.V.R. Dias, S. Singh, T.R. Cundari, *Angew. Chem., Int. Ed.* **2005**, *44*, 4907.

[52] (a) Y. Sarazin, D.L. Hughes, N. Kaltsoyannis, J.A. Wright, M. Bochmann, *J. Am. Chem. Soc.*, **2007**, *129*, 881, (b) Y. Sarazin, N. Kaltsoyannis, J.A. Wright, M. Bochmann, *Organometallics*, **2007**, *26*, 1811.

character to afford strong parallels to the Bochmann system. The presence of multiple arenes on our bis(imino)pyridine ligand, in conjunction with the weakly coordinating anion (OTf^-) should provide for a compelling study of both Tl-ligand, as well as Tl-arene π-interaction.

[4.2] Results and Discussion Part A: Synthesis and Structure of Tl(I) Bis(imino)pyridines

Reaction of soluble $Tl(O_3SCF_3)$ with ligands **1A** and **1C**, shown in Scheme 4.3, lead to the first Tl complexes of these ligands as bright yellow species **4.1** (71%) and **4.2** (84%). Microanalyses and NMR spectroscopy support the formation of the targeted Tl-ligand complexes, $[\{ArN{=}CPh\}_2(NC_5H_3)]Tl^+$ (Ar = 2,5-^{t}Bu$_2$C$_6$H$_3$ and 2,6-^{i}EtC$_6$H$_3$ respectively). The identity and detailed structural features of these compounds were documented by single crystal X-ray analysis with the results summarized in Figures 4.1, 4.2 and Tables 4.3 and 4.4. Compound **4.1** displayed the expected ligand array of coplanar N centres with the Tl(I) residing 1.27Å out of the mean plane defined by N1, N2, and N3. The metal centre is symmetrically positioned in the ligand cleft with a Tl-$N_{pyridine}$ distance of 2.646(6)Å, and both of the Tl-N_{imine} distances longer than 2.73Å, which is greater than the sum of the covalent radii for Tl (1.45Å) and N (0.71Å).[45] The shortest contact to the triflate anion is via an O atom, with a Tl-O1 distance of approximately 2.93Å.

Similarly, compound **4.2** displayed the expected ligand array of coplanar N centres and with the Tl(I) residing only about 0.8Å out of the mean plane defined by N1, N2, and N3. The metal centre is symmetrically positioned in the ligand cleft with all of the Tl-N distances longer than 2.73Å, which is greater than the aforementioned sum of the covalent radii.The shortest contact to the thallium centre is to an O atom of the triflate counterion, Tl-O1 = 2.613(2)Å. The effects of variation on the steric load of the NAr moieties of the ligand were revealed by the

distortions observed in the structure of **4.1** relative to compound **4.2**. The two N_{imine} centres (N1, N3) are twisted in the same direction and out of planarity with the N_{py} (N2) centre in **4.1**. The triflate anion is considerably further removed and the shortest Tl-O distance is increased by >0.3Å. The Tl centre in **4.1**, while still positioned symmetrically with respect to the ligand, is slightly closer to the N_{py} at 2.646(6)Å.

Scheme 4.3

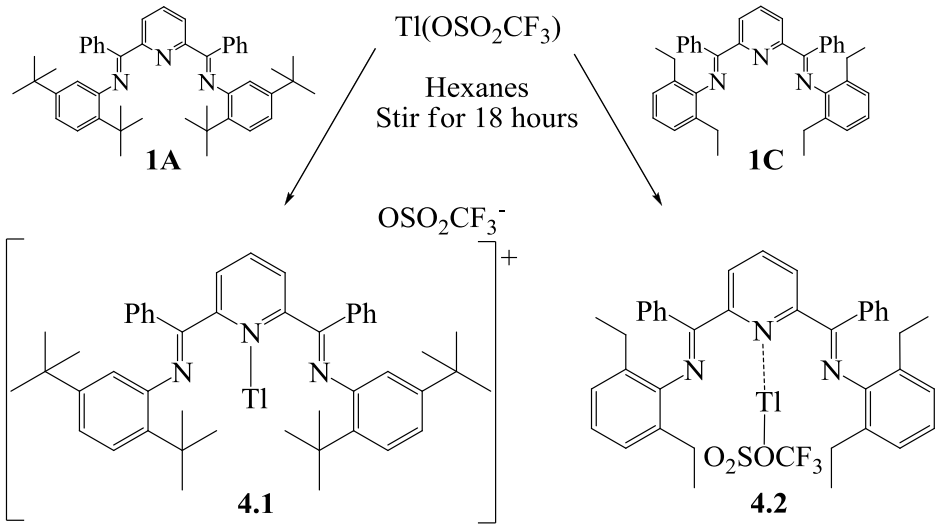

The most direct comparisons for the Tl(I)-nitrogen distances in **4.1** and **4.2** are with anionic polydentate tris(pyrazolyl)borate species. These compounds display shorter mean Tl-N distances of 2.63Å.[53] Thallium-amido distances show, as expected, considerably shorter bond distances. For example, monomeric methyl(aryl)amido, [TlN(Me)Ar] (Ar = (2,6-Mes_2C6H3) had a Tl-N distance of 2.364(3)Å.[54] The gas-phase monomer $TlN(SiMe_3)_2$ displayed a Tl-N distance of 2.15(1)Å and the the mononuclear thallium(I) 1,5-diaryl-1,3,5-triazapentadienides possessed average Tl-N distances of 2.67Å.[51,55]

[53] H.V.R. Dias, *Comprehensive Coordination Chemistry II*, **2004**, 3, 383.
[54] R.J. Wright, M. Brynda, P.P. Power *Inorg. Chem.* **2005**, *44*, 3368.
[55] K.W. Klinkhammer, S.J. Henkel, *Organomet. Chem.,* **1994**, 480, 167.

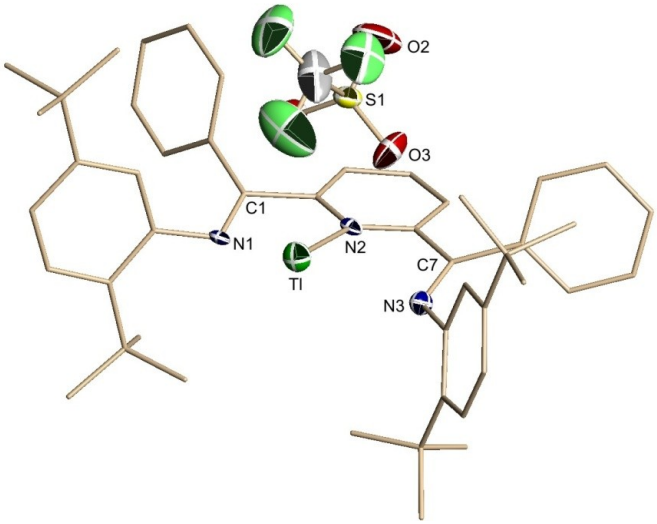

Figure 4.1: X-ray structure of compound **4.1** with hydrogen atoms and ether molecule omitted for clarity. Select bond lengths and angles are given in Tables 4.3 and 4.4.

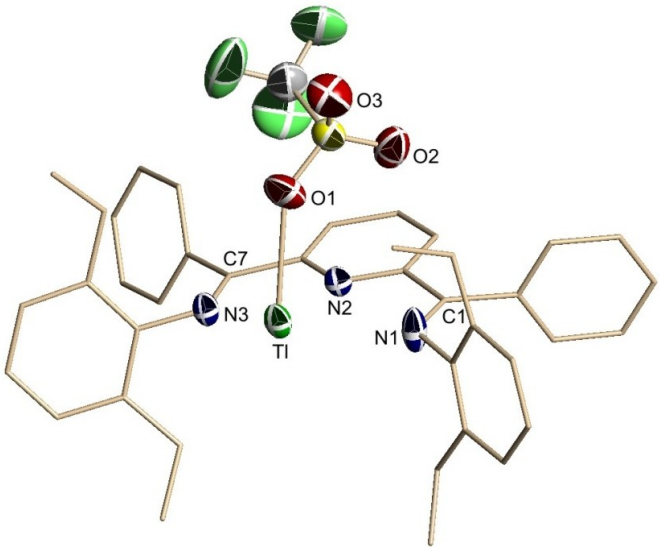

Figure 4.2: X-ray structure of compound **4.2** with hydrogen atoms and ether molecule omitted for clarity. Select bond lengths and angles are given in Tables 4.3 and 4.4.

Computational Studies: Computations offer a unique, and perhaps sole method to interrogate the metal-ligand interactions. Under a collaboration with Dr. Serge Gorelsky, a DFT computational study with the B3LYP functional and the mixed TZVP/LANL2DZ basis set was

undertaken to obtain a thorough understanding of the electronic nature of the Tl[bis(imino)pyridine]$^+$ cations and the interactions of the cation with the OTf$^-$ anion in compounds **4.1** and **4.2**. Electronic structure optimizations for compounds **4.1** and **4.2** gave molecular structures that were in agreement with experiment. The cation-anion interaction energy for **4.2** was determined to be -79.5kcal/mol with a bond order of only 0.20. Importantly, this interaction was equally distributed between the Tl and bis(imino)pyridine ligand. Turning attention to the interactions within the [{ArN=CPh}$_2$(NC_5H_3)]Tl$^+$ cation, the energy of the Tl-ligand interaction was found to be -64.4kcal/mol. Only a small part of this was bonding in nature and the computed bond orders of Tl and the N_{imine} centers were only 0.08 and with the N_{py} only 0.12. This overall bond order of only 0.28 is considerably less than a single bond and is dispersed over three sites and is consistent with the experimental observations. The bonding between the Tl(I) and ligand **1A** in compound **4.1** is very similar with a total value of only 0.24. The cation/ligand bonding in compounds **4.1** and **4.2** are less than half of that observed for the In analogues, [{ArN=CPh}$_2$(NC_5H_3)]In$^+$ (See Chapter 2).

[4.3] Results and Discussion Part B: Thallium Dimer Formation

A closer inspection of the structure of **4.2** exposed an expanded intermolecular relationship involving a Tl(I) cation-arene interaction between two of the [bis(imino)pyridine]Tl$^+$ cations and is represented in Figure 4.3. This feature positions the Tl$^+$ of one species at a distance of 3.4 Å over the N-Ar group of a neighboring cation. Likely due to the larger steric profile of the ^tBu substituted aryl group, an analogous intermolecular interaction was not observed in **4.1**. Thallium has established arene interactions. Given the fact that the bonding of the Tl$^+$ centre with the bis(imino)pyridine ligand **1C** and the triflate anion had been established as weak, a computational examination of this intermolecular cation-π interaction was investigated by a DFT computational optimization with the B3LYP functional and a TZVP/LANL2DZ basis set. In fact,

this "dimer" is very weakly bound with an interaction energy of only -1.9kcal/mol. This slight level of electron transfer involved a 6p type Tl accepting orbital. For comparison, the intramolecular Tl-arene interactions in monomeric methyl(aryl)amido, [TlN(Me)(2,6-$Mes_2C_6H_3$)] involved a pendant aryl moiety with a Tl-centroid distance of 3.026(2) Å and very low interaction energy of only -3 kcal/mol.[54] Similar Tl(I)-arene features were observed in mononuclear thallium(I) 1,5-diaryl-1,3,5-triazapentadienides ($TlN[C(C_3F_7)NAr]_2$; Ar = mesityl, 2,6-diisopropylphenyl), which exhibited an average Tl-centroid distance of 3.09Å.[55] A DFT study on these later species, gave an interaction energy of -13 kcal/mol with three MOs displaying significant interactions and involving considerable contributions from the Tl 6s orbital. The cation-π interaction that we have observed for **4.2** is currently the weakest reported crystallographically observed Tl-arene interaction.

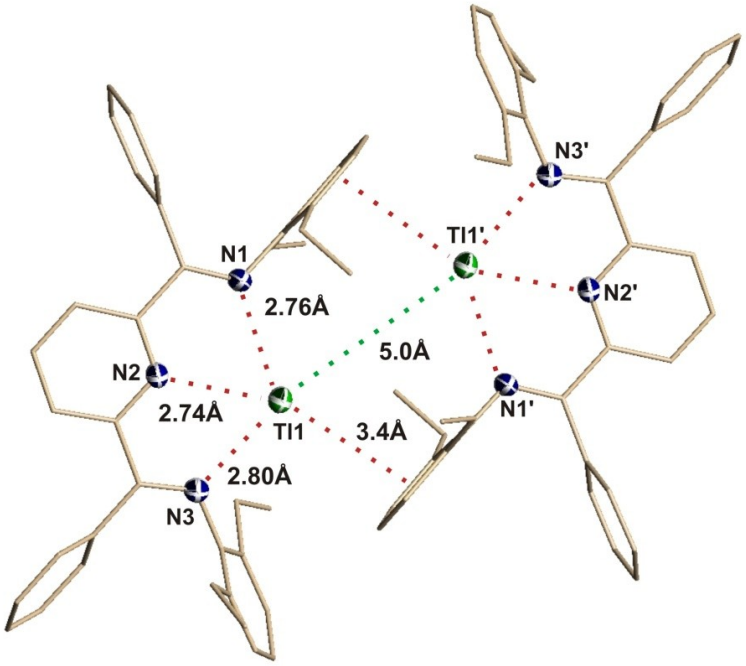

Figure 4.3: Expanded packing of the X-ray structure of **4.2** showing dimer formation via Tl-arene interactions. Hydrogen atoms and triflate anion are omitted for clarity.

[4.4] Results and Discussion Part C: Thallium Arene Interactions

In an effort to probe the capability and nature of these very weak cation/arene features, compound **4.1** was crystallized from benzene and toluene. Both of these solvents yielded Tl-arene adducts (**4.3** and **4.4** for benzene and toluene) as described in Scheme 4.4. Corresponding X-ray structures are reported in Figures 4.4 and 4.5. Upon closer structural investigation, expanded packing arrangements reveal inverted sandwich (metal–ligand–metal) structures with $[\{(2,5\text{-}^{t}Bu_2C_6H_3)N{=}CPh\}_2(NC_5H_3)]Tl^+$ cations bridged by either benzene or toluene as represented in Figure 4.6. The disposition of the Tl and bis(imino)pyridine ligand, as well as the Tl-N distances are similar to that observed in the parent species **4.1** (Tables 4.3 and 4.4). Average Tl-O distances of 2.87Å are shorter than those observed in **4.1** (2.93Å). Most interesting is the symmetrically bonded arene that resides between two Tl(I) centres with an inverted sandwich relationship/arrangement as shown in Figure 4.6 (a similar arrangement is also observed for **4.3**). The Tl-centroid distances of 3.33Å and 3.30Å for **4.3** and **4.4** respectively, suggests a weak Tl-arene interaction.

Scheme 4.4

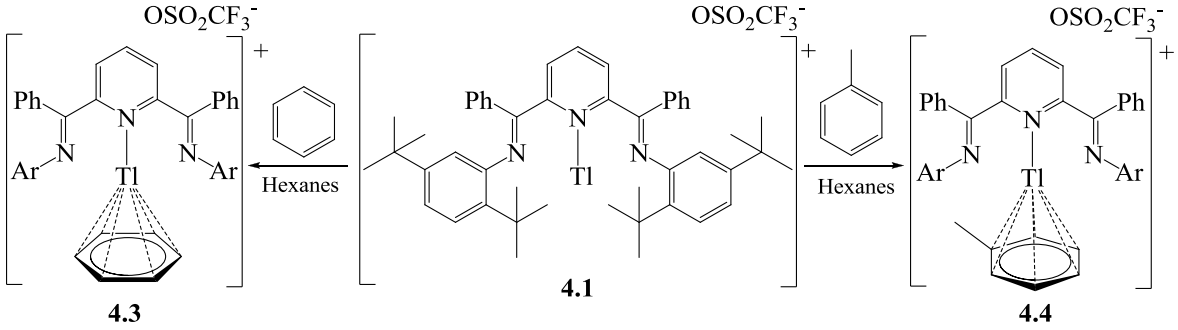

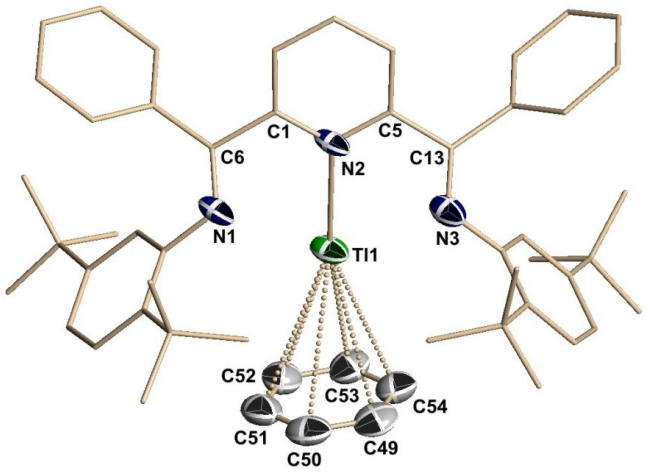

Figure 4.4: X-ray structure of compound **4.3** with hydrogen atoms and triflate anion omitted for clarity. Select bond lengths and angles are given in Tables 4.3 and 4.4.

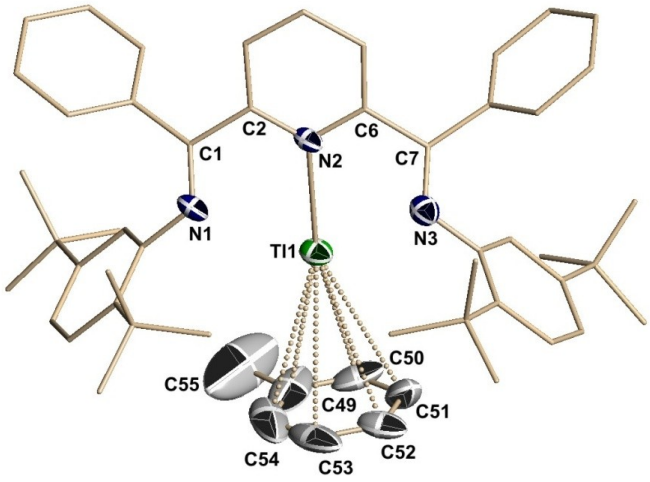

Figure 4.5: X-ray structure of compound **4.4** with hydrogen atoms and triflate anion omitted for clarity. Select bond lengths and angles are given in Tables 4.3 and 4.4.

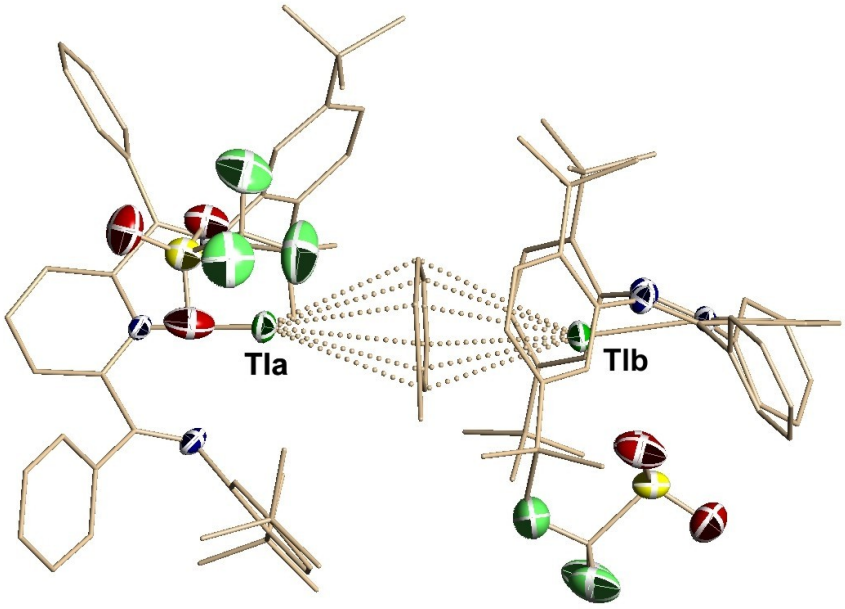

Figure 4.6: Expanded packing arrangement in the X-ray structure of **4.4** highlighting the inverted sandwhich (metal-arene-metal) geometry. Hydrogen atoms are ommited for clarity. A similar arrangement is observed for **4.3**.

Computational Studies: Computational analysis offers the only way to really probe the relationship between the thallium cation and the bridging arene; however, when using a conventional functional such as B3LYP this structurally characterized species separated into fragments. Turning to the CAM-B3LYP functional and using the mixed TZVP/LANL2DZ basis set, successful optimization was achieved on the full experimental structure **4.3** (Figure 4.6) including the triflate anions.[56] The fragment interactions between the neutral benzene and the two $[\{(2,5\text{-}^{t}Bu_2C_6H_3)N{=}CPh\}_2(NC_5H_3)]Tl^{+}(OTf)^{-}$ displayed an interaction energy of -4.8kcal/mol, bond order = 0.02, with a charge donation of only 0.02 electrons. Comparing with the recently reported Tl(I)-arene $[Tl(PhMe)_3]^{+}$ species (Scheme 4.2 (**ii**)) which show no close

[56] CAM-B3LYP is a "long-range corrected functional" provided in the Gaussian 09 suite. It effectively handles weak dispersion type interactions which fall below the threshold supported by the standard B3LYP functional.

contacts with anions and only Tl-arene interactions, reveals an average Tl-centroid distance of 2.97Å. DFT analysis on these compounds provided Mulliken charge of the Tl atom in the cation $[Tl(PhMe)_3]^+$ is 0.90, and the total interaction energy relative to Tl^+ and three free toluene molecules is -221 kJ mol^{-1} (73.7 kJ or 17.6 kcal/mol per Tl-arene), three MOs of the cation have low, but significant, Tl 6s contribution.[52] By comparison, our reported Tl-arene interactions are significantly weaker with an interaction energy of just -4.8kcal/mol.

[4.5] Results and Discussion Part D: Arene Interactions with Inverted Quadrupole

An additional probe of the nature of the Tl-arene interaction was attempted by crystallizing compound **4.1** from hexafluorobenzene. In hexafluorobenzene, the quadrupole moment is inverted relative to benzene, as is graphically illustrated in Figure 4.7. The electron density is situated on the fluoride groups along the ring periphery, as opposed to benzene, for which the bulk of negative charge is situated on the carbon atoms of the ring. The resulting crystallization product **4.5** is simply component **4.1** and two hexafluorobenzene groups co-crystallized, with no evidence of interaction with each other, as is illustrated in Figure 4.8(a). Upon closer inspection, and removal of **4.1** to improve clarity, expanded packing reveals an extended network of long-range interaction between the hexafluorobenze molecules (Figure 4.8(b)). Molecule orientation displays side-on arrangement whereby the δ- fluorine groups point towards the centre of the δ+ arene ring of neighbouring hexafluorobenzene molecules. It is a point of interest to note that these systems, although predisposed to weak interactions prefer to co-crystallize independently rather than show any sign of interaction with each other.

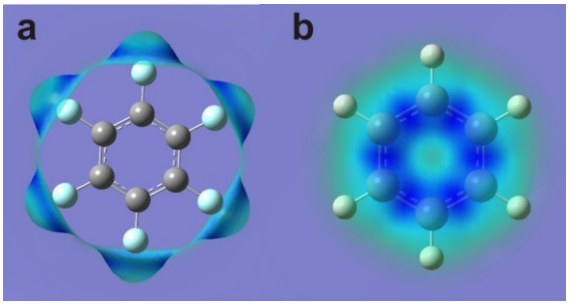

Figure 4.7: Isosurface representations of (**a**) hexafluorobenzene and (**b**) benzene, generated with Gaussian 09 utilizing B3LYP with the DGTZVP basis set.

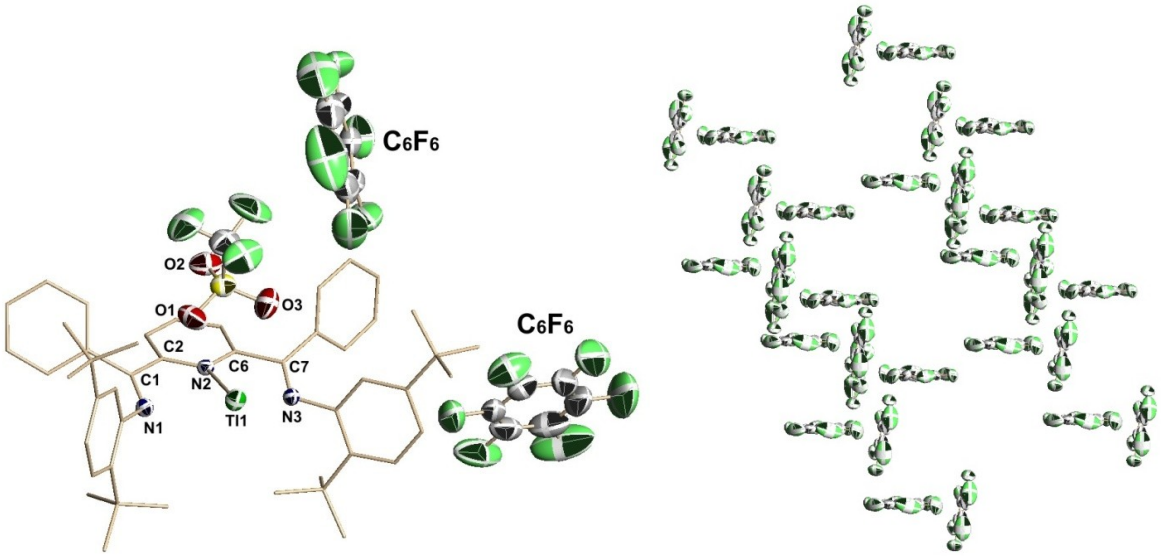

(a) **(b)**

Figure 4.8: (**a**) X-ray structure of compound **4.5** highlighting the non-interacting cocrystalization of **4.1** with two molecules of hexafluorobenzene. Hydrogen atoms are ommited for clarity. (**b**) Expanded packing arrangement of hexafluorobenzene molecules within the X-ray structure of **4.5**, thallium complex ommited for clarity.

[4.6] Conclusion

The first reported ligation of Tl^{+} with bis(imino)pyridine yielded unique complexes of Tl. These complexes feature unprecedentedly weak ligand-metal covalent interactions, surpassing

even our initial findings with In(I) (Chapter 2). The resulting Tl complexes behave as naked Tl^+ cations in a ligand cage. As per recent trends in thallium coordination chemistry, our complexes can also be stabilized via Tl-arene interactions. Isolation of dimeric species in reduced ligand steric environments (**4.2**), or inverted sandwhich (metal-arene-metal) bimetallic complexes under greater steric encumbrance revealed new examples of Tl-arene interactions (**4.3** and **4.4**). Long interaction distances as observed from X-ray structure, coupled with advanced DFT computations revealed these Tl-arene interactions to be the weakest reported to date. This further supports our theme of naked metal cations in essentially non-interacting ligand frameworks.

[4.7] Thallium Complex Experimental

General Methods. Reactions were performed in a glovebox with a nitrogen atmosphere. All solvents were sparged with nitrogen and then dried by passage through a column of activated alumina using an apparatus purchased from Anhydrous Engineering. Deuterated toluene was dried using activated molecular sieves. Thallium triflate was purchased from Strem Chemicals and used as received. All other chemicals were purchased from Aldrich and used without further purification. NMR spectra were run on a Bruker Avance 300 MHz spectrometer with C_7D_8 as solvent and internal standard. Elemental analyses for **4.1** and **4.2** were performed by Midwest Microlab LLC, Indianapolis IN.

Note on working with Thallium compounds: Due to the well established toxicity of thallium in the +1 oxidation state, care must be taken to prevent introduction into the body by inhalation, accidental ingestion through contaminated hands or gloves, or through the skin.[57] All thallium reagents and wastes, including contaminated solvents, were handled using multi-glove and

[57] S. Galvan-Arzate, A. Santamaria, *Toxicol. Lett.* **1998**, *99*, 1.

secondary containment procedures. All wastes were disposed of in accordance to government regulations.

(4.1) [Tl-2,6-Bis{1-[(2,5-ditertbutylphenyl)imino]-benzyl}pyridine][OSO_2CF_3]: $TlOSO_2CF_3$ powder (51 mg, 0.145 mmol) was added to a clear yellow solution of **1A** (100 mg, 0.151 mmol) in 5 mL of hexanes. The reaction mixture was sealed and allowed to stir for 18 h. The solution remains opaque yellow throughout. The solution was then held at -30°C for 24 h, and a bright yellow precipitate formed. This solution was filtered, and the precipitate was washed with 5 x 2 mL hexanes, and allowed to dry under vacuum, resulting in the isolation of a bright yellow powder in 71% yield. Bright yellow rod-like crystals suitable for X-ray analysis were grown by evaporation from cold ether at -30°C for several days. Furthermore, no evidence of decomposition of **4.1** is observed. ^{1}H NMR (C_6D_6, 23°C): δ 8.26-6.73(br m, 19 H, aromatic), 1.53(br s, 18H, *^{t}Bu*), 1.15(br s, 18H, *^{t}Bu*). ^{13}C NMR (C_6D_6, 23°C). δ 167.8(C=N imine), 157.7(py, *o*-C=N), 150.2(py, *m*-CH), 147.9(py, *p*-CH), 139.6(Ar-*^{t}Bu*, *i*-C), 138.7(Ph, *o*-CH), 136.2(Ar-*^{t}Bu*, *o*-CH), 131.1(Ph, *i*-C), 130.3(Ar-*^{t}Bu*, *p*-CH), [*(Ph, p-CH) and (Ar-^{t}Bu, m-C) are obscured by C_6D_6 peak 128-130ppm*], 126.7(Ar-*^{t}Bu*, *m*-CH), 122.7(Ph, *m*-CH), 120.4(Ar-*^{t}Bu*, *o*-C), 35.8(Ar-*^{t}Bu*, CH_3), 34.9(Ar-*^{t}Bu*, CH_3), 31.7(Ar-*^{t}Bu*, CH_3), 31.2(Ar-*^{t}Bu*, CH_3). Elemental analysis for $C_{48}H_{55}F_3TlN_3O_3S$ Calculated: C, 56.78; H, 5.46; N, 4.14 Found: C, 55.93; H, 5.33; N, 3.93.

(4.2) [Tl-2,6-Bis{1-[(2,6-diethylphenyl)imino]-benzyl}pyridine][OSO_2CF_3]: $TlOSO_2CF_3$ powder (63 mg, 0.178 mmol) was added to a clear yellow solution of **1C** (100 mg, 0.182 mmol) in 5 mL of hexanes. The reaction mixture was sealed and allowed to stir for 18 h. The solution remains opaque yellow throughout. The solution was then held at -30°C for 24 h, and a bright yellow precipitate formed. This solution was filtered, and the precipitate was washed with 5 x 2

mL hexanes, and allowed to dry under vacuum, resulting in the isolation of a bright yellow powder in 84% yield. Bright yellow rod-like crystals suitable for X-ray analysis were grown by evaporation from cold ether at -30^{o}C for several days. Crystallization yields a near 50:50 mix of bright yellow crystals corresponding to **4.2**, as well as pale yellow needles corresponding to free ligand **1C** as a result of product decomposition. NMR experiments were conducted in C_7D_8 as the complex appears to be stable in toluene over the time period required to obtain adequate spectra. However, two distinct conformers (*i* and *ii*) of **4.3** are observed, with *conformer i* being predominant, the respective peaks are tentatively assigned: ^{1}H NMR (C_7D_8, 23^{o}C): δ 8.35(br s, 1H, Ar-H, *Conformer ii*), 8.25(br s, 1H, Ar-H, *Conformer i*), 7.98(br s, 4H, Ar-H, *Conformer i*), 7.73-7.10(br m, 11H$_i$, 15H$_{ii}$, Ar-H, *Conformers i and ii*), 6.98-6.79 (br m, 4H, Ar-H, *Conformers i and ii*), 3.04(br m, 4H, -CH_2, *Conformer i*), 2.91(br m, 4H, -CH_2, *Conformer ii*), 2.69(br m, 4H, -CH_2, *Conformer i*), 2.45(br m, 4H, -CH_2, *Conformer ii*), 1.49(br m, 12H, -CH_3, *Conformer i*), 1.25(br m, 12H, -CH_3, *Conformer ii*). ^{13}C NMR (C_7D_8, 23^{o}C) *Conformer i*: δ 167.9 (C=N imine), 156.4(py, *m*-CH), 148.8(py, *o*-C=N), 139.1(py, *p*-CH), 135.9(Ar-CH), 132.9(Ar-CH), 131.3(Ar-CH), (Ar-CH and Ar-*i*-C *are obscured by C_7D_8 peaks at 127-129, and 125-126ppm*), 126.6(Ar-CH), 124.8(Ar-*i*-C), 124.3(Ar-*i*-C), 26.0(-CH_2), 14.9(-CH_3). *Conformer ii*: δ 165.4 (C=N imine), 155.8(py, *m*-CH), 146.2(py, *o*-C=N), 138.9(py, *p*-CH), 135.7(Ar-CH), 132.2(Ar-CH), 129.9(Ar-CH), (Ar-CH and Ar-*i*-C *are obscured by C_7D_8 peaks at 127-129, and 125-126ppm*), 126.1(Ar-CH), 123.9(Ar-*i*-C), 122.1(Ar-*i*-C), 25.5(-CH_2), 13.9(-CH_3). Elemental analysis for $C_{40}H_{39}F_3TlN_3O_3S$ Calculated: C, 53.19; H, 4.35; N, 4.65 Found: C, 52.79; H, 4.63; N, 4.36.

Crystallization of (4.1) with benzene and toluene: Under an atmosphere of N_2, approximately 20-30mg of **4.1** was dissolved in 0.75 mL of dry benzene or toluene respectively, with hexanes as countersolvent, the solution was then held at -30^{o}C for several days while crystals of **4.3** and

4.4 (respectively) were formed by slow diffusion process (Scheme 2). Yellow block like crystals were isolated on both accounts. Elemental analysis could not be obtained as arene adduct is removed under the strong vacuum necessary for sample preparation. The fluxional nature of the Tl-Arene interaction also makes characterization by NMR unfeasible.

[4.8] X-ray Structure Crystallographic Information: Thallium Complexes

Table 4.1: Summary of Data Collection and Crystallographic Parameters for **4.1-4.4.***

Compound	**4.1**	**4.2**	**4.3**	**4.4**
Empirical formula	$[C_{48}H_{55}F_3N_3O_3STl]$ $[C_4H_{10}O]_{0.15}$	$[C_{40}H_{39}F_3N_3O_3STl]$ $[C_4H_{10}O]_{0.25}$	$[C_{48}H_{55}F_3N_3O_3STl]$ $[C_6H_6]_{0.75}$	$[C_{48}H_{55}F_3N_3$-$O_3STl]$ $[C_7H_8]_{1.25}$
Formula weight	1026.50	921.70	1073.96	1132.56
Temperature (K)	202(2)	202(2)	200(2)	202(2)
λ(Å)	0.71073	0.71073	0.71073	0.71073
Crystal system	Triclinic	Triclinic	Monoclinic	Monoclinic
Space group	P-1	P-1	C2/c	C2/c
a (Å)	11.4925(13)	11.5837(4)	30.9941(17)	31.1041(7)
b (Å)	14.6601(16)	12.5411(4)	20.8284(13)	20.6691(5)
c (Å)	17.1790(15)	15.4083(5)	19.4245(12)	19.5116(5)
α (deg)	105.615(5)	113.570(2)	90	90.00
β (deg)	103.016(5)	99.759(2)	106.008(2)	106.2800(10)
γ (deg)	97.860(6)	97.068(2)	90	90.00
V ($Å^3$)	2655.1(5)	1976.33(11)	12053.4(12)	12040.9(5)
Z	2	2	8	8
ρ (calc) (Mg/m^3)	1.284	1.549	1.184	1.250
μ (mm^{-1})	3.129	4.194	2.760	2.766
Absorption correction	Semi-empirical from equivalents			
Final R indices [I>2σ(I)]				
R1[a]	0.0723	0.0256	0.0456	0.0329
*w*R2[b]	0.1733	0.0659	0.1324	0.0900

[a] $R1 = \Sigma \left| |F_o| - |F_c| \right| / \Sigma |F_o|$. [b] $wR2 = \left(\Sigma w \left(|F_o| - |F_c| \right)^2 / \Sigma w |F_o|^2 \right)^{1/2}$

*structure files available from CCDC

Table 4.2: Summary of Data Collection and Crystallographic Parameters for **4.5.**

Compound	**4.5**
Empirical formula	$[C_{48}H_{55}F_3N_3O_3STl]\ [C_6F_6]_2[C_6H_{14}]_{0.5}$
Formula weight	1430.59
Temperature (K)	202(2)
λ(Å)	0.71073
Crystal system	Triclinic
Space group	P-1
a (Å)	14.9435(16)
b (Å)	15.0791(16)
c (Å)	15.6496(16)
α (deg)	82.008(6)
β (deg)	70.548(5)
γ (deg)	82.521(6)
V ($Å^3$)	3279.5(6)
Z	2
ρ (calc) (Mg/m^3)	1.449
μ (mm^{-1})	2.581
Absorption correction	Semi-empirical from equivalents
Final R indices [I>2σ(I)]	
R1[a]	0.0520
*w*R2[b]	0.1093

[a] $R1 = \Sigma \left\| F_o \right| - \left| F_c \right\| / \Sigma \left| F_o \right|$. [b] $wR2 = \left(\Sigma w \left(\left| F_o \right| - \left| F_c \right| \right)^2 / \Sigma w \left| F_o \right|^2 \right)^{1/2}$

Table 4.3. Selected bond lengths (Å) for compounds **4.1-4.4**

4.1		**4.2**		**4.3**		**4.4**	
N1-C1	1.286(9)	N1-C1	1.271(3)	N1-C6	1.281(6)	N1-C1	1.281(3)
N3-C7	1.265(10)	N3-C7	1.274(3)	N3-C13	1.282(5)	N3-C7	1.288(4)
N2-C2	1.348(8)	N2-C2	1.337(3)	N2-C1	1.351(5)	N2-C2	1.339(4)
N2-C6	1.323(9)	N2-C6	1.340(3)	N2-C5	1.343(6)	N2-C6	1.346(3)
C1-C2	1.509(10)	C1-C2	1.500(3)	C1-C6	1.474(7)	C1-C2	1.496(4)
C6-C7	1.511(9)	C6-C7	1.504(3)	C5-C13	1.502(6)	C6-C7	1.489(4)
Tl1-N2	2.646(6)	Tl1-N2	2.7386(18)	Tl1-N2	2.654(3)	Tl1-N2	2.657(2)
Tl1-N1	2.816(5)	Tl1-N1	2.755(2)	Tl1-N1	2.827(4)	Tl1-N1	2.818(2)
Tl1-N3	2.815(6)	Tl1-N3	2.795(2)	Tl1-N3	2.809(4)	Tl1-N3	2.827(2)
Tl1-O1	2.928*	Tl1-O1	2.613(2)	Tl1-O1	2.867*	Tl1-O1	2.873*
--	--	--	--	Tl-Ar plane	[i] 3.325*	Tl-Ar plane	[i] 3.302*

Table 4.4: Selected bond angles (°) for compounds **4.1-4.4.**

4.1		**4.2**		**4.3**		**4.4**	
N1-C1-C2	116.9(6)	N1-C1-C2	118.8(2)	N1-C6-C1	117.5(4)	N1-C1-C2	116.8(3)
N3-C7-C6	115.7(6)	N3-C7-C6	118.3(2)	N3-C13-C5	115.7(4)	N3-C7-C6	117.1(2)
C1-C2-N2	116.3(6)	C1-C2-N2	117.88(19)	C6-C1-N2	116.7(4)	C1-C2-N2	116.8(2)
C7-C6-N2	116.8(6)	C7-C6-N2	116.67(19)	C13-C5-N2	116.2(3)	C7-C6-N2	117.1(2)
C2-N2-C6	118.7(6)	C2-N2-C6	118.32(19)	C1-N2-C5	118.8(3)	C2-N2-C6	119.1(2)
C2-N2-Tl1	119.8(5)	C2-N2-Tl1	119.05(14)	C1-N2-Tl1	119.8(3)	C2-N2-Tl1	120.23(16)
C6-N2-Tl1	120.2(4)	C6-N2-Tl1	121.02(14)	C5-N2-Tl1	120.1(3)	C6-N2-Tl1	119.46(17)
N2-Tl1-N1	60.06(17)	N2-Tl1-N1	59.84(6)	N2-Tl1-N1	59.25(12)	N2-Tl1-N1	59.49(6)
N2-Tl1-N3	59.15(18)	N2-Tl1-N3	58.64(6)	N2-Tl1-N3	59.23(10)	N2-Tl1-N3	59.68(7)
Tl1-N1-C1	110.3(4)	Tl1-N1-C1	120.88(17)	Tl1-N1-C6	110.9(3)	Tl1-N1-C1	111.64(17)
Tl1-N3-C7	111.4(5)	Tl1-N3-C7	120.72(16)	Tl1-N3-C13	111.3(3)	Tl1-N3-C7	110.57(19)
--	--	O1-Tl1-N2	77.83(7)	--	--	--	--

Table 4.5: Select Bond Lengths (Å) for **4.5.**

Bond Lengths (Å)		**Bond Angles** (^{o})	
N1-C1	1.277(4)	N1-C1-C2	117.3(3)
N3-C7	1.282(4)	N3-C7-C6	116.3(3)
N2-C2	1.343(4)	C1-C2-N2	116.5(3)
N2-C6	1.344(4)	C7-C6-N2	117.2(3)
C1-C2	1.498(4)	C2-N2-C6	118.9(3)
C6-C7	1.489(5)	C2-N2-Tl1	120.51(19)
Tl1-N2	2.624(3)	C6-N2-Tl1	119.4(2)
Tl1-N1	2.804(3)	N2-Tl1-N1	60.28(8)
Tl1-N3	2.808(3)	N2-Tl1-N3	59.85(8)
Tl1-O1	*2.819	Tl1-N1-C1	111.4(2)
--		Tl1-N3-C7	110.5(2)
--	--	N3-Tl1-N1	113.45(8)

[i]*distance from Tl to intersection with Ar plane formed by line drawn from Tl to Tl*

*** distance beyond the recognized bonding parameters in SHELXTL*

Chapter 5: *Tin(II), Formation of Cation-Anion Pairs*

[5.1] Introduction

In a continuing effort to expand the main group chemistry of the bis(imino)pyridine ligand, we looked at the neighbouring group 14 elements, from which we targeted tin(II). Like In(I), Sn(II) bears a $5s^2$ valence electron configuration, and once complexed to a donor ligand (such as bis(imino)pyridine) should behave as a Lewis base. Sn(II) does not share the same tendency towards disproportionation as its low valent group 13 congeners (Sn(II) is only slightly less stable than Sn(IV))[58], so Sn(II)-bis(imino)pyridine compounds could be more robust and thus suitable for reactivity testing previously unavailable to their In(I) analogues. Further commonality between indium and tin can be found in comparing covalent radii (1.39Å for Sn vs 1.42Å for In), making the comparison all the more compelling. However, unlike the case with In(I) and Ga(I), there is a myriad of inexpensive commercially available, and readily soluble Sn(II) starting materials. As such, the coordination and organometallic chemistry of tin is well established and suitably covered in countless journals and numerous books.[59]

Although the realm of tin coordination chemistry is well explored, and examples of tin coordination complexes are numerous, there are no reported bis(imino)pyridine compounds in literature. The closest examples being Sn(IV)-terpyridine complexes that feature well separated cation-anion pairs (Scheme 5.1 (**i**)).[60] Otherwise, reaction of Schiff base 2,6-pyridinediylbis(N-hydroxyphenylaldimine) with Sn(IV) yielded the molecular monomeric compound (**ii**) (Scheme

[58]Reduction potentials: [Sn^{2+}→Sn E^o=-0.14V],[Sn^{4+}→Sn^{2+} E^o=0.15V], C.E. Housecroft, A.G. Sharpe, *Inorganic Chemistry 3rd Ed.*, Pearson Prentice Hall, **2008**.
[59]M. Gielen, A. Davies, K. Pannell, E. Tiekink, Tin Chemistry: Fundamentals, Frontiers, and Applications, **2008** John Wiley & Sons, Ltd.
[60] M.K. Das, J. Buckle, P.G. Harrison, *Inorganica Chimica Acta*, **1972**, 6, 17.

5.1).[61] The complex features a bis(imino)pyridine backbone, however, due to absence of Sn-N_{py} bond, does not behave as a bis(imino)pyridine N,N',N ligated complex. Our goal was to synthesize and characterize the first bis(imino)pyridine complexes of Sn(II), and subsequently begin to explore potential reactivity.

Scheme 5.1

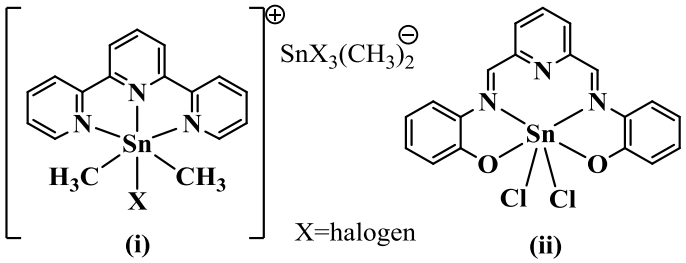

[5.2] Results and Discussion: Ligation of Bis(imino)pyridines to Sn(II) Halides

Initial attempts to generate a neutral monomeric Sn(II)-bis(imino)pyridine species by reaction of $SnBr_2$ with **1A** resulted in the isolation of a fine orange powder in poor yields (<50%), and EA results indicating large excess of inorganic species. Drawing comparison to our results from GaI_3 trials which yielded cation/anion pairs when reacted with **1A** and **1B**, we reacted **1A** with 2 equivalents of $SnBr_2$ (Scheme 5.2). The resulting fine orange powder was isolatead in 77% yield, and confirmed by both X-ray and EA to be an Sn(II) complex consisting of $[2,6\text{-}\{2,5\text{-}^{t}Bu_2C_6H_3N{=}CPh\}_2(NC_5H_3)]SnBr^{+}SnBr_3^{-}$ as a weakly interacting cation/anion pair **5.1** (Figure 5.1). Selected bond distances and angles for **5.1** are presented in Tables 5.2 and 5.3 respectively.

In the assignment of a coordination geometry for the Sn centre of the cation fragment, it is prudent to propose a location for a stereochemically active lone pair. Upon investigation

[61] H.A. Tayim, M. Absi, A. Darwish, S.K. Thabet, *Inorg. Nucl. Chem. Letters*, **1975**, 11, 395.

of X-ray structures (*vide infra*), a logical location for the lone pair is trans to the $N_{pyridine}$. The resulting geometry of the tin centre within this cation can be viewed as distorted square-base-pyramidal with the four-fold plane defined by the pyridine centre (N2), the two imine N groups (N1 and N3), and aforementioned lone pair situated trans to N2. As was observed for the In and Tl species, the Sn-N2 distance of 2.275(2)Å is shorter than the Sn-N_{imine} distances of 2.483(2)Å and 2.522(2)Å. The apical site of the pyramid is occupied by Br1. Trans to the bromide group is an open site bearing δ+ charge. This appears to facilitate long range dipole-dipole interaction with a Br atom of the $SnBr_3^-$ anion (3.3706(4)Å for Sn1-Br2 vs 2.6362(4)Å for Sn1-Br1). The N1-Sn1-N3 angle is 136.94(7)^o due to ligand geometric constraints, however the Br1-Sn1-Br2 angle of 155.727(15)^o indicates geometric influence of the basal lone pair. The geometry of the tin centre within the $SnBr_3^-$ anion is distorted tetrahedral with a lone pair, resulting in average Br-Sn-Br angles of 94.4^o vs 109.5^o for ideal tetrahedral. Within the anion, the "bridging" Br atom displays a slightly elongated Sn-Br bond (2.6608(4)Å for Sn2-Br2 vs 2.6123(6)Å and 2.6175(6)Å for Sn2-Br3 and Sn2-Br4 respectively).

Scheme 5.2

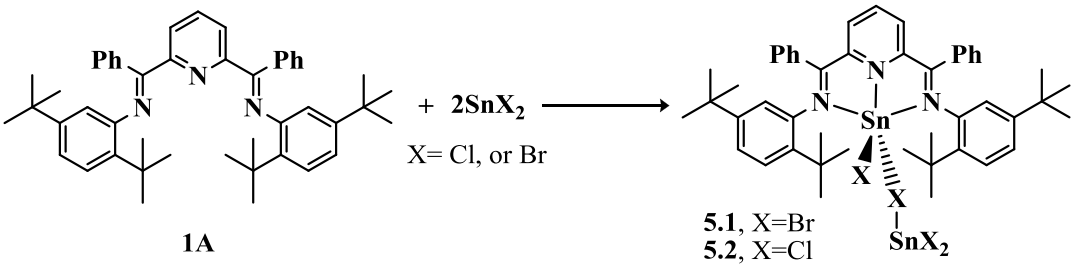

In analogous fashion, **1A** was reacted with 2 equivalents of $SnCl_2$ (Scheme 5.2). The resulting fine orange powder was isolated in 94% yield, and confirmed by both X-ray and microanalysis to be an Sn(II) complex consisting of [2,6-{2,5-

$^{t}Bu_2C_6H_3N{=}CPh\}_2(NC_5H_3)]SnCl^{+}SnCl_3^{-}$ as a weakly interacting cation/anion pair **5.2** (Figure 5.2). Selected bond distances and angles for **5.2** are presented in Tables 5.2 and 5.3 respectively. As with **5.1**, the geometry of the tin centre within the cation of **5.2** is distorted square-base-pyramidal with the four-fold plane defined by the pyridine centre (N2), the two imine N groups (N1 and N3), and a lone pair situated trans to N2. The Sn-N2 distance of 2.267(3)Å is shorter than the Sn-N_{imine} distances of 2.505(3)Å and 2.516(3)Å. The apical site is occupied by Cl1, trans to which is situated a δ+ open site facilitating long distance interactions with a Cl atom of the $SnCl_3^-$ anion (3.372Å for Sn1-Cl2 vs 2.4746(11)Å for Sn1-Cl1). The N1-Sn1-N3 angle is 137.66(9)^{o} due to ligand geometric constraints, however the Cl1-Sn1-Cl2 angle of 155.45^{o} indicates geometric influence of the basal lone pair as observed in **5.1**. The geometry of the tin centre within the $SnCl_3^-$ anion is similarly distorted tetrahedral. Within the anion, the interacting Cl atom displays a slightly elongated Sn-Cl bond (2.4918(12)Å for Sn2-Cl2 vs 2.4638(12)Å and 2.4493(12)Å for Sn2-Cl3 and Sn2-Cl4 respectively), indicating a slight amount of electron donor character.

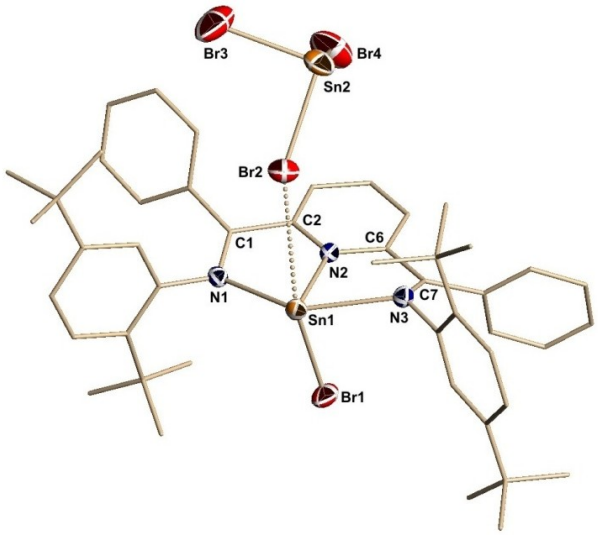

Figure 5.1: X-ray structure of compound **5.1** with hydrogen atoms omitted for clarity. Select bond lengths and angles are given in Tables 5.2 and 5.3.

Compounds **5.1** and **5.2** display similar bonding characteristics, with any slight differences arising simply from the differing covalent radii of Cl and Br. Crystallization of **5.2** from diethyl ether resulted in the isolation of [2,6-{2,5-$^{t}Bu_2C_6H_3N{=}CPh\}_2(NC_5H_3)$]$SnCl^{+}SnCl_3^{-}$ as a well separated cation/anion pair **5.2ii** (Figure 5.3). The open site bearing δ+ charge trans to the apical chloride remains empty, and the $SnCl_3^{-}$ anion is well separated by 13.260Å, and the co-crystallized ether molecule is well separated from both the Sn cation and anion centers and behaves as a non-interacting cocrystallized solvent. Thus providing further evidence that the cation-anion interaction is indeed dipole-dipole in nature, and not a Lewis-acid, Lewis-base interaction as it could alternatively be percieved. The presence of a Lewis acidic site would facilitate some level of interaction with the oxygen lone pairs of ether, especially in the absence of the now far removed $SnCl_3^{-}$ anion. General bonding features for **5.2** and **5.2ii** remain similar, however Sn1-N1 and Sn1-N3 interactions are slighly altered, perhaps a likely artifact of the altered crystallization environment as afforded by the definitive separation of the cation anion pair. In **5.2ii** Sn1-N1 and Sn1-N3 bonds are shortened to distances of 2.472(7)Å and 2.476(7)Å respectively vs. 2.505(3)Å and 2.516(3)Å in **5.2**. The increased N_{imine}-Sn donation is facilitated by a slight twist in ligand geometry to accommodate orbital alignment. N_{imine} distances to the Sn-pyridine plane change from 0.425Å and 0.534Å for N1 and N3 respectively in **5.2** to 0.240Å and 0.200Å in **5.2ii**, resulting in an overall increase in basal planarity.

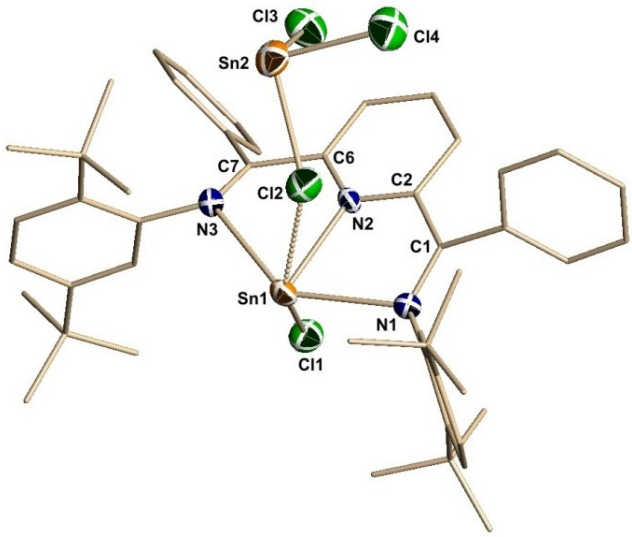

Figure 5.2: X-ray structure of compound **5.2** with hydrogen atoms and toluene omitted for clarity. Select bond lengths and angles are given in Tables 5.2 and 5.3.

In an ongoing attempt to generate neutral monomeric Sn(II)-bis(imino)pyridine species, $SnCl_2$ was reacted with **1D**, our least sterically encumberred ligand. However, as with **5.1** and **5.2**, the isolation of a fine orange powder in poor yields (sub 50%), and microanalysis results indicating large excess of inorganic species were indicative of a cation/anion pair species. Ligand **1D** was succesfully reacted with 2 equivalents of $SnCl_2$ (Scheme 5.3). The resulting fine orange powder was isolated in 96% yield, and confirmed by both X-ray and elemental analysis to be an Sn(II) complex consisting of [2,6-{2,6-$Me_2C_6H_3N{=}CPh\}_2(NC_5H_3)$]$SnCl^+SnCl_3^-$ as a weakly interacting cation/anion pair **5.3** (Figure 5.4). Selected bond distances and angles for **5.3** are presented in Tables 5.5 and 5.6 respectively.

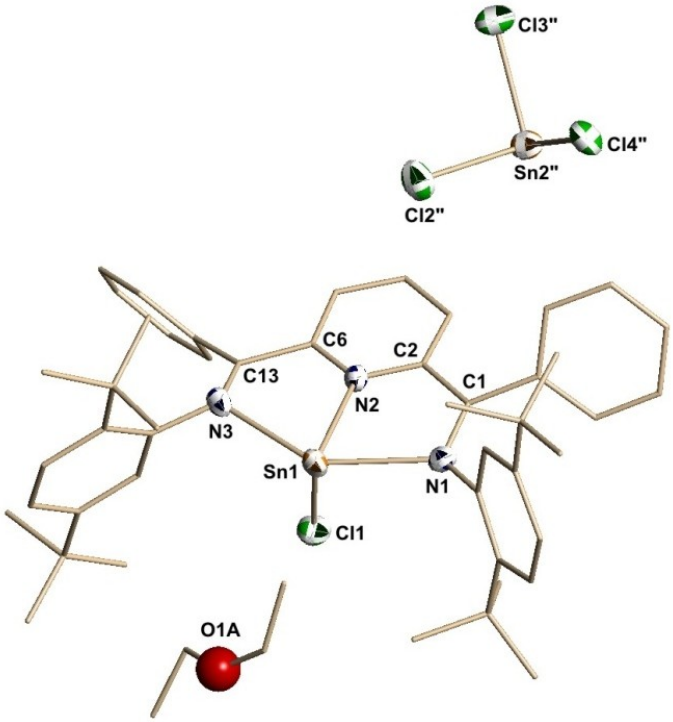

Figure 5.3: X-ray structure of compound **5.2ii** with hydrogen atoms omitted for clarity. Select bond lengths and angles are given in Tables 5.2 and 5.3.

Scheme 5.3

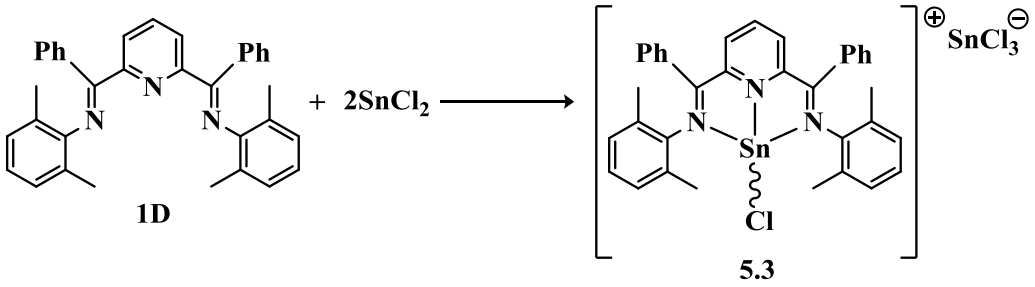

Analogous to **5.1** and **5.2**, the geometry of the tin centre within the cation of **5.3** is distorted square-base-pyramidal with the four-fold plane defined by the pyridine centre (N2), the two imine N groups (N1 and N3), and a lone pair situated trans to N2. The Sn-N2 distance of 2.2839(16)Å is shorter than the Sn-N_{imine} distances of 2.3839(18)Å and 2.4183(17)Å. The apical site is occupied by Cl1, trans to which is situated a δ+ open site

facilitating long distance interactions with a Cl atom of the $SnCl_3^-$ anion (3.824Å for Sn1-Cl4" vs 2.4464(7)Å for Sn1-Cl1). The N1-Sn1-N3 angle is 136.62(6)^o due to ligand geometric constraints, however the Cl1-Sn1-Cl4" angle of 148.25^o indicates geometric influence of the basal lone pair. The geometry of the tin centre within the $SnCl_3^-$ anion is similarly distorted tetrahedral. Within the anion, the interacting Cl atom displays a slightly elongated Sn-Cl bond (2.5118(8)Å for Sn2"-Cl4" vs 2.4680(7)Å and 2.4703(7)Å for Sn2"-Cl3" and Sn2"-Cl2" respectively), likely indicating a slight amount of electron donor character.

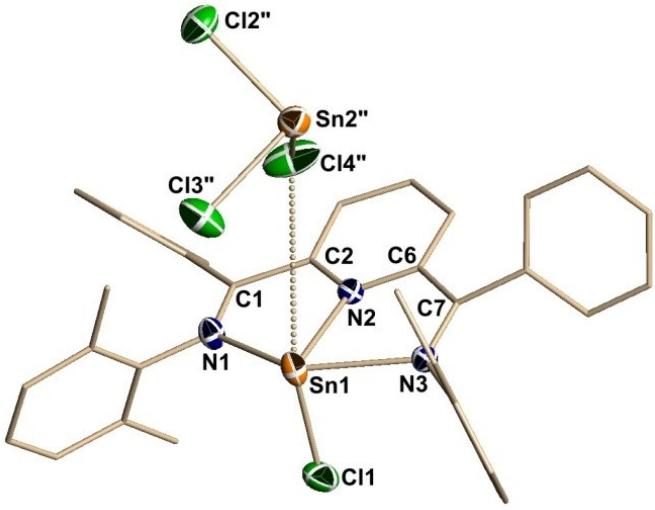

Figure 5.4: X-ray structure of compound **5.3** with hydrogen atoms and CH_2Cl_2 omitted for clarity. Select bond lengths and angles are given in Tables 5.5 and 5.6.

The Sn1-Cl4" bond (3.824 Å) in **5.3** is significantly longer than the Sn1-Cl2 bond (3.372Å) in **5.2**. This is seemingly counterintuitive as steric congestion around the Sn centre is relieved by incorporation of Me rather than ^{t}Bu groups, making the approach of $SnCl_3^-$ towards the δ+ site less sterically encumbered. One potential explanation could be that the $SnCl_3^-$ anion, as we had observed with the OTf anion in our indium chemistry (Chapter 2), is

not only stabilized by interactions to the tin centre, but also partially stablized by interactions with δ+ sites on the bis(imino)pyridine scaffold. Once steric bulk is reduced, these sites are no longer available, and apparent Sn1-Cl4" bond length becomes elongated, as there are less sites amenable to dipole-dipole interaction. The Sn-N_{imine} distances of 2.3839(18)Å and 2.4183(17)Å in **5.3** are shorter than those in **5.2ii** (2.472(7)Å and 2.476(7)Å) and significantly shorter than those of **5.2** (2.505(3)Å and 2.516(3)Å). The increased N_{imine}-Sn donation is facilitated by an even greater twist in ligand geometry than observed in **5.2ii**. N_{imine} distances to the Sn-pyridine plane are 0.256Å and 0.031Å for **5.3** vs 0.240Å and 0.200Å in **5.2ii**, and 0.425Å and 0.534Å in **5.2**.

To probe general reactivity of both the stereochemically active lone pair and the δ+ site trans to the apical halide, as well as anion exchange, a set of experiments were conducted on **5.3** (Scheme 5.4). Attempts to probe lone pair adduct formation with Lewis acid $B(C_6F_5)_3$ (**a**) yielded structure **5.3a**, which displays no interaction or even co-crystalization with $B(C_6F_5)_3$ (Figure 5.5). Trials (**b**),(**c**), and (**d**) entail the attempted crystalization of saturated solutions of **5.3** in isopropionitrile, propionitrile and aniline respectively, in order to probe potential interaction with the δ+ site with electron rich unsaturated C≡N bonds or N lone pairs. Orange plate like crystals suitable for X-ray crystallography were obtained from solution (**b**) with isopropionitrile, while (**c**) and (**d**) yielded no suitable crystals. The resulting structure **5.3b** indicates no direct Sn-isopropionitrile interaction, but rather a well separated cocrystalization (Figure 5.6). Like we have seen earlier with **5.2ii**, this lends further proof to the dipole-dipole nature of the cation-anion interaction. Attempted reaction with $K[BPh_4]$ (**e**) at room temperature showed no colour change and $K[BPh_4]$ appeared poorly soluble. Allowing the solution to stir for 6 hours at 50°C to facilitate dissolution of $K[BPh_4]$ resulted

in a translucent green, which upon immediate removal from the heat source precipitated grey $Sn(0)_s$, leaving behind a translucent yellow green solution from which no decomposition products could be clearly identified.

Scheme 5.4

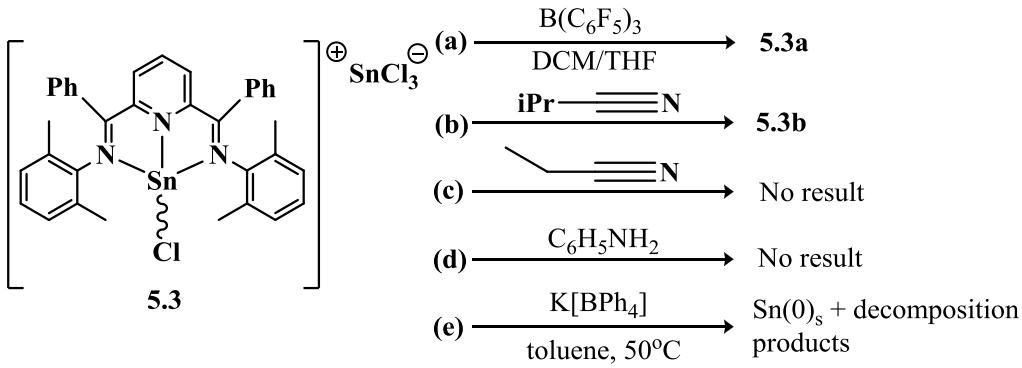

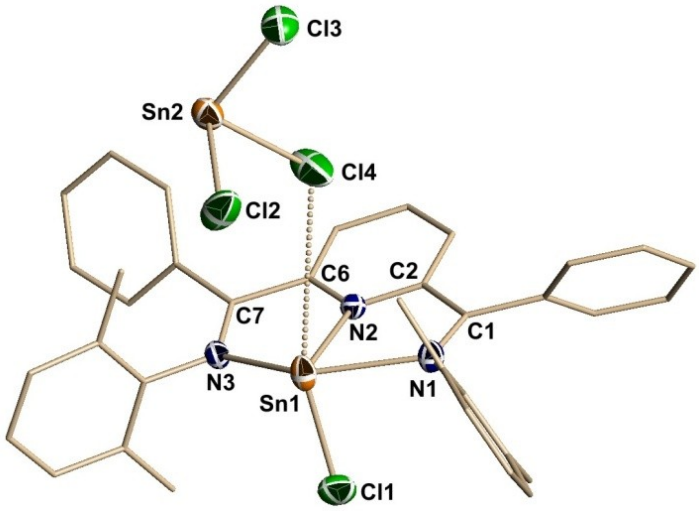

Figure 5.5: X-ray structure of compound **5.3a** with hydrogen atoms,CH_2Cl_2 and THF omitted for clarity. Select bond lengths and angles are given in Tables 5.5 and 5.6.

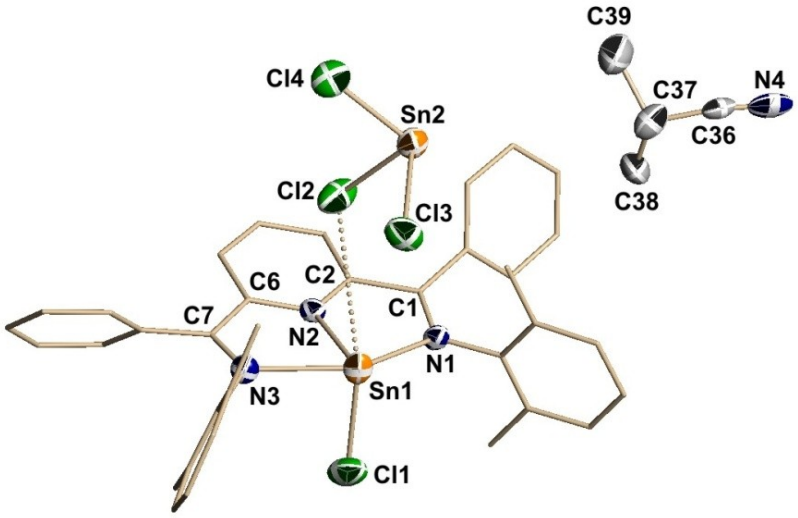

Figure 5.6: X-ray structure of compound **5.3** with hydrogen atoms omitted for clarity. Select bond lengths and angles are given in Tables 5.5 and 5.6.

[5.3] Conclusion

This is the first report of a succesful synthesis of bis(imino)pyridine complexes of tin in either II or IV oxidation states. The resulting complexes showed preferential formation of cation-anion pairs, even in the presence of reduced ligand bulk around the N,N',N binding pocket. This behaviour has been documented previously in our efforts with gallium, and is also prevalent in the aluminum literature.[7] Computational efforts will have to be employed to garner a better understanding of this behaviour, as well as the dipole-dipole nature of the anion-cation interaction. Furthermore, we attempted basic reactivity trials to elucidate potential activity at either the Lewis basic lone pair site, or the open δ+ sites of tin. Although early efforts point to no activity, efforts should remain ongoing as the availability of a Lewis basic site, coupled with complexes air stability remains compelling for future applications in either stoichiometric or catalytic organic transformations.

[5.4] Tin Complex Experimental

General Methods. Unless otherwise stated, reactions were performed in a glovebox with a nitrogen atmosphere. All solvents were sparged with nitrogen and then dried by passage through a column of activated alumina using an apparatus purchased from Anhydrous Engineering. Deuterated chloroform was dried using activated molecular sieves. Tin(II) halides were purchased from Strem Chemicals and used as received. All other reagents were purchased from Aldrich and used without further purification. NMR spectra were run on a Bruker Avance 500 MHz spectrometer with deuterated chloroform as a solvent and internal standard. Elemental analyses were performed by Midwest Microlab LLC, Indianapolis IN.

(5.1) [2,6-bis{2,5-^{t}Bu$_2$C$_6$H$_3$N=CPh}$_2$(NC$_5$H$_3$)]SnBr(SnBr$_3$): $SnBr_2$ powder (65 mg, 0.232 mmol) was added to a clear yellow solution of **1A** (100 mg, 0.151 mmol) in 8 mL of 1:3 toluene: hexanes. Colour change was immediate as the solution went from translucent yellow to a bright translucent red/orange, gradually becoming opaque. The reaction mixture was sealed and allowed to stir for 6 hours and then cooled to -30^{o}C overnight, over which time a bright orange precipitate formed. The solution was filtered, washed with 10 x 2 mL hexanes, and the solid was allowed to dry under vacuum. A bright orange powder of 5.1 was isolated in 77% yield. ^{1}H and ^{13}C NMR point to the existence of two conformers in solution. A principal *Conformer A*: ^{1}H NMR ($CDCl_3$, 500 MHz): δ 8.83(br t, 1H, py, *p*-CH), δ 8.43(br d , 2H, py, *m*-CH), δ 8.21(br d, 2H, aromatic), δ 7.95(br d, 2H, aromatic), 7.54-7.08(br m, 8H, aromatic), δ 6.94(br s, 2H, aromatic), δ 6.86(br s, 2H, aromatic), 1.56(br s, 9H, ^{t}*Bu*), 1.40(br s, 9H, ^{t}*Bu*), 1.14(br s, 9H, ^{t}*Bu*), 1.06(br s, 9H, ^{t}*Bu*). ^{13}C NMR ($CDCl_3$, 125 MHz). δ 168.9 (C=N imine), 153.4(py, *o*-C=N), 149.6(Ar-CH), 143.9 (Ar, *i*-C), 140.1(Ar-CH), 138.8(Ar-CH), 131.6(Ar-CH), 130.9(Ar-CH), 129.9(Ar, *i*-C), 129.4(Ar-CH), 128.8(Ar-CH), 124.4(Ar-CH), 124.1(Ar-^{t}*Bu*, C-^{t}*Bu*), 123.0(Ar-

^{t}Bu, C-*^{t}Bu*), 35.9(Ar-*^{t}Bu*, C-$(CH_3)_3$), 34.3(Ar-*^{t}Bu*, C-$(CH_3)_3$), 33.2(Ar-*^{t}Bu*, CH_3), 30.9(Ar-*^{t}Bu*, CH_3). *Conformer B*: ^{1}H NMR ($CDCl_3$, 500 MHz): δ 8.75(br t, 1H, py, *p*-CH), δ 8.39(br d , 2H, py, *m*-CH), δ 8.14(br m, 2H, aromatic), δ 7.83(br m, 2H, aromatic), 7.54-7.08(br m, 10H, aromatic), δ 6.48(br s, 2H, aromatic), 1.45(br s, 9H, *^{t}Bu*), 1.38(br s, 9H, *^{t}Bu*), 1.29(br s, 9H, *^{t}Bu*), 0.95(br s, 9H, *^{t}Bu*). ^{13}C NMR ($CDCl_3$, 125 MHz). δ 168.8 (C=N imine), 152.2(py, *o*-C=N), 149.5(Ar-CH), 146.4 (Ar, *i*-C), 141.1(Ar-CH), 139.6(Ar-CH), 133.8(Ar-CH), 133.1(Ar-CH), 132.2(Ar, *i*-C), 129.1(Ar-CH), 128.2(Ar-CH), 125.3(Ar-*^{t}Bu*, C-*^{t}Bu*), 123.9(Ar-*^{t}Bu*, C-*^{t}Bu*), 123.9(Ar-CH), 36.1(Ar-*^{t}Bu*, C-$(CH_3)_3$), 34.3(Ar-*^{t}Bu*, C-$(CH_3)_3$), 33.6(Ar-*^{t}Bu*, CH_3), 30.9(Ar-*^{t}Bu*, CH_3). Orange block like crystals suitable for X-ray analysis were grown by diffusion of hexanes into a saturated CH_2Cl_2 solution held at -30^{o}C for several days. Analysis for $C_{47}H_{55}Sn_2Br_4N_3$: Calculated, C 46.31, H 4.55, N 3.45, Found C 46.48, H 4.63, N 3.40.

(5.2) [2,6-bis{2,5-^{t}Bu$_2$C$_6$H$_3$N=CPh}$_2$(NC$_5$H$_3$)]SnCl(SnCl$_3$): $SnCl_2$ powder (52 mg, 0.274 mmol) was added to a clear yellow solution of **1A** (100 mg, 0.151 mmol) in 8 mL of 1:3 toluene: hexanes. Colour change was immediate as the solution went from translucent yellow to a bright translucent orange, gradually becoming opaque. The reaction mixture was sealed and allowed to stir for 6 hours and then cooled to -30^{o}C overnight, over which time a bright orange precipitate formed. The solution was filtered, washed with 10 x 2 mL hexanes, and the solid was allowed to dry under vacuum. A bright orange powder of **5.2** was isolated in 94% yield. Yellow plate like crystals suitable for X-ray analysis were grown by diffusion of hexanes into saturated solutions of either ether or toluene held at -30^{o}C for several days. ^{1}H and ^{13}C NMR point to the existence of one predominant species, with multiple conformers present in smaller ratios (5:1 or less for principal species vs conformers). The NMR spectra for the principal species is reported: ^{1}H NMR ($CDCl_3$, 500 MHz): δ 8.32(br t, 1H, py, *p*-CH), δ 7.87(br m , 2H, py, *m*-CH), 7.62-

7.03(br m, 14H, aromatic), δ 6.89(d, 2H, aromatic), 1.53(br s, 18H, ^{t}Bu), 1.04(br s, 18H, ^{t}Bu). ^{13}C NMR ($CDCl_3$, 125 MHz). δ 168.6 (C=N imine), 153.3(py, *o*-C=N), 152.0 (Ar, *i*-C), 149.6(Ar-CH), 143.5(Ar-CH), 139.9(Ar-CH), 132.6(Ar, *i*-C), 130.8(Ar-CH), 129.0(Ar-CH), , 128.7(Ar-CH), 128.2(Ar-CH), 124.3(Ar-^{t}Bu, C-^{t}Bu), 124.0(Ar-CH), 122.8(Ar-^{t}Bu, C-^{t}Bu), 36.1(Ar-^{t}Bu, C-$(CH_3)_3$), 34.3(Ar-^{t}Bu, C-$(CH_3)_3$), 33.4(Ar-^{t}Bu, CH_3), 30.8(Ar-^{t}Bu, CH_3). Elemental analysis was obtained by recrystallization in toluene, resulting in a 3:2 toluene adduct of **5.2**. Calculated for $[C_{47}H_{55}Sn_2Cl_4N_3]_3[C_7H_8]_2$: C 56.28, H 5.52, N 3.81, Found C 56.22, H 5.56, N 3.90.

(5.3) [2,6-bis{2,6-Me$_2$C$_6$H$_3$N=CPh}$_2$(NC$_5$H$_3$)]SnCl(SnCl$_3$): $SnCl_2$ powder (74 mg, 0.390 mmol) was added to a clear yellow solution of **1D** (100 mg, 0.203 mmol) in 8 mL of toluene. Colour change was immediate as the solution went from translucent yellow to a bright translucent orange, gradually becoming opaque. The reaction mixture was sealed and allowed to stir for 24 hours and then cooled to -30^{o}C overnight, over which time a bright orange precipitate formed. The solution was filtered, washed with 10 x 2 mL hexanes, and the solid was allowed to dry under vacuum. A bright orange powder of **5.3** was isolated in 96% yield. Orange block like crystals suitable for X-ray analysis were grown by diffusion of hexanes into a saturated CH_2Cl_2 solution held at -30^{o}C for several days. ^{1}H NMR ($CDCl_3$, 500 MHz): δ 8.52(br t, 1H, py, *p*-CH), δ 8.12(br d , 2H, py, *m*-CH), δ 7.45(br m, 2H, aromatic), δ 7.39(br m, 8H, aromatic) δ 7.16(br m, 2H, aromatic), δ 6.97(br m, 4H, aromatic), 2.30(vbr s, 12H, Me). ^{13}C NMR ($CDCl_3$, 125 MHz). δ 168.6 (C=N imine), 151.2(py, *o*-C=N), 144.9 (Ar, *i*-C), 141.1(Ar-CH), 133.1(Ar-CH), 131.7(Ar-CH), 131.1(Ar, *i*-C), 129.5(Ar-CH), 129.0(Ar-CH), 128.7(Ar-CH), 128.2(Ar-CH), 127.0(Ar-CH), 125.3(Ar-*Me*, C-*Me*), 20.1(Ar-*Me*, CH_3). Analysis for $C_{35}H_{31}Sn_2Cl_4N_3$: Calculated, C 48.16, H 3.58, N 4.81, Found C 48.38, H 3.78, N 4.71.

Testing Reactivity of (5.3): (**a**) 40 mg (0.05mmol) of **5.3** was dissolved in 5mL of CH_2Cl_2, to which was added an excess of $B(C_6F_5)_3$ (50 mg, 0.1mmol), and spiked with minimal THF to aid solubility. The solution was allowed to stir for 18 hours, over which time it remained translucent orange. The solution was then layered with ~2mL of hexanes and held at -30^oC for several days to allow for crystallization. Orange block like crystals suitable for X-ray crystallography were obtained. The resulting structure **5.3a** indicates no interaction or even co-crystalization with $B(C_6F_5)_3$. Trials (**b**),(**c**), and (**d**) entail the attempted crystalization of saturated solutions of **5.3** in isopropionitrile, propionitrile and aniline respectively, with hexanes as countersolvent. 20 mg (0.025mmol) of **5.3** were dissolved in each solvent, allowed to stir for 1 hour, filtered through a plug of celite, then placed within a larger vial with hexanes as countersolvent and held at -30^oC for several days to allow for crystallization. Orange plate like crystals suitable for X-ray crystallography were obtained from solution (**b**) with isopropionitrile, while (**c**) and (**d**) yielded no suitable crystals. The resulting structure **5.3b** indicates no direct Sn-isopropionitrile interaction, but rather a well separated cocrystalization. (**e**) 40 mg (0.05mmol) of **5.3** was dissolved in 10mL of toluene, to which was added a slight excess of $K[BPh_4]$ (20 mg, 0.056mmol). The reaction flask was sealed and removed from the glovebox, placed in a heated sandbath and allowed to stir for 6 hours at 50^oC to facilitate dissolution $K[BPh_4]$. The solution became translucent green, but upon immediate removal from the sandbath, grey $Sn(0)_s$ precipitated leaving behind a translucent yellow green solution from which no decomposition products could be clearly identified. The bonding features of **5.3a** and **5.3b** are similar to those of **5.3**.

[5.5] X-ray Crystallographic Information: Tin Complexes

Table 5.1. Summary of Data Collection and Crystallographic Parameters for **5.1-5.2ii**.*

Compound	**5.1**	**5.2**	**5.2ii**
Empirical formula	$C_{47}H_{55}Br_4N_3Sn_2$	$C_{47}H_{55}Cl_4N_3Sn_2$•(C_7H_8)	$C_{47}H_{55}Cl_4N_3Sn_2$ •$(ether)_{0.5}$
Formula weight	1218.96	1133.25	1073.14
Temperature (K)	200(2)	200(2)	200(2)
λ (Å)	0.71073	0.71073	0.71073
Crystal system	Monoclinic	Monoclinic	Triclinic
Space group	P2(1)/c	P2(1)/c	P-1
a (Å)	14.8198(2)	18.2152(5)	10.6251(5)
b (Å)	19.1524(3)	14.1924(4)	14.0413(7)
c (Å)	16.9799(3)	22.1938(6)	19.5349(10)
α (deg)	90	90	74.108(2)
β (deg)	91.2240(10)	111.5820(10)	77.877(3)
γ (deg)	90	90	75.277(2)
V ($Å^3$)	4818.39(13)	5335.2(3)	2679.9(2)
Z	4	4	2
ρ (calc) (Mg/m^3)	1.680	1.411	1.330
μ (mm^{-1})	4.388	1.173	1.165
Absorption correction		Semi-empirical from equivalents	
Final R indices [I>2σ(I)]			
R1[a]	0.0342	0.0417	0.0745
*w*R2[b]	0.0807	0.0781	0.1707

[a] $R1 = \Sigma \left| |F_o| - |F_c| \right| / \Sigma |F_o|$. [b] $wR2 = \left(\Sigma w \left(|F_o| - |F_c| \right)^2 / \Sigma w |F_o|^2 \right)^{1/2}$

*structure data available from CCDC.

Table 5.2. Selected bond lengths (Å) for compounds **5.1-5.2ii**.

5.1		**5.2**		**5.2ii**	
C(1)-C(2)	1.496(4)	C(1)-C(2)	1.480(5)	C(1)-C(2)	1.500(12)
C(6)-C(7)	1.481(4)	C(6)-C(7)	1.485(5)	C(6)-C(13)	1.484(11)
C(1)-N(1)	1.285(4)	C(1)-N(1)	1.301(4)	C(1)-N(1)	1.297(11)
C(7)-N(3)	1.280(3)	C(7)-N(3)	1.282(4)	C(13)-N(3)	1.288(11)
C(2)-N(2)	1.344(3)	C(2)-N(2)	1.340(4)	C(2)-N(2)	1.325(10)
C(6)-N(2)	1.347(3)	C(6)-N(2)	1.339(4)	C(6)-N(2)	1.344(10)
Sn(1)-N(1)	2.483(2)	Sn(1)-N(1)	2.505(3)	Sn(1)-N(1)	2.472(7)
Sn(1)-N(3)	2.522(2)	Sn(1)-N(3)	2.516(3)	Sn(1)-N(3)	2.476(7)
Sn(1)-N(2)	2.275(2)	Sn(1)-N(2)	2.267(3)	Sn(1)-N(2)	2.281(6)
Sn(1)-Br(1)	2.6362(4)	Sn(1)-Cl(1)	2.4746(11)	Sn(1)-Cl(1)	2.463(2)
Sn(2)-Br(2)	2.6608(4)	Sn(2)-Cl(2)	2.4918(12)	Sn(2)”-Cl(2)”	2.472(3)
Sn(2)-Br(3)	2.6123(6)	Sn(2)-Cl(3)	2.4638(12)	Sn(2)”-Cl(3)”	2.497(2)
Sn(2)-Br(4)	2.6175(6)	Sn(2)-Cl(4)	2.4493(12)	Sn(2)”-Cl(4)”	2.509(3)
Sn(1)-Br(2)	3.3706(4)	Sn(1)-Cl(2)	3.372*	Sn(1)-Cl(2)”	13.260*

**distance beyond the recognized bonding parameters in SHELXTL.*

Table 5.3: Selected bond angles (°) for compounds **5.1-5.2ii**.

5.1		**5.2**		**5.2ii**	
N(2)-Sn(1)-Br(1)	85.45(6)	N(2)-Sn(1)-Cl(1)	82.79(8)	N(2)-Sn(1)-Cl(1)	83.09(17)
N(1)-C(1)-C(2)	115.7(2)	N(1)-C(1)-C(2)	117.3(3)	N(1)-C(1)-C(2)	115.5(7)
N(3)-C(7)-C(6)	117.6(2)	N(3)-C(7)-C(6)	117.4(3)	N(3)-C(13)-C(6)	117.7(7)
N(1)-Sn(1)-N(2)	68.18(7)	N(1)-Sn(1)-N(2)	69.47(10)	N(1)-Sn(1)-N(2)	68.9(2)
N(3)-Sn(1)-N(2)	68.76(7)	N(3)-Sn(1)-N(2)	68.31(10)	N(3)-Sn(1)-N(2)	69.7(2)
N(1)-Sn(1)-N(3)	136.94(7)	N(1)-Sn(1)-N(3)	137.66(9)	N(1)-Sn(1)-N(3)	138.6(2)
N(1)-Sn(1)-Br(1)	93.75(5)	N(1)-Sn(1)-Cl(1)	95.20(7)	N(1)-Sn(1)-Cl(1)	92.40(17)
N(3)-Sn(1)-Br(1)	82.81(5)	N(3)-Sn(1)-Cl(1)	82.71(7)	N(3)-Sn(1)-Cl(1)	81.88(17)
C(1)-N(1)-Sn(1)	113.38(17)	C(1)-N(1)-Sn(1)	111.3(2)	C(1)-N(1)-Sn(1)	114.2(5)
C(7)-N(3)-Sn(1)	111.12(17)	C(7)-N(3)-Sn(1)	110.6(2)	C(13)-N(3)-Sn(1)	113.4(5)
C(1)-C(2)-N(2)	116.2(2)	C(1)-C(2)-N(2)	117.6(3)	C(1)-C(2)-N(2)	117.4(7)
C(7)-C(6)-N(2)	117.2(2)	C(7)-C(6)-N(2)	116.5(3)	C(13)-C(6)-N(2)	117.9(7)
C(2)-N(2)-Sn(1)	120.36(17)	C(2)-N(2)-Sn(1)	119.6(2)	C(2)-N(2)-Sn(1)	120.2(5)
C(6)-N(2)-Sn(1)	119.50(17)	C(6)-N(2)-Sn(1)	119.9(2)	C(6)-N(2)-Sn(1)	118.9(5)
C(2)-N(2)-C(6)	120.1(2)	C(2)-N(2)-C(6)	120.3(3)	C(2)-N(2)-C(6)	120.9(7)
Br(2)-Sn(2)-Br(3)	92.131(18)	Cl(2)-Sn(2)-Cl(3)	93.46(4)	Cl(2)”-Sn(2)”-Cl(3)”	93.57(9)
Br(2)-Sn(2)-Br(4)	97.956(17)	Cl(2)-Sn(2)-Cl(4)	92.49(4)	Cl(2)”-Sn(2)”-Cl(4)”	91.70(8)
Br(3)-Sn(2)-Br(4)	93.00(2)	Cl(3)-Sn(2)-Cl(4)	93.65(4)	Cl(3)”-Sn(2)”-Cl(4)”	94.48(9)
N(2)-Sn(1)-Br(2)	70.29(6)	--	--	--	--
N(1)-Sn(1)-Br(2)	78.29(5)	--	--	--	--
N(3)-Sn(1)-Br(2)	87.53(5)	--	--	--	--
Br(1)-Sn(1)-Br(2)	155.727(15)	--	--	--	--
Sn(1)-Br(2)-Sn(2)	152.513(16)	--	--	--	--

Table 5.4. Summary of Data Collection and Crystallographic Parameters for **5.3-5.3b**.

Compound	**5.3**	**5.3a**	**5.3b**
Empirical formula	$C_{35}H_{31}Cl_4N_3Sn_2$•(CH_2Cl_2)	$C_{35}H_{31}Cl_4N_3Sn_2$•$(CH_2Cl_2)_{0.25}$ $(THF)_{0.5}$	$C_{35}H_{31}Cl_4N_3Sn_2$ •$(C_4H_7N)_{0.5}$
Formula weight	957.73	930.09	907.36
Temperature (K)	200(2)	200(2)	200(2)
λ (Å)	0.71073	0.71073	0.71073
Crystal system	Monoclinic	Monoclinic	Monoclinic
Space group	P2(1)/c	P2(1)/c	P2(1)/c
a (Å)	13.7902(3)	13.9675(3)	14.3461(16)
b (Å)	18.1623(4)	17.9761(4)	17.440(2)
c (Å)	16.7627(3)	16.9189(4)	17.3094(19)
α (deg)	90	90	90
β (deg)	112.4330(10)	112.9150(10)	113.172(5)
γ (deg)	90	90	90
V ($Å^3$)	3880.71(14)	3912.78(15)	3981.4(8)
Z	4	4	4
ρ (calc) (Mg/m^3)	1.639	1.579	1.514
μ (mm^{-1})	1.730	1.615	1.552
Absorption correction	Semi-empirical from equivalents		
Final R indices [I>2σ(I)]			
R1[a]	0.0274	0.0355	0.1041
*w*R2[b]	0.0686	0.0991	0.2216

[a] $R1 = \Sigma \left| |F_o| - |F_c| \right| / \Sigma |F_o|$. [b] $wR2 = \left(\Sigma w \left(|F_o| - |F_c| \right)^2 / \Sigma w |F_o|^2 \right)^{1/2}$

Table 5.5. Selected bond lengths (Å) for compounds **5.3-5.3b**.

5.3		**5.3a**		**5.3b**	
C(1)-C(2)	1.493(3)	C(1)-C(2)	1.495(4)	C(1)-C(2)	1.476(16)
C(6)-C(7)	1.490(3)	C(6)-C(7)	1.493(4)	C(6)-C(7)	1.483(15)
C(1)-N(1)	1.283(3)	C(1)-N(1)	1.283(3)	C(1)-N(1)	1.268(14)
C(7)-N(3)	1.280(3)	C(7)-N(3)	1.283(3)	C(7)-N(3)	1.286(14)
C(2)-N(2)	1.345(3)	C(2)-N(2)	1.347(3)	C(2)-N(2)	1.331(14)
C(6)-N(2)	1.343(2)	C(6)-N(2)	1.336(3)	C(6)-N(2)	1.359(14)
Sn(1)-N(1)	2.3839(18)	Sn(1)-N(1)	2.379(2)	Sn(1)-N(1)	2.425(9)
Sn(1)-N(3)	2.4183(17)	Sn(1)-N(3)	2.422(2)	Sn(1)-N(3)	2.359(10)
Sn(1)-N(2)	2.2839(16)	Sn(1)-N(2)	2.282(2)	Sn(1)-N(2)	2.284(9)
Sn(1)-Cl(1)	2.4464(7)	Sn(1)-Cl(1)	2.4500(10)	Sn(1)-Cl(1)	2.430(4)
Sn(2)”-Cl(2)”	2.4703(7)	Sn(2)-Cl(2)	2.4610(10)	Sn(2)-Cl(2)	2.505(4)
Sn(2)”-Cl(3)”	2.4680(7)	Sn(2)-Cl(3)	2.4722(9)	Sn(2)-Cl(3)	2.458(4)
Sn(2)”-Cl(4)”	2.5118(8)	Sn(2)-Cl(4)	2.5176(10)	Sn(2)-Cl(4)	2.470(4)
Sn(1)-Cl(2)”	3.824*	Sn(1)-Cl(4)	3.757*	Sn(1)-Cl(2)	3.612*

**distance beyond the recognized bonding parameters in SHELXTL*

Table 5.6: Selected bond angles (°) for compounds **5.3-5.3b**.

5.3		**5.3a**		**5.3b**	
N(2)-Sn(1)-Cl(1)	92.08(5)	N(2)-Sn(1)-Cl(1)	92.60(6)	N(2)-Sn(1)-Cl(1)	94.8(2)
N(1)-C(1)-C(2)	115.97(18)	N(1)-C(1)-C(2)	116.1(2)	N(1)-C(1)-C(2)	116.8(10)
N(3)-C(7)-C(6)	115.86(17)	N(3)-C(7)-C(6)	115.7(2)	N(3)-C(7)-C(6)	115.1(10)
N(1)-Sn(1)-N(2)	69.16(6)	N(1)-Sn(1)-N(2)	69.10(8)	N(1)-Sn(1)-N(2)	67.8(3)
N(3)-Sn(1)-N(2)	68.20(6)	N(3)-Sn(1)-N(2)	68.25(8)	N(3)-Sn(1)-N(2)	68.5(3)
N(1)-Sn(1)-N(3)	136.62(6)	N(1)-Sn(1)-N(3)	136.50(8)	N(1)-Sn(1)-N(3)	135.3(3)
N(1)-Sn(1)-Cl(1)	85.74(5)	N(1)-Sn(1)-Cl(1)	85.66(7)	N(1)-Sn(1)-Cl(1)	88.5(2)
N(3)-Sn(1)-Cl(1)	88.15(5)	N(3)-Sn(1)-Cl(1)	88.04(6)	N(3)-Sn(1)-Cl(1)	85.8(3)
C(1)-N(1)-Sn(1)	118.63(13)	C(1)-N(1)-Sn(1)	118.71(18)	C(1)-N(1)-Sn(1)	115.2(7)
C(7)-N(3)-Sn(1)	116.12(13)	C(7)-N(3)-Sn(1)	115.88(17)	C(7)-N(3)-Sn(1)	120.3(8)
C(1)-C(2)-N(2)	116.25(17)	C(1)-C(2)-N(2)	115.6(2)	C(1)-C(2)-N(2)	115.4(9)
C(7)-C(6)-N(2)	115.67(17)	C(7)-C(6)-N(2)	115.9(2)	C(7)-C(6)-N(2)	115.5(10)
C(2)-N(2)-Sn(1)	119.51(13)	C(2)-N(2)-Sn(1)	119.82(17)	C(2)-N(2)-Sn(1)	120.0(7)
C(6)-N(2)-Sn(1)	119.83(13)	C(6)-N(2)-Sn(1)	119.86(17)	C(6)-N(2)-Sn(1)	119.8(7)
C(2)-N(2)-C(6)	119.73(17)	C(2)-N(2)-C(6)	119.3(2)	C(2)-N(2)-C(6)	119.3(9)
Cl(2)”-Sn(2)”-Cl(3)”	92.70(3)	Cl(2)-Sn(2)-Cl(3)	92.60(4)	Cl(2)-Sn(2)-Cl(3)	91.81(14)
Cl(2)”-Sn(2)”-Cl(4)”	96.84(3)	Cl(2)-Sn(2)-Cl(4)	90.37(4)	Cl(2)-Sn(2)-Cl(4)	96.88(13)
Cl(3)”-Sn(2)”-Cl(4)”	90.00(3)	Cl(3)-Sn(2)-Cl(4)	97.13(3)	Cl(3)-Sn(2)-Cl(4)	93.25(14)

Chapter 6: *Silver(I), Coordination Chemistry and Adduct Formation*

[[6.1] Introduction

In continuing our exploration of low valent group 13 congeners, our next goal was to move beyond our main group focus and explore the bis(imino)pyridine chemistry of analogous late transition metals. Owing to its similar covalent radius to both indium and thallium (1.45Å for Ag vs 1.42Å for In and 1.45Å for Tl)[45] and commercial availability of analogous starting material (AgOTf, similar to synthesized InOTf and commercially available TlOTf), silver became a new focus for reactivity with bis(imino)pyridine ligands.[62] However, unlike In(I) and Tl(I) which feature a $5s^2$ valence electron configuration, Ag(I) is $5s^0$. This represents a move away from our previous compounds which exhibit Lewis basic tendencies once complexed to a donor ligand such as bis(imino)pyridine (In(I), Tl(I), as reported in chapters 2 and 4 respectively). Resulting bis(imino)pyridine compounds of Ag(I) should display Lewis acidic behaviour previously inaccessible to their low valent group 13 congeners.

Furthermore, considering the prevalence of both silver reagents and pincer type geometries in synthetic inorganic and organometallic chemistry, we were surprised to find only one prior example of a silver complex featuring a pincer ligand array (Figure 6.1).[63] The synthesis of [(2,6-bis(5-methyl-1H-pyrazol-3-yl)pyridine)Ag(pyridine)$_2$][NO_3] is heavily reliant on choice of solvent. Pyridine is vital to the isolation of the Ag complex as a molecular monomeric cation/anion pair. Alternatively, use of DMF or H_2O results in formation of clusters, with the ligand pincer geometry dissolving to a bidentate conformation. As such, our initial motivation was not only to synthesize the first

[62] AgOTf is slightly light sensitive, and as a precaution, initial complex synthesis is carried out in darkened vials. Unlike InOTf, AgOTf is sufficiently more stable and not similarly prone to disproportionation/decomposition.
[63] Y. Zhou, W. Chen, D. Wang, *Dalton Trans.,* **2008**, 1444.

bis(imino)pyridine compounds of Ag(I), but also contribute to the extremely limited family of Ag pincer complexes.

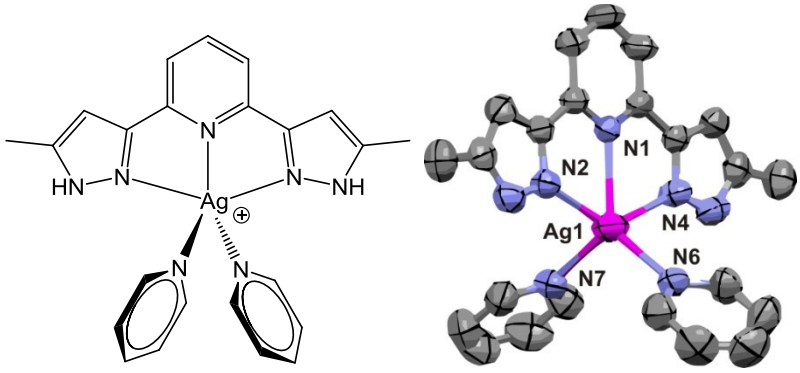

Figure 6.1: The first reported Ag(I)-pincer complex [(2,6-bis(5-methyl-1H-pyrazol-3-yl)pyridine)Ag(pyridine)$_2$][NO_3]. H atoms, and NO_3^- ommitted for clarity (ref. 63).

[6.2] Silver(I) and Adduct formation

With the goal of benchmarking Lewis acid site reactivity, we subjected our target Ag(I) bis(imino)pyridine compounds to reactivity trials towards the formation of adducts with Lewis bases. Our target donor class includes lone pair donors (pyridine), unsaturated C-C bonds (alkenes and alkynes), and arenes. Silver-pyridine interactions are common and featured in a variety of complexes. Formation of Ag-pyridine bonds is facilitated through classic Lewis-acid Lewis-base interactions via the nitrogen lone pairs of pyridine. The resulting adduct often serves to stabilize the otherwise reactive metal centre; one need only look at the aforementioned primary example of silver pincer complexes (Figure 6.1). There is also a growing literature reporting the formation of stable crystalline Ag-arene π-complexes with the arene bonded in the η^2 or η^3 mode in the solid state, but exhibit fluxional behaviour in solution.[64] Silver(I)-alkene

[64] P. Pérez-Galán, N. Delpont, E. Herrero-Gómez, F. Maseras, A. M. Echavarren, *Chem. Eur. J.* **2010**, *16*, 5324 and references therein.

and alkyne complexes are perhaps best known, and have been so for over seventy years.[65] Their study was largely facilitated by developments in IR spectroscopy, where coordination of olefins to Ag(I) is readily indicated by a shift in C-C stretching vibration to lower frequencies than the free olefin species.[66] Silver(I)-alkene and alkyne adducts serve as both precatalytic intermediates, and are also currently being explored for application as supramolecular synthons.[67]

Scheme 6.1

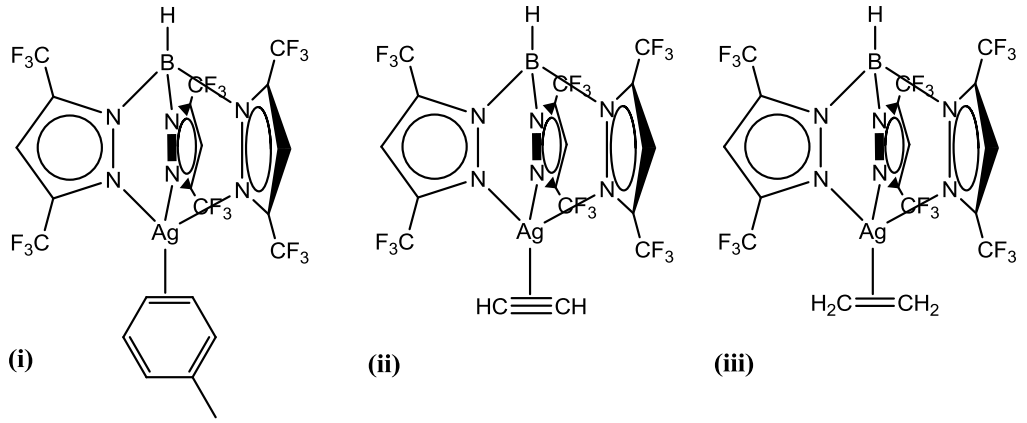

Perhaps the most notable recent examples of silver(I) adduct formation come from the Dias group.[68] The reaction of silver triflate with sodium-hydrotris(3,5-bis(trifluoromethyl)pyrazolyl)borate monohydrate in the presence of THF yields a monomeric silver(I)hydrotris(3,5-bis(trifluoromethyl)pyrazolyl)borate THF adduct (another example of lone pair interaction with Lewis acidic silver(I) centre, akin to pyridine).[69] Dissolution of the THF adduct in toluene results in the isolation of η^2 bound arene complex (Scheme 6.1 **(i)**). Adducts **(ii)**, and **(iii)** as shown in Scheme 6.1 were achieved by dissolving the silver complex in hexanes and bubbling through ethylene or acetylene respectively. The facile manner in which adducts are

[65] S. Winstein, H.J. Lucas, *J. Am. Chem. Soc.,* **1938**, 60, 836.
[66] H.W. Quinn, R.L. VanGilder, *Can. J. Chem.*, **1971**, 49, 1323.
[67] J. Burgess, P.J. Steel, *Coord. Chem. Rev.*, **2011**, 255, 2094.
[68] H.V.R. Dias, Z. Wang, W. Jin, *Inorg. Chem*., **1997**, 36, 6205.
[69] H.V.R. Dias, W. Jin, H.J. Kim, H.L. Lu, , *Inorg. Chem*., **1996**, 35, 2317.

interchanged is indicative of their silver-donor ligand interaction. Such weak transient activation of unsaturated bonds is important for developing Lewis-acid catalysis applications.

[6.3] Results and Discussion: Ligation of Bis(imino)pyridines to AgOTf

The first reported Ag complexes of the bis(imino)pyridine ligand frame were prepared by the addition of ligands **1A** and **1B** to $Ag(O_3SCF_3)$ (Scheme 6.2), which provided **6.1** and **6.2** as bright yellow crystalline solids in 69% and 84% yields respectively.[70] The ^{1}H and ^{13}C NMR spectra of these materials were consistent with the proposed formulation for compounds **6.1** and **6.2**. Of note is the appearance of broadened resonances and of diastereotopic methyl groups for the ^{i}Pr groups in **6.2** suggesting hindered rotation of the Ar-N_{imine} bonds. The identities and structural details of these species as bis(imino)pyridine complexes $[\{ArN{=}CPh\}_2(NPh)]Ag^{+}(OTf)^{-}$ (Ar = 2,5-$^{t}Bu_2C_6H_3$ **6.1**; 2,6-$^{i}Pr_2C_6H_3$ **6.2**) were established by single crystal X-ray analysis.

Scheme 6.2

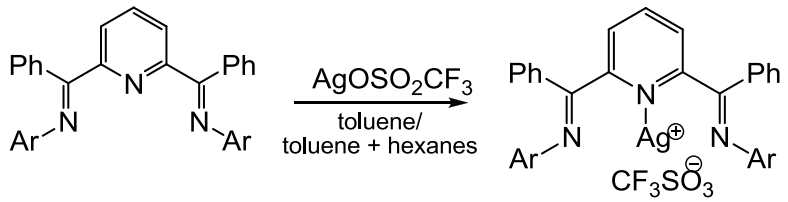

1A, 1B

6.1: Ar=2,4-$^{t}BuC_6H_3$
6.2 Ar=2,5-$^{i}PrC_6H_3$

Figures 6.2 and 6.3 summarize the structural features of complexes **6.1** and **6.2** respectively. In both cases, the constrained geometry, coplanar terdentate array provided by the bis(imino)pyridine ligand makes these compounds unique pincer complexes for

[70] Examples of dinuclear Ag complexes of tetraimine Schiff-base macrocycles are reported in; H. Adams, N. A. Bailey, W. D. Carlisle, D. E. Fenton, and G. Rossi, *J. Chem. Soc. Dalton Trans.*, **1990**. 1271

silver.[71,72] The Ag-N_{py} distances (Ag(1)-N(1) 2.270(9)Å for **6.1**; Ag(1)-N(2) 2.347(6)Å for **6.2**) are only slightly longer than Ag-N_{py} distances in bis(pyridine) complexes of Ag(OTf).[73] Significantly, these distances are substantially shorter than those observed in the In and Tl analogues $[\{ArN{=}CPh\}_2(NC_5H_3)]In^+(OTf)^-$ (Ar = 2,5-$^tBu_2C_6H_3$ **2.1**, 2,6-$^iPr_2C_6H_3$ **2.2**), and $[\{ArN{=}CPh\}_2(NC_5H_3)]Tl^+(OTf)^-$ (Ar = 2,5-$^tBu_2C_6H_3$ **4.1**, 2,6-$Me_2C_6H_3$ **4.2**). For the indium complexes there is minimal electron donation from the ligand and the respective In-N_{py} values of 2.495(5)Å and 2.502(5)Å reflect this. Even more extreme values can be found for thallium with Tl-N_{py} values of 2.646(6)Å and 2.7386(18)Å for **4.1** and **4.2** respectively. The Ag-N_{imine} distances of **6.1** (Ag(1)-N(2) 2.523(7)Å) and **6.2 (**Ag(1)-N(1) 2.526(9)Å, Ag(1)-N(3) 2.492(6)Å) are also shorter than the analogous In-N_{imine} distances for **2.1** (2.747(5)Å and 2.689(5)Å) or **2.2** (2.664(5)Å and 2.679(5)Å). Overall this pincer geometry leaves the hemisphere of the Ag^+ cation, that is opposite of the ligand, open to coordination. One of the oxygen sites of the triflate counterions approaches the open face of the silver centre oriented approximately perpendicular to the AgN_3 plane at distances of Ag(1)-O(1), 2.331(8)Å for **6.1** and 2.638(6)Å for **6.2**. These distances are slightly shorter than the corresponding distances between silver and triflate in the recently reported pyridine complexes of silver triflate.[45] The position and orientation of the triflate anion is the result of two effects: the empty Ag 5p orbital that is perpendicular to the AgN_3 plane (*vide infra*) and ligand/ligand

[71] Recent minireview of pyridine-derived tridentate pincer ligands. J.I. van der Vlugt, J.N.H. Reek *Angew. Chem. Int. Ed.* **2009**, *48*, 8832.

[72] Monovalent silver and gold compounds of anionic and neutral pincer ligands are reported but they do not display pincer geometries. For Ag(I) examples see: A. Fraix, M. Lutz, A.L. Spek, R.J. M. Klein Gebbink, G. van Koten, J.-Y. Salaün. P.-A. Jaffrè *Dalton Trans.*, **2010**, *39*, 2942. J. I. van der Vlugt, M.A. Siegler, M. Janssen, D. Vogt A. L. Spek *Organometallics* **2009**, *28,* 7025. J.C. DeMott, F. Basuli, U.J. Kilgore, B.M. Foxman, J.C. Huffman, O.V. Ozerov, D.J. Mindiola, *Inorg. Chem.*, **2007**, *46*, 6271. F.Camso, M.Camalli, H.Rimml, L. M. Venanzi *Inorg. Chem.* **1995**, *34*, 673. For examples of Au(I) see: M. Contel, M. Stol, M.A. Casado, G.P.M. van Klink, D.D. Ellis, A.L.Spek, G.van Koten *Organometallics* **2002**, *21*, 4556. M. Contel, D. Nobel, A. L. Spek, G. van Koten *Organometallics* **2000,** *19,* 3288. S.-J. Shieh, X. Hong, S.-M. Peng, C.-M. Che, *J. Chem. Soc., Dalton Trans.* **1994**, 3067.

[73] C. Di Nicola, Effendy, F. Marchetti, C. Nervi, C. Pettinari, W.T. Robinson, A.N. Sobolevb, A.H. White *Dalton Trans.*, **2010**, *39*, 908 and referenced therein.

electrostatic interactions that favor alignment of the negative charge density on the O centers with δ+ charges on the imino-carbon ligand sites.[30]

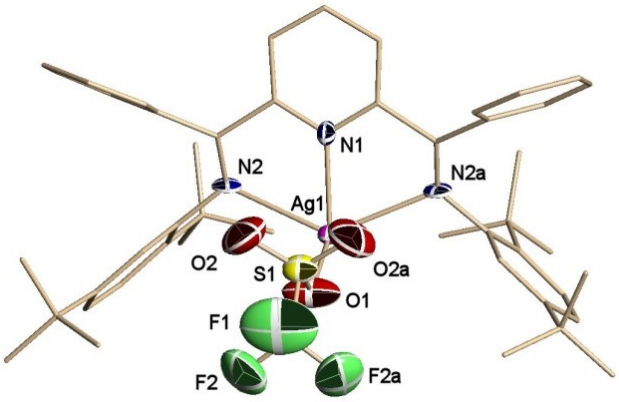

Figure 6.2: X-ray structure of compound **6.1**, with hydrogen atoms and $CHCl_3$ omitted for clarity. Select bond lengths and angles are given in Tables 6.4 and 6.6.

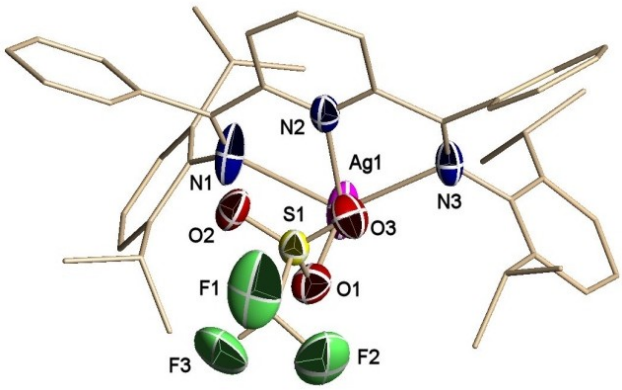

Figure 6.3: X-ray structure of compound **6.2**, with hydrogen atoms toluene omitted for clarity. Select bond lengths and angles are given in Tables 6.4 and 6.6.

Computational Analysis: In collaboration with Dr. Serge Gorelsky, a more intimate examination of the electronic features of compounds **6.1** and **6.2** was obtained through a DFT computational study using the B3LYP functional and the mixed DZVP/TZVP basis set.[74] The electronic interaction energy between the Ag[bis(imino)pyridine]$^+$ (LAg^+) cation and the OTf

[74] T. Jurca, S.I. Gorelsky, I. Korobkov, D.S. Richeson, *Dalton Trans*., **2011**, 40, 4394.

anion was determined to be similar for **6.1** and **6.2** with values of -85.7 and -84.5 kcal/mol, respectively. Furthermore, these compounds displayed similar cation/anion bond orders of 0.31-0.32 which corresponded to approximately 0.18-0.19 electron transferred from the triflate to the LAg^+ fragment. Two unoccupied acceptor orbitals on the LAg^+ fragment (LUFO and LUFO+2) participated in covalent component of bonding with the OTf^- anion. The Ag character of these fragment orbitals (FOs) was dominated by the empty Ag 5*s* orbital.[75]

Turning attention to the bonding interaction between the bis(imino)pyridine ligand and the silver centre within the LAg^+ cation, the computational results revealed that greater than 50% of the electronic interaction energy (**6.1** = -87.7 kcal/mol, **6.2** = -89.0 kcal/mol) is due to covalent bonding between the metal ion and the ligand. In both compounds the bis(imino)pyridine ligands donate 0.4 electrons to the Ag^+ ion. This donation comes primarily from the four highest occupied orbitals of the ligand that are shown in Figure 6.4. Four orbitals on the Ag^+ cation fragments accept this electron density: LUFO-LUFO+3. The LUFO of the Ag^+ centre has 100% 5*s* character and is a major contributor (60%) to the covalent bonding with the HOFO-6 ligand orbital. The three remaining unoccupied acceptor orbitals on the Ag cation are of 5*p* character; two of these orbitals (LUFO+1 and LUFO+2) lie in the ligand plane and accept σ-type electron density from the ligand donor orbitals HOFO and the HOFO-5/HOFO-1 combination respectively. The remaining metal acceptor orbital, LUFO+3, is the 5*p* Ag orbital oriented perpendicular to the ligand plane and is of π-symmetry and accepts very little electron density from the bis(imino)pyridine ligand.

[75] For comparison compound **2.2**, the In(I) analogue of compound **6.2**, exhibited a similar In-OTf distance (2.462(6)Å). However, a fragment orbital population analysis revealed that only 0.10 electrons are transferred from the anion to a cation FO that had a significant In-based component. This orbital was dominated (85%) by In 5p character. In these compounds the bulk of electron donation was actually to the ligand component of the $In[bis(imino)pyridine]^+$ cation. Analogous behaviour is also observed in our work with thallium (Chapter 4).

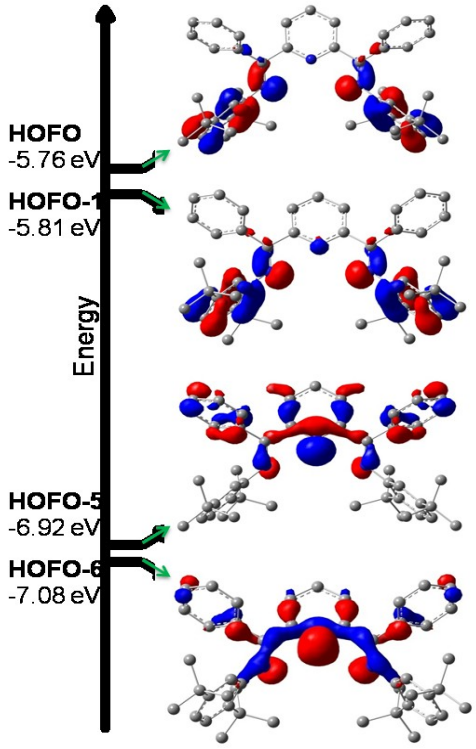

Figure 6.4: The four most significant donor orbitals of the pincer ligand in **6.1**. The energy of each orbital is provided with the label.

[6.4] Results and Discussion: Adduct Formation and Computational Analysis

The ligand array and geometry of cationic complexes **6.1** and **6.2** provide an interesting set of compounds to investigate the nature of interactions with common Lewis base ligands. The reactivity of the open face of compounds **6.1** and **6.2** with σ and π ligands was probed by the reactions shown in Scheme 6.3. Addition of pyridine, arene, alkyne or cyclooctene to the LAg^+ centres of **6.1** or **6.2** led to weak coordination of these species to the open site of the cation species. In fact, the LAg^+/donor interactions produce labile species that could be captured and examined by single crystal X-ray analysis but these adducts did not exhibit distinct NMR signals indicating that the coordinating species is released when compounds **6.1a-d** and **6.2a** were

dissolved in solution. Furthermore, preparation of samples of compounds **6.1a-d** and **6.2a** for elemental analysis led to results consistent with loss of the coordinating species (i.e pyridine, toluene, 2-butyne, cyclooctene).

Scheme 6.3

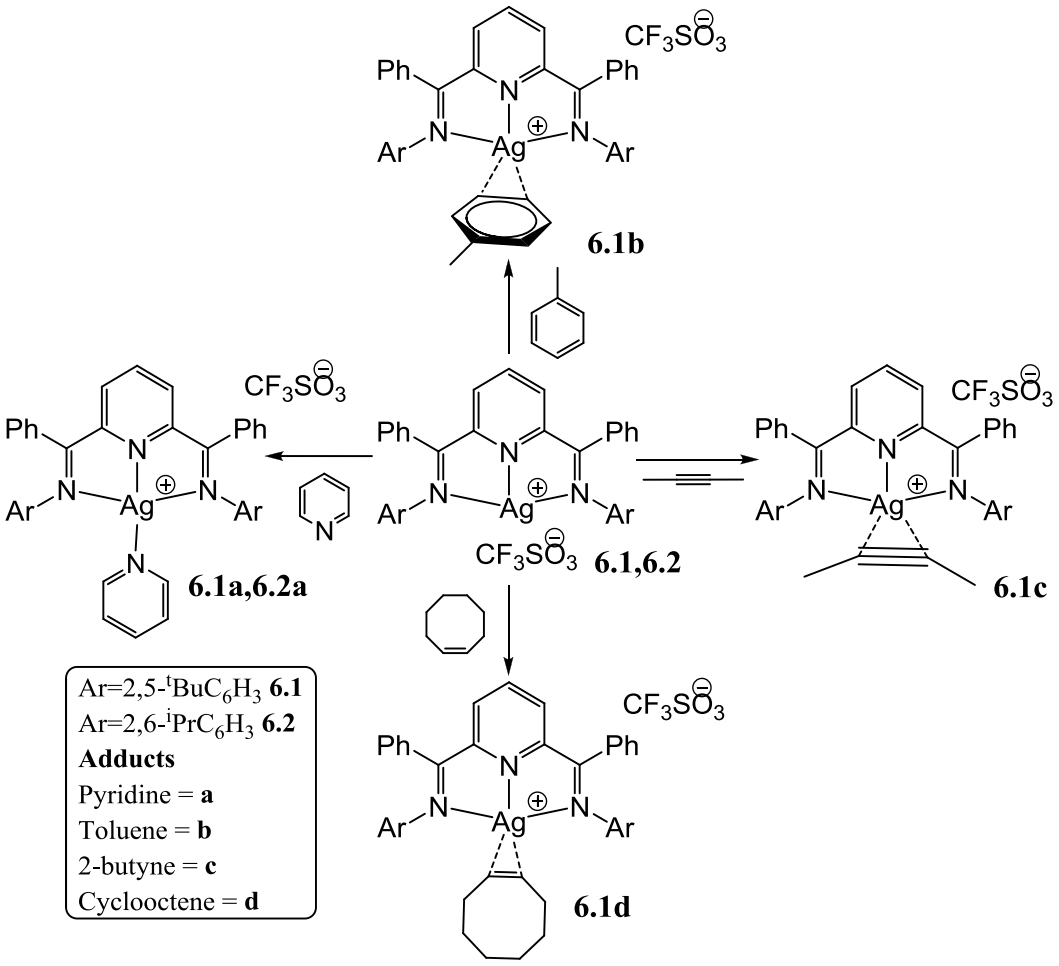

When **6.1** and **6.2** are recrystallized from pyridine, single crystals of the pyridine adducts **6.1a** and **6.2a** were repeatedly obtained which were analyzed by single crystal X-ray diffraction. The results are summarized in Figures 6.5 and 6.6 and Tables 6.4, 6.6, 6.5 and 6.7. Both compounds display LAg(pyridine)$^+$ cations with an LAg$^+$ fragment in a pincer geometry of a planar terdentate bis(imino)pyridine ligand array. The bonding parameters within the [bis(imino)pyridine]Ag$^+$ fragments of **6.1a** and **6.2a** are very similar to the parent

species. The coordinated pyridine fragment lies in the open face of the LAg^+ moiety to yield a distorted square planar metal centre within the limits due to the restrictions of the bis(imino)pyridine ligand. Interestingly, the plane of the coordinated pyridine ligands in these two compounds is nearly co-planar/coincides with that of the bis(imino)pyridine ligands. In the case of **6.1a**, the angle between the planes defined by the pyridyl group of the bis(imino)pyridine ligand and the coordinated pyridine ligand was 10.2(1)° with an analogous angle for **6.2a** of 25.9(1)°. This disposition appears to be a result of the steric pocket provided by the NAr groups. In both compounds, the triflate anion is more removed than in the parent compounds. The shortest Ag-triflate contact for **6.1a** was Ag(1)-O(2) at >3.0Å and in **6.2a** it was Ag(1)-O(1) at ≈2.7Å. The lability of the coordinated pyridine in compounds **6.1a** and **6.2a** was demonstrated by elemental analysis, whereby loss of pyridine adduct was evident even in samples subjected to minimal sample preparation/handling prior to combustion.

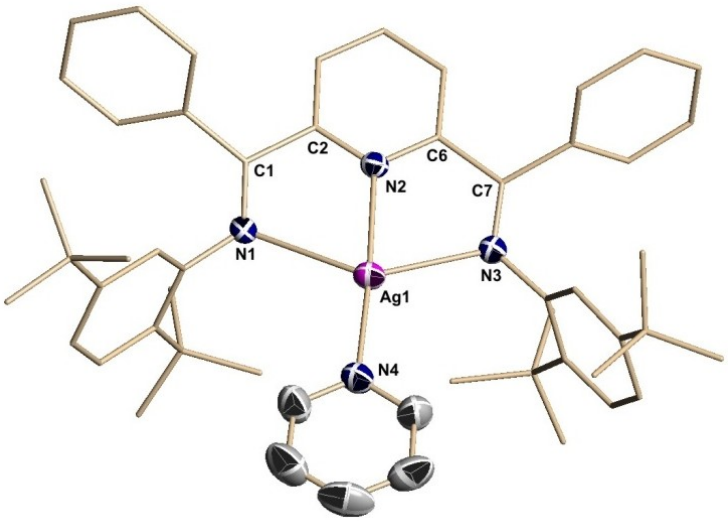

Figure 6.5: X-ray structure of compound **6.1a**, with hydrogen atoms and triflate counterions omitted for clarity. Select bond lengths and angles are given in Tables 6.5 and 6.7.

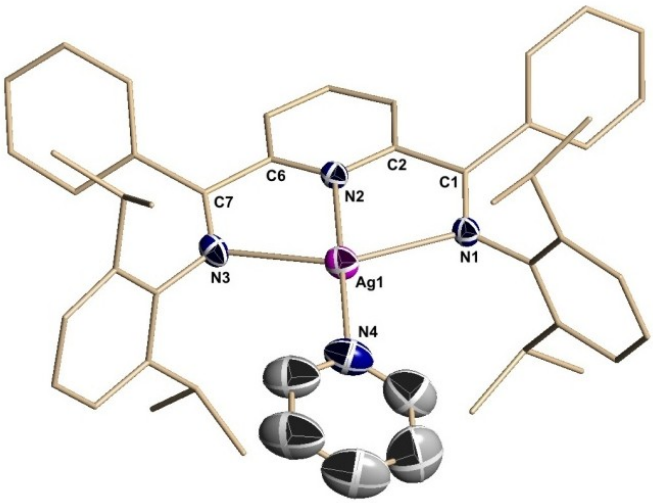

Figure 6.6: X-ray structure of compound **6.2a**, with hydrogen atoms and triflate counterions omitted for clarity. Select bond lengths and angles are given in Tables 6.4 and 6.6.

When **6.1** was crystallized from toluene, crystals of **6.1b** were isolated that demonstrate the Lewis acidity of the LAg^+ pincer cation (Figure 6.7). The coordination of toluene has displaced the OTf- anion to a distance >6.3Å and the silver centre bonds symmetrically to the *m*- and *p*-carbons of the toluene molecule. The distance between the Ag centre and the mean aromatic plane of 2.279Å and Kochi's geometric criteria gave a hapticity for **6.1b** of η=2.02.[76] Again, while the formation of crystals of **6.1b** was reproducible, attempts to obtain elemental analysis of this species was hindered by loss of toluene during sample isolation and transport.

Similarly, the alkyne adduct of **6.1** was obtained when this silver complex was crystallized in excess 2-butyne. The results of a single crystal X-ray analysis of this new compound **6.1c** are presented in summary form with Figure 6.8 and Tables 6.5 and 6.7. As with

[76] A.V. Vasilyev, S.V. Lindeman, J.K. Kochi, *Chem. Commun.,* **2001**, 909.

the pyridine and toluene adducts, **6.1a** and **6.1b**, the alkyne complex, **6.1c**, displayed a silver centre coordinated by the tridentate pincer ligand. Overall the Ag-N distances in the LAg^+ fragment ($Ag\text{-}N_{py}$ and $Ag\text{-}N_{imine}$) are similar to those observed for **6.1** and **6.1a-b**. Similarly, the Ag-OTf distance is increased relative to the starting material **6.1**. The 2-butyne is coordinated symmetrically to the Ag centre with Ag-C distances of 2.373(3)Å and 2.369(3)Å. This coordination only very slightly lengthens the C≡C bond distance with the observed value of 1.186(4)Å versus the reported value of 1.1160Å.[77] In addition, the alkyne moiety exhibits only a minor deviation from linearity with C(49)-C(50)-C(51) angle of 169.14(3)º. Overall, these features suggest little, if any, back donation from the metal centre to the 2-butyne. The alkyne is coordinated along the same vector as was observed for the pyridine coordination in **6.1a** and, like that compound, the C(50)-Ag(1)-C(49) plane approaches a co-planar orientation with that of the bis(imino)pyridine ligand with an observed angle between pyridine ring and alkyne plane of 31.8(5)º.

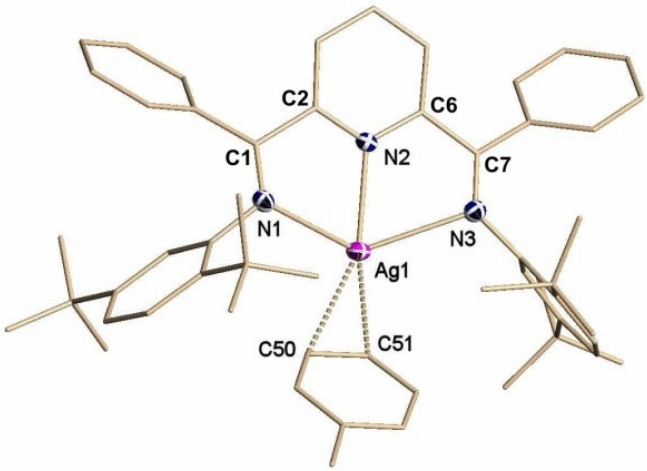

Figure 6.7: X-ray structure of compound **6.1b**, with hydrogen atoms and triflate counterions omitted for clarity. Select bond lengths and angles are given in Tables 6.5 and 6.7.

[77] NIST Computational Chemistry Comparison and Benchmark Database, NIST Standard Reference Database Number 101 , Release 15b, August 2011, Editor: Russell D. Johnson III, http://cccbdb.nist.gov/

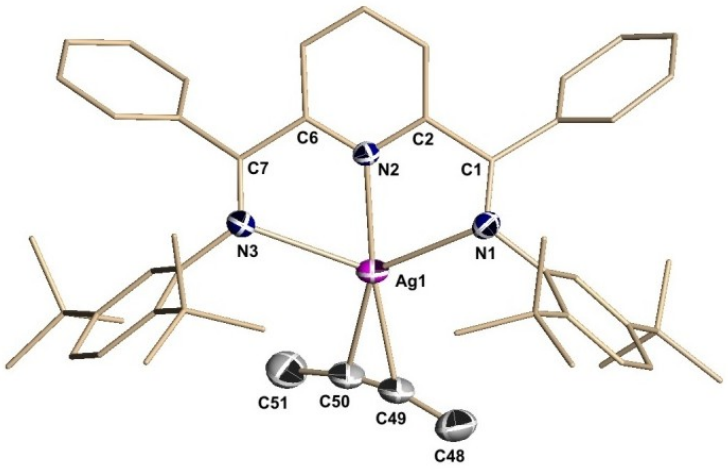

Figure 6.8: X-ray structure of compound **6.1c**, with hydrogen atoms and triflate counterions omitted for clarity. Select bond lengths and angles are given in Tables 6.5 and 6.7.

This compound can be compared to both trigonal planar and tetrahedrally coordinated Ag-alkyne complexes. The Ag-C_{alkyne} distances in **6.1c** are longer than those observed in the trigonal planar hexyne adduct of a triazapentadienyl Ag complex with Ag-C distances of 2.233Å and 2.241Å [78] as well as those in Ag(hfac)($Me_3SiCCSiMe_3$) ($hfac^-$ = $(CF_3COCHCOCF_3)^-$) with Ag-C_{alkyne} distances of 2.255(4)Å and 2.267(4)Å.[79] A trispyrazolyl borate complex of Ag(I) coordinates both acetylene (Ag-C_{alkyne} = 2.293(4)Å) and phenylacetylene (Ag-C_{alkyne} = 2.263(5)Å, 2.407(5)Å) to yield tetrahedral species.[68]

We explored the coordination of alkenes to the LAg^+ fragment by crystallizing compound **6.1** in excess cyclooctene. Single crystal X-ray analysis revealed this species to be compound **6.1d**, [LAg^+(cyclooctene)][OTf^-] with the results presented in Figure 6.9 and Table 6.5 and 6.7. Similar to compounds **6.1** and **6.1a-c**, the bis(imino)pyridine ligand provides a planar pincer coordination with a typical Ag(1)-N(2) distance (2.296(4)Å) and

[78] H.V.R. Dias, J.A. Flores, J. Wu, P. Kroll, *J. Am. Chem. Soc.*, **2009**, 131, 11249.
[79] W.J. Evans, D.G. Giarikos, D. Josell, J.W. Ziller, *Inorg.Chem.*, **2003** , 42, 8255.

only slightly asymmetrically to the N_{imine} sites of the ligand. The Ag-C_{olefin} distances (2.418(5)Å, 2.360(6)Å) are slightly longer than those of the four coordinate species [HB(3,5-$(CF_3)_2Pz)_3$]Ag-(H_2CCH_2) (Ag-C = 2.294(7)Å and 2.307(7)Å).[68] The cyclooctene adduct, **6.1d,** exhibited a C=C distance (C(48)-C(49) 1.361(8)Å) slightly elongated from the free cyclooctene value of 1.22(4)Å.[801] Like the pyridine and the alkyne adducts, the olefin displays a rather small angle with the bis(imino)pyridine ligand plane; the angle between the pyridine ring and olefin-Ag fragment is 27.8 (0.4)º. Lastly, Figure 6.10 shows expanded packing diagrams of the unit cell for **6.1a** and **6.1d**. Of note is the position of the triflate anion which resides over the δ+ sites of the ligand, and the lack of any short contacts between molecules. Similar cation-anion interaction is also observed for **6.1c** and **6.2a**.

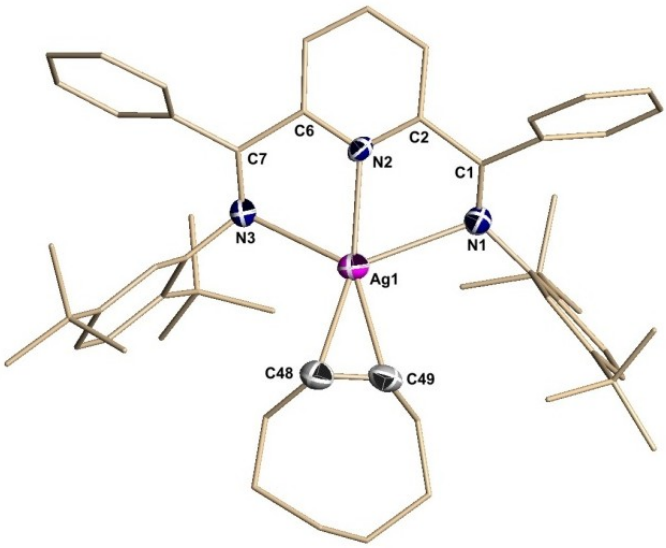

Figure 6.9: X-ray structure of compound **6.1d**, with hydrogen atoms and triflate counterions omitted for clarity. Select bond lengths and angles are given in Tables 6.5 and 6.7.

[80] V.V. Bbashilov, P.V. Petrovsky, V.I. Sokolov, F.M. Dolgushin, A.I. Yanovsky, Yu.T. Struchkov, *Izv. Akad. Nauk SSSR, Ser. Khim.*, **1996**, 1268.

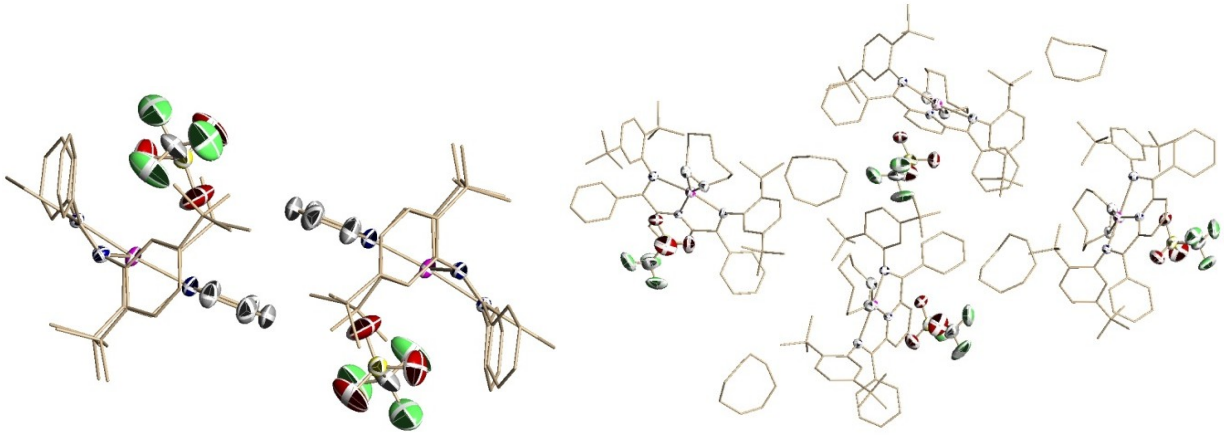

Figure 6.10: Crystal packing diagrams of **6.1a** and **6.1d**, with hydrogen atoms omitted for clarity. There are no significant long range interactions or short contact points between molecules.

Computational Analysis: The combination of our experimental observations on the nature of compounds **6.1a-d** and the analysis of the crystallographic features of these compounds indicated that they exhibit weak interactions between the LAg^+ cation and the ligands. In order to quantify the degree and details for the interactions between the [bis(imino)pyridine]Ag^+ cation and the coordinated moieties, and with the help of Dr. Serge Gorelsky, we examined the interaction of these fragments using computations with the resulting data summarized in Table 6.1.[81] Frequency analysis on the optimized structures confirmed that they were minima and provided the data for the calculation of free energy of adduct formation (ΔG_f) and sum of electronic and zero-point energies, ΔE, according to equation 2.

$$[\{ArN{=}CPh\}_2(NC_5H_3)]Ag]^+ + \mathbf{L'} \longrightarrow [\{ArN{=}CPh\}_2(NC_5H_3)]Ag\mathbf{L'}]^+ \quad (2)$$

Ar = 2,5-^{t}Bu$_2$C$_6$H$_3$ **6.1$^+$**; 2,6-^{i}Pr$_2$C$_6$H$_3$ **6.2$^+$**

L' = pyridine **6.2a**, toluene **6.1b**, 2-butyne **6.1c**, cyclooctene **6.1d**

[81] T. Jurca, S. Ouanounou, I. Korobkov, S.I. Gorelsky, D.S. Richeson, *Dalton Trans.,* **2012**, 41, 4765.

Table 6.1. Summary of Computational Results on Compounds **6.1b-d**, and **6.2a**.

	Ligand, **L'**	E_{int} (kcal/mol)	Bond order	Charge donation (electrons)	ΔG_f (kcal/mol)	ΔE (kcal/mol)
6.2a	pyridine	-23.9	0.25	0.11	-6.2	-18.9
6.1b	toluene	-12.9	0.44	0.19	1.2	-9.4
6.1c	2-butyne	-17.1	0.53	0.28	1.6	-9.6
6.1d	cyclooctene	-17.6	0.62	0.26	1.2	-11.0

The LAg^+/pyridine interactions in compound **6.2a** were examined with a DFT computational study using the B3LYP functional and the mixed DZVP/TZVP basis set. Full optimization of this compound yielded a structure in accord with the cation in **6.2a** including the features of the Ag-pyridine bonding. Our analysis indicated that the electronic interaction energy between the two fragments was -23.9 kcal/mol with donation of only 0.11 electrons from the N-based lone pair of the pyridine (e.g. 5.5% of the population of the HOFO). This corresponded to a bond order of 0.25 between the fragments. The two LAg^+ acceptor orbitals, LUFO and LUFO+2 (Figure 6.11), receive nearly equal components of this electron donation (2.3 and 3.9% respectively). In terms of Ag contribution, both of these orbitals consist mainly of the empty Ag *5s* orbital with the LUFO being 25% *5s* and 6% *5p* and the LUFO+2 being 53% *5s* and 7% *5p*. Significantly, almost 70% of the LUFO is actually based on the bis(imino)pyridine ligand. Furthermore, even the LUFO+2 is about 40% bis(imino)pyridine in character. Although the donation of electron density from a coordinated pyridine to the Ag *5s* orbital is as expected, the important role of the supporting ligand in this bonding, revealed in this analysis, is unexpected. The small value for the free energy of formation of this adduct is in agreement with our observations that the pyridine ligand is only weakly bound to the Ag centre.

A similar analysis of the bonding interactions between the LAg^+ cation and the toluene moiety was carried out. In order to facilitate the computations, the $LAg(toluene)^+$

cation in **6.1b** was modeled by replacing the 2,5-$^{t}Bu_2C_6H_3$ groups with simple phenyl rings. Similary, using the B3LYP functional and the mixed DZVP/TZVP basis set on this model yielded a structure in agreement with the cation in **6.1b**. The electronic interaction energy between the [bis(imino)pyridine]Ag^+ and the toluene fragments was determined to be -12.9 kcal/mol with a corresponding bond order of 0.44 and a charge transfer of 0.19 electrons from toluene to the silver fragment. The toluene/Ag interaction is σ in nature and involves the π-orbitals on toluene and LAg^+ fragment orbitals shown in Figure 6.11. As was observed with compound **6.2a**, **t**he silver fragment acceptor orbitals LUFO and LUFO+2 are the major recipients of electron donation from the toluene HOFO (4.4%) and HOFO-4 (2.5%). Again, the LUFO+2 is predominantly an Ag orbital. Again it was both interesting and unexpected that the other acceptor orbital was the bis(imino)pyridine-based π^*-orbital. This unusual bonding points to the important role of the bis(imino)pyridine ligand not only in stabilizing the pincer geometry of Ag^+ but in the formation of adducts. The interaction between the supporting bis(imino)pyridine ligand and the coordinated toluene is a key component in the adduct formation. The nearly zero value of the ΔG_f is, once again, consistent with the labile nature of this interaction.

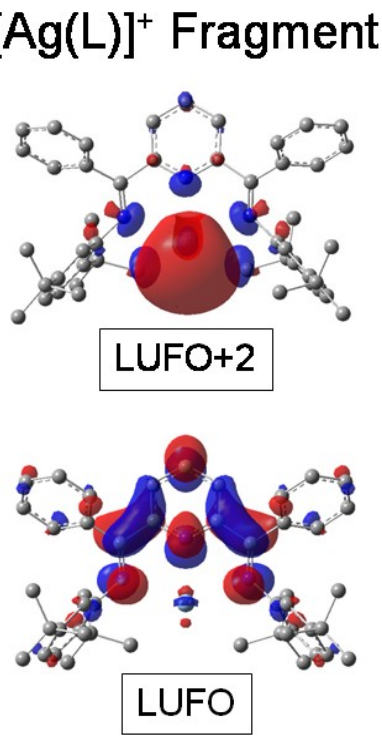

Figure 6.11: Fragment orbitals for the optimized cation fragment, [{(2,5-$tBu_2C_6H_3$)N=CPh}$_2$(NC_5H_3)]Ag^+. These are the FOs with the largest electron acceptor contributions to bonding in **6.2a**, and **6.1b-d**.

The 2-butyne ligand interacts more strongly with the LAg^+ cation of **6.1c** than the toluene in adduct **6.1b** as evidenced by a greater electronic interaction energy between the LAg^+ cation and the alkyne of -17.1 kcal/mol as well as a higher bond order (b.o. = 0.53) and greater degree of charge transfer from the alkyne to LAg^+ of 0.23 electrons. The only significant interaction is σ in nature and is donation of 8.9% of the electronic population from the alkyne HOFO (π bonding) to Ag. There was no significant back donation contribution to the Ag-alkyne interaction (i.e. into the LUFO of the alkyne) a feature consistent with the crystallographic data and supported by the observed lability of this adduct. In this case the donation from the alkyne moiety is distributed between the LUFO (3%) and LUFO+2 (5.9%) (see Figure 6.10). Once

again, adduct bonding involves acceptor orbitals that have significant bis(imino)pyridine ligand-based components. For example, the LUFO is only 20% Ag-centered with 80% bis(imino)pyridine character while the LUFO+2 is 68% on Ag 32% on the tridentate ligand. Consistent with the previous observations, the Ag contribution is dominated by the *5s* orbital (i.e. 65.4% *5s* for LUFO+2).

The degree and nature of the interaction between the LAg^+ cation and olefin in **6.1d** is similar to that observed in the alkyne complex **6.1c**. Specifically, the interaction energy between the fragments was determined to be -17.6 kcal/mol with a bond order of 0.62 and corresponding charge donation of 0.26 electrons. In this case, the olefin contributes 10.8% of the electron density in the HOFO (olefin π) through a σ interaction with the two cation acceptor orbitals: the LUFO (4.7%) and LUFO+2 (6.3%). The nature of these two orbitals was as observed for the other adducts with the LUFO being largely bis(imino)pyridine in nature (71% *versus* 29% Ag) and the LUFO+2 being 66% Ag with a substantial contribution (33%) from the supporting bis(imino)pyridine ligand.

[6.5] Conclusion

The first reported ligation of Ag^+ with bis(imino)pyridine yielded unique pincer complexes of Ag. Importantly ligand/anion interactions are shown to be significant general features in these species that impact on geometry and complex formation. Although this ligand coordinates more strongly to Ag^+ than In^+ and Tl^+, the Ag^+ center remains sufficiently Lewis acidic, which facilitated the study of adduct formation with weakly coordinating ligands, ranging from pyridine to arene, alkyne and olefin species. Furthermore, the resulting ligand/ligand interactions are a somewhat surprising common feature and these interactions have

important repercussions on complex formation. In addition to the conventional electron donation from the ligand to the metal centre, a remarkable contribution to the bonding in these species is an unusual donation to an essentially bis(imino)pyridine-based π*-orbital. This unconventional bonding interaction involving a non-innocent role of the bis(imino)pyridine ligand in adduct formation may have broader implications on the application of these and other transient species to organic transformations.

Lability and reactivity are fundamental objectives in chemistry which are in opposition to isolation and characterization of stable species. The capture and analysis of weakly bonded complexes has important implications on reactivity and can challenge and enhance concepts of bonding and stability. Because such species are fragile and vulnerable to transformation only some characterization tools may be applicable to their analysis, in contrast to the examination of unreactive, stable compounds. Computations can enhance the characterization and provide a springboard for defining more subtle features of intermolecular interactions that go beyond conventional electron transfer/donor bonds.

[6.6] Silver Complex Experimental

General Methods. Reactions were performed in a glovebox with a nitrogen atmosphere. All solvents were sparged with nitrogen and then dried by passage through a column of activated alumina using an apparatus purchased from Anhydrous Engineering. Deuterated chloroform was dried using activated molecular sieves. Metal halides were purchased from Strem Chemicals and used as received. All other chemicals were purchased from Aldrich and used without further purification. NMR spectra were run on a Bruker Avance 300 MHz spectrometer with $CDCl_3$ as

solvent and internal standard. Elemental analyses for **6.1,** and **6.2** were performed by Midwest Microlab LLC, Indianapolis IN.

(6.1) [Ag-2,6-Bis{1-[(2,5-ditertbutylphenyl)imino]-benzyl}pyridine][OSO_2CF_3]: $AgOSO_2CF_3$ powder (38 mg, 0.150 mmol) was added to a clear yellow solution of **1A** (100 mg, 0.151 mmol) in 8 mL of toluene. The reaction mixture was sealed, wrapped in aluminum foil due to light sensitivity of $AgOSO_2CF_3$ and allowed to stir for 14 hours, gradually becoming opaque yellow. Solution was then held at -20^oC overnight, over which time a bright yellow precipitate formed. Solution was filtered, washed with 5 x 2 mL hexanes, and allowed to dry under vacuum. A bright yellow powder was isolated in 69% yield. Large yellow cubic crystals suitable for X-ray analysis were grown by diffusion of saturated $CDCl_3$ solution in hexanes, and storing at -20^oC for several days. ^1H NMR ($CDCl_3$, 300 MHz): δ 7.89(br t, 1 H, py, *p*-CH), 7.60(br d , 2 H, py, *m*-CH), 7.40-7.10(br m, 12 H, aromatic), 6.96(br d, 1H, aromatic), 6.93(br d, 1 H, aromatic), 6.53(br d, 2 H, aromatic), 1.49(br s, 18H, ^tBu), 0.96(br s, 18H, ^tBu). ^{13}C NMR ($CDCl_3$, 75 MHz). δ 165.6(C=N imine), 152.7(py, *o*-C=N), 149.9(Ar-CH), 148.3 (Ar-CH), 138.9(Ar, *i*-C), 138.1(Ar-CH), 134.3(Ar, *i*-C), 129.8(Ar-CH), 129.3(Ar-CH), 128.3(Ar-CH), 126.1(Ar-CH), 125.0 (Ar-CH), 121.9(Ar-^tBu, C-^tBu), 120.7(Ar-^tBu, C-^tBu), 35.5(Ar-^tBu, C-$(CH_3)_3$), 34.2(Ar-^tBu, C-$(CH_3)_3$), 31.2(Ar-^tBu, CH_3), 30.9(Ar-^tBu, CH_3). Sample for elemental analysis was obtained by recrystallization in toluene, resulting in a 1:1 toluene adduct of **6.1** calculated (%) for $[C_{48}H_{55}AgF_3N_3O_3S][C_7H_8]$: C 65.34, H 6.28, N 4.16, found C 64.92, H 5.97, N 3.90.

(6.2) [Ag-2,6-Bis{1-[(2,6-diisopropylphenyl)imino]-benzyl}pyridine][OSO_2CF_3]: $AgOSO_2CF_3$ powder (42 mg, 0.164 mmol) was added to a clear yellow solution of **1B** (100 mg, 0.165 mmol) in 8 mL of 5:1 hexanes to toluene solution. The reaction mixture was sealed, wrapped in aluminum foil due to light sensitivity of $AgOSO_2CF_3$ and allowed to stir for 14 hours, gradually

becoming opaque yellow. Solution was then held at -20°C overnight, over which time a bright yellow precipitate formed. Solution was filtered, washed with 5 x 2 mL hexanes, and allowed to dry under vacuum. A bright yellow powder was isolated in 84% yield. Large yellow cubic crystals suitable for X-ray analysis were grown in a saturated solution of 1:1 toluene/hexanes, and storing at -20°C for several days. ^{1}H NMR ($CDCl_3$, 300 MHz): ^{1}H NMR ($CDCl_3$, 23°C): δ 7.98(t, 1H, py, *p*-CH), 7.79(d, 2H, py, *m*-CH), 7.42-6.95(br m, 16H, aromatic), 2.92(br m, 4H, ^{i}*Pr-CH*), 1.21(br d, 12H, CH_3), 0.91(br d, 12H, CH_3).^{13}C NMR ($CDCl_3$). δ 165.6(C=N imine), 152.3(py, *o*-C=N), 144.5(py, *m*-CH), 139.3(py, *p*-CH), 136.7(Ph, *m*-CH), 133.2(Ph, *o*-CH), 130.7(Ar-^{i}*Pr*, C-^{i}*Pr*), 129.4(Ar-^{i}*Pr*, CH), 129.3(Ph, *i*-C),128.4(Ph, *p*-CH), 125.8(Ar-^{i}*Pr*, C- ^{i}*Pr*), 123.6(Ar-^{i}*Pr*, CH), 28.7(Ar-^{i}*Pr*,CH_3), 24.6(Ar-^{i}*Pr*, CH-$(CH_3)_2$), 22.6(Ar-^{i}*Pr*,CH_3). Sample for elemental analysis was obtained by recrystallization in toluene, resulting in a 1:1 toluene adduct of **6.2** calculated (%) for $[C_{44}H_{47}AgF_3N_3O_3S][C_7H_8]$: C 64.15, H 5.81, N 4.40, found C 64.83, H 5.78, N 4.19.

Formation of Adducts 6.1a-d, 6.2a: Adducts **6.1a-d** and **6.2a** were prepared by dissolution of either **6.1** or **6.2** in a neat solution of the appropriate ligand species (~15mg of Ag complex in 1.5 mL of solvent). The solutions were allowed to stir for 1 hour and then filtered through a Celite plug into a small vial. This vial was left uncovered and placed within a larger vial with hexanes. The large vial was sealed and placed in the freezer at -30°C for several days. During this time some hexane diffused into the smaller, internal vial and crystals suitable for X-ray crystallography formed. All of these species produced crystals which were bright yellow and are either plates (**6.1a-c**) or blocks (**6.1d**, **6.2a**). Attempts to characterize adducts via NMR, elemental analysis and infrared were inconclusive. Adducts readily dissociate in solution, and decompose under standard preparation procedure for elemental analysis samples.

Infrared spectra were collected on a Hartmann & Braun BOMEM B-100 spectrometer. Samples of compounds **6.1** and **6.2** were prepared as KBr pellets. Samples of **6.1a-d** and **6.2a** were isolated from solution, dried only briefly to avoid loss of coordinated ligand, and prepared as smears on NaCl plates. All experiments were conducted under laboratory atmosphere. Values are reported in cm^{-1} and are ranked in order of decreasing intensity. The rank is provided in brackets. Absorbances with the same relative intensities were given identical ranking. Due to overlap of ligand and adduct peaks, results remain inconclusive.

6.1: 3060.2(26), 2961.3(9), 2906(15), 2867.1(14), 1598.1(12), 1586.3(11), 1494 (16), 1462.3(20), 1444.2(19), 1385.2(17), 1360.7(21), 1281.9(2), 1256.7(1), 1224(13), 1148.4(8), 1133.4(7), 1051.6(18), 1031.6(4), 928.2(27), 820.7(10), 777.6(25), 756.9(9), 719.1(23), 697.8(5), 637.2(3), 537.9(27), 517.4(24).

6.1a: 3078(11), 3052.4(14), 3025(10), 3000.5(13), 1921.5(19), 1873.4(18), 1632.7(17), 1597.4(8), 1580.7(3), 1482(9), 1437.8(2), 1216.7(16), 1146.6(15), 1068.2(12), 1030.5(6), 990.6(7), 747.8(4), 704.5(1), 602.8(5).

6.1b: 3086.5(10), 3062(7), 3027.1(4), 2920.2(5), 2872.1(12), 2734.1(21), 1942.6(16), 1858(17), 1803(18), 1736.6(22), 1604.3(6), 1523.5(14), 1495.7(3), 1460.9(8), 1379.3(13), 1178.7(15), 1081.3(11), 1030.1(9), 895.6(19), 785.3(20), 728.7(1), 694.4(2).

6.1c: 2958.8(2), 2922.9(1), 2862.8(4), 2738.2(10), 1598(13), 1444.8(3), 1375.1(8), 1275.7(9), 1249.9(7), 1162.2(11), 1028.5(6), 700.6(12), 637.8(5).

6.1d: 3015.2(4), 2926.7(1), 2851.8(2), 2682.1(13), 1710.9(22), 1650.2(16), 1466.1(5), 1448.5(8), 1357.9(15), 1277.4(14), 1264.1(14), 1242.7(11), 1175.1(18), 1117(19), 1069.6(20), 1024.7(21), 982.8(12), 971(18), 892.8(9), 874.4(18), 820.3(17), 765.4(10), 751.1(3), 701.9(6), 575.5(7).

6.2: 3059.4(22), 2959.6(11), 2927.2(16), 2868.3(17), 1622.6(10), 1600.1(21), 1581.7(13), 1492.7(25), 1462.6(14), 1444.1(12), 1383.8(19), 1362(26), 1328.2(19), 1281.7(5), 1246.6(3), 1220.4(9), 1154.4(4), 1080.6(20), 1049.4(15), 1026.9(1), 846.86(23), 772.9(8), 754.3(7), 707.3(10), 698.9(6), 635.22(2), 572(24), 515.9(18).

6.2a: 3078.7(6), 3025.4(7), 3000.9(10), 2008.7(18), 1928.3(17), 1822.1(19), 1597.3(9), 1581(3), 1482.3(11), 1438.2(2), 1275.6(16), 1216.6(15), 1147.1(14), 1068.2(13), 1030.9(8), 990.9(12), 748.6(5), 704.5(1), 602.7(4).

[6.7] X-ray Crystallographic Information: Silver Complexes and Adducts

Table 6.2. Summary of Data Collection and Crystallographic Parameters for **6.1**, **6.2** & **6.2a**.*

Compound	**6.1**	**6.2**	**6.2a**
Empirical formula	$[C_{48}H_{55}AgF_3$ $N_3O_3S][CHCl_3]_{2.5}$	$[C_{44}H_{47}AgF_3$ $N_3O_3S][C_7H_8]_{0.5}$	$[C_{44}H_{47}AgF_3$ $N_3O_3S]$ $[C_5H_5N]$ $[C_4H_6]_{0.35}$
Formula weight	1217.30	908.84	960.81
Temperature (K)	200(2)	200(2)	200(2)
λ (Å)	0.71073	0.71073	0.71073
Crystal system	Monoclinic	Orthorhombic	Monoclinic
Space group	P2(1)/m	Fdd2	P2(1)/c
a (Å)	9.6367(18)	46.000(6)	14.3389(16)
b (Å)	27.216(5)	47.725(6)	18.947(2)
c (Å)	11.094(2)	8.9835(12)	18.189(2)
α (deg)	90.00	90.00	90.00
β (deg)	91.654(3)	90.00	90.00
γ (deg)	90.00	90.00	90.00
V ($Å^3$)	2908.5(9)	19722(4)	4890.0(10)
Z	2	16	4
ρ (calc) (Mg/m^3)	1.390	1.224	1.305
μ (mm^{-1})	0.777	0.501	0.510
Absorption correction	Semi-empirical from equivalents		
Final R indices [I>2σ(I)]			
R1[a]	0.0811	0.0680	0.0403
*w*R2[b]	0.1666	0.1699	0.1109

[a] $R1 = \Sigma \left| |F_o| - |F_c| \right| / \Sigma |F_o|$. [b] $wR2 = \left(\Sigma w \left(|F_o| - |F_c| \right)^2 / \Sigma w |F_o|^2 \right)^{1/2}$

*structure data available from CCDC

Table 6.3. Summary of Data Collection and Crystallographic Parameters for **6.1a-d**.

Compound	**6.1a**	**6.1b**	**6.1c**	**6.1d**
Empirical formula	$[C_{48}H_{55}AgF_3N_3O_3S][C_5H_5N]$	$[C_{48}H_{55}AgF_3N_3O_3S][C_7H_8]$	$[C_{48}H_{55}AgF_3N_3O_3S][C_4H_6]_{1.5}$	$[C_{48}H_{55}AgF_3N_3O_3S][C_8H_{14}]_{1.5}$
Formula weight	997.98	1011.01	1000.01	1084.17
Temperature (K)	200(2)	200(2)	200(2)	200(2)
λ (Å)	0.71073	0.71073	0.71073	0.71073
Crystal system	Triclinic	Triclinic	Monoclinic	Orthorhombic
Space group	P-1	P-1	C2/c	Pca2(1)
a (Å)	11.1402(4)	11.1617(5)	32.106(3)	31.0722(11)
b (Å)	15.4794(5)	15.3550(6)	20.658(2)	9.7664(4)
c (Å)	15.6244(6)	16.0260(7)	19.954(2)	19.8728(7)
α (deg)	98.249(3)	76.361(2)	90.00	90.00
β (deg)	110.516(2)	78.113(2)	118.949(5)	90.00
γ (deg)	91.383(2)	69.665(2)	90.00	90.00
V ($Å^3$)	2489.27(15)	2479.56(18)	11581(2)	6030.7(4)
Z	2	2	8	4
ρ (calc) (Mg/m^3)	1.331	1.354	1.147	1.194
μ (mm^{-1})	0.504	0.506	0.433	0.421
Absorption correction	Semi-empirical from equivalents			
Final R indices [I>2σ(I)]				
R1[a]	0.0407	0.0569	0.0474	0.0452
*w*R2[b]	0.0822	0.1547	0.1396	0.1207

[a] $R1 = \Sigma \left| |F_o| - |F_c| \right| / \Sigma |F_o|$. [b] $wR2 = \left(\Sigma w \left(|F_o| - |F_c| \right)^2 / \Sigma w |F_o|^2 \right)^{1/2}$

Table 6.4. Selected bond lengths (Å) for compounds **6.1**, **6.2** & **6.2a**.

6.1		**6.2**		**6.2a**	
N2-C4	1.291(9)	N1-C1	1.263(11)	N1-C1	1.270(3)
--	--	N3-C7	1.284(9)	N3-C7	1.272(3)
N1-C3	1.324(9)	N2-C2	1.342(8)	N2-C2	1.338(2)
--	--	N2-C6	1.317(9)	N2-C6	1.338(3)
C3-C4	1.517(10)	C1-C2	1.483(10)	C1-C2	1.501(3)
--	--	C6-C7	1.503(9)	C6-C7	1.503(3)
Ag1-N1	2.270(9)	Ag1-N2	2.347(6)	Ag1-N2	2.2983(16)
Ag1-N2	2.523(7)	Ag1-N1	2.526(6)	Ag1-N1	2.5564(18)
--	--	Ag1-N3	2.492(6)	Ag1-N3	2.559(2)
Ag1-O1	2.331(8)	Ag1-O1	2.638(6)	Ag1-O1	*2.661
--	--	Ag1-C48	2.716(13)	Ag1-N4	2.212(2)

Table 6.5. Selected bond lengths (Å) for compounds **6.1a-d**.

6.1a		**6.1b**		**6.1c**		**6.1d**	
N1-C1	1.281(4)	N1-C1	1.284(4)	N1-C1	1.282(3)	N1-C1	1.292(7)
N3-C7	1.272(4)	N3-C7	1.279(4)	N3-C7	1.279(3)	N3-C7	1.291(7)
N2-C2	1.344(4)	N2-C2	1.341(4)	N2-C2	1.344(3)	N2-C2	1.324(6)
N2-C6	1.344(4)	N2-C6	1.340(4)	N2-C6	1.340(3)	N2-C6	1.335(7)
C1-C2	1.496(4)	C1-C2	1.497(4)	C1-C2	1.496(3)	C1-C2	1.505(8)
C6-C7	1.494(4)	C6-C7	1.499(4)	C6-C7	1.494(3)	C6-C7	1.505(8)
Ag1-N2	2.255(2)	Ag1-N2	2.287(2)	Ag1-N2	2.2757(19)	Ag1-N2	2.296(4)
Ag1-N1	2.638(2)	Ag1-N1	2.556(3)	Ag1-N1	2.596(2)	Ag1-N1	2.622(4)
Ag1-N3	2.537(3)	Ag1-N3	2.581(3)	Ag1-N3	*2.703	Ag1-N3	2.503(4)
Ag1-O2	*3.037	Ag1-O3	*6.935	Ag1-O1	*2.951	Ag1-O3	*2.865
Ag1-N4	2.187(3)	Ag1-C50	2.447(4)	Ag1-C49	2.373(3)	Ag1-C48	2.418(5)
--	--	Ag1-C51	2.464(4)	Ag1-C50	2.369(3)	Ag1-C49	2.360(6)
--	--	C50-C51	1.382(6)	C49-C50	1.186(4)	C48-C49	1.361(8)

**distance beyond the recognized bonding parameters in SHELXTL.*

Table 6.6: Selected bond angles (°) for compounds **6.1**, **6.2** & **6.2a**.

6.1		**6.2**		**6.2a**	
N2-C4-C3	116.6(7)	N1-C1-C2	118.4(6)	N1-C1-C2	117.44(17)
--	--	N3-C7-C6	115.8(6)	N3-C7-C6	116.41(19)
C4-C3-N1	115.7(7)	C1-C2-N2	116.8(7)	C1-C2-N2	117.45(17)
--	--	C7-C6-N2	118.1(7)	C7-C6-N2	117.37(17)
C3-N1-C3	117.1(10)	C2-N2-C6	121.1(7)	C2-N2-C6	118.82(17)
C3-N1-Ag1	121.3(5)	C2-N2-Ag1	119.3(5)	C2-N2-Ag1	119.75(13)
--	--	C6-N2-Ag1	119.6(5)	C6-N2-Ag1	120.68(13)
N1-Ag1-N2	68.85(15)	N2-Ag1-N1	67.3(2)	N2-Ag1-N1	68.57(6)
--	--	N2-Ag1-N3	67.40(18)	N2-Ag1-N3	67.95(6)
Ag1-N2-C4	110.7(5)	Ag1-N1-C1	113.5(4)	Ag1-N1-C1	111.36(13)
--	--	Ag1-N3-C7	116.0(4)	Ag1-N3-C7	112.97(14)
--	--	N2-Ag1-C48	157.1(2)	N2-Ag1-N4	173.07(8)

Table 6.7: Selected bond angles (°) for compounds **6.1a-d**.

6.1a		**6.1b**		**6.1c**		**6.1d**	
N1-C1-C2	117.4(3)	N1-C1-C2	116.7(3)	N1-C1-C2	116.9(2)	N1-C1-C2	115.3(5)
N3-C7-C6	117.0(3)	N3-C7-C6	116.0(3)	N3-C7-C6	116.4(2)	N3-C7-C6	117.0(5)
C1-C2-N2	116.8(3)	C1-C2-N2	116.7(3)	C1-C2-N2	117.11(19)	C1-C2-N2	116.3(4)
C7-C6-N2	116.9(3)	C7-C6-N2	116.5(3)	C7-C6-N2	117.86(19)	C7-C6-N2	115.7(5)
C2-N2-C6	118.9(3)	C2-N2-C6	119.0(3)	C2-N2-C6	118.73(19)	C2-N2-C6	119.1(4)
C2-N2-Ag1	121.7(2)	C2-N2-Ag1	119.08(19)	C2-N2-Ag1	118.98(14)	C2-N2-Ag1	120.5(3)
C6-N2-Ag1	119.38(19)	C6-N2-Ag1	121.9(2)	C6-N2-Ag1	122.06(15)	C6-N2-Ag1	120.3(3)
N2-Ag1-N1	67.72(8)	N2-Ag1-N1	68.55(9)	N2-Ag1-N1	68.11(7)	N2-Ag1-N1	66.63(15)
N2-Ag1-N3	69.01(9)	N2-Ag1-N3	66.98(9)	N2-Ag1-N3	*65.84	N2-Ag1-N3	68.21(15)
Ag1-N1-C1	107.26(19)	Ag1-N1-C1	108.0(2)	Ag1-N1-C1	106.23(15)	Ag1-N1-C1	105.6(3)
Ag1-N3-C7	109.2(2)	Ag1-N3-C7	111.4(2)	Ag1-N3-C7	*106.88	Ag1-N3-C7	111.5(3)
N2-Ag1-N4	173.64(11)	C50-Ag1-C51	32.69(14)	C49-Ag1-C50	28.96(10)	C48-Ag1-C49	33.1(2)
N1-C1-C2	117.4(3)	N1-C1-C2	116.7(3)	N1-C1-C2	116.9(2)	N1-C1-C2	115.3(5)

Chapter 7: *Re(I), Synthesis of Pincer Complexes*

[7.1] Introduction

In a departure from low valent main group and analogous late transition metal chemistry, we shifted our focus to rhenium(I). While we cannot claim a direct relation to our previous work, there is some thematic continuity in the aspect of exploring the chemistry of low-valent states. Rhenium has a wide range of oxidation states (-1,0,1,2,3,4,5,6,7) with 2,4,6,7 being the most common.[82] As such, work done with the less common +1 valence state provides a continuum to our previous efforts. Unlike most low-valent synthons we have used, the common Re(I) synthons of the form $Re(CO)_5X$ (X = Cl, Br, and I) are remarkably stable, so much so, that it often takes forcing conditions to initiate ligation. Initial loss of two CO groups is generally facile, but loss of the third requires more forcing conditions (often beyond the stability range of the ligand used), as such most $Re(CO)_5X$ derivatized complexes are of the form $L_nRe(CO)_3X$ (n = 1 for bidentate ligation, and 2 for monodentate).[83]

Scheme 7.1

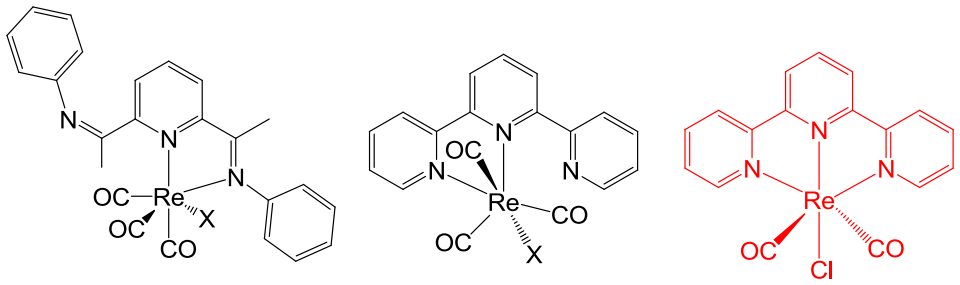

(i) X=Cl,Br, and I **(ii)** **(iii)**

[82] A.F. Holleman, E. Wiberg, N. Wiberg, Nils, (**1985**). "Rhenium" (in German). *Lehrbuch der Anorganischen Chemie* (91–100 ed.). Walter de Gruyter. pp. 1118–1123.

[83] T.A. Martin, C.E. Ellul, M.F. Mahon, M.E. Warren, D. Allan, M.K. Whittlesey, *Organometallics*, **2011**, *30*, 8, 2200.

Furthermore, there is a well-established precedent for reactivity of $Re(CO)_5X$ with bis(imino)pyridine ligands. As is generally observed with bidentate ligands, reaction with bis(imino)pyridine results in loss of two CO groups and formation of monomeric Re(I) complexes with the bis(imino)pyridine acting as a bidentate chelate ligand (Scheme 7.1 (**i**)). These complexes are highly stereochemically non-rigid in solution, most notably undergoing 1,4-metallotropic shifts, E,Z-isomerisation of the pendant imine group, as well as restricted C-C rotation of the free ligand arm.[84] There is also a broad array of analogous terpyridine chemistry with the $Re(CO)_5X$ synthon. Again, the reaction proceeds with loss of two CO groups and formation of monomeric Re(I) complexes where terpyridine acts as a bidentate chelate ligand (Scheme 7.1 (**ii**)). Stereochemically non-rigidity via 1,4-metallotropic shifts is also a common feature for the terpyridine chelates.[85]

There have been two main focal points of research for Re(I) complexes with bidentate chelating ligands. Structurally, the focus has been on dynamic NMR studies of complexes in solution, with the focus on the metallotropic shifts. There has also been a tremendous interest in the photophysical chemistry of Re(I) complexes bound to pyridine groups. Re(I) compounds are d^6 complexes whose lowest excited state often bears metal-ligand charge transfer character, and as a result can luminesce at room temperature in solution.[86] Our interest lies in the structural aspect, and more importantly in the challenges of synthesizing Re(I) complexes bearing pincer type geometry (via N,N',N chelation of bis(imino)pyridine ligands). While higher oxidation state rhenium complexes featuring pincer ligands bound in terdentate fashion are well known, there

[84] (a) K.G.Orrell, A.G. Osborne, V. Sik, M.W. daSilva, M.B. Hursthouse, D.E. Hibbs, K.M.A. Malik, N.G. Vassilev, *J. Organomet. Chem.*, **1997**, 538, 171; (b) J. Granifo, S.J. Bird, K.G. Orrell, A.G. Osborne, V. Sik, *Inorg. Chim. Acta*, **1999**, 295, 56.
[85] E.W. Abel, V.S. Dimitrov, N.J. Long, K.G. Orrell, A.G. Osborne, H.M. Pain, V. Sik, M.B. Hursthouse, M.A. Mazid, *J. Chem. Soc. Dalton Trans*, **1993**, 597.
[86] A. Juris, S. Campagna, I. Bidd, J.M. Lehn, R. Zeissel, *Inorg. Chem*., **1988**, 27, 4007.

are to our knowledge no crystallographically authenticated examples of low valent Re(I) complexes featuring terdentate ligation of a pincer ligand.[87] The terdentate terpyridine Re(I) complex (Scheme 7.1 (**iii**)) as reported by Juris *et al* is to our knowledge the only Re(I) pincer complex reported. Beyond the ^{1}H NMR, IR, and elemental analysis, little is known about this complex.[86] Our goal is to synthesize, crystallographically authenticate, and study the first low valent rhenium pincer complex of the bis(imino)pyridine class.

[7.2] Results and Discussion: Ligation of Bis(imino)pyridines to $Re(CO)_5X$

In a sealed reaction flask under N_2 atmosphere, ligand **1B** was reacted with 1 equivalent of $Re(CO)_5Br$ at 100^{o}C for 24 hours (Scheme 7.2). The resulting bright red/orange powder was isolated in 91% yield, and confirmed by both X-ray and elemental analysis to be the octahedral Re(I) complex 2,6-{2,6-$^{i}Pr_2C_6H_3N$=CPh}$_2$(NC_5H_3)$Re(CO)_3Br$ **7.1** (Figure 7.1). Selected bond distances and angles for **7.1** are presented in Tables 7.4 and 7.7 respectively. Ligand **1B** binds in a bidentate fashion through the pyridine nitrogen (N2) and one of the imine nitrogens (N1), while the other imine nitrogen (N3) is twisted out of the N,N',N plane. The geometry around the Re(I) centre is octahedral with the pyridine centre (N2), one imine N group (N1), and two CO carbons (C44 and C46) residing in a plane. The axial sites are defined by a CO carbon (C45) and a halide group (Br1). The Re-$N_{pyridine}$ distance of 2.208(3)Å is slightly longer than the Re-N_{imine} distance of 2.186(3)Å. The CO groups trans to the nitrogen donors exhibit similar M-C bond lengths (1.916(4)Å and 1.942(5)Å for groups trans to imine and pyridine respectively). The resulting CO bonds show slight elongation at 1.149(4)Å and 1.142(4)Å compared to 1.128Å for free CO. The Re-axial CO bond trans to the bromide group is slightly longer at 1.942(5)Å, and the resulting

[87] O.V. Ozerov, L.A. Watson, M. Pink, K.G. Caulton, *J. Am. Chem. Soc.,* **2007**, 129, 6003.

CO bond appears substantially shorter at 1.073(5)Å, indicating that the bulk of electron density is shared between Re and Br, and the apical CO is receiving less back-donation from the rhenium centre.

In analogous fashion to **7.1**, ligand **1B** was reacted with 1 equivalent of $Re(CO)_5Cl$ at 100°C for 24 hours (Scheme 7.2). The resulting bright red/orange powder was isolated in 98% yield, and confirmed by both X-ray and EA to be the octahedral Re(I) complex 2,6-{2,6-$^{i}Pr_2C_6H_3N{=}CPh\}_2(NC_5H_3)Re(CO)_3Cl$ **7.2** (Figure 7.2). Selected bond distances and angles for **7.2** are presented in Tables 7.4 and 7.7 respectively. As observed for ligand **1A** in **7.1**, ligand **1B** binds in a bidentate fashion through the pyridine nitrogen (N2) and one of the imine nitrogens (N1), while the other imine nitrogen (N3) is twisted out of the N,N',N plane. The geometry around the Re(I) centre is octahedral with a plane defined by the pyridine centre (N2), one imine N group (N1), and two CO carbons (C45 and C46). Once again, the axial sites are defined by a CO carbon (C44) and a halide group (Cl1). As expected, the Re-$N_{pyridine}$ distance of 2.2085(18)Å is slightly longer than the Re-N_{imine} distance of 2.1860(19)Å, these bond lengths are identical to those of **7.1**. The CO groups trans to the nitrogen donors exhibit similar M-C bond lengths (1.914(2)Å and 1.904(2)Å for groups trans to imine and pyridine respectively). The resulting CO bonds show slight elongation at 1.158(3)Å and 1.151(3)Å compared to 1.128Å for free CO, and on average are 0.01Å longer than those observed in **7.1**. The Re-axial CO bond trans to the chloride group, unlike observed in **7.1** is 1.916(5)Å, showing no distinct difference than the equatorial CO's, and the resulting CO bond appears slightly shorter at 1.147(3)Å; a less dramatic difference than observed in **7.1**. Overall these bond lengths are comparable to those of (**i**) (Scheme 7.1, X=Br), where Orrell *et al* report CO lengths of 1.150(10)Å, 1.156(10)Å, and 1.136(10)Å (for CO trans to the axial bromide).[84a]

Scheme 7.2

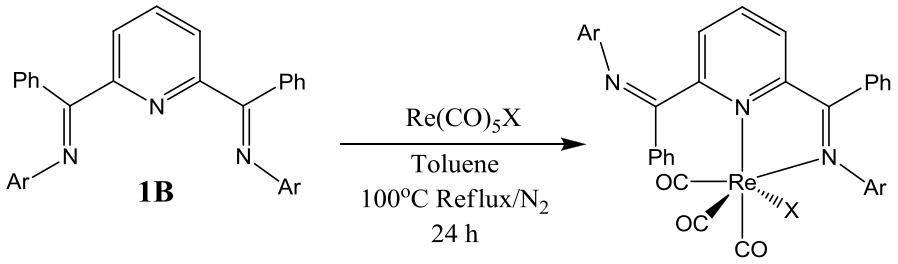

Ar=2,6-^{i}PrC$_6$H$_3$ **7.1** X=Br **7.2** X=Cl **7.1, 7.2**

With the goal of accessing low valent Re(I) pincer complexes, we subjected both **7.1** and **7.2** to conditions amenable to loss of CO, and subsequent ligand rearrangement to pincer geometry. Exposure of dilute solutions of **7.1** and **7.2** in toluene to UVA, UVB and UVC rays of increasing intensity resulted in no discernible colour change. Similarly, heating to temperatures above 200^{o}C had no discernible effect, as no colour change was observed, and resulting ^{1}H NMR spectra remain indicative of bidentate coordination of bis(imino)pyridine. In fact these complexes remain remarkably stable under all reasonable reaction conditions to which they were exposed. One possible explanation could be that the steric bulk imposed by the ^{i}Pr groups is too great to facilitate the formation of the desired terdentate geometry.

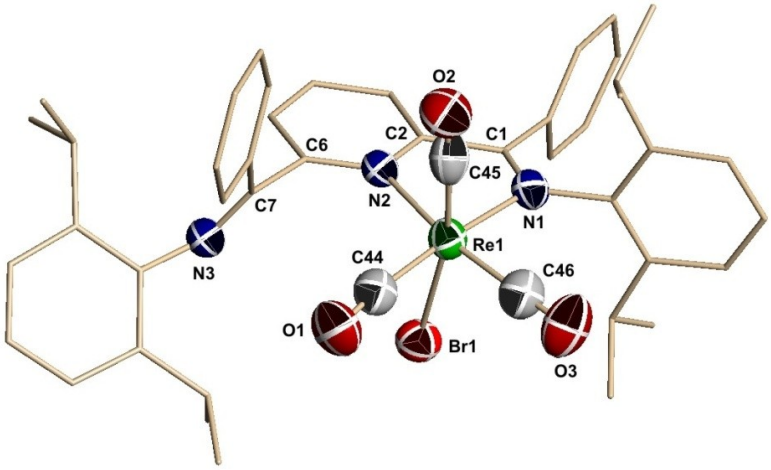

Figure 7.1: X-ray structure of compound **7.1** with hydrogen atoms, CH_2Cl_2 and THF omitted for clarity. Select bond lengths and angles are given in Tables 7.4 and 7.7.

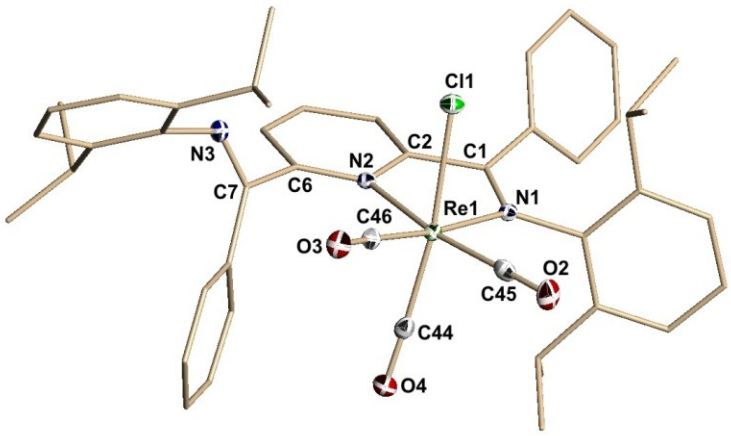

Figure 7.2: X-ray structure of compound **7.2** with hydrogen atoms,CH_2Cl_2 and THF omitted for clarity. Select bond lengths and angles are given in Tables 7.4 and 7.7.

Scheme 7.3

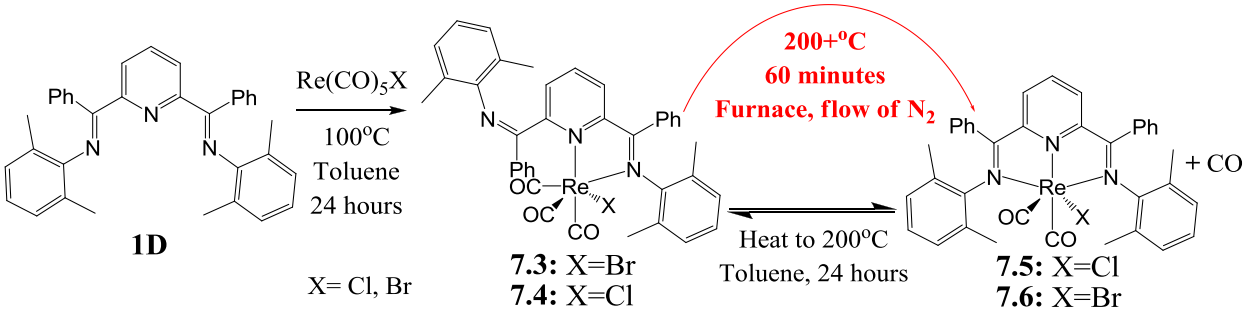

In an effort to ascertain the effect of ligand steric bulk, and with the goal of targeting a pincer type ligand geometry, efforts were refocused on our least stericaly hindered ligand **1D**. Analogous to the synthetic procedure for **7.1** and **7.2**, **1D** was reacted with 1 equivalent of $Re(CO)_5X$ (X = Br, and Cl respectively) at 100°C for 24 hours (Scheme 7.3). The resulting bright red/orange powders were isolated in yields of 85% and 97% (respectively for Br and Cl based synthons). Structures were confirmed by both X-ray and elemental analysis to be the octahedral Re(I) complexes 2,6-{2,6-$Me_2C_6H_3N$=CPh}$_2(NC_5H_3)Re(CO)_3Br$ **7.3** and 2,6-{2,6-$Me_2C_6H_3N$=CPh}$_2(NC_5H_3)Re(CO)_3Cl$ **7.4** (Figure 7.3 and 7.4). Selected bond distances and angles for **7.3** and **7.4** are presented in Tables 7.5 and 7.8 respectively.

As observed for ligand **1B** in compounds **7.1** and **7.2**, ligand **1D** binds in a bidentate fashion through the pyridine nitrogen (N2) and one of the imine nitrogens (N1), while the other imine nitrogen (N3) remains twisted out of the N,N',N plane. The geometry around the Re(I) centre is octahedral with a completely analogous ligand disposition. Two coordinated N centres, pyridine (N2), one imine N group (N1), and two CO carbons lay in a plane. The axial sites are defined by a CO carbon and a halide group (Br or Cl for **7.3** and **7.4** respectively). As expected, the Re-$N_{pyridine}$ distances of 2.249(12)Å and 2.2200(15)Å remain longer than the Re-N_{imine} distances of 2.171(12)Å and 2.1655(18)Å for **7.3** and **7.4** respectively. IR reveals CO stretches at 2024, 1932, and 1897 cm^{-1} for **7.3**, and 2013, 1918, and 1896 cm^{-1} for **7.4** (Table 7.10). Free CO stretch is observed at 2143 cm^{-1}, indicating a range of back donation for the three CO groups on the rhenium centre. Correlating to CO bond lengths in the crystal structures, the most elongated bonds (smallest wavenumber) correspond to CO groups trans to the N-pyridine group, whereas the least elongated (largest wavenumber) correspond to CO groups trans to the N-imine group. The CO group trans to the halide does however trend towards significant elongation/activation of the CO bond. These trends reflect those observed in literature.[84b,85,88]

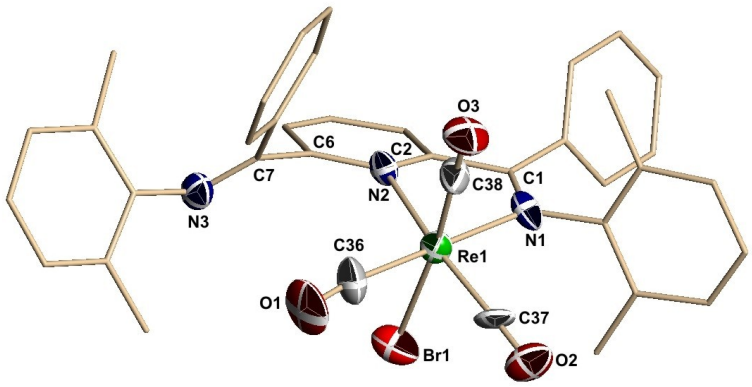

Figure 7.3: X-ray structure of compound **7.3** with hydrogen atoms,CH_2Cl_2 and THF omitted for clarity. Select bond lengths and angles are given in Tables 7.5 and 7.8.

[88] M. Schutte, G. Kemp, H. Visser, A. Roodt, *Inorg. Chem.*, **2011**, *50* (24), 12486.

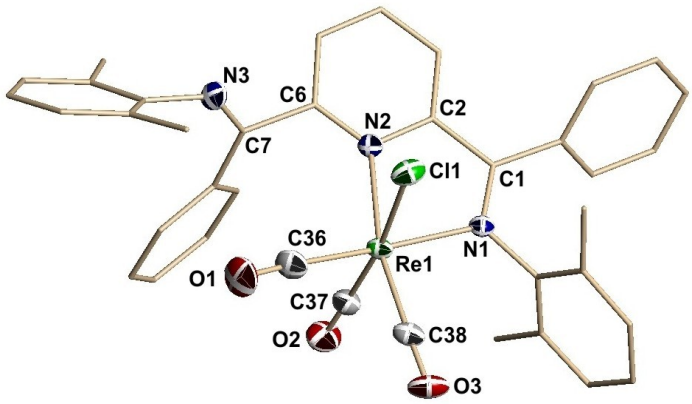

Figure 7.4: X-ray structure of compound **7.4** with hydrogen atoms,CH_2Cl_2 and THF omitted for clarity. Select bond lengths and angles are given in Tables 7.5 and 7.8.

Heating solutions of **7.3** and **7.4** to temperatures of 200^{o}C for 24 hours resulted in a colour change from red, to a very intense dark red/brown, and workup lead to the isolation of dark red/brown powders. Resulting ^{1}H NMR spectra show two products, one being unreacted starting material, either **7.3** or **7.4**, and a secondary set of peaks with simplified signals, indicative of a symmetric bis(imino)pyridine ligand as expected with terdentate coordination. The product distribution ratios in the ^{1}H NMR are approximately 3:1 for **7.3** to terdentate complex, and 1:1 for **7.4** to respective terdentate complex. In an attempt to garner complete conversion to tridentate complex, solutions were allowed to stir for 48-72 hours, and monitored by ^{1}H NMR. There is no significant change in product distribution ratios, potentially owing to a high temperature equilibrium in solution, coupled with the fact that CO is not continually removed from the reaction vessel.

To circumvent the solution equilibrium that prevents full conversion to the desired pincer geometry, experiments were repeated in the solid-state, utilizing a furnace and heating to 200^{o}C under a flow of nitrogen. As **7.4** showed a greater propensity for conversion than

7.3, our immediate efforts focused on the chloride derivative. Placing **7.4** powder in a furnace at 200°C under a flow of nitrogen for 1 hour results in conversion to a dark brown powder, which was confirmed by both X-ray, NMR and elemental analysis to be the octahedral Re(I) complex 2,6-{2,6-$Me_2C_6H_3N$=CPh}$_2$(NC_5H_3)Re(CO)$_2$Cl **7.5** (Figure 7.5). Loss of CO and subsequent rearrangement of the imine side arm affords the desired pincer ligand geometry, and the resulting powder is isolated in 97% yield and requires no further workup. Selected bond distances and angles for **7.5** are presented in Tables 7.6 and 7.9 respectively.

The geometry around the Re(I) centre is octahedral with the four-fold plane defined by the pyridine centre (N2), imine nitrogens (N1, and N3), and a CO carbon (C37). The axial sites are defined by a CO carbon (C36) and a chloride (Cl1). As expected for the pincer geometry, the Re-$N_{pyridine}$ distance of 2.0672(16)Å is slightly shorter than the Re-N_{imine} distances of 2.0964(15)Å and 2.1089(16)Å, these bond lengths are significantly shorter than those observed for bidentate complexes **7.1-4** indicating a stronger L-M interaction. This indicates that the terdentate configuration is prefered, but the barrier to formation with regard to initial loss of CO is high. The CO groups exhibit similar bond lengths of 1.160(3)Å and 1.158(3)Å, and IR stretches of 1919 and 1849 cm^{-1} (Table 7.10), which are not dissimilar to those observed in **7.3** and **7.4**, albeit on the long end of the ranges observed prior, this is expected as terdentate ligation is facilitated by loss of CO group trans to N_{imine}, which was shown to receive the least amount of back donation. The Re-Cl bond length of 2.4751(5)Å is also similar to those observed in **7.2** and **7.4** (2.4630(6)Å and 2.4778(6)Å respectively). Repeating the synthetic procedure with **7.3** required an increased temperature of 240°C and a reaction time of 1 hour to achieve complete conversion to pincer complex. The reaction

resulted in isolation of dark brown powder in 95% yield, which was confirmed by both NMR and elemental analysis to be the octahedral Re(I) complex 2,6-{2,6-$Me_2C_6H_3N$=CPh}$_2$(NC_5H_3)Re(CO)$_2$Cl **7.6**.[89] However, crystals suitable for X-ray crystallography could not be obtained. Infra-Red reveals CO stretches of 1906 and 1837 cm^{-1} which correspond closely to those observed in **7.5** (Table 7.10).

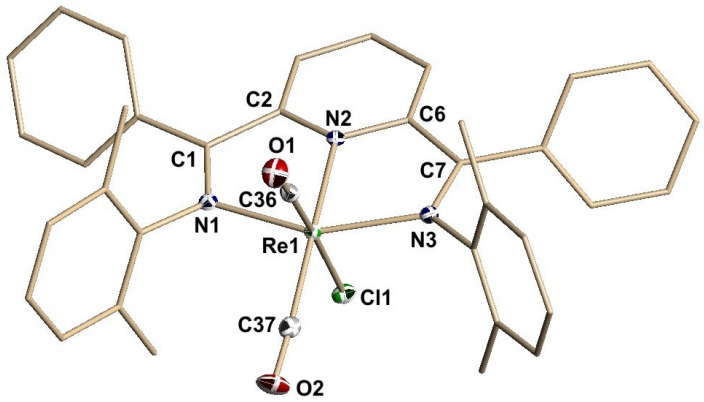

Figure 7.5: X-ray structure of compound **7.5** with hydrogen atoms,CH_2Cl_2 and THF omitted for clarity. Select bond lengths and angles are given in Tables 7.6 and 7.9.

Having isolated our target Re(I) pincer complex, the next step was to make it amenable for reactivity testing, an area of potential interest given the wide oxidation state range of rhenium. One problem in that regard is not only the lack of coordination sites on **7.5**, but also the fact that none of the bonded groups are sufficiently labile. To address this issue, we attempted to exchange the chloride group for a triflate, which is known to be a labile anion, and should provide an open site for interaction with the Re centre. Reaction of **7.5** with a slight excess of AgOTf resulted in the isolation of dark brown/purple powder. Attempted ^{1}H NMR spectra were unclear due to severe broadening, indicative of a paramagnetic species. Attempted crystallization of the powder yielded multiple components,

[89] Elemental analysis confirms the formula, and both ^{13}C and ^{1}H NMR are nearly identical to that observed for **7.5** leading to the assertion that **7.6** is similarly an octahedral Re(I) complex with pincer type geometry.

only two of which could be identified, but neither sufficiently isolable for elemental analysis or NMR studies. The principal component in the crystal mixture was bright yellow plate-like crystals, which were shown to be the bidentate rhenium-triflate complex **7.7** (*vide infra*), with the secondary component being small brown needle-like crystals. X-ray crystallography confirmed the product to be the octahedral Re(I) complex K[2,6-{2,6-$Me_2C_6H_3N$=CPh}$_2$(NC_5H_3)Re(CO)$_2$Cl] **7.8** (Figure 7.6). Selected bond distances and angles for **7.8** are presented in Tables 7.6 and 7.9 respectively.

Scheme 7.4

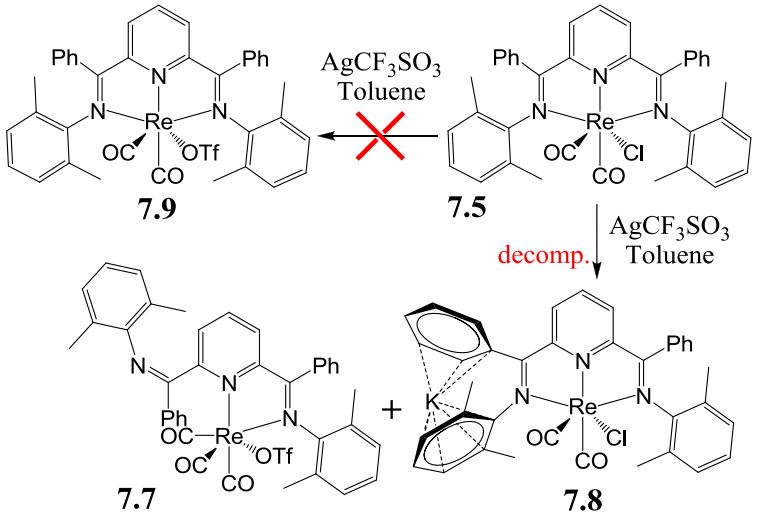

General structural features of **7.8** echo those observed in **7.5**, with the only difference being the π-bonded K^+ ion interacting with the N-aryl and phenyl backbone arenes. In conjunction with the broadened peaks in the ^{1}H NMR, this is indicative of a radical ligand species.[90] Unfortunately, this species could not be adequately separated to obtain magnetic measurement. What is perhaps most peculiar is the introduction of K+, the only potential source of which was the Celite used durring sample preparation.[91] Celite is for the most part understood to be inert, as such this would indicate that the transient species generated which

[90] This is similar to what was observed with the gallium compound **3.3**.
[91] Celite, or diatomaceous earth contains 1.4% K_2O + Na_2O: Sigma Aldrich.

result in the formation of **7.6** and **7.8** are highly reactive.[92] In an ongoing effort to isolate a pincer type complex with the triflate substituent, we took a step backwards and targeted the direct synthesis of **7.6**, and subsequent solid state conversion to the desired pincer geometry.

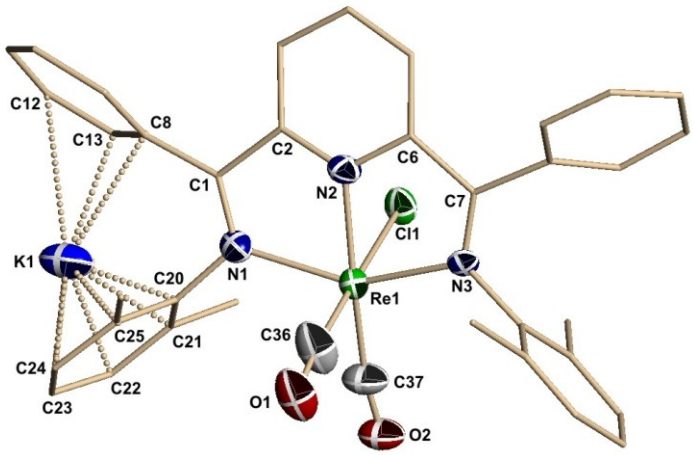

Figure 7.6: X-ray structure of compound **7.8** with hydrogen atoms, and THF omitted for clarity. Select bond lengths and angles are given in Tables 7.6 and 7.9.

Reaction of **7.4** with a slight excess of AgOTf resulted in the isolation of bright yellow/orange powder in a moderate 55% yield. Both X-ray and elemental analysis confirmed the product to be the octahedral Re(I) complex 2,6-{2,6-$Me_2C_6H_3N$=CPh}$_2$(NC_5H_3)Re(CO)$_3$(OTf) **7.7** (Figure 7.7). Selected bond distances and angles for **7.7** are presented in Tables 7.5 and 7.8 respectively. The geometry around the Re(I) centre is octahedral with the four-fold plane defined by the pyridine centre (N2), one imine N group (N1), and two CO carbons (C36 and C38). The axial sites are defined by a CO carbon (C37) and triflate oxygen (O1). As observed prior, the Re-$N_{pyridine}$ distance of 2.228(2)Å is slightly longer than the Re-N_{imine} distance of 2.154(2)Å, these bond lengths are similar to those observed for previous complexes with bidentate ligand coordination. The CO bonds for groups trans to the

[92] Presence of K+ in bulk was confirmed via Inductive Coupled Plasma Emission Spectrometry (ICPES), which showed a 2.5% K to Re ratio.

$N_{pyridine}$ and N_{imine} are relatively similar at 1.146(4)Å and 1.150(4)Å respectively. IR reveals CO stretches at 2030, 1931, and 1912 cm^{-1} (Table 7.10). Correlation to bond lengths observed in the crystal structure show that the greatest amount of elongation occurs in the CO group trans to the triflate moiety (slightly longer than values observed for CO trans to halide groups), and the $N_{pyridine}$ donation is not as significant as prior examples. However, values remain well within previously observed ranges.

Scheme 7.5

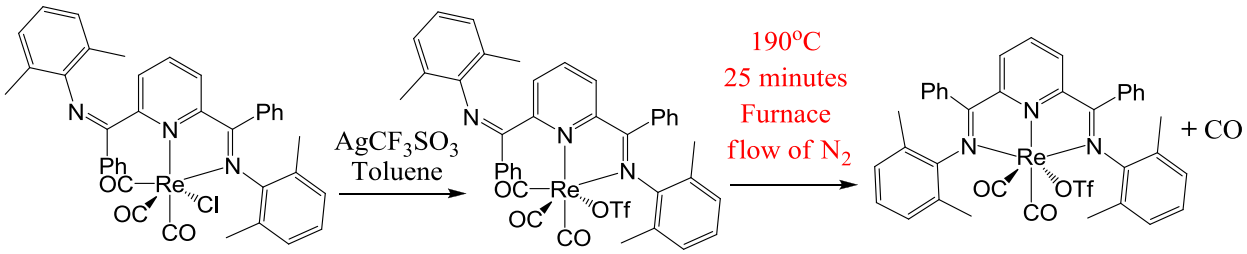

7.4 **7.7** **7.9**

Placing **7.7** powder in a furnace at 190°C under a flow of nitrogen for 25 minutes results in conversion to a dark brown powder, which was confirmed by both X-ray, NMR and EA to be the octahedral Re(I) complex 2,6-{2,6-$Me_2C_6H_3N$=CPh}$_2$(NC_5H_3)Re(CO)$_2$(OTf) **7.9** (Figure 7.8).[93] Loss of CO and subsequent rearrangement of the imine side arm affords the desired pincer ligand geometry, and the resulting powder is isolated in 93% yield and requires no further workup. Selected bond distances and angles for **7.9** are presented in Tables 7.5 and 7.9 respectively. The geometry around the Re(I) centre is octahedral with the four-fold plane defined by the pyridine centre (N2), imine nitrogens (N1, and N3), and a CO carbon (C37). The axial sites are defined by a CO carbon (C36) and a triflate oxygen (O3). As expected for the pincer geometry, the Re-$N_{pyridine}$ distance of 2.028(17)Å is slightly shorter than the Re-N_{imine} distances of 2.136(170)Å and 2.073(16)Å, these bond lengths are

[93] Higher temperatures or prolonged reaction results in decomposition. The powder turns black and there are multitudes of peaks in the ^{1}H NMR.

significantly shorter than those observed for bidentate complexes **7.1-4**, indicating a stronger L-M interaction similar to that observed in **7.5**. The observed CO bond lengths reveal 1.21(3)Å for the group trans to $N_{pyridine}$ and 1.18(3)Å for the group trans to N_{imine}. IR stretches of 1915 and 1855 cm^{-1} (Table 7.10), remain similar to those observed in **7.5** and **7.6**.

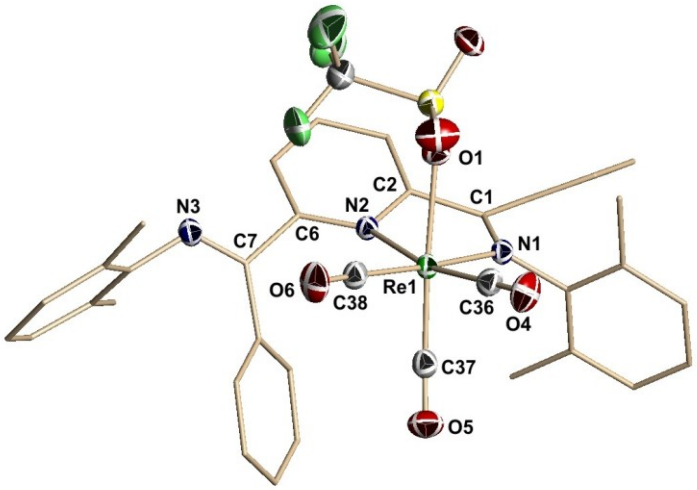

Figure 7.7: X-ray structure of compound **7.7** with hydrogen atoms,CH_2Cl_2 and THF omitted for clarity. Select bond lengths and angles are given in Tables 7.5 and 7.8.

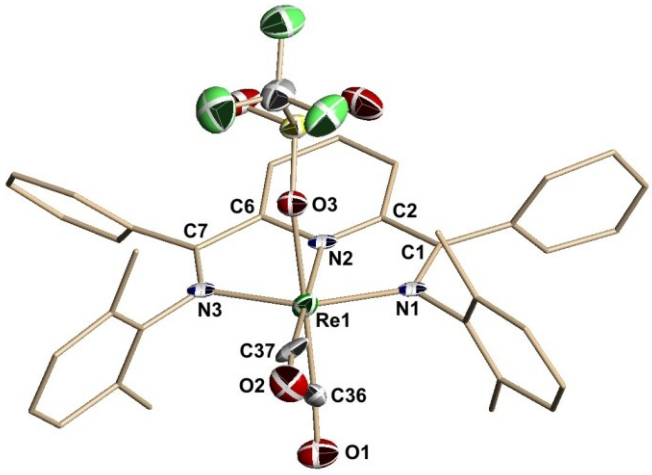

Figure 7.8: X-ray structure of compound **7.9** with hydrogen atoms,CH_2Cl_2 and THF omitted for clarity. Select bond lengths and angles are given in Tables 7.6 and 7.9.

[7.3] Electrochemistry Experiments for Complexes 1D, 7.4 and 7.5

Cyclic voltammograms (CV) of **1D**, **7.4** and **7.5** reveal quasi-reversible reduction waves (Figure 7.9). For **7.4** and **7.5**, the waves are assigned as successive one-electron reductions of the bis(imino)pyridine ligand within the respective rhenium complex; CV of **1D** reveals only one reversible reduction within the window afforded by acetonitrile. Formation of ML^{2-} species is not uncommon for bis(imino)pyridines, which have been shown to facilitate the formation of *mono*-, *di*-, and *tri*-anionic complexes.[94] Similar electrochemical behaviour has been noted previously for related aromatic N-donor ligand systems (diimine and pyridine based).[95] No oxidation waves were observed within the solvent window.

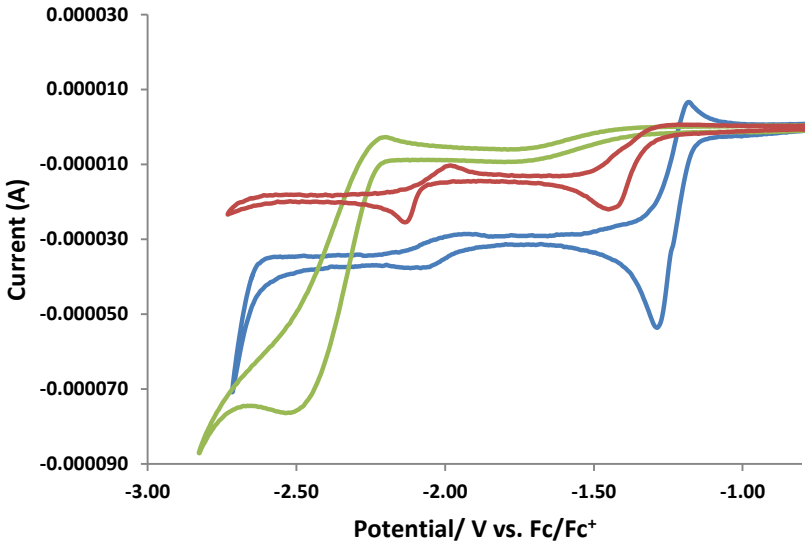

Figure 7.9: Cyclic voltammogram of **1D** (**green**), **7.4** (**red**) and **7.5** (**blue**)**:** Potential measured against Fc/Fc^+ couple in acetonitrile. *Further details in General Experimental.*

[94] (a)K.G. Caulton, *Eur. J. Inorg. Chem.* **2012**, 435–443.; (b) Q. Knijnenburg, S. Gambarotta, P. H. M. Budzelaar, *Dalton Trans.,* **2006**, 5442–5448.
[95] (a)F. Paolucci, M. Marcaccio, C. Paradisi, S. Roffia, C.A. Bignozzi, C. Amatore, *J. Phys. Chem. B,* **1998**, *102,* 4759-4769; (b) G.J. Stor, F. Hartl, J.W. van Outersterp, D.J. Stufkens, *Organometallics*, **1995**, 14, 1115-1131.; (c) M. S. Jana, A.K. Pramanik, S. Kundu, T.K. Mondal, *Polyhedron*, **2012**, http://dx.doi.org/10.1016/j.poly.2012.03.044

Bidentate complex **7.4** displays quasi-reversible reduction waves with cathodic maxima at -1.45 V and -2.13 V ($E_{1/2}$ -2.07V) vs ferrocene/ferrocenium (Fc/Fc^{+}) couple. Terdentate complex **7.5** displays a similar pattern, with cathodic maxima at -1.29 V ($E_{1/2}$ -1.25V) and -2.04 V ($E_{1/2}$ -1.98V) . The potential separation between the two redox processes (680 mV for **7.4** and 750 mV for **7.5**) is a typical value for aromatic N-donor ligands bound to rhenium(I).[95a,96] The drastic difference in potentials between the first reduction in **7.4** and **7.5** (-1.45 and -1.29 V respectively), and that of free ligand **1D** (-2.52 V, $E_{1/2}$ -2.36V) illustrates the electrostatic stabilization of the reduced forms of the ligand by the rhenium(I) cation. Furthermore, the shift to less negative potential when going from bidentate **7.4** to terdentate **7.5** (+160mV for the first reduction step and +90mV for the second) indicates an increase in electrostatic stabilization of the reduced ligand in the tridentate conformation. This is not surprising as ligand-metal contact has increased from two, to three N-donor interactions.

[7.4] Conclusion

We were succesful in expanding the low-valent Re(I) chemistry of the bis(imino)pyridine ligand framework. We succesfully developed a highly efficient solid-state synthetic methodology to access the first crystallographically authenticated low valent rhenium pincer complexes. Conversion was facilitated in part by the high temperatures which overcome the large energetic barrier for removal of CO, and also by the continous N_2 flow in our solid state process which serves to remove CO from the reaction environment and prevent the equilibria observed in solution. Furthermore, we also found an efficient route to generate pincer complexes bearing the weakly bound triflate anion for future reactivity studies and potential catalytic applications. Electrochemistry experiments reveal similar two electron ligand based redox processes for both bidentate and terdentate structures, with the

[96] B. D. Rossenaar, F. Hartl, D.J. Stufkens, *Inorg. Chem*., **1996**, 35, 6194-6203.

reduction being slightly more facile for the terdentate geometry. Further experiments would focus on a theoretical elucidation of the energies involved in the loss of CO and structural rearrangement to terdentate geometry. The seemingly facile redox activity coupled with the open site as facilitated by the triflate derivatives **7.7** and **7.9** are compelling for future reactivity studies.

[7.5] Rhenium Complex Experimental

General Methods. Reactions were performed in a glovebox with a nitrogen atmosphere. All solvents were sparged with nitrogen and then dried by passage through a column of activated alumina using an apparatus purchased from Anhydrous Engineering. Deuterated chloroform was dried using activated molecular sieves. Rhenium starting materials were purchased from Strem Chemicals and used as received. All other chemicals were purchased from Aldrich and used without further purification. NMR spectra were run on Bruker Avance 300 and 500 MHz spectrometers with $CDCl_3$ as solvent and internal standard. Elemental analyses for **7.1-8** were performed by Midwest Microlab LLC, Indianapolis IN. Solid state reactions were carried out in a Lindberg Blue M Mini-Mite Tube Furnace (model TF55035A-1). Electrochemical measurements were performed with a Princeton Applied Research (PAR) 2273 potentiostat/galvanostat running Power Suite 2.58 electrochemical software using a one-compartment 3-electrode cell. Platinum wire working and counter electrodes, silver wire pseudo-reference electrode, and 0.1 M tetrabutylammonium bromide (Sigma Aldrich, 99.0%) in acetonitrile (Fisher Scientific, 99.9%) supporting electrolyte were employed; ferrocene was added as an internal standard at the end of each experiment. The electrochemical cell was degassed with nitrogen prior to measurement. Cyclic voltammograms of 5 mM **1D**, **7.4** and **7.5** were recorded at 50 mV s^{-1}. A nitrogen environment was maintained in the cell throughout all measurements.

(7.1) 2,6-{2,6-^{i}Pr$_2$C$_6$H$_3$N=CPh}$_2$(NC$_5$H$_3$)Re(CO)$_3$Br: $Re(CO)_5Br$ powder (95 mg, 0.234 mmol) was added to a clear yellow solution of **1B** (150 mg, 0.247 mmol) in 8 mL of toluene, in which $Re(CO)_5Br$ remained insoluble. The reaction mixture was placed in a Teflon sealed flask and allowed to stir at 100^{o}C for 24 hours, over which time a bright red/orange precipitate formed. Solution was filtered, washed with 5 x 2 mL hexanes, and allowed to dry under vacuum. A bright red/orange powder was isolated in 91% yield. Large red block like crystals suitable for X-ray analysis were grown in a saturated solution of cyclooctadiene with hexanes as countersolvent, and storing at -20^{o}C for several days. ^{1}H NMR ($CDCl_3$, 500 MHz): δ 8.08(br t , 1H, py, aromatic), δ 7.99(br d, 1H, py, aromatic), δ 7.65(br d, 1H, aromatic), δ 7.41(br m, 3H, aromatic), δ 7.35-6.98(br m, 13H, aromatic), δ 3.53(br m, 1H, C(H)-^{i}Pr), δ 3.39(br m, 1H, C(H)-^{i}Pr), δ 3.05(br m, 1H, C(H)-^{i}Pr), δ 2.77(br m, 1H, C(H)-^{i}Pr), δ 1.33-1.01(br d, 18H, Me), δ 0.71-0.53(br m, 6H, Me), ^{13}C NMR ($CDCl_3$, 125 MHz). δ 195.6(CO), 195.0(CO), 186.5(CO), 178.4 (C=N imine), 164.0(py, C=N imine), 163.3(*o*-C=N), 158.2(*o*-C=N), 145.0(Ar, *i*-C), 144.2(Ar, *i*-C), 140.2(Ar, *i*-C), 139.8(Ar, *C-iPr*), 138.8(Ar-CH), 132.7(Ar, *i*-C), 132.6(Ar, *C-iPr*), 131.1(br, Ar-CH), 131.0(br, Ar-CH), 130.7(Ar-CH), 129.9(Ar-CH), 129.0(Ar-CH), 128.8(Ar-CH), 128.4(Ar-CH), 128.2(Ar-CH), 128.0(Ar-CH), 125.3(Ar, *C-iPr*), 124.5(Ar-CH), 124.2(Ar-CH), 123.7(Ar-CH), 123.3(Ar-CH), 28.7(Ar-*iPr*, CH), 28.3(Ar-*iPr*, CH), 28.1(Ar-*iPr*, CH), 27.9(Ar-*iPr*, CH), 26.9(Ar-*iPr*, CH_3), 26.6(Ar-*iPr*, CH_3), 24.9(Ar-*iPr*, CH_3), 24.6(Ar-*iPr*, CH_3), 24.3(Ar-*iPr*, CH_3), 23.7(Ar-*iPr*, CH_3), 21.6(Ar-*iPr*, CH_3), 21.5(Ar-*iPr*, CH_3). Sample for elemental analysis was obtained by recrystallization in cyclooctadiene, resulting in a 1:2 cyclooctadiene adduct of **7.1** calculated (%) for $[C_{46}H_{47}ReBrN_3O_3]_2[C_8H_{12}]$: C 59.28, H 5.57, N 4.15, found C 59.05, H 5.16, N 4.11.

(7.2) 2,6-{2,6-^{i}Pr$_2$C$_6$H$_3$N=CPh}$_2$(NC$_5$H$_3$)Re(CO)$_3$Cl: $Re(CO)_5Cl$ powder (200 mg, 0.553mmol) was added to a clear yellow solution of **1B** (400 mg, 0.659 mmol) in 8 mL of toluene, in which $Re(CO)_5Cl$ remained insoluble. The reaction mixture was placed in a Teflon sealed flask and allowed to stir at 100^{o}C for 24 hours, over which time a bright red/orange precipitate formed. Solution was filtered, washed with 5 x 2 mL hexanes, and allowed to dry under vacuum. A bright red/orange powder was isolated in 91% yield. Large orange block like crystals suitable for X-ray analysis were grown in a saturated solution of THF with hexanes as countersolvent, and storing at -20^{o}C for several days. ^{1}H NMR ($CDCl_3$, 500 MHz): δ 8.08(br t , 1H, py, aromatic), δ 7.97(br d, 1H, py, aromatic), δ 7.64(br d, 1H, aromatic), δ 7.48-7.37(br m, 3H, aromatic), δ 7.32(br m, 1H, aromatic), δ 7.26-7.10(br m, 10H, aromatic),δ 7.03(br m, 2H, aromatic), δ 3.44(br m, 1H, C(H)-^{i}Pr), δ 3.11(br m, 2H, C(H)-^{i}Pr), δ 3.03(br m, 1H, C(H)-^{i}Pr), δ 1.29(br d, 3H, Me), δ 1.16(v br m, 12H, Me), δ 1.02(br d, 3H, Me), δ 0.93(br d, 3H, Me), δ 0.57(br d, 3H, Me). ^{13}C NMR ($CDCl_3$, 125 MHz). δ 195.4(CO), 195.3(CO), 187.5(CO), 178.4 (C=N imine), 164.2(py, C=N imine), 163.2(*o*-C=N), 158.0(*o*-C=N), 145.2(Ar, *i*-C), 144.2(Ar, *i*-C), 140.2(Ar, *i*-C), 139.9(Ar, *C-iPr*), 138.7(Ar-CH), 135.8-134.9(v br d,Ar, *C-iPr*), 132.7(Ar, *i*-C), 132.4(Ar, *C-iPr*), 131.5(Ar-CH), 131.4(Ar-CH), 131.0(Ar-CH), 130.8(Ar-CH), 130.7(Ar-CH), 129.9(Ar-CH), 128.7(Ar-CH), 128.4(Ar-CH), 128.2(Ar-CH), 128.1(Ar-CH), 128.0(Ar-CH), 125.3(Ar, *C-iPr*), 124.5(Ar-CH), 124.1(Ar-CH), 123.8(Ar-CH), 123.5(Ar-CH), 28.5(Ar-*iPr*, CH), 28.3(Ar-*iPr*, CH), 28.0(Ar-*iPr*, CH), 27.9(Ar-*iPr*, CH), 26.6(Ar-*iPr*, CH_3), 26.5(Ar-*iPr*, CH_3), 24.9(Ar-*iPr*, CH_3), 24.5(Ar-*iPr*, CH_3), 24.1(Ar-*iPr*, CH_3), 23.6(Ar-*iPr*, CH_3), 22.2(Ar-*iPr*, CH_3), 21.7(Ar-*iPr*, CH_3). Sample for elemental analysis was obtained by recrystallization in THF, resulting in a 2:1 THF adduct of **7.2** calculated (%) for $[C_{46}H_{47}ReBrN_3O_3S][C_4H_8O]_2$: C 61.26, H 6.28, N 3.97, found C 61.72, H 5.87, N 3.98.

(7.3) 2,6-{2,6-$Me_2C_6H_3N$=CPh}$_2$(NC_5H_3)Re(CO)$_3$Br: $Re(CO)_5Br$ powder (95 mg, 0.234 mmol) was added to a clear yellow solution of **1D** (150 mg, 0.305 mmol) in 8 mL of toluene, in which $Re(CO)_5Br$ remained insoluble. The reaction mixture was placed in a Teflon sealed flask and allowed to stir at 100^{o}C for 24 hours, over which time a bright red/orange precipitate formed. Solution was filtered, washed with 5 x 2 mL hexanes, and allowed to dry under vacuum. A bright red/orange powder was isolated in 85% yield. Large red plate like crystals suitable for X-ray analysis were grown in a saturated solution of THF with hexanes as countersolvent, and storing at -20^{o}C for several days. ^{1}H NMR ($CDCl_3$, 500 MHz): δ 8.24(br d , 1H, py, aromatic), δ 8.09(br t, 1H, py, aromatic), δ 7.62(br d, 1H, aromatic), δ 7.47-6.88(br m, 15H, aromatic) 6.84(br d, 1H, aromatic), δ 6.80(br d, 1H, aromatic), δ 2.65(br s, 3H, Me), δ 2.44(br s, 3H, Me), δ 1.96(br s, 3H, Me), δ 1.66(br s, 3H, Me). ^{13}C NMR ($CDCl_3$, 125 MHz). δ 195.7(CO), 194.9(CO), 185.3(CO), 177.9 (C=N imine), 163.9(py, C=N imine), 163.0(*o*-C=N), 157.9(*o*-C=N), 148.5(Ar, *i*-C), 147.1(Ar, *i*-C), 139.1(Ar-CH), 133.3(Ar, *i*-C), 133.2(Ar, *C*-CH_3), 131.3(Ar-CH), 131.1(Ar-CH), 131.0(Ar-CH), 130.9(Ar, *C*-CH_3), 130.5(Ar-CH), 129.2(Ar-CH), 128.7(Ar-CH), 128.7(Ar-CH), 128.6(Ar-CH), 128.5(Ar-CH), 128.4(Ar-CH), 128.3(Ar-CH), 128.2(Ar-CH), 128.1(Ar-CH), 127.8(Ar-CH), 126.1(Ar, *C*-CH_3), 123.9(Ar-CH), 122.5(Ar, *C*-CH_3), 21.1(Ar-*Me*, CH_3), 18.7(Ar-*Me*, CH_3), 18.6(Ar-*Me*, CH_3), 18.4(Ar-*Me*, CH_3). Elemental analysis calculated (%) for [$C_{38}H_{31}ReBrN_3O_3$]: C 53.90, H 4.05, N 4.96, found C 54.01, H 3.93, N 5.05.

(7.4) 2,6-{2,6-$Me_2C_6H_3N$=CPh}$_2$(NC_5H_3)Re(CO)$_3$Cl: $Re(CO)_5Cl$ powder (68 mg, 0.190 mmol) was added to a clear yellow solution of **1D** (100 mg, 0.203 mmol) in 8 mL of toluene, in which $Re(CO)_5Cl$ remained insoluble. The reaction mixture was placed in a Teflon sealed flask and allowed to stir at 100^{o}C for 24 hours, over which time a bright orange precipitate formed.

Solution was filtered, washed with 5 x 2 mL hexanes, and allowed to dry under vacuum. A bright red/orange powder was isolated in 97% yield. Large red plate like crystals suitable for X-ray analysis were grown in a saturated solution of THF with hexanes as countersolvent, and storing at -20^{o}C for several days. ^{1}H NMR ($CDCl_3$, 500 MHz): δ 8.21(br d , 1H, py, aromatic), δ 8.09(br t, 1H, py, aromatic), δ 7.59(br d, 1H, aromatic), δ 7.45-6.83(br m, 16H, aromatic) 6.80(br d, 1H, aromatic), δ 2.60(br s, 3H, Me), δ 2.41(br s, 3H, Me), δ 1.99(br s, 3H, Me), δ 1.71(br s, 3H, Me). ^{13}C NMR ($CDCl_3$, 125 MHz). δ 196.3(CO), 195.1(CO), 186.0(CO), 178.1 (C=N imine), 163.9(py, C=N imine), 162.8(*o*-C=N), 157.7(*o*-C=N), 148.3(Ar, *i*-C), 147.2(Ar, *i*-C), 139.2(Ar-CH), 133.4(Ar, *i*-C), 133.1(Ar, *C-CH$_3$*), 131.4(Ar-CH), 131.1(Ar-CH), 131.0 (Ar, *C-CH$_3$*), 130.9(Ar-CH), 130.5(Ar-CH), 130.0(Ar-CH), 128.8(Ar-CH), 128.7(Ar-CH), 128.6(Ar-CH), 128.4(Ar-CH), 128.2(Ar-CH), 128.1(Ar-CH), 127.7(Ar-CH), 126.9 (Ar-CH), 126.2(Ar, *C-CH$_3$*), 123.9(Ar-CH), 122.8(Ar, *C-CH$_3$*), 20.3(Ar-*Me*, CH_3), 18.7(br, Ar-*Me*, CH_3), 18.4(Ar-*Me*, CH_3). Elemental analysis calculated (%) for [$C_{38}H_{31}ReClN_3O_3$]: C 57.10, H 3.91, N 5.26, found C 57.48, H 3.92, N 5.38.

(7.5) 2,6-{2,6-Me$_2$C$_6$H$_3$N=CPh}$_2$(NC$_5$H$_3$)Re(CO)$_2$Cl: 2,6-{2,6-$Me_2C_6H_3N$=CPh}$_2$(NC_5H_3)Re(CO)$_3$Cl (**7.4**) powder (120 mg, 0.149 mmol) was placed in a ceramic boat, inside a quartz tube under flow of N_2 and placed inside a furnace. The reaction was allowed to run for 1 hour at 200^{o}C, after which the boat was removed and allowed to cool. A dark brown/red powder was isolated in 97% yield. Small dark brown prism like crystals suitable for X-ray analysis were grown in a saturated solution of THF with hexanes as countersolvent, and storing at -20^{o}C for several days. ^{1}H NMR ($CDCl_3$, 500 MHz): δ 7.66(br d , 2H, py, *m*-CH), δ 7.42(br t, 2H, aromatic), δ 7.33(br t, 2H, aromatic), δ 7.16(br t, 2H, aromatic) δ 7.07(br m, 3H, aromatic), δ 7.01(br d, 2H, aromatic), δ 6.96(br d, 2H, aromatic), δ 6.81(br t, 2H,

aromatic), δ 6.70(br d, 2H, aromatic), δ 2.76(br s, 6H, Me), δ 2.12(br s, 6H, Me). ^{13}C NMR ($CDCl_3$, 125 MHz). δ 221.8 (CO), 174.6 (C=N imine), δ 166.2 (CO), 161.8(py, *o*-C=N), 151.2 (Ar, *i*-C), 138.1(Ar-CH), 132.5(Ar, *i*-C), 132.1(Ar, *i*-C), 130.9(Ar-CH), 130.0(Ar-CH), 128.8(Ar-CH), 128.6(Ar-CH), 128.5(Ar-CH), 128.3(Ar-CH), 128.2(Ar-CH), 127.9(Ar-CH), 127.8(Ar-CH), 126.8(Ar, *i*-C), 126.2 (Ar-CH), 124.4(Ar-CH), 20.2(Ar-*Me*, CH_3), 19.1(Ar-*Me*, CH_3). Elemental analysis calculated (%) for [$C_{37}H_{31}ReClN_3O_3$]: C 57.61, H 4.05, N 5.45, found C 57.43, H 4.03, N 5.44.

(7.6) 2,6-{2,6-Me$_2$C$_6$H$_3$N=CPh}$_2$(NC$_5$H$_3$)Re(CO)$_2$Br: 2,6-{2,6-$Me_2C_6H_3N$=CPh}$_2$(NC_5H_3)Re(CO)$_3$Br (**7.3**) powder (60 mg, 0.071 mmol) was placed in a ceramic boat, inside a quartz tube under flow of N_2 and placed inside a furnace. The reaction was allowed to run for 1 hour at 240^{o}C, after which the boat was removed and allowed to cool. A dark brown/red powder was isolated in 95% yield. Small dark prism-like crystals were grown from a variety of solvents (ether, THF, chloroform) but were consistently too small and unsuitable for X-ray analysis. ^{1}H NMR ($CDCl_3$, 500 MHz): δ 7.66(br m , 2H, py, *aromatic*), δ 7.49-6.88(br m, 13H, aromatic), δ 6.83(br t, 2H, aromatic), δ 6.72(br d, 2H, aromatic), δ 2.82(br s, 6H, Me), δ 2.14(br s, 6H, Me). ^{13}C NMR ($CDCl_3$, 125 MHz). δ 221.6 (*v br* CO), 174.9 (C=N imine), 167.1 (CO), 161.9(py, *o*-C=N), 151.8 (Ar, *i*-C), 138.4(Ar-CH), 133.1(Ar, *i*-C), 132.3(Ar, *i*-C), 131.3(Ar-CH), 130.4(Ar-CH), 129.2(Ar-CH), 128.9(Ar-CH), 128.6(Ar-CH), 128.4(Ar-CH), 128.2(Ar-CH), 127.1(Ar, *i*-C), 126.6 (Ar-CH), 124.6(Ar-CH), 21.7(Ar-*Me*, CH_3), 19.6(Ar-*Me*, CH_3). Elemental analysis calculated (%) for [$C_{37}H_{31}ReBrN_3O_3$]: C 54.48, H 3.83, N 5.15, found C 53.94, H 3.78, N 5.09.

(7.7) 2,6-{2,6-Me$_2$C$_6$H$_3$N=CPh}$_2$(NC$_5$H$_3$)Re(CO)$_3$(CF$_3$SO$_3$): 2,6-{2,6-$Me_2C_6H_3N$=CPh}$_2$(NC_5H_3)Re(CO)$_3$Cl (**7.4**) powder (150 mg, 0.187 mmol) and slight excess of

AgOTf (51 mg, 0.200 mmol) was added to 8 mL of toluene, in a darkened reaction flask. The reaction mixture was allowed to stir for 18 hours, over which time a bright yellow precipitate formed. Solution was filtered, washed with 5 x 2 mL hexanes, redisolved in DCM and filtered through a plug of Celite, and concentrated under vacuum. A bright yellow powder was isolated in 55% yield. Yellow plate like crystals suitable for X-ray analysis were grown in a saturated solution of THF with hexanes as countersolvent, and storing at -20^{o}C for several days. . ^{1}H NMR ($CDCl_3$, 500 MHz): δ 8.21(br d , 1H, py, aromatic), δ 8.42(br d, 1H, py, aromatic), δ 8.19(br t, 1H, aromatic), δ 7.65(br d, 1H, aromatic), δ 7.45(br t, 1H, aromatic), δ 7.37(br m, 2H, aromatic), δ 7.32(br m, 2H, aromatic), δ 7.28-7.11(br m, 4H, aromatic), δ 7.03(br m, 3H, aromatic), δ 6.93(br t, 2H, aromatic), δ 6.84(br d, 1H, aromatic), δ 6.77(br d, 1H, aromatic), δ 2.49(br s, 3H, Me), δ 2.38(br s, 3H, Me), δ 2.02(br s, 3H, Me), δ 1.52(br s, 3H, Me). ^{13}C NMR ($CDCl_3$, 125 MHz). δ 195.9(CO), 194.6(CO), 187.4(CO), 179.6 (C=N imine), 163.7(py, C=N imine), 163.3(*o*-C=N), 157.5(*o*-C=N), 147.4(Ar, *i*-C), 147.2(Ar, *i*-C), 140.3(Ar-CH), 133.4(Ar, *i*-C), 132.4(Ar, *C-CH$_3$*), 131.9(Ar-CH), 131.4(Ar-CH), 131.3(Ar-CH), 130.7(Ar-CH), 130.5(Ar, *C-CH$_3$*), 130.1(Ar, *C-CH$_3$*), 129.5(Ar-CH), 128.9(Ar-CH), 128.8(Ar-CH), 128.7(Ar-CH), 128.4(Ar-CH), 128.0(Ar-CH), 127.7(Ar-CH), 127.2(Ar-CH), 126.2 (Ar, *C-CH$_3$*), 124.2(Ar-CH), 18.8(Ar-*Me*, CH_3), 18.4(Ar-*Me*, CH_3), 18.3(Ar-*Me*, CH_3), 18.2(Ar-*Me*, CH_3).Sample for elemental analysis was obtained by recrystallization in $CHCl_3$, resulting in a 1:1 $CHCl_3$ adduct of **7.7** calculated (%) for $[C_{39}H_{31}F_3N_3O_6ReS][CHCl_3]$: C 46.54, H 3.12, N 4.07, found C 46.85, H 3.22, N 4.22.

(7.8) Reaction of 2,6-{2,6-Me$_2$C$_6$H$_3$N=CPh}$_2$(NC$_5$H$_3$)Re(CO)$_2$Cl with AgOTf: 2,6-{2,6-$Me_2C_6H_3N$=CPh}$_2$(NC_5H_3)Re(CO)$_2$Cl (7.5) powder (105 mg, 0.136 mmol) and slight excess of AgOTf (26 mg, 0.140 mmol) was added to 8 mL of toluene, in a darkened reaction

flask. The reaction mixture was allowed to stir for 18 hours, over which time no discernible colour change was observed. Solution was filtered, washed with 5 x 2 mL hexanes to afford 108 mg of dark maroon powder. Attempted crystallization resulted in the isolation of **7.7** and **7.9**, along with other species unsuitable for crystallography. Attempted ^{1}H NMR showed extreme broadening, pointing to a paramagnetic species. Elemental analysis or further magnetic measurements could not be conducted due to sample impurity.

(7.9) 2,6-{2,6-$Me_2C_6H_3N$=CPh}$_2$(NC_5H_3)Re(CO)$_2$(CF_3SO_3): 2,6-{2,6-$Me_2C_6H_3N$=CPh}$_2$(NC_5H_3)Re(CO)$_3$(CF_3SO_3) (**7.7**) powder (50 mg, 0.055 mmol) was placed in a ceramic boat, inside a quartz tube under flow of N_2 and placed inside a furnace. The reaction was allowed to run for 25 minutes at 190^{o}C, after which the boat was removed and allowed to cool. A dark brown/red powder was isolated in 93% yield. Small orange plate like crystals suitable for X-ray analysis were grown in a saturated solution of $CHCl_3$ with hexanes as countersolvent, and storing at -20^{o}C for several days. ^{1}H NMR ($CDCl_3$, 500 MHz): δ 7.59(br d , 2H, py, *m*-CH), δ 7.49-6.99(br m, 13H, aromatic), δ 6.81(br t, 2H, aromatic), δ 6.71(br d, 2H, aromatic), δ 2.66(br s, 6H, Me), δ 2.19(br s, 6H, Me). ^{13}C NMR ($CDCl_3$, 125 MHz). δ 220.4 (CO), 178.9 (C=N imine), 169.1 (CO), 163.9(py, *o*-C=N), 150.4 (Ar, *i*-C), 140.7(Ar-CH), 131.7(Ar, *i*-C), 131.6(Ar, *i*-C), 131.3(Ar-CH), 129.4(Ar-CH), 129.3(Ar-CH), 128.9(Ar-CH), 128.6(Ar-CH), 128.3(Ar-CH), 128.2(Ar-CH), 127.3(Ar-CH), 126.7(Ar, *i*-C), 126.6 (Ar-CH), 126.4(Ar-CH), 19.4(Ar-*Me*, CH_3), 19.0(Ar-*Me*, CH_3). Elemental analysis calculated (%) for [$C_{38}H_{31}F_3N_3O_5ReS$]: C 51.58, H 3.53, N 4.75, found C 51.31, H 3.44, N 4.80.

[7.6] X-ray Crystallographic Information: Rhenium Complexes

Table 7.1. Summary of Data Collection and Crystallographic Parameters for **7.1** & **7.2**.*

Compound	**7.1**	**7.2**
Empirical formula	$[C_{46}H_{47}ReBrN_3O_3][C_8H_{12}]_2$	$[C_{46}H_{47}ReClN_3O_3][C_4H_8O]_2$
Formula weight	1172.33	1055.72
Temperature (K)	200(2)	100(2)
λ (Å)	0.71073	0.71073
Crystal system	Monoclinic	Monoclinic
Space group	P2(1)/c	P2(1)/c
a (Å)	11.2917(2)	10.6850(2)
b (Å)	24.4721(4)	24.6759(5)
c (Å)	20.4997(4)	18.4443(3)
α (deg)	90.00	90.00
β (deg)	94.5900(10)	92.3360(10)
γ (deg)	90.00	90.00
V ($Å^3$)	5646.55(18)	4859.02(16)
Z	4	4
ρ (calc) (Mg/m^3)	1.379	1.443
μ (mm^{-1})	2.905	2.606
Absorption correction	Semi-empirical from equivalents	
Final R indices [I>2σ(I)]		
R1[a]	0.0356	0.0232
*w*R2[b]	0.0727	0.0525

$$^{a}R1 = \Sigma \left| |F_o| - |F_c| \right| / \Sigma |F_o|. \quad ^{b}wR2 = \left(\Sigma w \left(|F_o| - |F_c| \right)^2 / \Sigma w |F_o|^2 \right)^{1/2}$$

*structures available from CCDC

Table 7.2. Summary of Data Collection and Crystallographic Parameters for **7.3, 7.4** & **7.7**.

Compound	**7.3**	**7.4**	**7.7**
Empirical formula	$[C_{38}H_{31}ReBrN_3O_3]$ $[C_4H_8O]_{0.5}$	$[C_{38}H_{31}ReClN_3O_3][C_4H_8O]$	$[C_{38}H_{31}Re(CF_3SO_3)N_3O_3]$ $[C_4H_8O]$
Formula weight	879.82	871.41	985.03
Temperature (K)	296(2)	200(2)	200(2)
λ (Å)	0.71073	0.71073	0.71073
Crystal system	Triclinic	Triclinic	Triclinic
Space group	P-1	P-1	P-1
a (Å)	9.645(3)	8.4994(3)	8.6739(2)
b (Å)	13.366(4)	13.6344(4)	12.3727(3)
c (Å)	15.955(5)	16.6194(5)	19.2872(4)
α (deg)	107.958(13)	102.8350(10)	87.8370(10)
β (deg)	99.607(15)	97.3350(10)	83.6820(10)
γ (deg)	90.663(14)	93.202(2)	76.1410(10)
V ($Å^3$)	1924.7(11)	1855.36(10)	1997.29(8)
Z	2	2	2
ρ (calc) (Mg/m^3)	1.518	1.560	1.638
μ (mm^{-1})	4.235	3.393	3.163
Absorption correction	Semi-empirical from equivalents		
Final R indices [I>2σ(I)]			
R1[a]	0.0667	0.0201	0.0298
*w*R2[b]	0.1285	0.0513	0.0602

[a] $R1 = \Sigma \left| |F_o| - |F_c| \right| / \Sigma |F_o|$. [b] $wR2 = \left(\Sigma w \left(|F_o| - |F_c| \right)^2 / \Sigma w |F_o|^2 \right)^{1/2}$

Table 7.3. Summary of Data Collection and Crystallographic Parameters for **7.5, 7.7** & **7.9**.

Compound	**7.5**	**7.8**	**7.9**
Empirical formula	$[C_{37}H_{31}ReClN_3O_2]$ $[C_4H_8O]_{1.5}$	$K[C_{37}H_{31}ReClN_3O_2]$ $[C_4H_8O]$	$[C_{37}H_{31}Re(CF_3SO_3)N_3O_3]$ $[CHCl_3]$
Formula weight	879.45	882.50	1004.29
Temperature (K)	296(2)	200(2)	200(2)
λ (Å)	0.71073	0.71073	0.71073
Crystal system	Monoclinic	Orthorhombic	Triclinic
Space group	P2(1)/n	P2(1)2(1)2(1)	P-1
a (Å)	9.2686(3)	12.8841(4)	13.8597(11)
b (Å)	18.1949(6)	16.9962(6)	15.6045(11)
c (Å)	22.0310(7)	18.3333(6)	18.8333(14)
α (deg)	90.00	90.00	81.639(4)
β (deg)	98.035(2)	90.00	84.582(4)
γ (deg)	90.00	90.00	78.114(4)
V ($Å^3$)	3678.9(2)	4014.6(2)	3934.7(5)
Z	4	4	4
ρ (calc) (Mg/m^3)	1.588	1.460	1.695
μ (mm^{-1})	3.422	3.236	3.407
Absorption correction	Semi-empirical from equivalents		
Final R indices [I>2σ(I)]			
R1[a]	0.0170	0.0613	0.0814
*w*R2[b]	0.0407	0.1514	0.1921

[a] $R1 = \Sigma \left| |F_o| - |F_c| \right| / \Sigma |F_o|$. [b] $wR2 = \left(\Sigma w \left(|F_o| - |F_c| \right)^2 / \Sigma w |F_o|^2 \right)^{1/2}$

Table 7.4. Selected bond lengths (Å) for compounds **7.1** & **7.2**.

7.1		**7.2**	
C(1)-C(2)	1.477(5)	C(1)-C(2)	1.480(3)
C(6)-C(7)	1.510(5)	C(6)-C(7)	1.514(3)
C(1)-N(1)	1.292(4)	C(1)-N(1)	1.294(3)
C(7)-N(3)	1.269(4)	C(7)-N(3)	1.273(3)
C(2)-N(2)	1.372(4)	C(2)-N(2)	1.371(3)
C(6)-N(2)	1.347(4)	C(6)-N(2)	1.337(3)
Re(1)-N(1)	2.186(3)	Re(1)-N(1)	2.1860(19)
Re(1)-N(2)	2.208(3)	Re(1)-N(2)	2.2085(18)
Re(1)-Br(1)	2.6112(4)	Re(1)-Cl(1)	2.4630(6)
Re(1)-C(44)	1.916(4)	Re(1)-C(44)	1.914(2)
Re(1)-C(45)	1.942(5)	Re(1)-C(45)	1.904(2)
Re(1)-C(46)	1.912(4)	Re(1)-C(46)	1.916(2)
C(44)-O(1)	1.149(4)	C(44)-O(1)	1.147(3)
C(45)-O(2)	1.073(5)	C(45)-O(2)	1.158(3)
C(46)-O(3)	1.142(4)	C(46)-O(3)	1.151(3)

Table 7.5. Selected bond lengths (Å) for compounds **7.3, 7.4** & **7.7**.

7.3		**7.4**		**7.7**	
C(1)-C(2)	1.46(2)	C(1)-C(2)	1.481(3)	C(1)-C(2)	1.489(4)
C(6)-C(7)	1.49(2)	C(6)-C(7)	1.511(3)	C(6)-C(7)	1.505(4)
C(1)-N(1)	1.303(18)	C(1)-N(1)	1.297(2)	C(1)-N(1)	1.288(4)
C(7)-N(3)	1.285(18)	C(7)-N(3)	1.276(3)	C(7)-N(3)	1.275(4)
C(2)-N(2)	1.376(18)	C(2)-N(2)	1.368(2)	C(2)-N(2)	1.364(4)
C(6)-N(2)	1.350(18)	C(6)-N(2)	1.339(3)	C(6)-N(2)	1.348(4)
Re(1)-N(1)	2.171(12)	Re(1)-N(1)	2.1655(18)	Re(1)-N(1)	2.154(2)
Re(1)-N(2)	2.249(12)	Re(1)-N(2)	2.2200(15)	Re(1)-N(2)	2.228(2)
Re(1)-Br(1)	2.623(2)	Re(1)-Cl(1)	2.4778(6)	Re(1)-O(1)	2.200(2)
Re(1)-C(36)	1.93(2)	Re(1)-C(36)	1.930(2)	Re(1)-C(36)	1.908(3)
Re(1)-C(37)	1.907(17)	Re(1)-C(37)	1.905(2)	Re(1)-C(37)	1.882(3)
Re(1)-C(38)	1.91(2)	Re(1)-C(38)	1.900(2)	Re(1)-C(38)	1.923(3)
C(36)-O(1)	1.127(18)	C(36)-O(1)	1.142(3)	C(36)-O(4)	1.150(4)
C(37)-O(2)	1.152(17)	C(37)-O(2)	1.152(3)	C(37)-O(5)	1.162(4)
C(38)-O(3)	1.135(18)	C(38)-O(3)	1.156(3)	C(38)-O(6)	1.146(4)

Table 7.6. Selected bond lengths (Å) for compounds **7.5, 7.8** & **7.9**.

7.5		**7.8**		**7.9**	
C(1)-C(2)	1.474(3)	C(1)-C(2)	1.487(16)	C(1)-C(2)	1.54(3)
C(6)-C(7)	1.477(3)	C(6)-C(7)	1.458(16)	C(6)-C(7)	1.47(3)
C(1)-N(1)	1.315(3)	C(1)-N(1)	1.266(14)	C(1)-N(1)	1.37(3)
C(7)-N(3)	1.309(3)	C(7)-N(3)	1.290(15)	C(7)-N(3)	1.30(3)
C(2)-N(2)	1.355(2)	C(2)-N(2)	1.327(15)	C(2)-N(2)	1.27(3)
C(6)-N(2)	1.353(2)	C(6)-N(2)	1.360(15)	C(6)-N(2)	1.44(3)
Re(1)-N(1)	2.0964(15)	Re(1)-N(1)	2.151(9)	Re(1)-N(1)	2.073(16)
Re(1)-N(2)	2.0672(16)	Re(1)-N(2)	2.074(8)	Re(1)-N(2)	2.028(17)
Re(1)-N(3)	2.1089(16)	Re(1)-N(3)	2.127(8)	Re(1)-N(3)	2.136(17)
Re(1)-Cl(1)	2.4751(5)	Re(1)-Cl(1)	2.477(3)	Re(1)-O(3)	2.198(13)
Re(1)-C(36)	1.897(2)	Re(1)-C(36)	1.844(14)	Re(1)-C(36)	1.86(2)
Re(1)-C(37)	1.914(2)	Re(1)-C(37)	1.900(13)	Re(1)-C(37)	1.87(3)
C(36)-O(1)	1.160(3)	C(36)-O(1)	1.208(16)	C(36)-O(1)	1.18(3)
C(37)-O(2)	1.158(3)	C(37)-O(2)	1.154(15)	C(37)-O(2)	1.21(3)
--	--	K(1)-C(20)	2.145(14)	--	--
--	--	K(1)-C(21)	2.141(14)	--	--
--	--	K(1)-C(22)	2.231(18)	--	--
--	--	K(1)-C(23)	2.247(18)	--	--
--	--	K(1)-C(24)	2.286(16)	--	--
--	--	K(1)-C(25)	2.243(13)	--	--
--	--	K(1)-C(8)	2.795(12)	--	--
--	--	K(1)-C(13)	2.306(15)	--	--

Table 7.7. Selected bond angles (°) for compounds **7.1** and **7.2**.

7.1		**7.2**	
N(3)-C(7)-C(6)	111.5(3)	N(3)-C(7)-C(6)	112.0(2)
C(7)-C(6)-N(2)	123.0(3)	C(7)-C(6)-N(2)	122.30(19)
C(6)-N(2)-Re(1)	129.4(2)	C(6)-N(2)-Re(1)	129.80(15)
N(1)-Re(1)-N(2)	75.52(10)	N(1)-Re(1)-N(2)	75.61(7)
N(1)-C(1)-C(2)	117.3(3)	N(1)-C(1)-C(2)	116.5(2)
C(1)-C(2)-N(2)	116.9(3)	C(1)-C(2)-N(2)	117.26(19)
C(6)-N(2)-C(2)	117.0(3)	C(6)-N(2)-C(2)	117.56(19)
Re(1)-N(1)-C(1)	116.6(2)	Re(1)-N(1)-C(1)	115.46(16)
Re(1)-N(2)-C(2)	113.2(2)	Re(1)-N(2)-C(2)	112.36(14)
N(2)-Re(1)-C(44)	105.25(13)	N(2)-Re(1)-C(46)	105.23(8)
N(2)-Re(1)-C(45)	90.60(14)	N(2)-Re(1)-C(44)	94.96(8)
N(2)-Re(1)-C(46)	169.12(13)	N(2)-Re(1)-C(45)	169.20(9)
N(2)-Re(1)-Br(1)	81.33(7)	N(2)-Re(1)-Cl(1)	79.41(5)
N(1)-Re(1)-C(44)	173.70(14)	N(1)-Re(1)-C(46)	173.06(8)
N(1)-Re(1)-C(45)	96.45(14)	N(1)-Re(1)-C(44)	99.18(8)
N(1)-Re(1)-C(46)	93.61(14)	N(1)-Re(1)-C(45)	93.86(9)
N(1)-Re(1)-Br(1)	88.70(7)	N(1)-Re(1)-Cl(1)	84.55(5)

Table 7.8. Selected bond angles (°) for compounds **7.3, 7.4** and **7.7**.

7.3		**7.4**		**7.7**	
N(3)-C(7)-C(6)	110.6(14)	N(3)-C(7)-C(6)	112.93(19)	N(3)-C(7)-C(6)	114.2(3)
C(7)-C(6)-N(2)	121.1(14)	C(7)-C(6)-N(2)	121.67(16)	C(7)-C(6)-N(2)	121.4(3)
C(6)-N(2)-Re(1)	127.8(10)	C(6)-N(2)-Re(1)	128.01(13)	C(6)-N(2)-Re(1)	128.3(2)
N(1)-Re(1)-N(2)	74.9(5)	N(1)-Re(1)-N(2)	74.69(6)	N(1)-Re(1)-N(2)	74.23(9)
N(1)-C(1)-C(2)	116.4(13)	N(1)-C(1)-C(2)	116.07(17)	N(1)-C(1)-C(2)	115.6(3)
C(1)-C(2)-N(2)	117.3(13)	C(1)-C(2)-N(2)	116.43(15)	C(1)-C(2)-N(2)	114.5(3)
C(6)-N(2)-C(2)	118.0(12)	C(6)-N(2)-C(2)	117.76(16)	C(6)-N(2)-C(2)	117.2(3)
Re(1)-N(1)-C(1)	117.5(11)	Re(1)-N(1)-C(1)	118.37(14)	Re(1)-N(1)-C(1)	117.38(19)
Re(1)-N(2)-C(2)	110.5(9)	Re(1)-N(2)-C(2)	113.43(12)	Re(1)-N(2)-C(2)	109.69(18)
N(2)-Re(1)-C(36)	103.2(6)	N(2)-Re(1)-C(36)	105.41(8)	N(2)-Re(1)-C(38)	101.32(11)
N(2)-Re(1)-C(37)	167.4(6)	N(2)-Re(1)-C(38)	167.22(8)	N(2)-Re(1)-C(36)	168.19(11)
N(2)-Re(1)-C(38)	97.3(6)	N(2)-Re(1)-C(37)	96.45(8)	N(2)-Re(1)-C(37)	103.58(12)
N(2)-Re(1)-Br(1)	81.4(3)	N(2)-Re(1)-Cl(1)	80.48(5)	N(2)-Re(1)-O(1)	76.06(8)
N(1)-Re(1)-C(36)	177.1(7)	N(1)-Re(1)-C(36)	174.41(9)	N(1)-Re(1)-C(38)	175.43(11)
N(1)-Re(1)-C(37)	94.2(6)	N(1)-Re(1)-C(38)	92.63(8)	N(1)-Re(1)-C(36)	99.01(11)
N(1)-Re(1)-C(38)	95.1(6)	N(1)-Re(1)-C(37)	97.89(8)	N(1)-Re(1)-C(37)	93.94(12)
N(1)-Re(1)-Br(1)	90.4(3)	N(1)-Re(1)-Cl(1)	87.45(5)	N(1)-Re(1)-O(1)	82.23(8)

Table 7.9. Selected bond angles (°) for compounds **7.5, 7.8** and **7.9**.

7.5		**7.8**		**7.9**	
N(1)-C(1)-C(2)	115.30(16)	N(1)-C(1)-C(2)	114.4(9)	N(1)-C(1)-C(2)	112(2)
N(3)-C(7)-C(6)	115.88(17)	N(3)-C(7)-C(6)	117.6(10)	N(3)-C(7)-C(6)	116(2)
C(1)-C(2)-N(2)	112.38(16)	C(1)-C(2)-N(2)	114.7(10)	C(1)-C(2)-N(2)	109(2)
C(7)-C(6)-N(2)	112.56(17)	C(7)-C(6)-N(2)	112.3(11)	C(7)-C(6)-N(2)	113(2)
C(2)-N(2)-C(6)	121.51(16)	C(2)-N(2)-C(6)	122.9(9)	C(2)-N(2)-C(6)	117(2)
C(2)-N(2)-Re(1)	118.18(13)	C(2)-N(2)-Re(1)	117.1(8)	C(2)-N(2)-Re(1)	125.8(17)
C(6)-N(2)-Re(1)	117.92(12)	C(6)-N(2)-Re(1)	117.4(8)	C(6)-N(2)-Re(1)	116.7(14)
N(1)-Re(1)-N(2)	75.79(6)	N(1)-Re(1)-N(2)	74.9(4)	N(1)-Re(1)-N(2)	74.2(7)
N(3)-Re(1)-N(2)	75.95(6)	N(3)-Re(1)-N(2)	75.7(4)	N(3)-Re(1)-N(2)	77.4(7)
N(1)-Re(1)-N(3)	151.72(6)	N(1)-Re(1)-N(3)	150.4(3)	N(1)-Re(1)-N(3)	151.6(7)
N(2)-Re(1)-C(37)	170.88(7)	N(2)-Re(1)-C(37)	169.8(5)	N(2)-Re(1)-C(37)	170.2(8)
N(2)-Re(1)-C(36)	105.01(7)	N(2)-Re(1)-C(36)	105.1(7)	N(2)-Re(1)-C(36)	103.1(9)
N(2)-Re(1)-Cl(1)	79.67(4)	N(2)-Re(1)-Cl(1)	79.1(3)	N(2)-Re(1)-O(3)	81.8(6)

[7.7] IR stretch of CO

Infra-Red spectra were collected using a Varian 640 FT-IR spectrometer using an ATR attachment.

Table 7.10: Infra-Red CO stretch for compounds **7.3-7,** & **7.9**.

	7.3	**7.4**	**7.5**	**7.6**	**7.7**	**7.9**
ν(CO)	2024s	2013s	1919s	1906s	2030s	1915s
cm^{-1}	1932s	1918s	1849s	1837s	1931s	1855s
	1897s	1896s			1912s	

Chapter 8: *Conclusion*

This project began with a much more narrow scope than it eventually grew into. We chose the bis(imino)pyridine ligand scaffold for a variety of reasons: ease of synthesis, ability to tune sterics on the N-aryl sidearms, and established utility as a pincer-type ligand with a lack of precedence within the main group metal catalogue. We were aware of several aspects of ligand non-innocence, such as ability to be reduced, whether by loss of proton on the backbone, or simply taking on additional electrons into the extended π-system. Ultimately, we were looking to use bis(imino)pyridine ligands as a standard Werner type complex, where we exploit the lone pair donor ability of the N,N',N binding pocket, along with increased steric bulk to facilitate the synthesis and subsequent kinetic stabilization of reactive indium(I) complexes. We were successful in doing so, and these complexes were the first example of their kind. However, and much to our delight, our computational studies revealed that we had uncovered something much more interesting than the main group coordination chemistry we initially targeted. This would shape the remainder of the work in this thesis, and hopefully continue to inspire much more work after my time in the lab has passed.

The ligand-metal covalent interaction for bis(imino)pyridine to the indium(I) centre was found to be so weak, that for all intents and purposes, it could be considered as a naked cation surrounded by a ligand cage. Yet these compounds remain sufficiently stable to be handled and characterized, and if stored in air and moisture free environments display longevity on the order of months, and even years. This is in direct contrast to the classical understanding of ligand-metal interaction, whereby we tacitly assume a donation or sharing of a discrete number of electrons, e.g. two electrons as would be the case for nitrogen atoms. Similar work was repeated with thallium(I), with the resulting Tl(I)bis(imino)pyridine complexes being the first of their

kind reported, and to our delight the results followed the same trend. However, this time around the binding was even weaker. Furthermore, our Tl(I)bis(imino)pyridine complexes also displayed Tl-arene interactions, resulting in the formation of Tl-arene bound dimers and inverted-sandwich bimetallic complexes. Computational studies revealed these arene interactions to also be the weakest ever reported, thus further challenging conventional views of ligand-metal interaction.

We attempted similar chemistry with gallium, with the goal of synthesizing Ga(I) complexes. Our efforts in that regard fell short due to lack of appropriate Ga(I) synthons, compounded by gallium's strong tendency to disproportionate to Ga(0) and Ga(III) species. We were however successful in developing a one pot synthetic methodology for Ga(III)bis(imino)pyridine complexes, and were also successful in characterizing the first Ga(III)bis(imino)pyridine radical complex. Keeping in theme with low-valent main group metals, we then looked at tin(II), whose similar $5s^2$ valence configurations drew compelling parallels to our indium(I) chemistry. These efforts led to the successful synthesis of the first ever tin(II)bis(imino)pyridine complexes. Furthermore, these complexes display weak binding interactions with their anionic component. These remain a promising target for future computational studies.

Furthermore, we expanded our work to silver(I). With a similar covalent radius, charge, and commercial availability of starting material, silver was a logical choice. We successfully synthesized the first Ag(I)bis(imino)pyridine complexes, which consequently were also only the second ever reported pincer complexes of silver. Due to the different electronic landscape of the transition metals, our resulting silver complexes did not exhibit weak ligand-metal interactions on the magnitude of those we observed in the main group. However they remained sufficiently

weak to allow the silver centre to be strongly cationic. This prompted studies into Lewis-acid reactivity at the silver site with a variety of donors (alkene, alkyne, aromatic, and lone pair). We successfully collected crystallographic data for transient intermediates of these weakly bound adducts. Computational studies thereof revealed another unexpected facet of bis(imino)pyridine ligand non-innocence; adduct formation was not only facilitated via adduct-silver interactions, but also via adduct-ligand interactions. This was something unexpected, and something which would likely be overlooked in the absence of a thorough computational evaluation, as the classical approach would be to attribute adduct formation to interaction of Lewis-basic donors with the Lewis-acidic metal centre.

Our final foray was into an unfamiliar field. Rhenium(I) chemistry has a longstanding and well established chemistry with the bis(imino)pyridine ligand framework. However, due to the nature of Re(I) synthons ($Re(CO)_5X$, X=Cl, Br, and I), resulting ligation of bis(imino)pyridine, as well as other terdentate ligands such as terpyridine always occurs in bidentate fashion. This is due to the energetic barrier associated with loss of a third CO group necessary to facilitate the pincer geometry. As such, there have been no crystallographically authenticated examples of low valent rhenium pincer complexes, with only one poorly characterized example as anecdotal evidence. Our goal was to synthesize the first low valent rhenium pincer complex. By developing a solid state reaction methodology we were able to synthesize an array of rhenium(I) pincer complexes with relative ease in near quantitative yields. These complexes are the first examples of their kind, and we hope are the stepping stones towards developing previously inaccessible low valent rhenium chemistry.

From a coordination chemistry perspective, we were successful in synthesizing a wide array of new compounds, ranging from refined examples of previous work, to completely novel

examples which we hope will set the trend towards future development of the field. In a broader sense, I believe our work has not only revealed several new aspects of bis(imino)pyridine ligand non-innocence, but has also challenged conventional concepts of ligand-metal interaction. In doing so, our work has contributed to the broader fundamental understanding of bonding interactions.